
# Developing Improved Civil Aircraft Arresting Systems



**DETAILS**

196 pages | | PAPERBACK
ISBN 978-0-309-11813-2 | DOI 10.17226/14340

**AUTHORS**

Matthew A Barsotti; John M H Puryear; David J Stevens; Transportation Research Board

AIRPORT COOPERATIVE RESEARCH PROGRAM

ACRP REPORT 29

# Developing Improved Civil Aircraft Arresting Systems

**Matthew A. Barsotti**
**John M. H. Puryear**
**David J. Stevens**
**Protection Engineering Consultants, LLC**
Austin, TX

*Subject Areas*
Aviation

Research sponsored by the Federal Aviation Administration

TRANSPORTATION RESEARCH BOARD

WASHINGTON, D.C.
2009
www.TRB.org

## AIRPORT COOPERATIVE RESEARCH PROGRAM

Airports are vital national resources. They serve a key role in transportation of people and goods and in regional, national, and international commerce. They are where the nation's aviation system connects with other modes of transportation and where federal responsibility for managing and regulating air traffic operations intersects with the role of state and local governments that own and operate most airports. Research is necessary to solve common operating problems, to adapt appropriate new technologies from other industries, and to introduce innovations into the airport industry. The Airport Cooperative Research Program (ACRP) serves as one of the principal means by which the airport industry can develop innovative near-term solutions to meet demands placed on it.

The need for ACRP was identified in *TRB Special Report 272: Airport Research Needs: Cooperative Solutions* in 2003, based on a study sponsored by the Federal Aviation Administration (FAA). The ACRP carries out applied research on problems that are shared by airport operating agencies and are not being adequately addressed by existing federal research programs. It is modeled after the successful National Cooperative Highway Research Program and Transit Cooperative Research Program. The ACRP undertakes research and other technical activities in a variety of airport subject areas, including design, construction, maintenance, operations, safety, security, policy, planning, human resources, and administration. The ACRP provides a forum where airport operators can cooperatively address common operational problems.

The ACRP was authorized in December 2003 as part of the Vision 100-Century of Aviation Reauthorization Act. The primary participants in the ACRP are (1) an independent governing board, the ACRP Oversight Committee (AOC), appointed by the Secretary of the U.S. Department of Transportation with representation from airport operating agencies, other stakeholders, and relevant industry organizations such as the Airports Council International-North America (ACI-NA), the American Association of Airport Executives (AAAE), the National Association of State Aviation Officials (NASAO), and the Air Transport Association (ATA) as vital links to the airport community; (2) the TRB as program manager and secretariat for the governing board; and (3) the FAA as program sponsor. In October 2005, the FAA executed a contract with the National Academies formally initiating the program.

The ACRP benefits from the cooperation and participation of airport professionals, air carriers, shippers, state and local government officials, equipment and service suppliers, other airport users, and research organizations. Each of these participants has different interests and responsibilities, and each is an integral part of this cooperative research effort.

Research problem statements for the ACRP are solicited periodically but may be submitted to the TRB by anyone at any time. It is the responsibility of the AOC to formulate the research program by identifying the highest priority projects and defining funding levels and expected products.

Once selected, each ACRP project is assigned to an expert panel, appointed by the TRB. Panels include experienced practitioners and research specialists; heavy emphasis is placed on including airport professionals, the intended users of the research products. The panels prepare project statements (requests for proposals), select contractors, and provide technical guidance and counsel throughout the life of the project. The process for developing research problem statements and selecting research agencies has been used by TRB in managing cooperative research programs since 1962. As in other TRB activities, ACRP project panels serve voluntarily without compensation.

Primary emphasis is placed on disseminating ACRP results to the intended end-users of the research: airport operating agencies, service providers, and suppliers. The ACRP produces a series of research reports for use by airport operators, local agencies, the FAA, and other interested parties, and industry associations may arrange for workshops, training aids, field visits, and other activities to ensure that results are implemented by airport-industry practitioners.

## ACRP REPORT 29

Project 07-03
ISSN 1935-9802
ISBN 978-0-309-11813-2
Library of Congress Control Number 2009941761



### COPYRIGHT INFORMATION



### NOTICE

The project that is the subject of this report was a part of the Airport Cooperative Research Program conducted by the Transportation Research Board with the approval of the Governing Board of the National Research Council. Such approval reflects the Governing Board's judgment that the project concerned is appropriate with respect to both the purposes and resources of the National Research Council.

The members of the technical advisory panel selected to monitor this project and to review this report were chosen for recognized scholarly competence and with due consideration for the balance of disciplines appropriate to the project. The opinions and conclusions expressed or implied are those of the research agency that performed the research, and while they have been accepted as appropriate by the technical panel, they are not necessarily those of the Transportation Research Board, the National Research Council, or the Federal Aviation Administration of the U.S. Department of Transportation.

Each report is reviewed and accepted for publication by the technical panel according to procedures established and monitored by the Transportation Research Board Executive Committee and the Governing Board of the National Research Council.

The Transportation Research Board of the National Academies, the National Research Council, and the Federal Aviation Administration (sponsor of the Airport Cooperative Research Program) do not endorse products or manufacturers. Trade or manufacturers' names appear herein solely because they are considered essential to the clarity and completeness of the project reporting.

*Published reports of the*

**AIRPORT COOPERATIVE RESEARCH PROGRAM**

*are available from:*

Transportation Research Board
Business Office
500 Fifth Street, NW
Washington, DC 20001

*and can be ordered through the Internet at*

http://www.national-academies.org/trb/bookstore

Printed in the United States of America

THE NATIONAL ACADEMIES
*Advisers to the Nation on Science, Engineering, and Medicine*

The **National Academy of Sciences** is a private, nonprofit, self-perpetuating society of distinguished scholars engaged in scientific and engineering research, dedicated to the furtherance of science and technology and to their use for the general welfare. On the authority of the charter granted to it by the Congress in 1863, the Academy has a mandate that requires it to advise the federal government on scientific and technical matters. Dr. Ralph J. Cicerone is president of the National Academy of Sciences.

The **National Academy of Engineering** was established in 1964, under the charter of the National Academy of Sciences, as a parallel organization of outstanding engineers. It is autonomous in its administration and in the selection of its members, sharing with the National Academy of Sciences the responsibility for advising the federal government. The National Academy of Engineering also sponsors engineering programs aimed at meeting national needs, encourages education and research, and recognizes the superior achievements of engineers. Dr. Charles M. Vest is president of the National Academy of Engineering.

The **Institute of Medicine** was established in 1970 by the National Academy of Sciences to secure the services of eminent members of appropriate professions in the examination of policy matters pertaining to the health of the public. The Institute acts under the responsibility given to the National Academy of Sciences by its congressional charter to be an adviser to the federal government and, on its own initiative, to identify issues of medical care, research, and education. Dr. Harvey V. Fineberg is president of the Institute of Medicine.

The **National Research Council** was organized by the National Academy of Sciences in 1916 to associate the broad community of science and technology with the Academy's purposes of furthering knowledge and advising the federal government. Functioning in accordance with general policies determined by the Academy, the Council has become the principal operating agency of both the National Academy of Sciences and the National Academy of Engineering in providing services to the government, the public, and the scientific and engineering communities. The Council is administered jointly by both the Academies and the Institute of Medicine. Dr. Ralph J. Cicerone and Dr. Charles M. Vest are chair and vice chair, respectively, of the National Research Council.

The **Transportation Research Board** is one of six major divisions of the National Research Council. The mission of the Transportation Research Board is to provide leadership in transportation innovation and progress through research and information exchange, conducted within a setting that is objective, interdisciplinary, and multimodal. The Board's varied activities annually engage about 7,000 engineers, scientists, and other transportation researchers and practitioners from the public and private sectors and academia, all of whom contribute their expertise in the public interest. The program is supported by state transportation departments, federal agencies including the component administrations of the U.S. Department of Transportation, and other organizations and individuals interested in the development of transportation. **www.TRB.org**

**www.national-academies.org**

## CRP STAFF FOR ACRP REPORT 29



## ACRP PROJECT 07-03 PANEL
### Field of Design



## AUTHOR ACKNOWLEDGMENTS

The research reported herein was performed under ACRP Project 07-03 by Protection Engineering Consultants (PEC).

Mr. Matthew A. Barsotti, M.S., Principal at PEC, was the Principal Investigator (PI). The other authors of this report were Mr. John M. H. Puryear, M.S., Project Engineer at PEC; and David J. Stevens, Ph.D., P.E., Senior Principal and Co-PI at PEC. Testing and evaluation support was provided by Mr. Jason Patton, Research Engineer at Southwest Research Institute (SwRI). Supporting research was provided by Timothy Walilko, Ph.D., Senior Engineer at Applied Research Associates (ARA); Subhash Narang, Ph.D., Principal at Shakti Technologies; Eric B. Williamson, Ph.D., P.E., Associate Professor at the University of Texas at Austin; and Maria C. Garci Juenger, Assistant Professor at the University of Texas at Austin. Airport operations consultation was provided by Gordon S. Chace, A.A.E., C.A.E.

The authors wish to acknowledge the assistance provided by Engineered Arresting Systems Corporation (ESCO), which provided valuable data and information regarding the EMAS system.

The authors would also like to acknowledge the companies that generously provided design concepts and materials for evaluation: Grid Technologies, Inc.; Norsk Glassgjenvinning AS; Pittsburgh Corning; and Tensar International.

The informative airport survey results would not have been possible without the participation of the many airport management personnel, who painstakingly gathered information regarding their facilities and experiences. The Minneapolis-St. Paul Metropolitan Airport Commission and the Port Authority of New York and New Jersey provided site tours and ongoing information to the research team. Many individuals at the FAA provided valuable references and insight, including David Rathfelder, E.C. Hunnicutt, and Ryan King.

Jim Day, P.E., Nielen Stander, Ph.D., and Willem Roux, Ph.D. (Livermore Software Technology Corporation) have continually provided outstanding technical help and advice with various LS-DYNA and LS-OPT questions and issues. Oleh Baran, Ph.D. (DEM Solutions) provided ongoing assistance with Discrete Element Modeling (DEM) facets of the project.

# FOREWORD

By Marci A. Greenberger
Staff Officer
Transportation Research Board

*ACRP Report 29: Developing Improved Civil Aircraft Arresting Systems* is a report that evaluates alternative materials that could be used for an engineered material arresting system (EMAS), as well as potential active arrestor designs for civil aircraft applications. Currently, there is only one manufacturer that has been approved by the FAA. This report provides an evaluation of (1) cellular glass foam, (2) aggregate foam, (3) engineered aggregate, and (4) a main-gear engagement active arrestor system. Airport operators will find the updated cost information and performance considerations useful, airport planning firms will be aided by evaluating future options with respect to runway dimensions and land requirements, and manufacturers of alternative products will be encouraged to see the performance characteristics of other materials and the potential process by which they may be able to gain approval.

---

There are many airports today that are land constrained and therefore unable to comply with FAA design standards to ensure that there is adequate room at runway ends for overruns. There can be many reasons why an airport does not have the space and would wish to pursue an alternative. An EMAS is one such alternative.

However, there is currently only one system that meets the FAA standards for arresting civil aircraft. The cost associated with acquiring and installing the cellular material is high, installation is labor-intensive, and there are no tests with which to verify the durability and integrity over time. There have been several ideas for alternative civil aircraft arresting systems submitted to the FAA; however, none have undergone testing or been submitted with the appropriate data necessary for approval.

Under ACRP 07-03, Protection Engineering Consultants was asked to (1) identify and evaluate the most promising alternatives, (2) identify the steps that must be taken to have those alternatives approved for use within the United States, (3) conduct a sensitivity analysis of the FAA's design and performance parameters for civil aircraft arresting systems and the potential effects on system design that result from varying one or more of the parameters (e.g., aircraft leaving the runway at 60 knots rather than 70 knots), and (4) document the advantages and disadvantages of each alternative.

This report provides alternatives to the current system, the steps required to pursue approval, and the performance characteristics of the candidate materials. The research team accomplished these objectives in part by (1) conducting a literature review, (2) surveying airport operators with installed systems, (3) reviewing FAA design parameters and holding discussions with the FAA, and (4) conducting an in-depth engineering evaluation of the arresting capabilities for the candidate systems.

# CONTENTS

SUMMARY

# Developing Improved Civil Aircraft Arresting Systems

## Introduction

Passenger aircraft can overrun the available runway area during takeoff and landing, creating accidents involving aircraft damage and loss of life. The increasing speed and weight of modern passenger aircraft require longer runways, but many airports are land-locked by surrounding buildings, bodies of water, or geographic features that prevent runway extension. These facts, combined with the increasing volume of air traffic, make overrun risks more relevant today than when many U.S. airports were first constructed.

To mitigate overruns that take place, the Federal Aviation Administration (FAA) now requires that all runways have a Runway Safety Area (RSA) beyond the normal runway surface, typically with a length of 1,000 ft. This area provides an additional deceleration zone for planes that cannot stop before reaching the runway end. However, some airports do not have sufficient land area to meet this requirement. In such cases, the airport can install an arrestor system that provides an equivalent to the standard RSA. This use of arrestor systems permits the airport to satisfy the FAA requirement within a smaller land space.

Currently, the only type of civil aircraft arresting system that meets FAA standards is an Engineered Material Arresting System (EMAS). A number of airports have installed EMAS, and these arrestors have demonstrated the ability to bring aircraft to a stop in several overrun incidents.

However, various issues and concerns regarding the current EMAS technology exist. At many airports, the land area at the end of a runway is inadequate to accommodate a full-sized EMAS system. The costs associated with acquiring and installing an EMAS are high due to the labor-intensive assembly process. The durability of the system over time is unknown, and no tests are currently available that can verify that an installed EMAS maintains its original design characteristics.

The objective of this research was to advance the development of alternative civil aircraft arresting systems to safely decelerate aircraft that overshoot the runway. The research sought to evaluate alternatives to the current EMAS technology, with the goal of finding options that might offer better performance, lower cost, or higher durability. The research involved technical and non-technical aspects such as candidate system evaluation, cost estimation, standards-related investigation, and airport surveys. A number of candidate systems and materials were evaluated; some were similar in function to the current system, while some were categorically different.

## EMAS Nomenclature

In general, the FAA advisory circular regarding EMAS provides latitude regarding the materials and construction methods that may be used; multiple EMAS designs could exist. At present, however, only one manufacturer has an approved EMAS design, which is the Engineered Arresting

Systems Corporation, or ESCO. In general use, the term "EMAS" has largely become synonymous with this ESCO product. Nevertheless, "EMAS" as a system definition could be expanded in the future to include a number of other arrestors besides this current product. Many of the new arrestor system concepts discussed in this report, if eventually approved and fielded, would qualify as EMAS systems.

As such, it is necessary to clarify the nomenclature that will be followed in this report. When technical comparisons are made regarding the design, construction, and performance of "EMAS," the term will refer to the systems presently deployed. When regulatory discussions are undertaken, the term will refer to the general requirements that pertain to the current and future passive arrestor systems. When clarification is required, qualifications such as "current EMAS," "current EMAS design," or "current EMAS technology" will be used to denote the ESCO product.

## EMAS Description

An EMAS is a surface-based arrestor constructed as a large bed that resides in the RSA beyond the end of a runway (Figure S-1). EMAS dimensions can vary considerably, but typical dimensions are approximately 300 ft in length by 150 ft in width, with a nominal 75-ft setback from the runway end. Depending on the available space in the RSA, it can be more cost-effective to install shorter EMAS beds with longer setbacks.

The current EMAS design features 4-ft by 4-ft blocks of cellular (foamed) cement, usually in one of two compressive strengths. The blocks have narrow gaps between them for venting and drainage, and the tops of these joints are sealed against rain. The depth of the blocks varies depending on the bed design. The sides of the bed stair-step for pedestrian and emergency vehicle access. These side step blocks are not considered in performance calculations for the arresting bed. Prior to installing an EMAS, the site must be prepared with a paved surface that provides a solid foundation for the bed and adequate drainage.

Two generations of EMAS are currently installed at U.S. airports. The older JBR-501 design used painted cement board tops for the individual blocks and caulking to seal the joints in between. The newer JBR-502 design uses plastic tops, which do not require painting, and silicone tape to seal the joints.

As the only current FAA-approved arresting system, the current EMAS design will serve as a baseline for the arrestor alternatives examined in this research.

*Figure S-1. EMAS arrestor, Minneapolis–St. Paul (MSP) airport.*

### Research Approach

The research was divided into two phases. The first, the study phase, included research, identification of alternatives, and an initial down-selection of the most promising candidate arrestor concepts. The second, the experimentation phase, focused on evaluating the candidate concepts through testing and modeling.

## Survey of U.S. Airport Operators

To obtain information and opinions regarding the existing EMAS from end-users, a survey was taken of 14 U.S. airports, and site visits were made to three. The information obtained was a mixture of objective data and subjective opinions. The airport operators were asked questions regarding past and present experience with EMAS pertaining to installation, maintenance, overrun performance, and its related costs. Additionally, a smaller survey of pilots and pilot organizations was undertaken. Many suggestions, opinions, and concerns were voiced. However, this summary will focus on the cost components.

For baseline cost information regarding EMAS, the study referred to FAA Order 5200.9, *Financial Feasibility and Equivalency of Runway Safety Area Improvements and Engineered Material Arresting Systems.* It provided guidelines for estimating the costs to establish an EMAS at an airport and for estimating the life-cycle costs of a system.

Airport operators were asked to provide the preparatory paving cost and installation cost for each arrestor installed at their airports. Eight airports provided preparatory paving and installation costs for a total of 11 arrestors. By way of comparison, the cost design values according to FAA Order 5200.9 were based on five separate EMAS installations.

The mean cost values reported by the airports are shown in Table S-1. They were normalized by the associated pavement and bed areas. The survey costs were corrected for inflation and are expressed in 2007 dollars. For comparison, the suggested values of preparatory paving cost and installation cost from FAA Order 5200.9 are included in the table, in 2007 dollars. As shown, the mean reported paving and installation costs were significantly higher than the design costs estimated in FAA Order 5200.9. Actual costs also appeared to exceed the expectations of FAA Order 5200.9 with regard to annual maintenance.

While the survey included more airports than the original data set used to create Order 5200.9, it did not include all EMAS systems installed at U.S. airports. It is possible that the average costs could shift if the remaining airports were included.

Although essentially based on anecdotal experiences, the researchers have noted a general lack of awareness regarding the existence, usage, and function of EMAS among airline pilots. This lack of awareness has been observed in both newer and seasoned pilots. It is unclear whether the

**Table S-1. Normalized mean costs from survey compared with FAA Order 5200.9 (2007 dollars).**

| | FAA Order 5200.9 | Survey |
|---|---|---|
| Normalized Preparatory Paving Cost per Square Foot | $15 | $48 |
| Normalized Installation Cost per Square Foot | $85 | $134 |
| Cost to Establish EMAS (CTEE) per Square Foot | $100 | $182 |
| Cost for 150 x 300-ft Bed | $4.5M | $8.2M |

awareness is higher for pilots that typically land at airports with EMAS. Unfortunately, response from the pilot community was limited during the survey process.

## Review of FAA Parameters

The design parameters for an EMAS are based on FAA requirements contained in Advisory Circular 150/5220-22A. These parameters were reviewed to determine their relative impact on the cost, size, and performance of installed arrestors.

### Exit Speed

Exit speed is how fast an aircraft is travelling when it rolls past the end of the runway. The advisory circular requires that an EMAS have a standard design exit speed of 70 knots (standard case) and a minimum of 40 knots (non-standard case). In designing an arrestor, the bed construction would be specified to ensure that the aircraft serviced by the runway could be stopped with these exit speeds. The 70-knot standard is intended to enable arrest of 90% of overruns, which historical data indicated was statistically the case. The 40-knot minimum is provided as an exception for airports with highly constrained RSAs.

A review of the overrun data collected in a recent ACRP study on aircraft overruns and undershoots indicated that the 70-knot requirement may no longer be sufficient to reach the intended 90% arrest rate (*ACRP Report 3*). Analysis of the new data conducted during this research effort suggests that the 90% threshold may have shifted to just above 80 knots. This could affect the design speeds for aircraft arrestors if a 90% criterion is to be maintained. Additional investigation may be warranted regarding the accuracy of the reported data that was used in the assessment.

### Damage to Aircraft

The advisory circular requires that the arrestor not cause structural damage to the aircraft. This mandate has a direct impact on the arrestor's cost and performance. The requirements could be altered to permit overloading of the aircraft landing gear if certain criteria are met. For example, if an aircraft continues to penetrate beyond 75% of the bed length, it could enter an "all or nothing" zone, where the resistance of the bed increases in a final attempt to arrest the aircraft. The landing gear may be damaged, but that may be preferable to the alternative of failing to stop the aircraft. A more robust approach could include an overall risk assessment for the facility and the aircraft serviced by the runway, since the consequences of an unimpeded overrun would not be equal for all facilities.

### Cost

The sensitivity of EMAS cost was assessed in the vicinity of the 40-knot minimum and 70-knot standard exit speeds. The impact of shifting the exit speeds of the advisory circular was assessed.

- The estimated length and cost of an EMAS with a 50-knot design exit speed is about 60% greater than an EMAS with a 40-knot design exit speed.
- The estimated length and cost of an EMAS with an 80-knot design exit speed is about 30% greater than an EMAS with a 70-knot design speed.

Thus, increasing the exit speed requirements would have a direct cost and size impact on arrestor bed installations.

## Commercialization Study

A commercialization study was undertaken to assess the requirements for a manufacturer to bring a new arrestor system to market. The study examined necessary steps to obtain FAA approval and identified barriers to market entry.

One barrier to entry that was identified is a lack of predictive tools for manufacturers to assess aircraft landing gear loads. Without this predictive capability, it would prove difficult to satisfy the safe-design requirements specified in Advisory Circular 150/5220-22A.

The FAA computer program, "ARRESTOR," though an old code at present, can predict arresting distances for various bed geometries. It models a general crushable foam material and permits the user to specify different compression strengths to be modeled. As such, ARRESTOR could serve the up-and-coming manufacturers who do not have in-house predictive codes.

ARRESTOR currently contains a limited library of aircraft: the B707, B727, and B747. Only one of these aircraft is still in broad service, the B747. To serve as a modern planning tool, a broader range of aircraft should be considered for ARRESTOR. Alternately, a new design program could be developed. The Arrestor Prediction Code (APC) developed in the current effort could serve as the basis for such a replacement.

## Identification and Selection of Alternatives

The identification of different arrestor alternatives to EMAS was approached through several means. The FAA William J. Hughes Technical Center supplied a list of manufacturers that had previously contacted them with different proposed arrestor concepts, materials, or designs. Those companies were subsequently contacted to determine if there was still active interest in arrestor development. Additionally, the research team reviewed historical arrestor designs and brainstormed to develop new concepts.

Following the identification of alternatives, taxonomy was developed to classify the different options and provide clarity of comparison. An initial assessment of the alternatives led to the selection of several promising candidates for detailed research in the experimentation phase of the effort.

The maturity of the different concepts varied widely. Some companies simply had an alternative crushable material that could be used in a similar manner as the cellular cement of current EMAS, but with potentially improved durability. Other companies had more well-developed ideas, including patents, design drawings, and calculations for energy absorption. The broad range of maturity required an initial assessment of the alternatives in order to determine the most promising concepts for inclusion in the experimentation stage of the research.

Based on the initial screening and down-selection process, four arrestor candidates were selected for the experimentation phase of the effort:

1. Glass foam arrestor concept (passive),
2. Aggregate foam arrestor concept (passive),
3. Engineered aggregate arrestor (passive), and
4. Main-gear engagement active arrestor concept (active).

Please note that the TRB and ACRP do not endorse specific products. Research results are provided to assist in the evaluation of options by others.

### Candidate 1: Glass Foam

Cellular glass foam was proposed as a material and would be made as a modification of an existing insulating product (Figure S-2). The material would be used in a large bed either composed of blocks akin to the current EMAS design or constructed as a monolithic structure. The

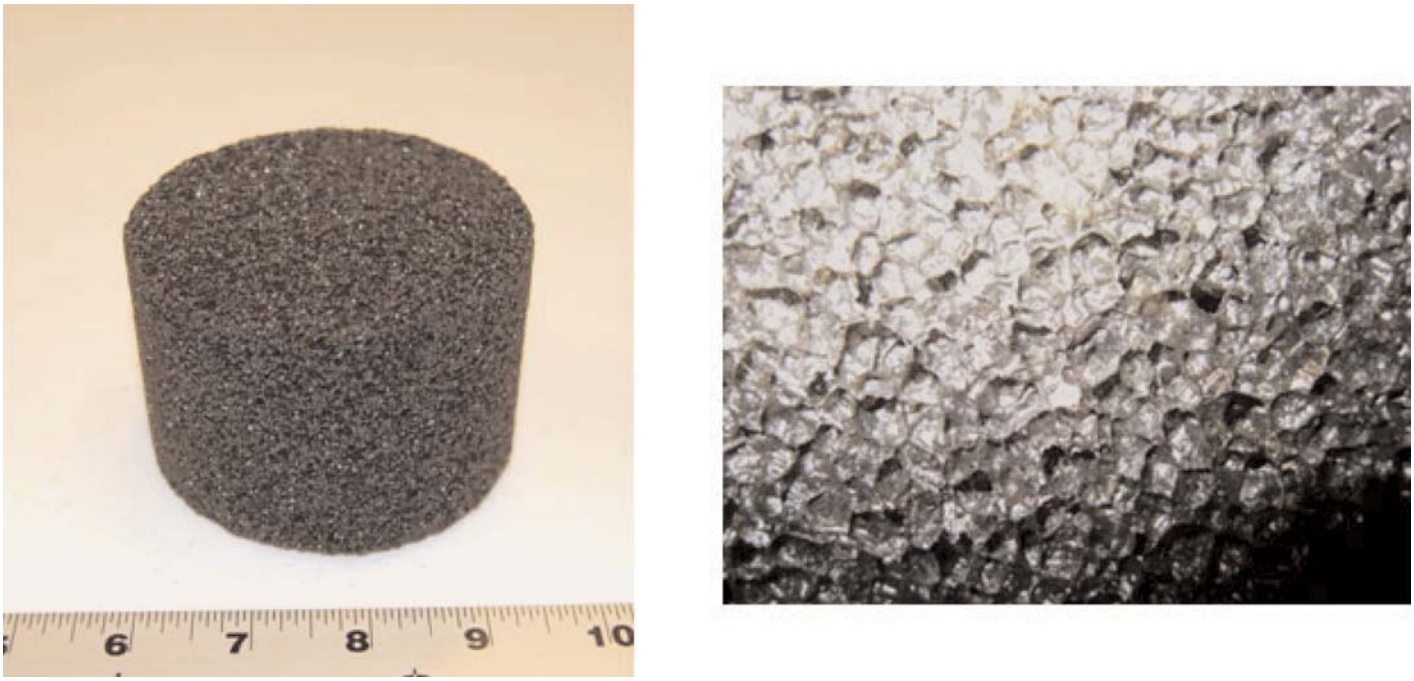


*Figure S-2. Cellular glass foam material.*

chemical makeup and closed-cell properties of glass foam suggested good chemical resistance, excellent durability to the environment, and resistance to water absorption. The potential improvement in durability suggested the possibility of reduced maintenance and replacement needs for an arrestor using this material.

The glass foam material offered relatively similar mechanical properties to that of cellular cement because both materials are low-density crushable foams. However, glass foam in general appeared to be less fragile, easier to handle, and potentially more durable than the cellular cement. Additionally, adhesives and moisture sealants are available for glass foams that permit joining and weatherproofing.

Because the glass foam material is generally manufactured in blocks sized at approximately $24 \times 18 \times 6$ inches, two variants are possible (Figure S-3):

1. **Block Method.** The block method would use 4-ft square blocks of the foam, analogous to the current EMAS construction approach. The blocks would be constructed by adhering multiple smaller blocks together, followed by the potential addition of top and/or bottom cap materials. The sides of the block could potentially be sprayed with a sealant to further weatherproof the blocks. These blocks would be transported to and installed at a runway in essentially the same manner as the current EMAS beds.
2. **Monolithic Method.** The monolithic method would be assembled on-site at the runway by stacking and gluing blocks into a single large structure. The final assembly would then be fitted with a continuous top cover layer composed of a roll/spray-on polymer. This layup would preclude the need for joint seams, sealants, and maintenance, which are required for the current EMAS design. Moisture sealing of the vertical sides of individual blocks would be unnecessary. Monolithic layups such as this have been used in building roof applications.

## Candidate 2: Aggregate Foam

An aggregate foam arrestor concept was proposed. The arrestor would use rough-broken foam aggregate made from recycled glass (Figure S-4). The foamed, or aerated, glass material has

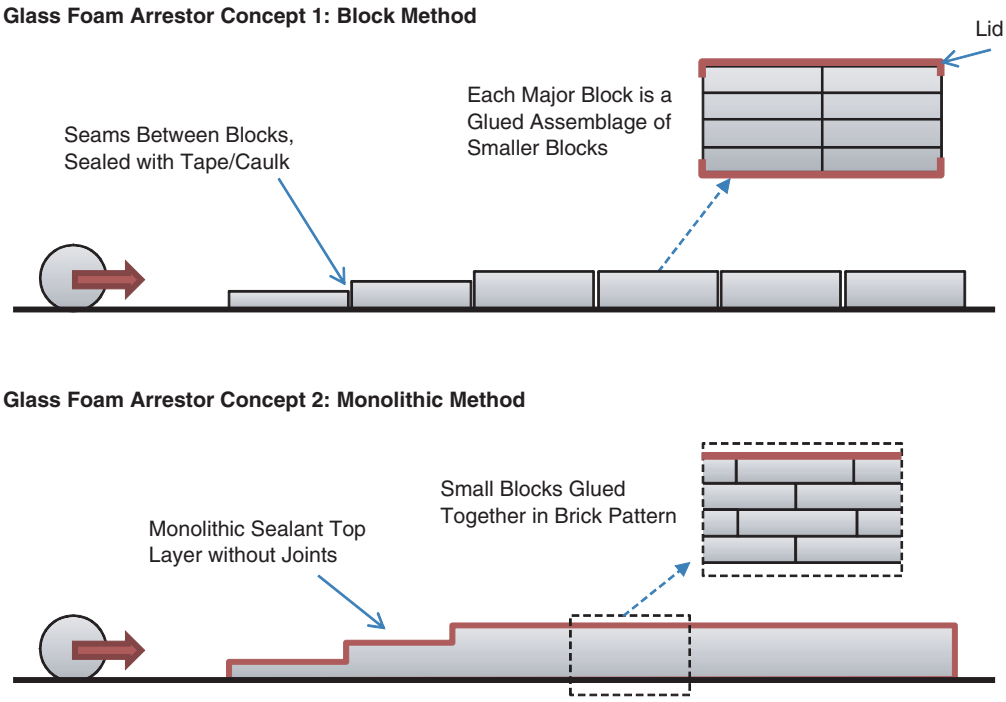


***Figure S-3. Glass foam arrestor variants: block method (top) and monolithic method (bottom).***

***Figure S-4. Aggregate foam material: microstructure (upper-left), as a pile (upper-right), and individual pieces (bottom).***

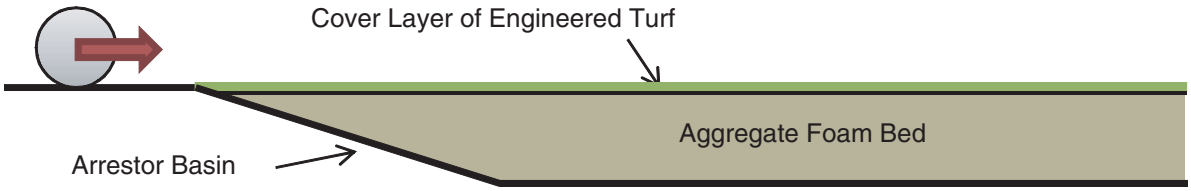


*Figure S-5. Aggregate foam arrestor concept.*

nominally 80% void space by volume. Its closed-cell microstructure makes it resistant to water absorption and degradation.

An arrestor using the aggregate foam would be constructed by creating a basin and filling it with the material. An engineered turf would serve as a top cover layer for the bed (Figure S-5), which can serve several purposes:

1. Prevent material dispersion due to jet blast;
2. Mitigate material spraying during overrun by an aircraft tire, thus limiting engine ingestion hazard;
3. Regulate water drainage and potential ice crust formation in winter; and
4. Act as a structural component to prevent lightweight land vehicles from penetrating the arrestor bed.

This simple fill-and-cover construction would likely produce lower manufacture and installation costs than the block construction methods used at present. This potential advantage is offset by the possibility that the material could settle over time and result in altered arresting performance.

## Candidate 3: Engineered Aggregate

An engineered aggregate arrestor concept was proposed. Its primary material is a spherical engineered aggregate that has excellent flow properties and resists settling and compaction that are more typical for angular gravels (Figure S-6).

This material would reside in a shallow bed and be covered with a reinforced turf layer. However, the engineered aggregate may also be used without a turf layer, which has been done at four airports in the UK. Other top layer materials are possible, such as a thin asphalt skim coat. Figure S-7


*Figure S-6. Engineered aggregate.*

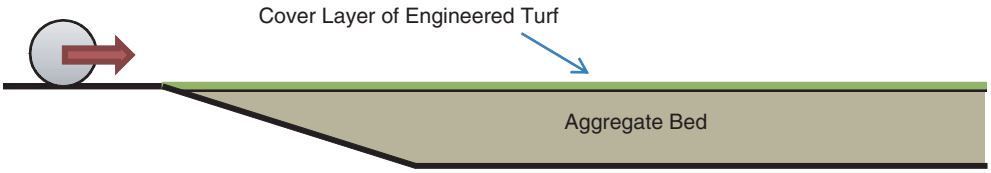


***Figure S-7. Engineered aggregate arrestor concepts.***

illustrates the cover-layer variant of the engineered aggregate arrestor concept. The confining top layer would serve similar purposes as that of the aggregate foam concept.

The engineered aggregate solution offered the advantage of construct-in-place simplicity, requiring no fabrication of blocks or cure time. Repairs after overruns would essentially involve shoveling or scraping the material back into place, with little material replacement required.

## Candidate 4: Main-Gear Engagement System

Active arresting systems have long been used to arrest military aircraft. Prior attempts have been made to adapt them for use with civil transport aircraft, using over-wing barrier nets to engage the wings and fuselage in the absence of a tail hook. To surpass these predecessors, any new attempts to adapt the active systems would require innovation and new sensor approaches. However, the active systems offer elegance and a decided performance advantage over passive systems. As such, they were revisited in this effort and re-examined for feasibility.

The active system concept evaluated was a main-gear engagement cable-based arrestor. For this concept, a cable-based arrestor would pop up from underneath to engage the main landing gear as the aircraft passes by. Military-style arrestor brakes would retain the cable at either end to decelerate the aircraft (Figure S-8). An aircraft identification system would determine the type of plane being engaged, and embedded runway sensors would detect the overrun event, compute aircraft speed, and determine the timing for deployment. The system would, therefore, be automated and not require manual activation. Pilot overrides could be included if desired.

One of the main advantages of the cable-based arrestor is that the nose gear would not be engaged. As shown in Figure S-9, the nose gear would only be loaded vertically due to the weight of

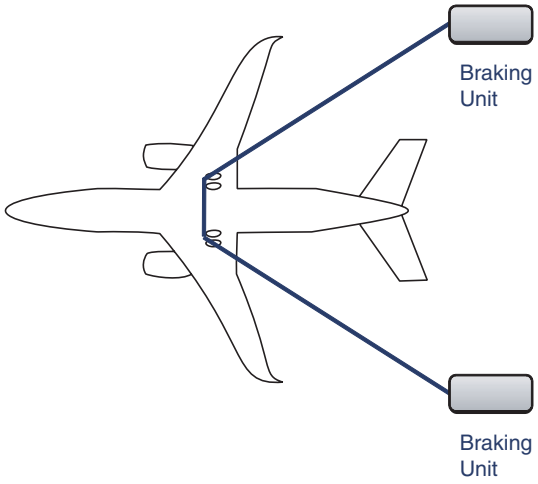


***Figure S-8. Main-gear engagement active arrestor.***

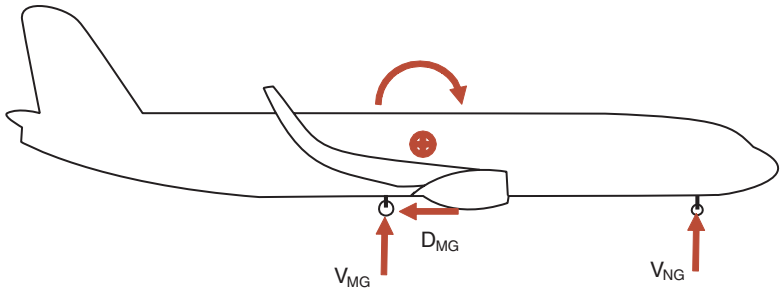


***Figure S-9. Loads on aircraft subjected to active arrestor deceleration.***

the aircraft and pitching moment. This main-gear engagement approach circumvents the weakness of the crushable bed systems: it does not subject the nose gear to drag loads. Consequently, it would be possible to achieve higher decelerations and shorter stopping distances. Further, with automated servo control of the braking units, it could obtain uniform decelerations for a wide range of aircraft weights. Therefore, the deceleration performance could readily exceed that of passive arrestor beds.

## Experimentation Overview

The research funding did not support full-scale testing on a broad enough basis to be meaningful for the effort. Because the experimentation phase was intended to compare the most promising alternatives to the current EMAS technology, and because there were several candidates to evaluate, a modeling-centric approach was adopted. Within this approach, various physical tests were performed in order to characterize the materials involved and to provide a basis for calibrating high-fidelity computer models of the systems. The models were then used to assess the performance of the arrestor concepts in different configurations and for different aircraft.

The candidate systems and evaluation methods are given in Table S-2. As the table indicates, the passive systems shared similar evaluation approaches, but the active system differed.

Crushable material technologies were emphasized most because they have a proven track record; finding a similar material solution with better life-cycle performance would provide a useful alternative in the near-term.

**Table S-2. Summary of evaluation methods for candidates.**

| Category | System | Evaluation Approach |
|---|---|---|
| Crushable material systems | • Candidate 1: Glass foam<br>• Candidate 2: Aggregate foam | • Material testing<br>• One-wheel bogey testing |
| Displaceable material systems | • Candidate 3: Engineered aggregate | • Numerical modeling to develop tire/material response surfaces<br>• Overall aircraft response evaluation using an aircraft suspension model |
| Active systems | • Candidate 4: Main-gear engagement active system | • Extended paper study<br>• Analytical spreadsheet model |

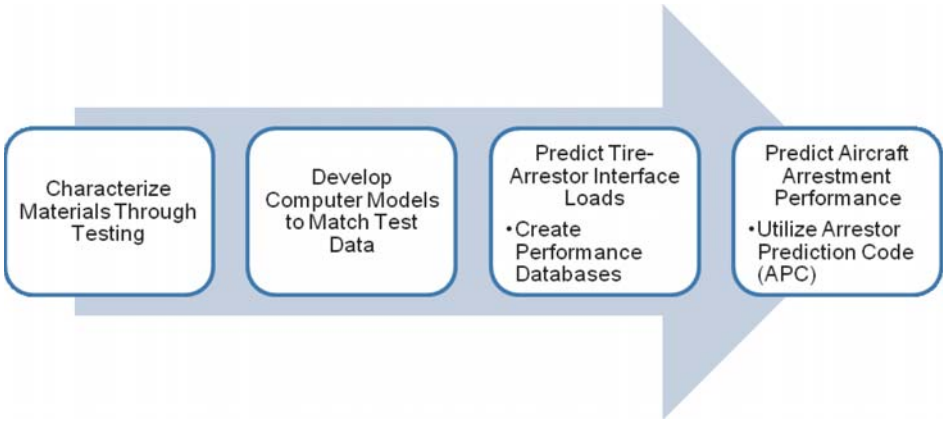


***Figure S-10. Simplified diagram of modeling and testing approach.***

Aggregate systems have historically experienced a discrepancy of acceptance, seeing use in the UK but not in the U.S. The evaluation approach outlined herein offers the promise of resolving the question of predictable arresting performance.

The evaluation method for the passive systems was composed of (1) modeling and (2) physical testing. Figure S-10 illustrates a simplified version of the modeling and testing approach.

The active system approach required a feasibility study to determine its merit. As such, a small task was dedicated to completing a more detailed paper/analytical study.

Early in the research effort, ESCO provided best-case EMAS arrestment prediction data for three aircraft from different size regimes: the CRJ-200, B737-800, and B747-400 (Figure S-11). In order to compare the candidate systems' performance with these EMAS baseline cases, aircraft computer models for each were developed. As such, these three aircraft are cited throughout the evaluation.

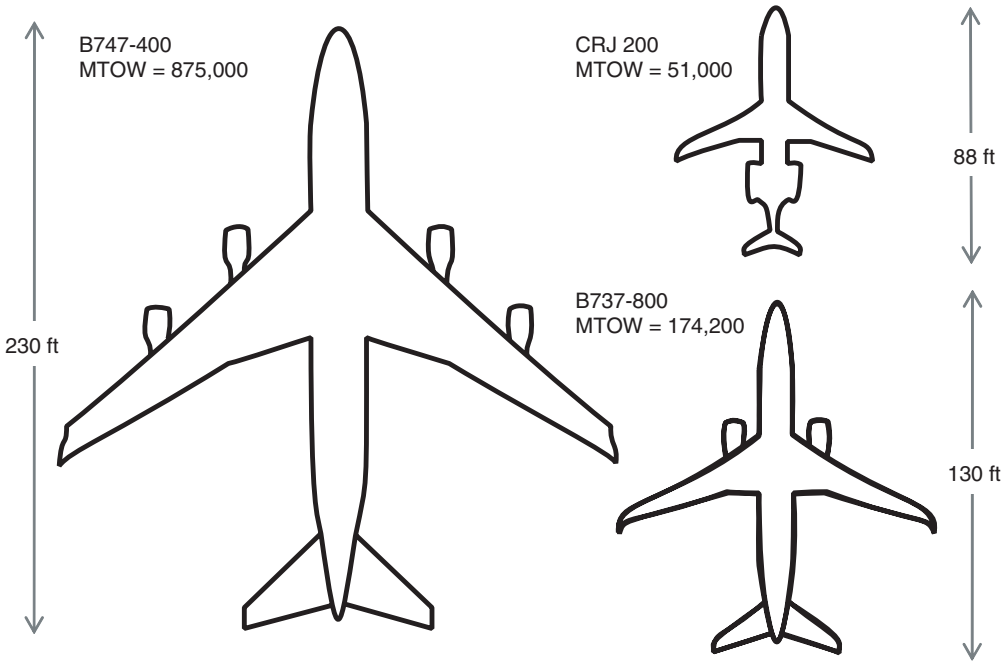


***Figure S-11. Three evaluation aircraft for the effort.***

## Passive System Evaluation Results

### Overview

The experimentation phase evaluated three passive arrestor candidate systems:

1. Glass foam arrestor,
2. Aggregate foam arrestor, and
3. Engineered aggregate arrestor.

Each demonstrated relative strengths and weaknesses. All three options provide concepts with increased material durability over cellular cement, which would likely result in longer life cycles and decreased maintenance requirements.

### Performance Comparison

The performance of the different candidates can be compared in two primary ways: based on (1) single-aircraft or (2) multi-aircraft bed designs. When comparing single-aircraft bed designs, the thickness of each bed and its material properties are optimized for the plane of interest. However, the bed designs for the different aircraft may not be compatible with one another. For example, a best-case design for the B747-400 was typically found to overload the landing gear of the CRJ-200.

When comparing multi-aircraft bed designs, a single bed is designed for best-case performance with all three of the subject aircraft simultaneously. A single-bed thickness and material property are determined such that the overall performance is optimized for all three aircraft.

The single-aircraft comparisons always produce the shortest feasible stopping distances. However, the multi-aircraft comparisons are more relevant to actual applications at airports, where arrestor beds are designed as a compromise between the different aircraft serviced.

Figure S-12 compares the best single-aircraft bed designs for the three alternatives and compares them to the current EMAS technology. The four sets of bars show very similar trends in terms of relative stopping lengths for the different aircraft. The glass foam stopping distances are slightly shorter than those of the current EMAS (except for the B737-800, where it is slightly longer), while the other two concepts would require slightly longer beds. The performance similarity of

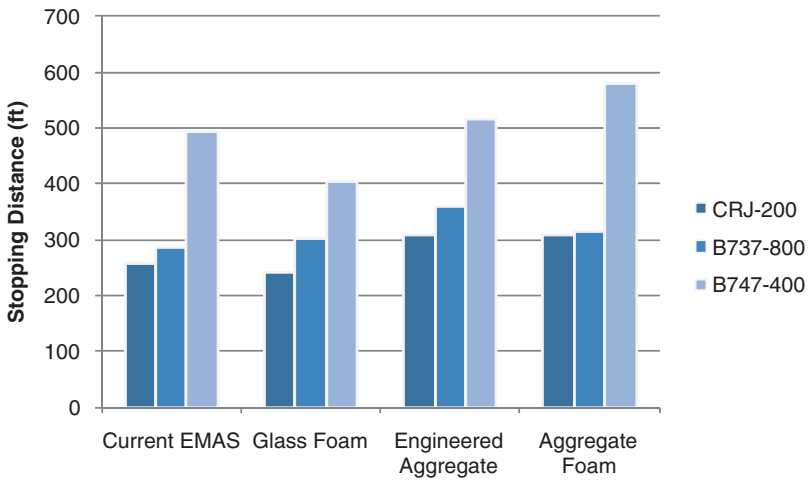


***Figure S-12. Comparison of single-aircraft bed performance for all candidates: distance travelled in bed for full arrest assuming 70-knot exit speed.***

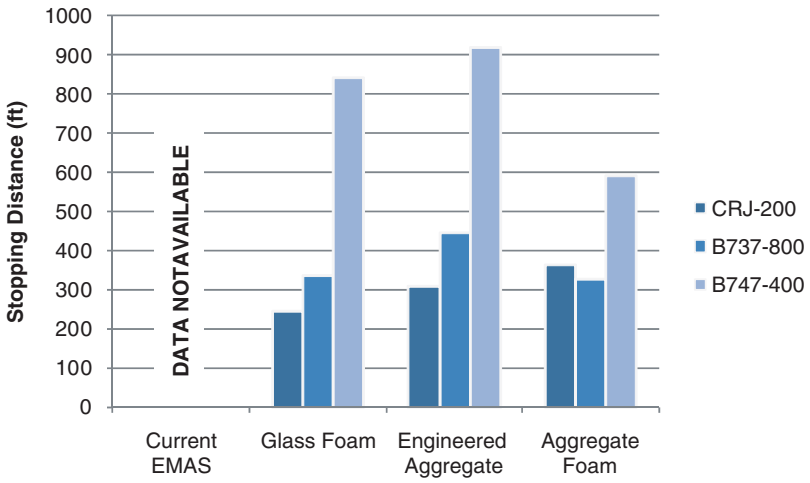


***Figure S-13. Comparison of multi-aircraft bed performance for all candidates: distance travelled in bed for full arrest assuming 70-knot exit speed.***

glass foam and the current EMAS is not surprising because both designs use crushable foam block material with similar mechanical behavior. However, this comparison of single-aircraft performance is ultimately less relevant to real applications than the multi-aircraft comparisons that follow.

Figure S-13 compares the best multi-aircraft arrestor bed designs for the three alternatives. In each case, the B747-400 required the longest bed for arrestment from a 70-knot exit speed. It should be noted that performance predictions for the existing EMAS have not been included in the figure because the design cases provided did not apply to multi-aircraft bed designs. In general, the material could be assumed to follow a similar trend to glass foam, owing to the mechanical similarities just discussed.

In comparing Figure S-12 with Figure S-13, the trend for leading and trailing concepts shifts considerably. The differences illustrate how substantially the multi-aircraft performance deviates from aircraft considered individually. For the multi-aircraft case, bars of similar height indicate improved equality in the treatment of the three aircraft. Of the three concepts, the aggregate foam shows the most consistent performance, with dramatic reduction in the stopping distance for the B747-400.

As an example, for a bed with a practical 400-ft length, the exit speeds for each aircraft are as shown in Table S-3. The 400-ft bed would obtain a full 70-knot exit speed rating for the CRJ-200 with all arrestor concepts. Both the glass foam and aggregate foam beds would further obtain a 70-knot rating for the B737-800, while the engineered aggregate falls behind at only 63 knots. For the B747-400, none of the beds obtains a full 70-knot rating; the aggregate foam leads at 56 knots and the engineered aggregate falls to below the minimum allowable speed at 39 knots.

**Table S-3. Comparison of multi-aircraft bed performance: exit speeds for full arrest in 400-ft bed.**

| Aircraft | Glass Foam | Engineered Aggregate | Aggregate Foam |
|---|---|---|---|
| **CRJ-200** | 70+ | 70+ | 70+ |
| **B737-800** | 70+ | 63 | 70+ |
| **B747-400** | 46 | 39 | 56 |

Overall, the performance of the three concepts can be summarized as below:

- The aggregate foam concept provided the best overall mixed-fleet bed performance, showing the smallest spread in arrestor performance for the three aircraft. However, the bed design must be correctly specified to prevent oscillatory "porpoising" behavior of the aircraft.
- The engineered aggregate produced speed-dependent landing gear loads. This would typically require designs to hedge against overloading by under-designing them, resulting in longer arrests than illustrated above.
- The glass foam beds produced the most predictable and constant decelerations without speed dependence or porpoising effects.

## Environmental Performance Comparison

From an environmental performance standpoint, all three alternatives appear likely to offer superior performance to the current EMAS technology. The environmental performance estimates are based on some test data, historical usage of the materials, and engineering judgment. An exhaustive environmental test program has not been undertaken as part of this program.

Life-cycle performance has been assumed to result from a combination of the core materials used and the protective measures taken to shield those materials from the elements.

From a materials standpoint, the glass foam and aggregate foam concepts both use closed-cell glass foams that inherently resist water penetration. The engineered aggregate is composed of hard spherical pellets. All three of these materials appear to offer superior inherent resistance to general handling and moisture/chemical exposure when compared to cellular cement.

With regard to protective measures, methods for covering and sealing the three candidate materials against moisture, standing water, jet blast, and freezing conditions have been examined (see respective chapters). For the aggregate foam and engineered aggregate approaches, the use of geo-plastics and geo-textiles could render the beds essentially isolated from water entrainment and freeze–thaw damage. The glass foam material could be packaged in a manner similar to that of the current EMAS cellular cement or equipped with an alternative monolithic sealed top layer.

## Cost Comparison

The relative costs for the current EMAS and the candidate systems are compared in Figure S-14 and Figure S-15, using survey cost assumptions and estimates from Order 5200.9, respectively. The general trends appear similar in either case, with the aggregate foam concept providing the least expensive alternative, and the glass foam providing the most expensive alternative. The costs in the figures denote the total cost to establish such a system and do not include life-cycle costs of bed replacement and maintenance.

## Summary Comparison

Glass foam provided equivalent dynamic behavior to the currently approved EMAS system. Its performance, cost, and construction are also similar to the current EMAS. However, use of glass foam with a monolithic construction offers reduced maintenance and a longer service life. Additionally, glass foam could be constructed using a stratified depth-varying layup, which would likely improve multi-aircraft bed performance.

Aggregate foam provided a novel approach that featured excellent multi-aircraft bed performance due to its depth-varying crushable material; this would effectively lead to shorter arrestor beds. Its cost was the lowest of the alternatives, combining an inexpensive material with a simple installation process.

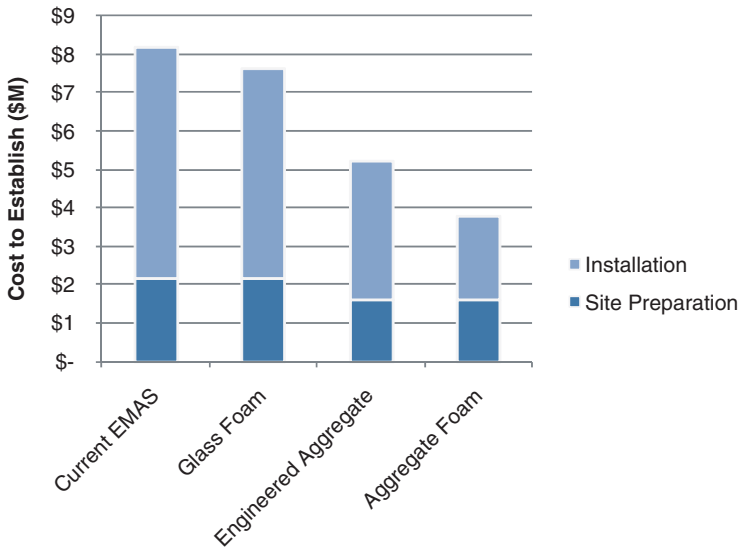


***Figure S-14. Relative estimated cost comparison assuming survey costs (150′ x 300′ bed).***

Engineered aggregate features the most durable candidate arrestor material, much of which could be reused after an arresting event. It has a cost that falls between the other concepts. Its speed-dependent nature produces weaker multi-aircraft performance, which would require longer arrestor beds to obtain the same exit speed ratings.

## Active System Evaluation Results

The main-gear engagement active system concept offered multiple advantages not available in passive surface-based arrestor beds. Feedback control offered the potential for ideal deceleration of aircraft. The energy-absorbing brakes could adjust automatically to apply less load on a small

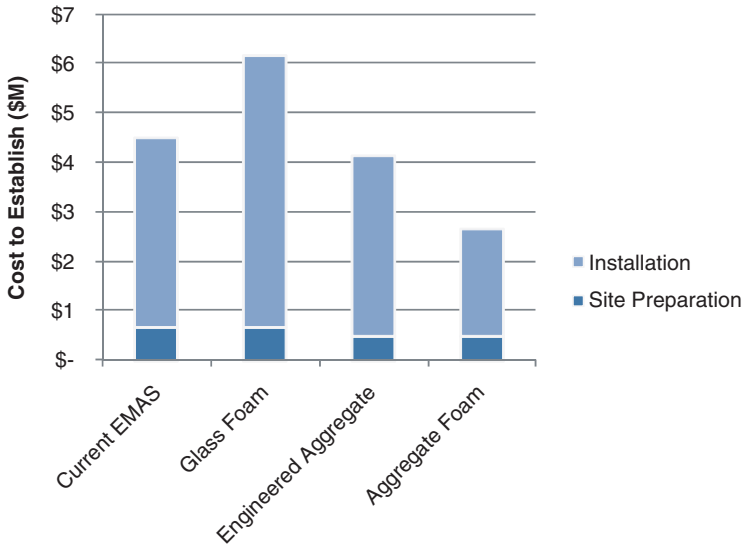


***Figure S-15. Relative estimated cost comparison assuming Order 5200.9 costs (150′ x 300′ bed).***

plane than a large one, enabling one arrestor to treat all aircraft equally. The overall effect of these advantages would be shorter arresting distances for the entire design fleet of aircraft.

Load calculations undertaken confirmed that the essential mechanics for the arrestor system would function as anticipated. Tension regulation in the cable would be essential to prevent overloading of the landing gear.

Despite these promising features, a number of complicating issues remain for the active system concept:

- Aircraft identification and speed calculation would be required for the system to function correctly. Systems to accomplish both could likely be developed, although research of such facets has not yet been undertaken.
- Cable sizes are of concern because the thicker cables required for rapidly arresting large planes could be heavy enough to damage smaller ones.
- The cable engagement process would likely result in damage to landing gear doors, actuators, wiring, and hydraulic features on the front side of the main struts.
- The window of time for deploying the system could be narrow when the aircraft has low slung engines because the vertical path of the cable or net must miss the engine nacelles yet engage the main strut above the tires.
- The geometry of some aircraft would exclude the possibility of engaging the main gear. These aircraft could not be engaged and arrested by a main-gear cable/net system.

For these reasons, the active system approach is feasible for stopping aircraft, but the main-gear engagement concept should be eliminated from consideration. Over-wing barrier net systems have been developed in the past, and they may still offer the best overall engagement approach. Past engagement issues for the nets could be resolved using automation concepts as discussed, thereby eliminating the need for direct triggering by airport personnel.

## Conclusions

In the first phase, research was done into multiple studies of different topics relevant to developing arrestor alternatives. After identifying promising alternatives, several candidate concepts were selected for detailed evaluation in the second, experimentation phase. In the second phase, testing and modeling were used to evaluate the performance of the candidates. This section summarizes important conclusions from both phases of research.

### Study Phase

The survey of U.S. airport operators revealed that actual EMAS costs appear to exceed the predicted values contained in FAA Order 5200.9 in terms of preparatory paving, installation, and maintenance. While the survey included more airports than the original data set used to create Order 5200.9, it did not include all EMAS systems installed at U.S. airports. It is possible that the average costs could shift once the remaining airports were included. However, since the survey data for the cost to establish an EMAS (CTEE) was 1.8 times higher than the predicted value, an update to the guidance document may be advisable.

A review of aircraft overrun data led to a revised probability curve for aircraft overrun exit speeds. This revised curve indicated that 90% of aircraft overruns may no longer take place at or below an exit speed of 70 knots. The new curve suggests that the 90% threshold may have shifted to just above 80 knots. This could affect the design speeds for aircraft arrestors if a 90% criterion is to be maintained. Additional investigation may be warranted regarding the accuracy of the reported data that was used in the assessment. However, increasing the 70-knot standard exit

speed or the 40-knot minimum exit speed requirements would have a notable impact on the size and cost of arrestor systems.

The FAA EMAS design requirements currently prohibit damage to the aircraft, which typically results in arrestor bed designs constrained by the rearward nose-gear loads. More aggressive decelerations would be possible if the designs were permitted to collapse the nose gear as long as the main gear remained intact. Prior EMAS testing suggests that this may pose minimal hazards to aircraft occupants. However, aircraft with low-slung engines could potentially be damaged and/or ingest arrestor material in such cases, and the risks of these effects have not been quantified. Additional concerns would apply to turbo-prop aircraft, where propeller damage could present additional hazards. It may be advantageous to revisit the requirements regarding landing gear loading in order to determine if case-by-case exceptions may be permissible. In some circumstances, the benefits of aggressive arrestor performance may outweigh the risks of failing to stop an overrun.

The approval and commercialization study determined that the current lack of a general predictive software tool presents a barrier for new entrants to the arrestor system field. Development of such a tool, or an update of the older ARRESTOR code, should be considered.

Although based on anecdotal experiences, the researchers have noted a seeming lack of awareness regarding the existence, usage, and function of EMAS among airline pilots. This lack of awareness has been observed in both newer and seasoned pilots. It is unclear whether awareness is greater among pilots that typically land at airports with EMAS. Unfortunately, response from the pilot community was limited during the survey process. Nevertheless, it may be beneficial to consider pursuit of an educational effort to increase awareness of the existence and function of EMAS within the pilot community.

## Experimentation Phase

The experimentation phase of the effort involved an extensive evaluation of four arrestor candidates:

1. Glass foam arrestor (passive),
2. Aggregate foam arrestor (passive),
3. Engineered aggregate arrestor (passive), and
4. Main-gear engagement active arrestor (active).

A combined modeling and simulation effort successfully replicated each candidate in order to evaluate its merit and compare it with the existing EMAS performance.

### *Passive System Evaluation*

The findings of this research indicate that a fieldable system is feasible for all three passive system candidates.

The aggregate foam concept offers superior multi-aircraft performance due to its depth-varying material properties. This multi-aircraft performance is arguably the most important factor for keeping arrestor beds short, reducing land requirements, and increasing the rated aircraft exit speeds. Additionally, it provides a substantially lower estimated cost per square foot. However, because the aggregate foam concept uses a novel crushable material and cover layer, the number of unknowns is greater. The arrestor materials require additional evaluation in order to produce high-confidence performance estimations. Overall, the combination of unknown factors and anticipated cost and performance improvements make it a moderate-risk/high-payoff concept.

Conversely, the glass foam concept is the most conservative of the three alternatives in terms of development risk and payoff. Glass foam provides an alternative to the current EMAS technology

with promising improvements regarding service life and maintenance, but at equivalent cost and performance. The mechanics of the material are predictable with relatively few unknown factors. Overall, the combination of unknown factors and anticipated cost and performance improvements make it a low-risk/moderate-payoff concept.

Finally, the engineered aggregate concept provides a feasible alternative, but one without a particular distinguishing advantage. It provides cost savings and increased material durability. However, the speed-dependent arrestor performance generally requires longer arrestor beds and diminishes the multi-aircraft performance. As with the aggregate foam, the materials to be used will require additional characterization in order to make high-confidence performance estimations. Overall, the combination of unknown factors and anticipated cost and performance improvements make it a moderate-risk/low-payoff concept.

The selection of one or more of these alternatives for fielding and approval is a task that requires consideration by the relevant stakeholders, which include the government, airport community, and manufacturers. Each candidate offers different advantages, risk levels, and payoff potential. Depending on the development track that is pursued, manufacturer investment may be required. The extensiveness of subsequent development plans and the associated costs may determine the feasibility of such participation. As a precursor to any such development, it is recommended that the concepts for pursuit be determined and that the relevant manufacturers be contacted for preliminary discussions of development scope and participation.

### *Active System Evaluation*

The main-gear engagement active system candidate is not recommended for additional pursuit. While stopping the aircraft proved mechanically feasible, engaging the main-gear struts involved multiple complexities, including damage to landing gear features, damage to landing gear bay doors, and timing and deployment complexity. Additionally, some aircraft geometries made capture infeasible altogether.

Nevertheless, active systems remain feasible if barrier nets are used for engagement. Using the suggested sensor and activation methods, an automated system could be developed that would eliminate the need for manual triggering, but permit pilot overrides. The active system approach offers the highest theoretical deceleration limits, which could produce substantially shorter arrestment distances than any passive system alternative.

The survey findings indicate that endeavors to implement an active civil aircraft arresting system would meet with resistance by the aviation community. If pursued, it is recommended that an educational component be included to increase awareness and reduce misconceptions regarding such systems.

## Final Conclusions

The research effort achieved its stated objective, which was to advance the development of alternative civil aircraft arresting systems. The research evaluated four alternatives to the current cellular cement EMAS technology and successfully identified options that can provide improved performance, lower cost, and/or higher durability.

Pursuing full development and testing of one or more of these candidate systems would be the next step toward obtaining requisite FAA approval. Once fielded, the new arrestor system would provide additional options to airport operators for achieving RSA compliance. Increasing the choices available would allow decision makers to select the arrestor option that best fits with the budgetary, climate, and space constraints of the facility.

CHAPTER 1

# Introduction

## 1.1. Project Background

Passenger aircraft can overrun the available runway area during takeoff and landing, creating accidents involving aircraft damage and loss of life. The increasing speed and weight of modern passenger aircraft require longer runways, but many airports are landlocked by surrounding buildings, bodies of water, or geographic features that prevent runway extension. These facts, combined with the increasing volume of air traffic, make overrun risks more relevant today than when many U.S. airports were first constructed.

To mitigate overruns that take place, the Federal Aviation Administration (FAA) now requires that all runways have a Runway Safety Area (RSA) beyond the normal runway surface, typically with a length of 1,000 ft. This area provides an additional deceleration zone for planes that cannot stop before reaching the runway end. However, some airports do not have sufficient land area to meet this requirement. In such cases, the airport can install an arrestor system that provides an equivalent to the standard RSA. This use of arrestor systems permits the airport to satisfy the FAA requirement within a smaller land space (*1*).

Currently, the only type of civil aircraft arresting system that meets FAA standards is an Engineered Material Arresting System (EMAS). A number of airports have installed EMAS, and these arrestors have demonstrated the ability to bring aircraft to a stop in several overrun incidents.

However, various issues and concerns regarding the current EMAS technology exist. The costs associated with acquiring and installing an EMAS are high due to the labor-intensive assembly process. At many airports, the land area at the end of a runway is inadequate to accommodate a full-sized EMAS system. In such cases, either additional land must be developed for accommodation or a reduced-performance EMAS must be installed. The durability of the system over time is unknown, and no tests are currently available that can verify that an installed EMAS maintains its original design characteristics.

The objective of this research was to advance the development of alternative civil aircraft arresting systems to safely decelerate aircraft that overshoot the runway. The research sought to evaluate alternatives to the current EMAS technology, with the goal of finding options that might offer better performance, lower cost, or higher durability. The research involved technical and non-technical aspects such as candidate system evaluation, cost estimation, standards-related investigation, and airport surveys. A number of candidate systems and materials were evaluated; some were similar in function to the current system while some were categorically different.

## 1.2. EMAS Nomenclature

In general, the FAA advisory circular regarding EMAS provides latitude regarding the materials and construction methods that may be used; multiple EMAS designs could exist (*1*). At present, however, only one manufacturer has an approved EMAS design, which is the Engineered Arresting Systems Corporation, or ESCO. In general use, the term "EMAS" has largely become synonymous with this ESCO product. Nevertheless, "EMAS" as a system definition could be expanded in the future to include a number of other arrestors besides this current product. Many of the new arrestor system concepts discussed in this report, if eventually approved and fielded, would qualify as EMAS systems.

As such, it is necessary to clarify the nomenclature that will be followed in this report. When technical comparisons are made regarding the design, construction, and performance of "EMAS," the term will refer to the systems presently deployed. When regulatory discussions are undertaken, the term will refer to the general requirements that pertain to the current and future passive arrestor systems. When clarification is required, qualifications such as "current EMAS," "current EMAS design,"

or "current EMAS technology" will be used to denote the ESCO product.

## 1.3. EMAS Description

An EMAS is a surface-based arrestor constructed as a large bed that resides in the RSA beyond the end of a runway (Figure 1-1). EMAS dimensions can vary considerably, but typical dimensions are approximately 300 ft in length by 150 ft in width, with a nominal 75-ft setback from the runway end. Depending on the available space in the RSA, it can be more cost-effective to install shorter EMAS beds with longer setbacks.

The current EMAS design features 4-ft by 4-ft blocks of cellular (foamed) cement, usually in one of two compressive strengths. The blocks have narrow gaps between them for venting and drainage, and the tops of these joints are sealed against rain. The depth of the blocks varies depending on the bed design. The sides of the bed stair-step for pedestrian and emergency vehicle access. These side step blocks are not considered in performance calculations for the arresting bed. Prior to installing an EMAS, the site must be prepared with a paved surface that provides a solid foundation for the bed and adequate drainage.

Two generations of EMAS are currently installed at U.S. airports. The older JBR-501 design used painted cement board tops for the individual blocks and caulking to seal the joints in between. The newer JBR-502 design uses plastic tops, which do not require painting, and silicone tape to seal the joints.

As the only current FAA-approved arresting system, the current EMAS design will serve as a baseline for the arrestor alternatives examined in this research.

## 1.4. Research Approach

The research was divided into two phases. The first "Study" phase included research, identification of alternatives, and an initial down-selection of the most promising candidate arrestor concepts. The second "Experimentation" phase focused on evaluating the candidate concepts through testing and modeling.

Table 1-1 presents a basic guide to the report. Chapters 2 through 6 discuss the findings of the study phase, which focused on information gathering and evaluation. These sections examine the overall context for arrestors, including historical and current usage, an EMAS cost evaluation, the impact of FAA requirements, and processes for approving new arrestor systems.

Chapter 7 is a key transitional chapter, which identifies different potential systems and places them within the broader context of past and present arrestor approaches. This chapter includes conceptual discussion of the key mechanical distinctions between the different concepts from a performance standpoint. The candidates selected for detailed evaluation are identified and briefly described.

Chapters 8 through 14 discuss the experimentation phase of the research, beginning with an overview of the evaluation process. Each candidate is subsequently examined on an individual basis in Chapters 9 through 14. These chapters contain substantial technical content, but also examine the estimated system costs and the requirements to transition into fielded systems.

Finally, Chapter 15 provides overall conclusions for the effort, including a general research summary and a comparison of the different candidate systems.

*Figure 1-1. EMAS arrestor, Minneapolis–St. Paul (MSP) Airport.*

**Table 1-1. Guide to report.**

| | Chapter | Content |
|---|---|---|
| **Introduction** | Chapter 1. Introduction | Project background and research introduction |
| **Study Phase** | Chapter 2. Literature Review | Discuss research findings on indicated topics |
| | Chapter 3. Survey of U.S. Airport Operators | |
| | Chapter 4. Review and Documentation of FAA Parameters | |
| | Chapter 5. Sensitivity Analysis | |
| | Chapter 6. Approval and Commercialization Study | |
| **Transition Chapter** | Chapter 7. Identification and Initial Assessment of Alternatives | Important background preceding candidate assessment |
| **Experimentation Phase** | Chapter 8. Experimentation Overview | Overview of evaluation approach to candidate systems |
| | Chapter 9. Glass Foam Arrestor Concept | Detailed evaluation of candidate systems |
| | Chapter 10. Engineered Aggregate Arrestor Concept | |
| | Chapter 11. Aggregate Foam Arrestor Concept | |
| | Chapter 12. Depth-Varying Foam Material | |
| | Chapter 13. Summary of Passive System Candidates | |
| | Chapter 14. Main-Gear Engagement Active System Concept | |
| **Conclusion** | Chapter 15. Conclusions | Overall conclusions for research |
| **Appendices** | Appendix A. Bibliography | Additional research details |
| | Appendix B. Survey Details | |
| | Appendix C. EMAS Calculations | |
| | Appendix D. Active Arrestor Calculations | |
| | Appendix E. Human Injury Study | |
| | Appendix F. Tire Models | |
| | Appendix G. Arrestor Prediction Code | |

CHAPTER 2

# Literature Review

## 2.1. General

The literature review began with research into past arrestor system development and current arrestor requirements by the FAA. This research identified a number of technical areas of interest, which then turned into second- and third-stage literature research. Altogether, over 130 references were collected and reviewed on a spectrum of topics pertinent to arrestor systems. A summary of important information gleaned from this research is given in this section; the annotated bibliography (Appendix A) contains a more complete listing of documents. Table 2-1 summarizes the scope of the literature review.

## 2.2. Historical Aircraft Arrestor Research and Development

Substantial historical work has been done in the area of arrestor system development. FAA and industry documentation was reviewed, sometimes requiring retrieval in hard-copy form due to the age of the material.

Civil arrestor research in the 1980s examined the usage of materials such as clay, sand, gravel, water, and foam to develop a "soft ground" arrestor, as discussed by Cook (*2*). These materials are passive in nature, with no moving parts. The arrestment of the aircraft is accomplished by these materials as they impart a drag load on the landing gear, absorbing kinetic energy and bringing the aircraft to a stop. Cook discusses how materials such as clay, sand, and water were not appropriate for various reasons. For sand and clay materials, the mechanical behavior could not be consistently predicted due to sensitivity to moisture content. Water could be shown to perform well mechanically, but only at speeds less than 50 knots, with the additional disadvantages of attracting waterfowl and freezing in cold climates. Subsequent research was undertaken to examine different variants of foam arrestor (*3*), from which it was determined that a cementitious foam provided advantages over polymer foams. Gravel spray caused by the aircraft tire was identified as a potential engine ingestion hazard. Additional, limited documentation was reviewed for gravel arresting system research undertaken in the United Kingdom (UK) (*4*).

The emphasis on development shifted, taking a direction that focused on crushable materials such as phenolic foam and cellular cement (sometimes referred to as aerated/foamed cement/concrete). White and Agrawal (*5*) outline that the advantage of the crushable foam materials is predictability of the drag load imparted on the landing gear and constant mechanical properties over a broad temperature range. Cellular cement eventually became the material of choice due to its near-zero rebound after crushing and chemically inert composition.

Computer modeling and simulation have played a substantial role throughout the development of these passive arresting technologies. Initially, predictive codes had been developed for the modeling of taxi, takeoff, and landing on soil landing strips (*6*). These methods were adapted to the soft-ground arresting concept to evaluate different materials. Landing gear loads for the main and nose gear struts have been a historical area of scrutiny (*2*). Loadings to the nose gear in particular were noted, since materials like gravel could jeopardize the integrity of the gear and cause potential collapse.

One military code, FITER1, was adapted for civil arresting applications and called "ARRESTOR," documented by Cook et al. (*7*). It featured three aircraft (B707, B727, and B747) and could be used to model different foam arresting bed geometries. Heymsfield et al. (*8*) have recently used the ARRESTOR code to perform sensitivity analyses on various parameters. This program has presently been superseded in capability by a proprietary predictive code used by the EMAS manufacturer, ESCO.

Active arresting systems that use military-type friction brakes (BAK-12, etc.) have been adapted to civilian aircraft in the past. Documentation in our research has been sparse on this subject, however, and the majority of knowledge gained on the subject has been through discussions with ESCO and by reviewing

**Table 2-1. Literature review summary.**

| Document Type | Topical Areas |
|---|---|
| Government research | Arrestor systems |
| Government regulations | Aircraft and landing gear dynamics |
| Journal papers | Airport operations |
| Patents | Modeling and simulation |
| Manufacturer specifications and research | Material science |
| Reference books | |
| Magazine/newspaper/Internet articles | |

a number of their product brochures. Active arresting systems have seen the most widespread use for military aircraft with tail hooks. To arrest civilian aircraft, netting systems are used to either wrap over the aircraft wings or engage the main landing gear struts. The former approach presents hazards for occupant emergency egress from the aircraft, as the netting can block exit hatches. The latter approach has technical difficulties due to widely varying landing gear geometries.

## 2.3. Recent Arrestor Research

Due to some of the present concerns regarding the life-cycle performance of the arrestors, Minneapolis–St. Paul Airport (MSP) has conducted several limited research and testing efforts. Stouffer (*9*) performed in-situ environmental tests on the arrestor bed and found a high relative humidity inside the bed, indicating the trapping of moisture inside the blocks. Stehly (*10*) conducted testing on some older blocks of the MSP 12R/30L arrestor, including fire-truck overruns and rough in-situ compression tests. Both tests indicated that performance degradation had occurred since the 1999 installation.

Design reports for arrestor beds were reviewed (*11*), as well as relevant excerpts from airport certification manuals (*12*). The design reports indicate that, in actual practice, the exit-speed performance of a given arrestor bed can vary widely across the aircraft fleet; some aircraft will be arrested at higher speeds than others.

Some literature was found pertaining to gravel truck arresting systems, typically used for arresting runaway trucks on downhill roadways. Rogers (*13*) discusses cold-weather testing information that demonstrates the potential for aggregate arresting beds to freeze over and become ineffective in harsh winter environments.

## 2.4. Landing Gear and Aircraft Dynamics

Landing gear was studied by the project team following the review of soft-ground arrestors. A key performance metric for soft-ground arresting systems is the consistency and predictability of the loads imparted to the landing gear: loadings that are too high can damage or fail the gear, and loadings that are too low will not efficiently arrest the aircraft. Accurate prediction of these loads cannot be obtained without also capturing the dynamic response of the aircraft and landing gear. Much like driving a car over speed bumps, the suspension response can dictate the overall degree of bounce and subsequent pitching, or "porpoising," that occurs. Inconsistent materials can lead to more porpoising, and hence higher loads on the landing gear.

While many documents have been reviewed, a few will be singled out here. Currey (*14*) provides a general text describing the fundamentals of design and analysis of landing gear, allowing for the general sizing of struts, tires, etc. Pritchard's (*15*) overview of landing gear dynamics provides a substantial array of simulation options, which will be employed in the second phase of the effort. Chester (*16*) outlines a modeling approach for a generalized aircraft of varying size, with a focus on landing gear dynamics and overall airframe response. Altogether, we find that relevant variables to the current problem include strut stiffness and stroke length, tire pressure and dimensions, aircraft mass and moments of inertia, etc. Since these properties for an actual aircraft are proprietary manufacturer information, the information from these references will prove beneficial for approximation.

Experimental studies undertaken by the FAA have been reviewed. Micklos and DeFiore (*17*) discuss video analysis techniques for determining aircraft parameters based on observations of aircraft landings. Tipps et al. (*18*) describe landing gear load factor statistical studies based on in-service aircraft measurements. These and similar reports focus on determining the level of loading that in-service aircraft *actually experience,* often with a focus toward determining the appropriateness of the current Federal Aviation Regulations (FAR) requirements. As such, they have less relevance to the current effort, where load *limits* for aircraft are the focus.

## 2.5. Airport Operations

In order to understand the implications of arrestor design on airport operations, several sections of CFR Part 14 were reviewed (*19, 20*).

FAA Order 5200.8 outlines the Runway Safety Area Program (*21*). The intent of the program is to ensure that all Part 139 airports in the United States are brought into compliance with RSA requirements. Historical data shows that most overruns take place at speeds of 70 knots or less, and that aircraft typically come to rest within 1,000 ft of the end of the runway (Section 4.4.1). Consequently, a standard RSA has a typical length of 1,000 ft. For airports not in compliance, five remedial measures are described: relocating runways, reducing runway length, a combination approach, the use of declared

distances, or the installation of an EMAS. From an operations standpoint, any arrestor developed must accomplish the goal specified by the EMAS advisory circular: to arrest aircraft with an exit speed of 70 knots, thereby providing protection that is equivalent to a standard RSA (*1*).

The current status of the Part 139 airports is summarized in an FAA database (*22*), which was consulted for determining the survey participant pool.

## 2.6. Accidents and Incidents

Two major studies have documented historical overrun accidents and incidents. In 1990, David (*23*) conducted an extensive review of overruns and summarized historical event data, including the distance travelled and the final location of the aircraft with respect to the runway end and centerline. DOT/FAA/CT 93-80 (*5,* p. 1) gives a histogram summarizing the exit speed distribution. This plot produced the historical basis for associating an exit speed of 70 knots or less with capturing roughly 90% of overruns. The arrestors have historically used 70 knots as a design objective for this reason.

In 2007, Hall et al. (*24*) revisited the topic with a study for TRB/ACRP. This research involved newer data compiled from several database sources pertaining to landing overruns, landing undershoots, and takeoff overruns. The database compiled in that study was obtained and reviewed, and served as a subsequent basis for the risk assessment of this effort. The 90% exit speed appears to have shifted since the previous research, and per the current data, it appears that the threshold could now be higher than 70 knots (Chapter 5).

AC 150/5200-37 presents guidance on safety management systems (SMS) and includes relevant risk assessment approaches (*25*). It has become apparent through the literature review that the reliability and risk for passive arrestors is less understood than for military-type systems. The military systems have been well characterized and are required to pass a 97.5% reliability criterion; no parallel currently exists for civil systems. The SMS guidance presents a paradigm to be adopted with civil arresting systems.

National Transportation Safety Board (NTSB) incident reports for several overruns were reviewed, including some involving arrestor beds (*26–28*). These documents provide some information in terms of exit speed and distance travelled through the arrestor beds. However, detailed information regarding the loading and deceleration effected by the arrestors is not provided.

## 2.7. Financial

FAA Order 5200.9 provided guidelines for estimating the costs to establish an EMAS at an airport (*29*). It provided a process for estimating the life-cycle costs of a system and established guidelines for comparing that cost to maximum feasible thresholds. The data contained therein served as a baseline for comparison with the airport operator survey (Chapter 3).

## 2.8. Patents

Various patents, dated from 1962 to the present, were identified pertaining to aircraft arrestor concepts. These patents are given in the annotated bibliography (Appendix A).

CHAPTER 3

# Survey of U.S. Airport Operators

To obtain information and opinions regarding the existing EMAS from end-users, a survey was taken of 14 U.S. airports, and site visits were made to three. This section summarizes the findings of the survey data and personnel interviews. As such, the information is a mixture of objective data and subjective opinions. The opinions and ideas expressed are those of the participating individuals and do not reflect the positions or recommendations of the ACRP.

## 3.1. Site Visits

In July 2007, site visits were made to three airports with EMAS arrestors: John F. Kennedy International (JFK), LaGuardia Airport (LGA), and Minneapolis–St. Paul International (MSP). At each of these airports, discussions were held with operations, maintenance, and management personnel regarding their experiences with EMAS.

### 3.1.1. JFK Airport Site Visit

JFK has two arrestors installed at the facility, as detailed in Table 3-1. Runway designations indicate the departure end of the runway where the EMAS is installed.

Several overrun incidents have occurred at JFK since the installation of the arrestor beds. Airport management personnel believe that two or three of these overruns could have resulted in aircraft damage or occupant injury if the arrestor systems had not been present.

JFK has a maintenance agreement with the manufacturer, which performs quarterly inspections; on-site maintenance personnel perform daily visual checks of the arrestors. The beds experience some washout of material. Personnel have related that there does not seem to be a good method at present for determining moisture content inside the arrestor beds. Painting and re-caulking have been historical maintenance issues with the bed and are included in the manufacturer maintenance agreement.

Site preparation was a significant cost for the airport at the time of installation. Since installation, landing light arrays that come up through the bed are difficult to access due to the obstruction created by the arrestor blocks.

Factors that JFK personnel identified for future improvement to the arrestor included better quantification of life-cycle characteristics, such as (1) the effects of rainfall on the arrestor bed, (2) the effects of freeze–thaw cycles on degradation of the arrestor material, and (3) the effects of good or poor maintenance on long-term performance.

### 3.1.2. LGA Airport Site Visit

LGA airport has two EMAS arrestors installed at the facility, as shown in Table 3-2.

LGA has a maintenance agreement with the manufacturer, which performs quarterly inspections; on-site maintenance personnel perform daily visual checks of the arrestors. Painting and joint re-caulking have been historical maintenance issues with the bed, and are included in the manufacturer maintenance agreement. The painting and caulking repairs typically must be done at night due to the associated runway closure, but night temperatures and the required cure times can make this difficult. Drainage seems to be an issue; water can be seen to seep out of the arrestor for a day after a substantial rain. Figure 3-1 and Figure 3-2 show some maintenance issues; repair of such issues is fairly routine.

Factors that LGA personnel identified for future improvement to the arrestor included similar life-cycle considerations as for the JFK facility. Additionally, they expressed a desire to see future arrestor construction handled more like other paving projects, with standardized ASTM material tests/specifications and multiple vendors that could bid on the work. They hope to see strides made toward including embedded sensors in future arrestors, allowing for ongoing monitoring of the internal environment of the arrestor blocks. They would like metrics for characterizing the aging of an arrestor, allowing

**Table 3-1. EMAS specifications for JFK airport.**

| Parameter | EMAS 1 | EMAS 2 |
|---|---|---|
| **Runway** | 4R | 22L |
| **Length** | 392 ft | 405 ft |
| **Width** | 200 ft | 227 ft |
| **Setback** | 35 ft | 35 ft |

**Table 3-2. EMAS specifications for LGA airport.**

| Parameter | EMAS 1 | EMAS 2 |
|---|---|---|
| **Runway** | 22 | 13 |
| **Length** | 275 ft | 327 ft |
| **Width** | 170 ft | 170 ft |
| **Setback** | 35 ft | 35 ft |

comparison of current expected performance as a percentage of the original level.

### 3.1.3. MSP Airport Site Visit

MSP airport has one EMAS arrestor installed at the facility, as shown in Table 3-3. It should be noted that this bed was installed in 1999, and it featured an older version of the current EMAS technology. It was later refurbished, but not replaced, to provide for improved drainage; maintenance issues for this bed should not be considered typical since the construction was atypical.

The MSP arrestor has exhibited unusual degradation problems, with severe "soft tops" occurring on multiple blocks in the bed. The tops appear cup-shaped, and walking on the surface of the bed produces an atypical crunching sound (Figure 3-3). This deformation can be visually observed to increase after a rain or when the temperature rises. The material inside apparently deteriorated, leading to washout of a substantial volume (Figure 3-4). Explanations for the basis of the deterioration vary, and include things such as inadequate maintenance, poor drainage, or insufficient techniques for the refurbishment process. Airport personnel speculated that moisture entrapment in the arrestor combined with the severe freeze–thaw cycles of the Minneapolis climate led to the degradation.

In response to the deterioration issues, MSP engaged in small-scale research efforts. The humidity inside the bed was measured and found to be approximately 100% (*9*). Rough in-situ compression tests were performed on blocks of the bed prior to removal and replacement (*10*). Though the tests only produced approximate measurements, they indicated that there was a substantial loss of compressive strength in the material. A notable change in compressive strength would have performance implications when compared with the original design specifications of the bed.

MSP used the manufacturer for arrestor maintenance on an as-needed basis until 2006, when MSP assumed such tasks. The manufacturer continues to perform annual inspections and undertakes repairs.

MSP considered positive aspects of the arrestor design to include its passive nature, minimal mechanical complexity, and minimal impact on airport operations.

During discussions with MSP personnel regarding future development, some interesting observations were made. MSP has seen a decrease in mid-size aircraft traffic at the airport, with the majority of air traffic falling into smaller (under 99K lb) or larger (over 300K lb) size brackets; this could influence the design process as it affects the set of design aircraft for a facility. Secondary arrestors, such as fail-safe net arrestors positioned at the end of the arrestor bed, were considered a favorable concept. Similar to JFK and LGA, there was a strong desire for

***Figure 3-1. LGA arrestor (left) out-washing of material and (right) peeling of joint tape.***

*Figure 3-2. LGA arrestor: peeling paint.*

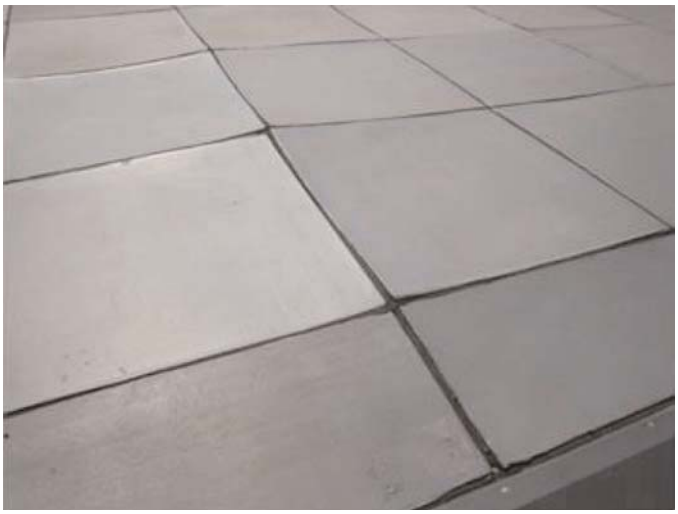

*Figure 3-3. MSP Airport: soft tops on EMAS blocks.*

instrumentation, embedded or otherwise, that could characterize the arrestor bed's internal condition and expected performance capabilities.

## 3.2. Participating Survey Airports

Surveys were sent to 16 airports, and 14 of those airports returned completed surveys. The airport names, location IDs, aircraft rescue and fire fighting (ARFF) indexes, approximate number of annual operations, and number of EMAS arrestors are shown in Table 3-4.

## 3.3. Standard EMAS

FAA AC 150/5220-22a defines an EMAS as standard if it has the capacity to arrest an aircraft at 70 knots (*1*). A non-standard EMAS is compliant if it has the capacity to arrest an aircraft at the minimum exit speed of 40 knots. To assess airport conformity with these requirements, airports with an EMAS were asked whether each of their arrestors was standard. Airports that returned surveys had installed 11 arrestors altogether. Four of those 11 arrestors were listed as standard, and 7 of them were listed as non-standard (Figure 3-5).

Each EMAS receives an exit speed rating for all the aircraft that it must service. Typically, some aircraft can be arrested at higher exit speeds than others. Airports were asked to provide the design aircraft and corresponding exit speed ratings for each EMAS.

For the 11 arrestor systems of the survey, 37 aircraft/exit-speed combinations were reported. These combinations constituted the design cases for the arrestors. The distribution of design cases over intervals from 0 to 80 knots is shown in Figure 3-6. Of all the design cases, 14% of the aircraft had design exit speeds below 40 knots; 62% had design speeds between 40 and 70 knots; and 24% had design exit speeds greater than 70 knots. For the cases below 40 knots, it should be noted that the arrestor beds involved still met the 40-knot standard for a number of aircraft, but not all aircraft listed.

**Table 3-3. EMAS specifications for MSP airport.**

| Parameter | EMAS 1 |
|---|---|
| Runway | 12R |
| Length | 160 ft |
| Width | 216 ft |
| Setback | 630 ft |

## 3.4. FAA Requirements

As part of the survey, airport operators were questioned about FAA requirements pertaining to arrestors. When asked whether FAA requirements for arrestor bed performance are too rigid, 8% responded *yes,* 54% responded *no,* and 38% responded *no opinion.* Similarly, when asked whether FAA requirements for RSA dimensions are too rigid, 31% responded *yes,* 46% responded *no,* and 23% responded *no opinion.* These results are also shown in Figure 3-7.

Airport operators were also asked to provide verbal commentary on FAA requirements concerning arrestor bed performance and RSA dimensions. Those comments are summarized in the following list:

- The 70-knot requirement for the standard arrestor could be lower;
- FAA regulations could consider that, in some cases, an RSA with an arrestor is safer than an RSA that satisfies general dimensional requirements; and
- FAA regulations could consider permitting damage to nose gear in extreme overrun scenarios.

*Figure 3-4. MSP airport: material out-wash.*

## 3.5. Installation

### 3.5.1. Cost

Airport operators were asked to provide the preparatory paving cost and installation cost for each arrestor installed at their airport. A total of 8 airports provided preparatory paving and installation costs for a total of 11 arrestors. These arrestors were installed from 1999 to 2007. By way of comparison, the cost design values according to FAA Order 5200.9 were based on 5 separate EMAS installations.

The mean cost values reported by the airports are shown in Table 3-5. They were normalized by the associated pavement and bed areas. The survey costs were corrected for inflation and are expressed in 2007 dollars. For comparison, the suggested values of preparatory paving cost and installation cost from FAA Order 5200.9 are included in the table, in 2007 dollars (30).

**Table 3-4. Airports participating in the survey of U.S. airport operators (*29*).**

| Airport Name | Loc. ID | ARFF Index | Annual Operations | No. EMAS |
|---|---|---|---|---|
| Anchorage International | ANC | E | 289,472 | 0 |
| Baton Rouge Metropolitan | BTR | C | 94,852 | 1 |
| Boston Logan International | BOS | E | 409,066 | 2 |
| Denver International | DEN | E | 586,151 | 0 |
| Minneapolis–St. Paul International | MSP | E | 475,000 | 1 |
| Nashville International | BNA | C | 215,830 | 0 |
| New York Kennedy International | JFK | E | 411,145 | 2 |
| New York La Guardia Airport | LGA | D | 404,990 | 2 |
| Pittsburgh International | PIT | D | 237,696 | 0 |
| Roanoke Regional | ROA | B | 86,091 | 1 |
| San Diego International | SAN | D | 220,485 | 1 |
| Seattle Tacoma International | SEA | E | 340,058 | 0 |
| Teterboro | TEB | E | 250,000 | 1 |
| Ronald Reagan Washington National | DCA | C | 278,151 | 0 |

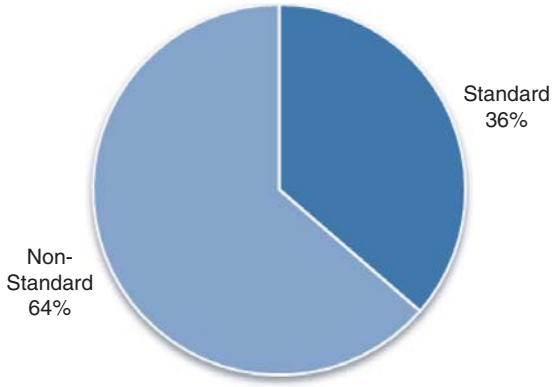


*Figure 3-5. Percentage of standard and non-standard EMAS.*

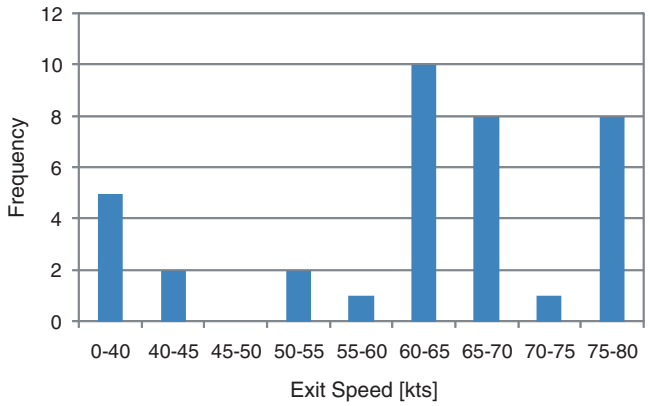


*Figure 3-6. Exit speed histogram for design aircraft cases of survey.*

As shown, the mean reported paving and installation costs were significantly higher than the design costs estimated in FAA Order 5200.9.

Figure 3-8 compares the total cost to establish an EMAS (CTEE) based on the survey data and cost estimates from Order 5200.9. The CTEE is the sum of the preparatory and installation costs. Individual data points indicate the costs for the arrestor beds from the surveyed airports. For the purposes of comparison, the survey and estimated Order 5200.9 costs were normalized to a runway width of 150 ft and converted to 2007 dollars.

Figure 3-9 compares the estimated life-cycle cost over a 20-year period, calculated per the methods outlined in Order 5200.9. The life-cycle costs are based on a combination of the CTEE, the annual maintenance costs, and a full bed replacement after 10 years. Using this method, the life cycle costs can be calculated using either the reported survey costs or estimates based on Order 5200.9.

In the plot, the longer-dashed line defines the maximum feasible cost in FAA Order 5200.9, which is considered the per-RSA upper cost threshold for EMAS. If life-cycle costs for the RSAs are calculated using the estimated EMAS costs from Order 5200.9, the data points fall below the maximum feasible cost line. However, when actual reported costs from the survey are used, the overall cost trend is substantially higher than the threshold.

A point of contrast with the CTEE data is that the life-cycle costs are calculated per RSA, rather than per EMAS bed. Typically, a runway has an EMAS located on only one end. However, for one of the surveyed airports, two EMAS beds were on the same runway. This case is shown in the right-most two data points of Figure 3-8, which are merged into one per-RSA data point on the right side of Figure 3-9.

### 3.5.2. Inconvenience

Airport operators were asked to rate the inconvenience of installing an EMAS from one (none) to five (severe). Eight operators responded, and the results are shown in Figure 3-10.

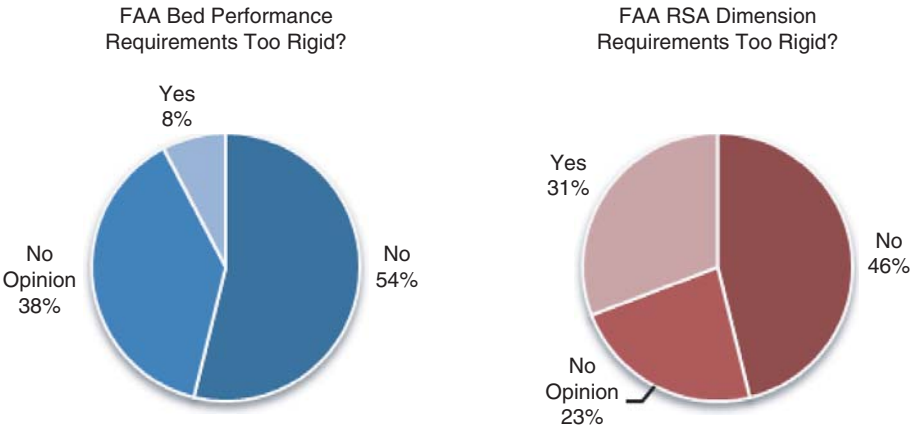


*Figure 3-7. Airport operator perception of FAA requirements.*

**Table 3-5. Normalized mean costs from survey compared with FAA Order 5200.9 (2007 dollars).**

| | FAA Order 5200.9 | Survey |
|---|---|---|
| Normalized Preparatory Paving Cost per Square Foot | $15 | $48 |
| Normalized Installation Cost per Square Foot | $85 | $134 |
| Cost to Establish EMAS (CTEE) per Square Foot | $100 | $182 |
| Cost for 150 x 300-ft Bed | $4.5M | $8.2M |

From the figure, installation of an EMAS was moderately inconvenient, with an average rating of 3.4.

Operators were also asked to provide verbal commentary on the cost and inconvenience of installing the arrestor beds. These comments are characterized as follows:

- Installing the arrestors is too expensive;
- The need to repave the surface supporting the arrestor is expensive and inconvenient; and
- Future arrestor installations will be subjected to wetland and environmental permit approval.

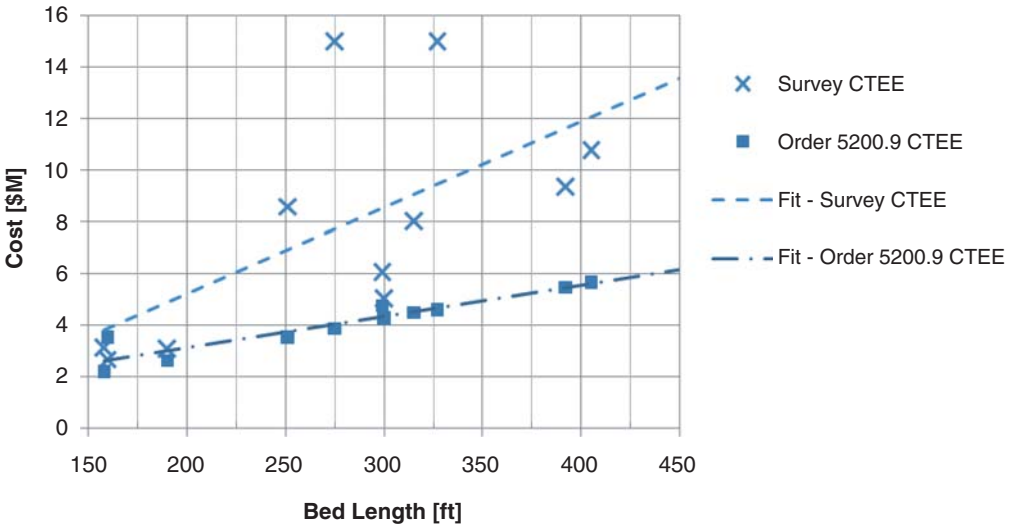


*Figure 3-8. Comparison of cost to establish EMAS (CTEE) per bed from Order 5200.9 and project survey (2007 dollars).*

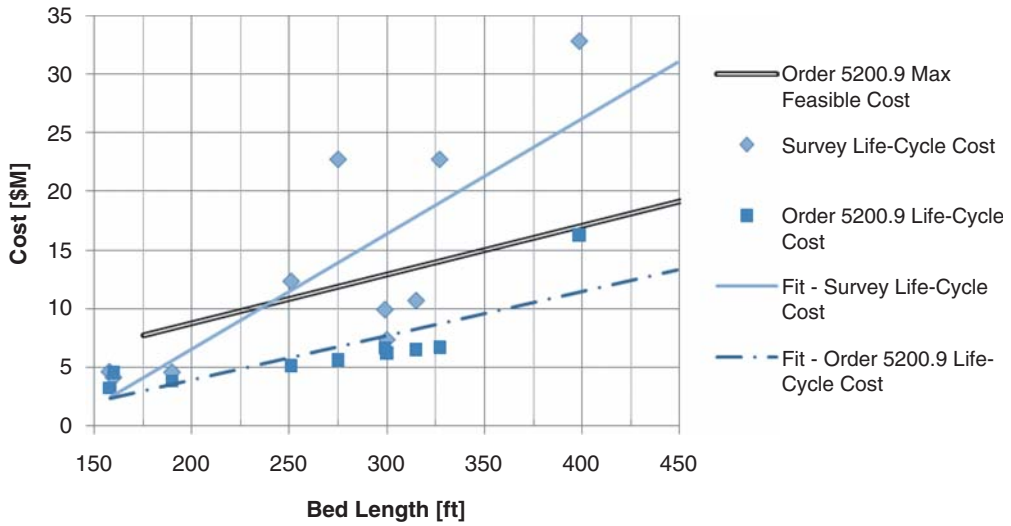


*Figure 3-9. Comparison of life-cycle costs for EMAS per RSA from Order 5200.9 and project survey (2007 dollars).*

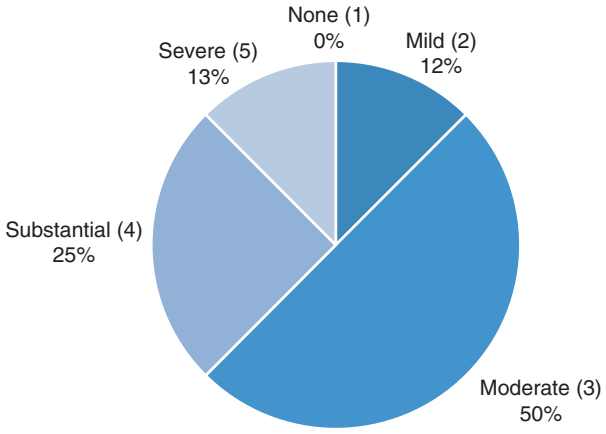


***Figure 3-10. Inconvenience of arrestor system installation.***

## 3.6. Maintenance

Airport operators were asked to provide the annual cost of maintaining their arrestors. Six airports provided annual maintenance costs for eight beds. Those maintenance costs were divided by the area of the associated arrestor bed to obtain a cost per square foot of arrestor bed. There was a significant amount of scatter in the maintenance costs reported by airports, and the average was significantly higher than the values suggested by FAA Order 5200.9. The results are shown in Table 3-6. Mean, high, and low costs are included in the table and compared to the value in Order 5200.9. For comparison, the survey values were divided by the Order 5200.9 value to provide a ratio to its value.

**Table 3-6. Maintenance costs from survey compared with Order 5200.9 values.**

| | Mean | Low | High | Order 5200.9 |
|---|---|---|---|---|
| **Maintenance Cost [$/ft$^2$]** | $3.05 | $0.11 | $6.89 | $0.36 |
| **Ratio of Order 5200.9** | 8.5 | 0.3 | 19.1 | 1.0 |

To assess the durability of the current EMAS technology, airports were asked to rate the severity of maintenance requirements for the arrestors on a scale of 1 (none) to 5 (severe). Airports were questioned about maintenance requirements in the following six categories: peeling paint, leaching of the material, caulking failure, joint tape debonding, soft tops on arrestor bed, and drainage problems. The severity of maintenance requirements by category, with respect to the year that the arrestor was installed, are shown in Figure 3-11 (left). Responses for arrestors that were installed in the same year were averaged. Average maintenance, which is the average of the maintenance numbers from each of these six categories, is included in Figure 3-11 (right).

From Figure 3-11, airport operators perceive the current EMAS to require a significant amount of maintenance. In fact, for all years prior to 2006 (except 2004), the average maintenance requirement was above three. That is, in most cases, airport operators perceive the arrestors to require maintenance closer to severe than to none.

Whether the airport had a maintenance contract with the manufacturer had little effect on the average maintenance required. That is, the weighted average maintenance

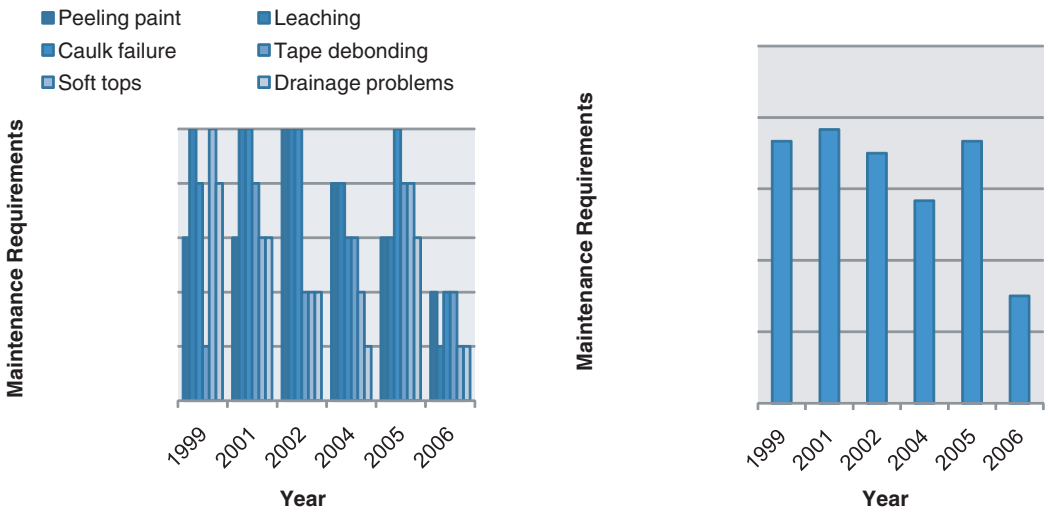


***Figure 3-11. Maintenance by category (left) and average maintenance (right).***

for arrestors with a manufacturer contract was 3.0, while the weighted average maintenance for arrestors without a manufacturer contract (maintenance was performed either by local contractors or airport personnel) was 2.7.

In addition to providing numerical responses, airport operators provided verbal commentary on the maintenance requirements. When asked to describe the negative traits of their EMAS systems, many cited maintenance problems. Their responses are summarized as follows:

- Arrestor beds require continual maintenance and inspection, which are both expensive and inconvenient;
- The durability of the arrestors is uncertain, and the effect of possible deterioration on performance is unknown;
- Airports with arrestors installed prior to 2003 mentioned that the top layer of the beds tended to deteriorate; and
- The arrestor beds are susceptible to being damaged by airport operations vehicles.

When airport operators were asked about what changes should be made to the arrestor design, the durability was again a significant concern. Comments pertaining to durability and maintenance are summarized below:

- A means should be developed for assessing the arresting capability of an installed arrestor;
- The inconvenience of maintaining the bed should be decreased;
- Adherence of paint should be improved; and
- The method of taping and caulking to seal tops of bed blocks could be improved.

It should be noted that the manufacturer has developed a second-generation top—colored plastic as opposed to the first-generation painted cement board—that it claims is more durable.

## 3.7. Observations for Survey Regarding EMAS

The survey respondents and site visit personnel had a variety of opinions, ideas, and desires regarding the current EMAS technology. Issues regarding maintenance varied due to differences in region, bed age, etc. With respect to the maintenance-related responses, it should be considered that EMAS designs have been improved over time, and now use different environmental protection measures than in the past. Not all user responses reflected experience with the most recent version of available EMAS designs.

Many respondents expressed a desire to incorporate integrated sensing technologies into the arrestor beds to monitor their physical condition over time. Representatives from the FAA indicated that such sensing methods may or may not be feasible for the future due to several technical complications. Laboratory tests have underscored the difficulties associated with this concept.

Costs for an EMAS appear to exceed the expectations of FAA Order 5200.9 with regard to the three main categories: preparation, installation, and maintenance. While the survey included more airports than the original data set used to create Order 5200.9, it did not include all EMAS systems installed at U.S. airports. It is possible that the average costs could shift once the remaining airports were included.

## 3.8. Perception of Active Arrestor

### 3.8.1. Survey of U.S. Airport Operators

Airport operators were asked how comfortable they would be with installing a net-based or cable-based active arrestor for civil aircraft. The possible responses were *not comfortable, low, moderate,* and *highly comfortable.* The results are shown in Figure 3-12. A full 86% of respondents were either not comfortable or had low comfort with use of an active arrestor for civil aircraft. None of the operators responded with "highly comfortable."

### 3.8.2. Other Aviation Organizations

As part of the survey effort, 23 individuals, many representing pilot organizations, were contacted to provide input on the appropriateness of active arrestors for civil aircraft. Appendix B provides a list of the organizations contacted. These individuals were selected to provide insight into the perspective of pilots and other aviation personnel.

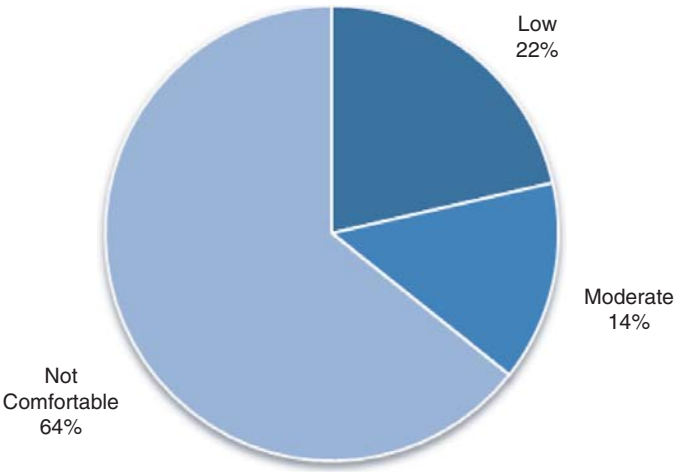


***Figure 3-12. Level of comfort with active arrestor.***

Of the 23 individuals contacted, only 3 completed the circulated questionnaire. Therefore, available comments from this group cannot be taken as representative of the broader aviation or pilot communities. However, their comments, which are summarized below, provide some insight into how deployment of an active arrestor for civil aircraft would be received.

- Active arrestors are inappropriate for civil aircraft:
  - Active arrestors involve too many potential complications.
  - Net-based or cable-based engagement would likely hinder passenger egress once the aircraft has stopped.
- Any activation of the arrestor should be under the control of the pilot, not the air traffic controller.
- The location of any arrestor at an airport should be noted on airport diagram charts using a standardized format.

## 3.9. Observations for Survey Regarding Active Arrestors

Overall, the concept of an active arrestor was not well received by the survey participants. Contributing issues that have been identified include the historical need for personnel to activate such an arrestor, determining whether ground personnel or pilots would have control over the activation, and a sense of unreliability due to the mechanical complexity of such systems.

Countering these concerns, several automated triggering concepts have been developed that could remove the need for manual activation, and pilot control or override can be incorporated in such systems (Section 7.7). Later sections discuss that the reliability of active systems can actually be higher than that of the current EMAS technology, even though passive systems have no moving parts (Section 5.2.2).

CHAPTER 4

# Review and Documentation of FAA Parameters

## 4.1. Relevant Literature

Of the documents reviewed, those most relevant to determining the basis of FAA parameters governing the arrest of civil aircraft are as follows:

AC 150/5220-9a. *Aircraft Arresting Systems on Civil Airports.* FAA, 2006.

AC 150/5220-22a. *Engineered Materials Arresting Systems (EMAS) for Aircraft Overruns.* FAA, 2005.

Order 5200.9. *Financial Feasibility and Equivalency of Runway Safety Area Improvements and Engineered Material Arresting Systems.* FAA, 2004.

Order 5200.8. *Runway Safety Area Program.* FAA, 1999.

*Runway Safety Area Status Database.* FAA, 2007.

## 4.2. Parameter Diagram

Figure 4-1 illustrates the FAA parameters governing civil aircraft arrestors. Parameters specifically cited in the EMAS advisory circular (or elsewhere) are shown with underscores.

At the most general level, the parameters were categorized as either inputs or outputs. Many of the inputs listed are essentially *requirements,* and these requirements can apply to the initial or final conditions of an arresting event. The manner in which the FAA drafts its requirements will govern the *outputs:* arrestor cost, size, performance, and so on. As such, one could summarize by saying that the inputs are *requirements* and the outputs are *consequences* of the requirements. Changes in the requirements will have an impact on system cost, the manner of the arrestor function, and so on.

## 4.3. Parameter Relationships

Figure 4-2 illustrates a detailed version of the prior parameter diagram, showing the relationships from a standpoint of designing and installing an arrestor.

The performance requirements, as set forward by the FAA, combined with the site constraints, would drive the selection of an appropriate arrestor type for the facility. For civil applications, there is currently only one EMAS option; however, this could broaden upon approval of other alternatives.

Given the performance requirements of the standards and the site constraints, the specific arrestor design for the facility would be determined. This final system design determines the cost for the system installation. The arrestor *type* determines the nature of the maintenance and repairs required, directly affecting those cost components. The arrestor type also has the most substantial impact on the installation time, service life, and downtime during repairs. The particular specifications of the *installed system* do not have a great effect on the time components.

From a regulatory standpoint, the performance requirements put forward by the FAA regarding exit speeds and the post-event aircraft condition (permissible level of damage) have the most tangible impact on system cost. While other factors may affect cost as well, the connectivity is more difficult to quantify. Chapter 5 demonstrates the cost impact of these parameters.

Figure 4-3 illustrates the parameter relationships for an overrun event. Within this context, design considerations are no longer relevant. The diagram assumes that all design decisions were previously made and that an arrestor system has been installed at the facility.

During an arresting event, the initial conditions (upper left) of the aircraft type, exit speed, etc., interact with the arrestor system to produce a performance output. The arrestor translates the overrun conditions into deceleration loads on the plane, an overall stopping distance, etc.

The arrestor type and specifications will impact the performance significantly. As the research later shows, different arrestor types have different inherent performance capabilities.

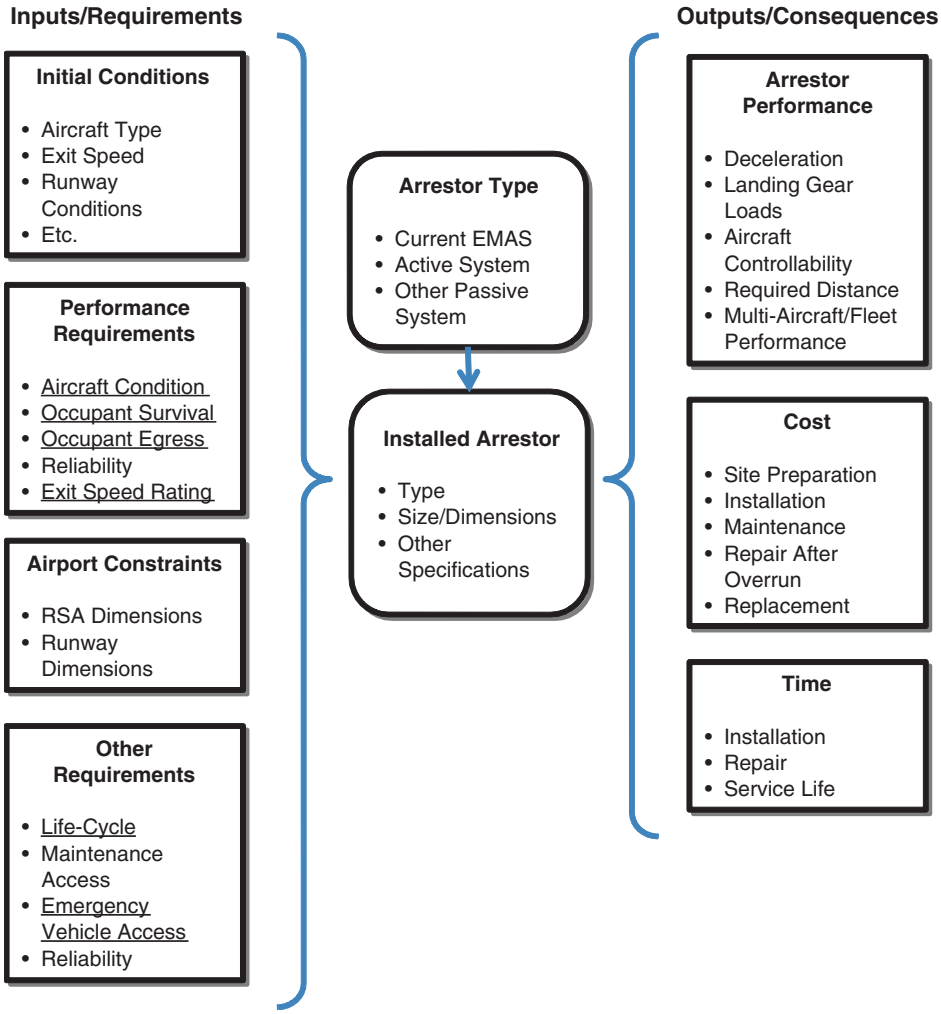


*Figure 4-1. Diagram of FAA parameters.*

## 4.4. Critical Parameters

### 4.4.1. Exit Speed

FAA AC 150/5220-22A requires that an EMAS have a standard design exit speed of 70 knots and a minimum of 40 knots (*1*). The 70-knot standard is intended to enable arrest of 90% of overruns. The 40-knot minimum is provided as an exception for airports with highly constrained RSAs. A review of the overrun data collected in subsequent ACRP research (*24*) indicated that the 70-knot requirement may no longer be sufficient to reach the intended 90% arrest rate (Chapter 5).

### 4.4.2. Damage to Aircraft

FAA AC 150/5220-22A requires that the arrestor not structurally damage the aircraft. However, this requirement could potentially be revised to permit a degree of flexibility in the interests of reducing overall risk.

More aggressive decelerations would be possible if the designs were permitted to overload/collapse the nose gear, as long as the main gear remained intact. While this certainly results in a monetary impact with regard to aircraft damage, prior EMAS testing suggests that it may pose minimal hazards to aircraft occupants in some cases. In the event of a nose gear collapse, some aircraft would be more adversely affected than others would. Aircraft with low-slung engines could potentially undergo engine damage and/or ingest arrestor material; the risks of these effects have not been quantified. Additional concerns would apply to turbo-prop aircraft, where propeller damage could present additional hazards.

As an example of potential implementation, if a plane continues to penetrate beyond 75% of an arrestor bed's length, it could enter an "all or nothing" zone, in which the resistance of the bed increases in a final attempt to arrest the aircraft. Nose gear collapse could be preferable to the consequences of failing to stop the aircraft, depending on what hazards lie beyond the arrestor bed.

A robust approach could consider an overall risk assessment, as the consequences of an un-averted overrun will not be equal for all facilities. It is suggested that the requirements

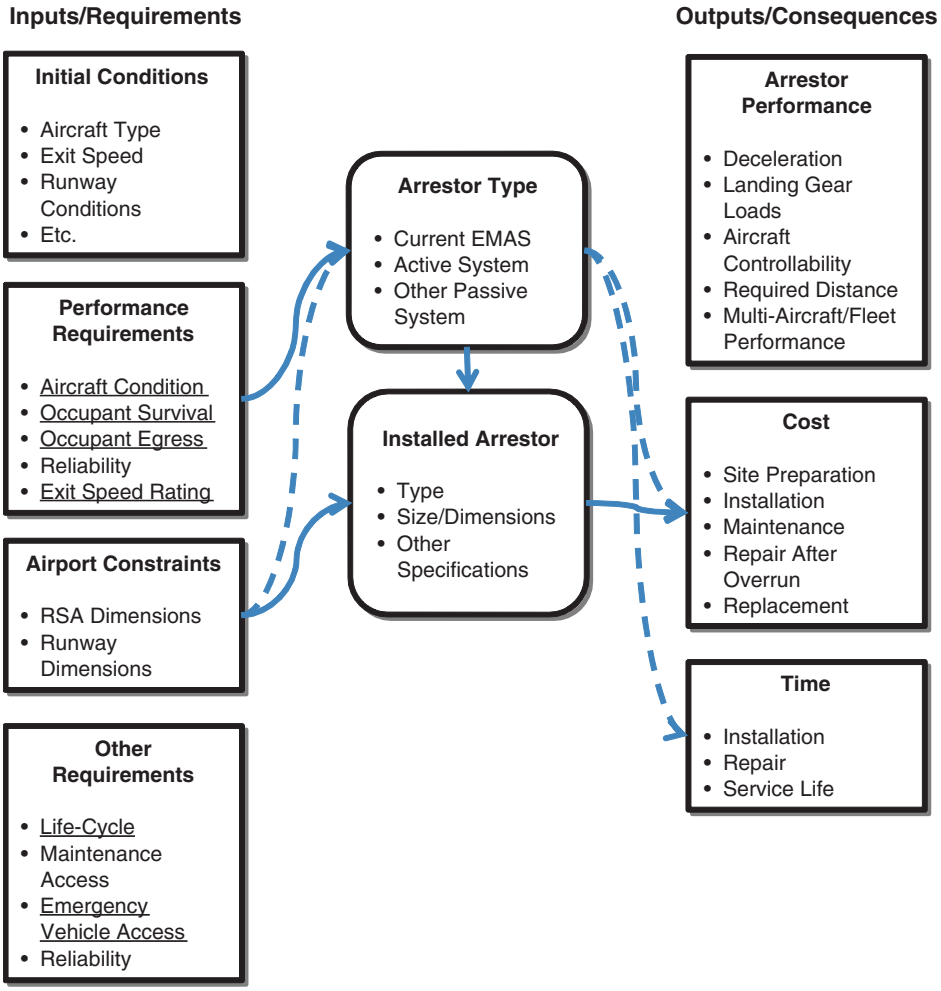


***Figure 4-2. Diagram of FAA parameters: detail for system design and installation.***

concerning landing gear loading be revisited in order to determine if case-by-case exceptions may be permissible.

### 4.4.3. Collateral Damage

To date, there has been minimal discussion in FAA literature about assessing collateral damage in the event of an aircraft overrun. As a resource for future consideration, aircraft damage and occupant injury have been included in the risk analysis software developed in recent ACRP research (*24*). For airports with highly constrained RSAs, it may be advisable to include a metric for collateral damage. FAA AC 150/5200-37 (*25*) provides a basic framework for risk-oriented planning.

### 4.4.4. Occupant Injury

A document found during the literature review indicated that arrestments should be limited to under 1 g, based on occupant injury criteria (*31*). Several individuals from the FAA stated that a 1 g limit might stem from FAR landing gear loading criteria, but that they were not aware of any such injury criterion. This topic was investigated further by enlisting a human injury expert. The subsequent research indicated that the deceleration injury threshold is substantially higher than 1 g. The conclusion, in the absence of other evidence, is that the 1 g deceleration limit mentioned in the reference previously cited was likely errant. Details regarding the human injury analysis are given in Appendix E.

### 4.4.5. Deceleration Thresholds

Table 4-1 summarizes deceleration thresholds for aircraft damage and occupant injury.

For the nose gear criterion, the 0.23 g deceleration assumes that no rearward loading is applied to any other part of the aircraft (main gear, thrust reversers, etc.). For the main-gear deceleration of 1.13 g, a similar assumption has been made. Both

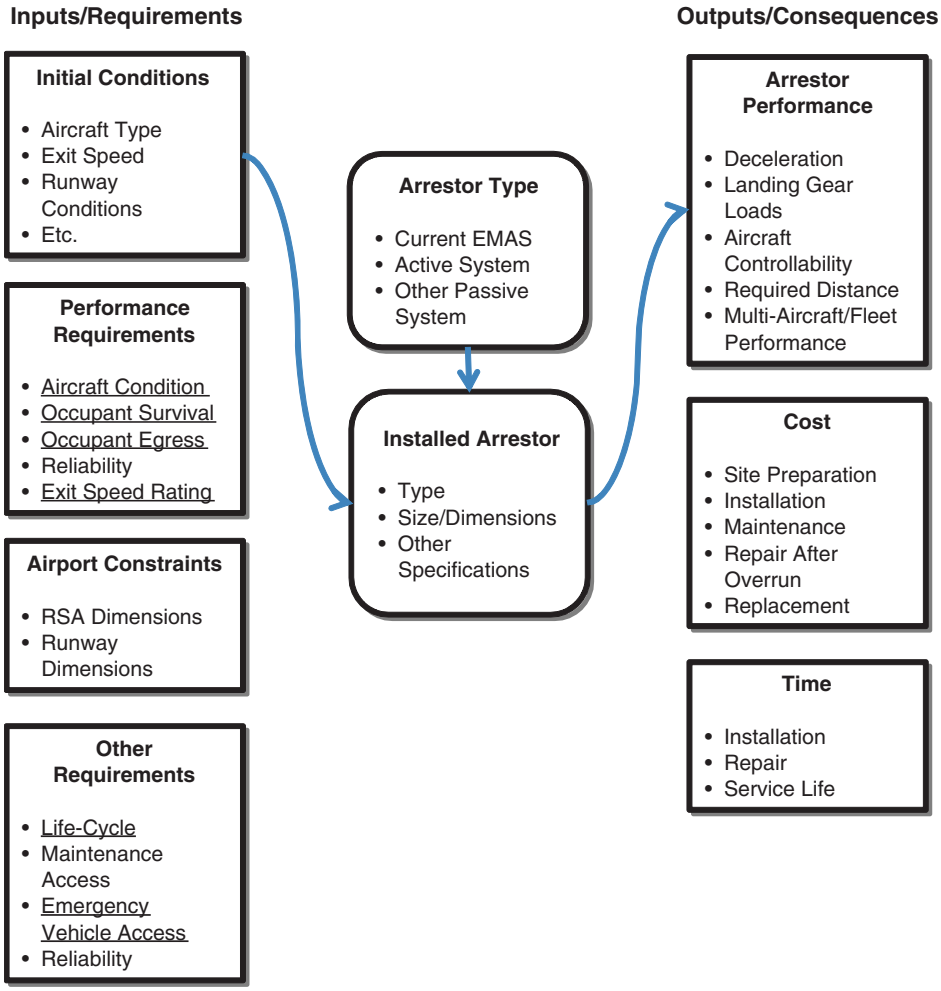


***Figure 4-3. Diagram of FAA parameters: detail for arresting event performance.***

**Table 4-1. Deceleration thresholds for aircraft damage and occupant injury.**

| Event/Criteria | | Deceleration |
|---|---|---|
| Nose Gear Rearward Failure | | 0.23 g |
| Main-Gear Rearward Failure | | 1.13 g |
| Combined Main- and Nose-Gear Rearward Failure | | 1.36 g |
| Traumatic Brain Injury (TBI) Threshold | Long duration (typical arrest) | 4.00 g |
| | Short duration (<1 sec) | 9.00 g |
| *Typical EMAS Deceleration (Section 5.2.1)* | | *~ 0.35 to 0.85 g* |

of these values represent cases that, in practice, are probably unattainable. Surface-based arrestors will apply a deceleration load to the main and nose gear struts simultaneously.

As such, the combined main and nose gear deceleration of 1.36 g is the most useful landing gear metric. It represents the theoretical limit for aircraft deceleration that could be obtained by perfectly distributed loading of the main and nose gear struts, such that all struts were at their maximal loading thresholds simultaneously. While not realistically attainable, the 1.36 g deceleration would represent the ideal case.

The long-duration traumatic brain injury (TBI) threshold is most appropriate for application to typical aircraft arrests, which would last for several seconds. For short-duration pulsed loads, the 9 g limit could be assumed instead. Details regarding the human injury analysis are given in Appendix E.

Given the deceleration thresholds indicated, the aircraft limit loads would constrain the arrestment rate, rather than occupant injury criteria. The landing gear loads have been the historical limitation for EMAS designs. The nose and main gear are not loaded in an ideal fashion, with the nose gear load generally limiting the obtainable decelerations to 0.35 to 0.85 g.

Perhaps the only realistic way in which to obtain higher decelerations for an aircraft is via an active arrestor system, using either cables or barrier nets to engage the aircraft. Such systems would open the possibility of exceeding the 1.36 g limitation, at which point the 4 g TBI criterion would become the performance constraint. Obviously, arrestment distances could be reduced significantly. Offsetting this advantage, airframe damage could result from such loads on the aircraft. Assessing the potential impact to the aircraft was beyond the research scope.

CHAPTER 5

# Sensitivity Analysis

ESCO generously supplied the research team with plots of velocity versus distance for several EMAS design cases. The cases were best-performance arrestor designs for three aircraft: the CRJ-200, B737-800, and B747-400. From these plots, a substantial amount of data was derived for the sensitivity analysis. Technical details for the following subsections are found in Appendix C.

## 5.1. Introduction

The sensitivity analysis investigated the dependence of cost and reliability on mechanical parameters. Life-cycle issues, such as the durability of the bed, were not considered as part of the sensitivity analysis. Only the parameters discussed in Chapter 4 that have bearing on the mechanics of arrestment are included in this sensitivity analysis (Table 5-1).

### 5.1.1. Reliability

The reliability of an EMAS refers to the percentage of overruns arrested for a given configuration. Reliability is inherently a probabilistic measure, and there are two empirical studies that have been conducted to establish relationships between cumulative percentage of overruns and exit speed. The first of these was discussed in DOT/FAA/CT-93/80 (*5*). A more recent study was conducted by the ACRP (*24*). Both studies were considered as part of this analysis.

Data was extracted from Figure 1 in DOT/FAA/CT-93/80 and from an overrun database compiled by the ACRP. The two sets of data were used to create cumulative distribution plots of overruns as a function of exit speed. As Figure 5-1 shows, the trends of the older and newer data differ.

### 5.1.2. Cost

The cost parameter in Table 5-1 refers to the total initial cost for an EMAS, including the preparatory paving cost and installation cost, but not recurring maintenance costs. There are two possible premises for the cost estimates: FAA Order 5200.9 and the cost data from the Survey of U.S. Airport Operators (Chapter 3) (30). Results presented in this section used normalized cost values, and therefore did not depend on which cost estimates were used.

## 5.2. Results and Discussion

### 5.2.1. Design Cases

For the purposes of the sensitivity analysis, standard design conditions were assumed: a 75-ft setback, no reverse thrust, and a 0.25 braking friction coefficient. The decelerations of the three design aircraft—CRJ-200, B737-800, and B747-400—were significantly different. Figure 5-2 shows the mean decelerations and error bars representing one standard deviation, the data of which was extracted manually from ESCO-provided deceleration plots.

As a brief aside, we note here that the B747 has less than one-half of the deceleration of a CRJ-200, which underscores an inherent limitation of crushable material arrestors. Even in the best-case designs (shown here), they simply are not as effective on some plane types as others. Section 7.5 gives further explanation regarding the mechanical basis for the gross difference in deceleration.

For the sensitivity analysis, exit speed was varied in the vicinity of the 40-knot minimum and 70-knot standard exit speeds. This showed the impact on cost and reliability if the requirements of the EMAS advisory circular were shifted by 5 to 10 knots. All three design aircraft were used for the study, and the results associated with each aircraft type were normalized and averaged.

### 5.2.2. Reliability

To assess the sensitivity of arrestor bed reliability to changes in the critical values of exit speed, cumulative percentage of

**Table 5-1. Sensitivity analysis parameters.**

| Input Parameters to Vary | Output Parameters from Models |
|---|---|
| Exit speed – arbitrary | Stopping distance |
| Geometry variations<br>• Width<br>• Setback | Reliability<br>• DOT/FAA/CT-93/80 exit speed probability curve<br>• Revised exit speed probability curve |
| Aircraft type<br>• CRJ200 ER<br>• B737-800<br>• B747-400 | Cost<br>• FAA Order 5200.9<br>• Survey data |
| Aircraft braking condition<br>• Braking<br>• Skidding<br>• Free-rolling | |

overrun occurrences were calculated for exit speeds 5 and 10 knots greater than the current minimum and standard exit speeds of 40 and 70 knots. The basis of the calculations was the revised overrun probability curve. The results are shown in Figure 5-3 and Figure 5-4.

From Figure 5-3, an EMAS with a 40-knot design exit speed would likely arrest fewer than 50% of aircraft overruns. If the design exit speed is increased to 50 knots, the EMAS would likely arrest 60% of aircraft. As shown in Figure 5-4, an EMAS with a 70-knot design exit speed would arrest 80% of all aircraft. Increasing that design speed to 80 knots would likely result in 88% of overrunning aircraft being arrested.

By way of comparison, active arrestors used for military aircraft achieve a minimum of 97.5% reliability. These active systems are described in detail in Section 7.7. It is noteworthy that, despite that fact that active arrestors are mechanical systems with a number of moving components, they are able to achieve significantly higher reliability than an EMAS designed for the standard 70-knot design exit speed. The passive nature of the EMAS concept does not assure inherently superior reliability over an active arrestor. This comparison comes with a caveat that the reliability numbers for the active systems presume solid engagement with the aircraft; with civil aircraft, engagement proves to be the most challenging aspect of using active arrestors (Chapter 14).

Furthermore, the function of active arrestor systems can be tested periodically as the system ages to confirm correct operation. As was mentioned in Section 3.6, the reliability of the current EMAS design after installation is uncertain because

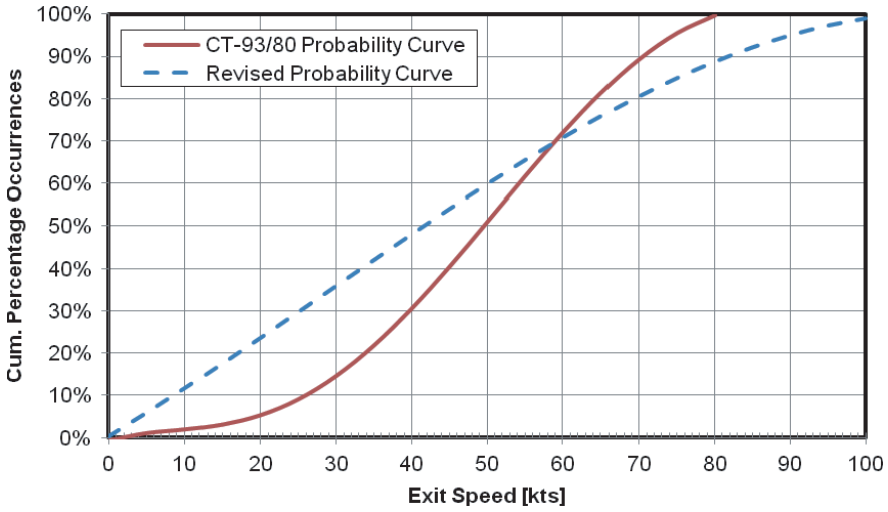


***Figure 5-1. Exit speed probability curves.***

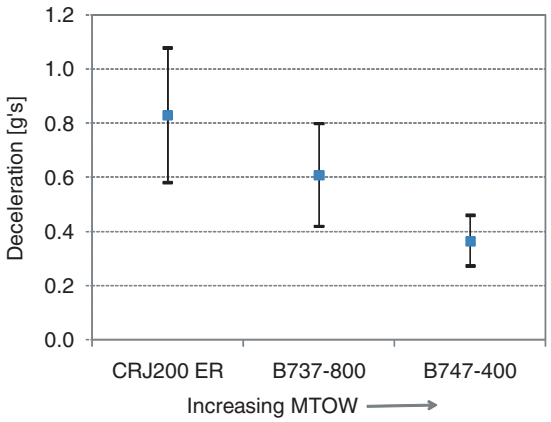


*Figure 5-2. Mean EMAS deceleration of design aircraft.*

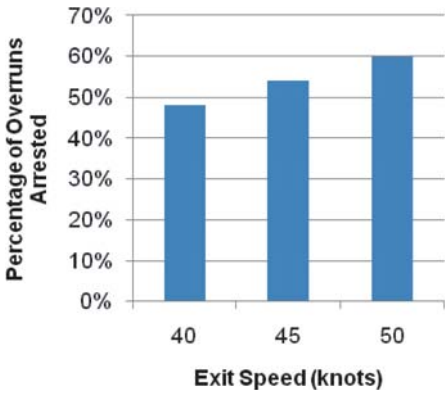


*Figure 5-3. Reliability impact of increasing the minimum exit speed requirement.*

the internal condition cannot presently be tested. In light of the survey data, it must be acknowledged that it is possible that degradation of the cellular cement could decrease the performance—and hence, reliability—of EMAS without being detected.

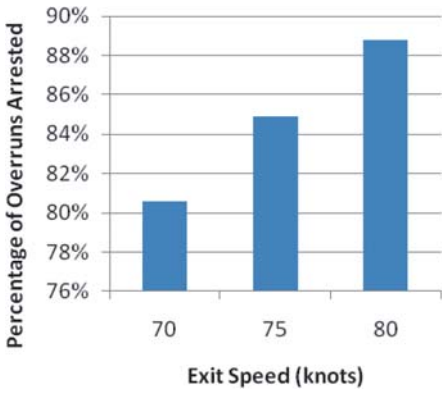


*Figure 5-4. Reliability impact of increasing the standard exit speed.*

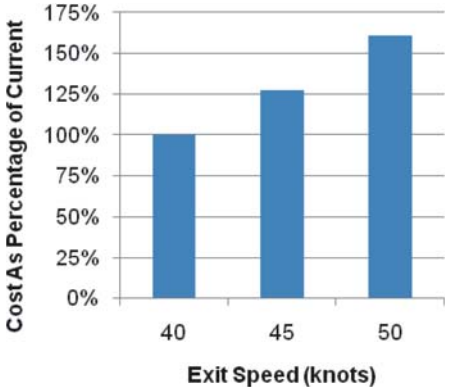


*Figure 5-5. Cost impact of increasing the minimum exit speed requirement.*

### 5.2.3. Cost

As shown in Figure 5-5 and Figure 5-6, cost sensitivity was assessed in the vicinity of the 40-knot minimum and 70-knot standard exit speeds. Sensitivity is expressed in terms of arrestor bed costs for the current design exit speeds. The estimated cost of an EMAS with a 50-knot design exit speed is 60% greater than the cost of an EMAS with a 40-knot design exit speed. In addition, the estimated cost of an EMAS with an 80-knot design exit speed is about 30% greater than the cost of an EMAS with a 70-knot design speed. It should be noted that these cost impacts would apply to any type of EMAS and would not be confined to the current EMAS design.

Thus, if the 70-knot exit speed in the EMAS advisory circular were increased to 80 knots, in order to return to the targeted reliability of 90%, future construction costs could be expected to increase by 30%, on average.

As shown in Figure 5-7, cost is essentially proportional to bed length. From a physics standpoint, the distance that a tire rolls through an EMAS is proportional to absorbed energy,

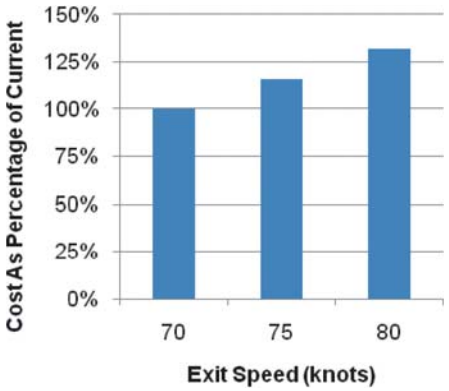


*Figure 5-6. Cost impact of increasing the standard exit speed.*

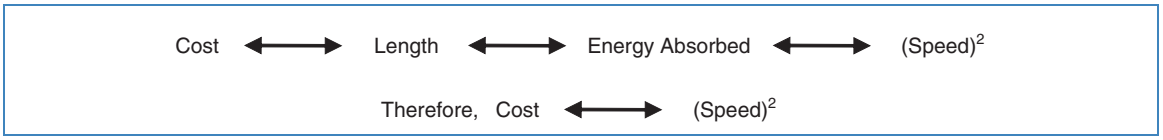


***Figure 5-7. Proportionality of cost and exit speed, per-plane basis.***

which is in turn proportional to the square of the exit speed. Thus, it was expected that the cost would be essentially proportional to the square of the exit speed. For example, the ratio of the square of $50^2$ to $40^2$ is 1.56, or 156%, which is consistent with the cost ratio in Figure 5-5.

The actual ratios in Figure 5-5 and Figure 5-6 were based on the cost data from the Survey of U.S. Airport Operators and the cost estimates in FAA Order 5200.9 (*30*). Therefore, the cost increase proportionalities shown are supported by cost data and the physics of aircraft arrest.

CHAPTER 6

# Approval and Commercialization Study

## 6.1. Approval Process for New Arrestor Development

The researchers engaged in discussions with both the FAA and manufacturers regarding the approval of new arrestor systems. Currently, only one EMAS system has obtained FAA approval, and new entrants to the arrestor market often cannot determine what steps to take toward gaining approval for their new designs. All parties concurred that a process is needed whereby new arrestor systems can be developed and gain FAA approval.

As a starting point, the FAA has stated that the essential performance requirements contained in AC 150/5220-22a will be required for other arresting system alternatives. The FAA has determined that the Airport Engineering/Airport Safety and Standards division, AAS-100, will act as the primary point of contact for companies submitting concepts.

Discussions with the FAA generated a number of ideas regarding the approval process. This report outlines a potential approval process, intended as a starting point for ongoing dialogue and modification.

Based on the historical development of the EMAS concept and the technical issues involved in arrestor systems, a two-branch approval process is proposed (Figure 6-1). A normal approval process would be required for arrestors substantially different from the current EMAS design. For systems that do not differ substantially, however, a shorter "equivalence" process is recommended. When a manufacturer submits a concept to the FAA, the first step would require identifying whether or not the system qualifies as a design equivalent to the current EMAS or constitutes a different dynamic approach. This determination will then dictate what further steps the manufacturer would need to take for approval.

## 6.2. Normal Approval Process

The "normal" approval process would require the stages outlined in Figure 6-2. This process does not assume that an arrestor is passive, nor that it engages the aircraft at the tire/ground interface. The normal process is intended for application to a full spectrum of design concepts. It requires that a manufacturer undertake (1) initial data collection, (2) feasibility calculations, (3) first-principles computer modeling, and (4) small-scale testing. The results would be submitted to the FAA as an application for a Cooperative Research and Development Agreement (CRDA). The CRDA would then facilitate full-scale aircraft testing, which should be required for systems fundamentally dissimilar from the existing EMAS design. After testing, the manufacturer would be required to demonstrate the ability to predict system performance with a computer model, as applied to different sizes and types of aircraft. Finally, the manufacturer would apply for FAA approval of the system.

## 6.3. Equivalent Approval Process

Obviously, the normal process would require substantial financial investment and involve several complex steps. For some applicants, these factors could preclude involvement, thus stalling potential improvements to the current EMAS approach. The "equivalence" process of Figure 6-3 allows for a simplification to the normal approach if certain conditions are met.

The equivalence process would require that the new concept constitute an equivalent to the current EMAS design at a mechanical level. It is restricted to replacement materials that are laid out in a geometrically similar bed and produce a dynamically analogous load on the landing gear. An aggregate system, for example, would *not* constitute such an equivalent, since it has other physical mechanisms at work than a crushable foam material (Section 7.4). Meanwhile, another crushable foam *could* constitute such an equivalent. To date, many crushable materials have been proposed as alternatives to cellular cement (Sections 7.3 and 7.4). The cellular cement could be replaced with a different crushable medium of similar properties and still obtain analogous arresting performance.

Further, the term "equivalent" is not intended to prevent new materials from superseding cellular cement. It requires

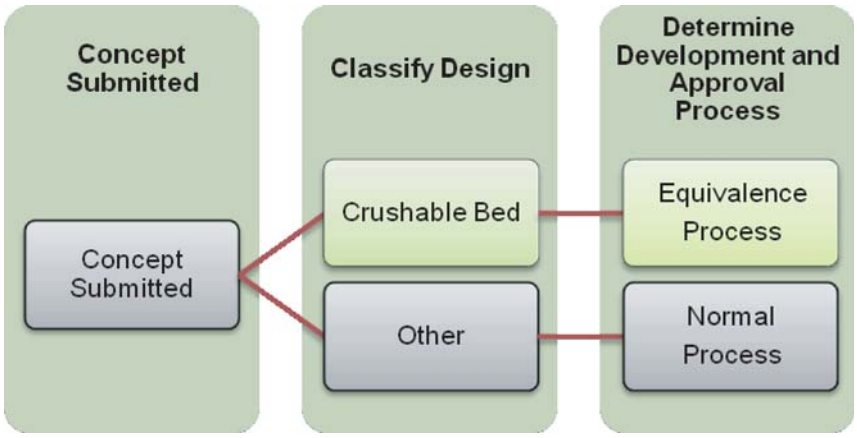


*Figure 6-1. Approval paths for system approval.*

that the mechanical behavior be sufficiently analogous to permit the same predictive models to be employed (i.e., the ARRESTOR code, etc.). However, improvements in other areas, such as life-cycle performance, would be encouraged.

To demonstrate equivalence, the manufacturer would (1) conduct thorough material testing, (2) generate feasibility calculations, (3) perform small-scale tests, and (4) make the case for equivalence in report form. The FAA would then review this report and make a determination as to how compelling the data appears.

## 6.4. Updating of the ARRESTOR Code

For the near-term development of alternative materials via the equivalent approval process, it would be necessary to have a prediction and planning program. ARRESTOR, though an old code at present, can predict arresting distances for various bed geometries. It models a general crushable foam material and permits the user to specify different compression strengths to be modeled. As such, ARRESTOR could serve the

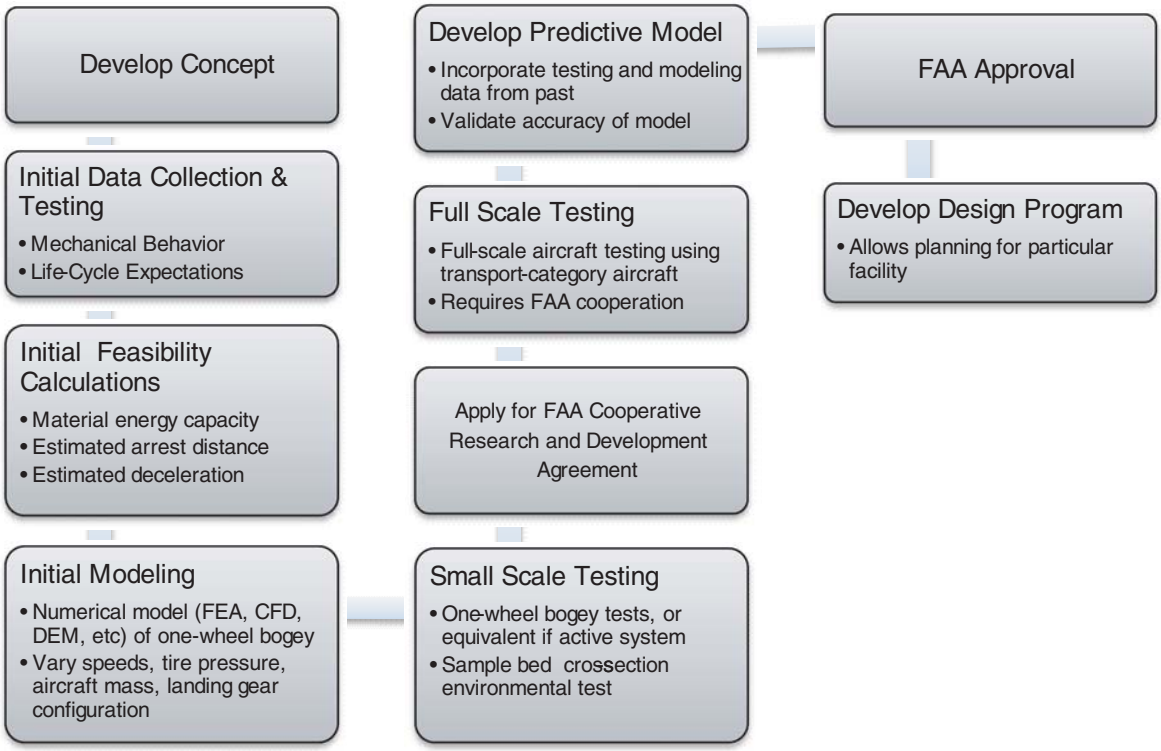


*Figure 6-2. Proposed normal approval process for new arrestor systems in general.*

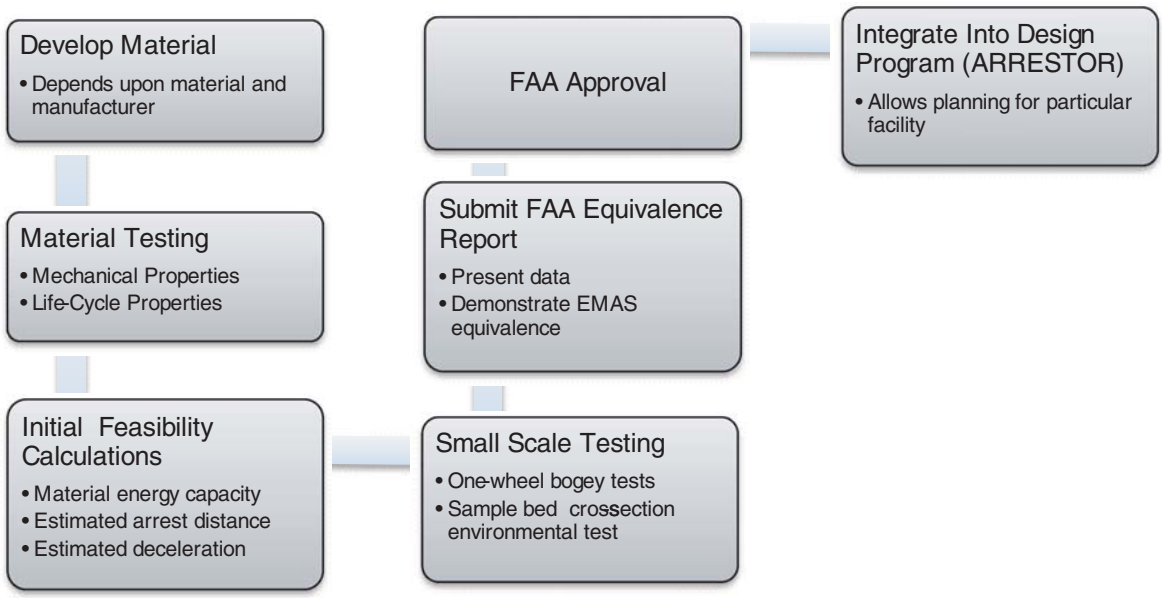


***Figure 6-3. Proposed equivalence approval path for new crushable bed arrestor systems.***

up-and-coming manufacturers who do not have in-house predictive codes.

ARRESTOR currently has a limited library of aircraft: the B707, 727, and 747. Only one of these aircraft is still in broad service, the B747. To act as a modern planning tool, a broader range of aircraft is needed. It is possible to accomplish this through two means. First, the aircraft manufacturers could be solicited for actual aircraft data. Second, the code could use a generalized aircraft model of arbitrary size, combined with parametric variation across a range of values. Other approaches may be possible.

Alternately, a new design program could be developed. The Arrestor Prediction Code (APC) developed in the current effort (Appendix G) could serve as the basis for such a replacement. For new manufacturers to participate actively in the arrestor system market, an updated predictive code would be necessary.

CHAPTER 7

# Identification and Initial Assessment of Alternatives

## 7.1. General Approach

The identification and ideation of different arrestor alternatives was approached through several avenues:

- Vendors with design ideas were contacted,
- Internal brainstorming meetings were undertaken,
- Technical literature was reviewed, and
- General web searches were undertaken.

Following the identification of alternatives, taxonomy was developed to classify the different options and provide clarity of comparison. An initial assessment of the alternatives led to the selection of several promising candidates for detailed research in the experimentation phase of the effort. Please note that the TRB and ACRP do not endorse specific products. Research results are provided to assist in the evaluation of options by others.

## 7.2. Vendor-Developed Alternatives

The FAA William J. Hughes Technical Center supplied a list of manufacturers that had previously contacted them with different proposed arrestor concepts, materials, or designs. Those companies were subsequently contacted to determine if there was still active interest in arrestor development.

The maturity of the different concepts varied widely. Some companies simply had an alternative crushable material that could be used in a similar manner as the current cellular cement design, but with potentially improved durability. Other companies had more well-developed ideas, including patents (Appendix A), design drawings, and calculations for energy absorption. The broad range of maturity required an initial assessment of the alternatives (Section 7.4) in order to determine the most promising concepts for inclusion in the experimentation stage of the research.

## 7.3. Classification of Alternatives

When trying to sort through the myriad of ideas developed and identified, it became apparent that some of the concepts did not differ as greatly as initially assumed. For instance, within the domain of crushable foams, there is minimal difference in the dynamic arrestment process expected for different materials. A crushable polymer foam, a crushable cellular cement, and a crushable metal foam will function in a fairly similar manner where their compressive (crush) strengths and other material properties are the same. There are many foams available, and delving into the nuances that separate them has minimal benefit. This is especially true when compared with the differences, for example, between crushable foam arrestors and gravel arrestors. The dynamic responses of these arrestors are quite different.

The classification structure that was developed divided the alternatives by *dynamic behavior*. Table 7-1 shows the classification for the different concepts in abbreviated form. Section 7.4 expands upon this table and indicates those alternatives that were selected for the detailed research. Subsequent chapters discuss the detailed research findings.

The systems were grouped into two broad classifications: passive systems, with no moving parts, and active systems, with moving mechanical components. Thereafter, they were grouped into four categories based on the energy absorption approach used.

1. **Crushable Materials.** Crushable materials absorb energy through permanent deformation of the material, either through brittle fracture or plastic deformation.
   - The aircraft is engaged at the tire/ground interface.
   - Current EMAS and phenolic foam beds are examples of crushable material systems.
2. **Displaceable Materials.** Displaceable materials do not undergo a physical breakdown of the material itself. Instead, the material is moved, and energy is absorbed through momentum transfer or the internal friction of the material. The mechanical behavior of these materials is fundamentally dissimilar from the crushable material and results in a different dynamic system response.
   - The aircraft is engaged at the tire/ground interface.

**Table 7-1. Classification of alternatives.**

| | Category | Subcategory | Technology | Covering Layer Applicable | Current Civil Use | Detailed Research |
|---|---|---|---|---|---|---|
| PASSIVE SYSTEMS | Crushable Materials | Crushable foams | Cellular cement (current EMAS) | Yes | Yes | |
| | | | Phenolic foam | Yes | | |
| | | | Metal foam | Yes | | |
| | | | Glass foam | Yes | | Yes |
| | | | Depth-varying foam | Yes | | Yes |
| | | Loose crushable fill | Glass aggregate foam | Yes | | Yes |
| | | Crushable aggregates with binder | Pumice aggregate | Yes | | |
| | | | Styrofoam aggregate | Yes | | |
| | | | Hollow microspheres | Yes | | |
| | | | Ceramic glass aggregate | Yes | | |
| | Displaceable Materials | Soil | Clay | | | |
| | | | Sand | Yes | | |
| | | Loose aggregates | Gravel | Yes | | |
| | | | Engineered aggregate | Yes | Yes | Yes |
| | | Fluids | Water or Glycol pond | Yes | | |
| ACTIVE SYSTEMS | Cable/Net Systems | Braking devices | Hydraulic brake | | | Yes |
| | | | Water impeller | | | |
| | | | Textile | | | |
| | | | Eddy-current brake | | | |
| | | Engagement devices | Over-wing barrier nets | | | |
| | | | Landing gear strut engagement | | | Yes |
| | Mechanical Surface Systems | | Surface of spring-supported panels | Yes | | |

- Water ponds are included in this category, as are beds of loose aggregate (gravel, etc.) where the individual pieces are compacted and moved, but not generally broken.

3. **Cable and Netting Systems.** Cable and netting systems utilize two components: (1) braking devices to absorb energy (water, hydraulic, electro-magnetic, etc.), and (2) an engagement system that connects the aircraft and the braking device (cables, nets, etc.).
   - Engagement can be done with an aircraft tail hook, the main gear, or the wings.
   - Military arrestors, such as the BAK-12, are included in this category.
4. **Mechanical Surface Systems.** Mechanical surface systems use mechanical components that absorb energy as the aircraft rolls across different movable panels at ground level.
   - The aircraft is engaged at the tire/ground interface.
   - The concepts in this category are few, encapsulated in the referenced U.S. Patent 6,969,213 (*32*); nevertheless, this approach represents a categorically different arresting method.

The *Subcategory* and *Technology* columns show progressively more detail on the concepts in each category.

The *Covering Layer Applicable* column indicates whether a given concept can be combined with a covering layer. Covering layers are often used to preserve the crushable or displaceable materials from the environment, jet blast, and so on. The current EMAS design uses such a "covering layer." The latest generation uses thin plastic tops, while the prior generation used cement board tops. Water ponds historically had different covering concepts suggested to keep the water clean and prevent evaporation or animal intrusion. For new arrestor candidates, a variety of creative covering layer concepts have been suggested by different vendors, all with similar purposes—to provide a durable top layer that protects the medium while not interfering with its arresting function.

The *Detailed Research* column indicates whether a given technology underwent further evaluation in the experimentation phase of the research.

It should be noted that combined approaches could be used by coupling a passive arresting bed with an active net or cable-based arresting system.

## 7.4. Initial Assessment of Alternatives

The preliminary vetting process involved two components: (1) an initial physics analysis to determine if a concept had the energy capacity and physical feasibility to arrest and aircraft, and (2) analysis of other factors, such as flammability, environmental considerations, life-cycle performance, and so on.

Table 7-2 gives the assessment criteria that were used to evaluate different concepts. In the analysis findings that follow, criteria of minimal relevance to different technologies are often excluded from the discussion.

As previously shown in Table 7-1, the array of alternatives is broad. Table 7-3 expands upon Table 7-1 with evaluation comments. Arresting alternatives selected as candidates for the experimental investigation are denoted with a "C." For alternatives not selected, the evaluation comments provide rationales for exclusion.

## 7.5. Crushable Material Systems

### 7.5.1. Drag Loading Dynamics

In general, all of the crushable material alternatives function on the same physical premise. The aircraft tires compact the material as they roll forward through it. The compaction of the material can take several forms at the microscale: brittle fracture, plastic deformation, reduction in void space, and so on. However, at the macroscale, the effect is similar: the aircraft is slowed by the drag load of the material and the energy absorbed is proportional to the volume of material compacted (Figure 7-1).

Some materials, such as phenolic foam, exhibit a rebound after compaction, where the material rises back up to a small extent after the tire rolls over it. This rebound is inherently inefficient and undesirable. The currently used cellular cement is advantageous because it has nearly zero rebound.

### 7.5.2. Essential Material Properties

To select a crushable material that is suitable for an arrestor bed, several properties must be considered. Figure 7-2 illustrates a typical compression stress-strain curve for a crushable foam.

The load increases up to a plateau value, typically designated as the compressive strength of the foam ($\sigma_u$). During the plateau stage, the foam is compacted, and the void spaces of the foam microstructure collapse. When the void spaces have been fully compacted, the plateau ends and the material hardens. The degree of compression that has occurred at the end of this plateau will be referred to as the maximum compressive strain of the material ($\varepsilon_{max}$). In actuality, further compression can take place, but not without dramatically higher compression forces. For the purposes of the arrestor applications, the concept of maximum compressive strain is useful.

The maximum compression helps determine the overall energy absorption potential for the material because energy absorption relates to the area under the stress-strain curve. Greater maximum compression strain values correspond to long plateau regions in the load curve and high energy absorption.

### 7.5.3. Effect of Landing Gear Configuration

The configuration of the tires on the aircraft's struts directly affects the efficiency of the crushable material systems. Figure 7-3 shows several landing gear tire configurations; in each case, only the leading tires participate in crushing the material and generate drag load. However, the vertical load on the strut is divided among all the tires. The dual configuration, and analogs to it, forms the most efficient coupling, since all tires participate in generating drag load. The dual tandem and tridem configurations are less efficient, regardless of the particular crushable material used. These efficiency reductions would typically only apply to the main struts of the aircraft because inline tires are uncommon for the nose gear.

The pneumatic pressure of the tires has an effect on the tire-material interface. Often referred to as "flotation," the ground pressure affects how much the tires sink into a soft

**Table 7-2. Assessment criteria for concept evaluation.**

| Criteria/Requirements | Comments |
|---|---|
| **Arresting Performance** | |
| Energy absorption | The system must have the energy absorption capacity to arrest the aircraft. |
| Mechanical engagement | The system must effectively engage the aircraft for the energy capacity to be employed. |
| Scalability | The system must either actively or inherently scale its stopping force appropriate to the aircraft size/type to prevent overly abrupt deceleration of smaller aircraft while not sacrificing capabilities with larger aircraft. |
| Reliability | Device complexity in general will increase maintenance-related concerns and reliability. However, passive systems also have associated reliability despite the absence of moving parts. |
| **Post-Arrest Factors** | |
| Emergency personnel access to aircraft | System must permit emergency personnel and vehicles to access the aircraft after an arrest. |
| Emergency egress of passengers | System must permit emergency exits to open and allow evacuation of passengers. |
| **Costs** | |
| Purchase/installation cost | May be resolvable with refinement of production process and volume production. Some facilities may support higher cost than others. |
| Repair cost | Some alternatives will have little to no repair costs following an overrun, depending on the materials used. |
| Maintenance cost | Both active and passive systems have been shown to require maintenance. |
| **Life-Cycle Factors** | |
| Pollution hazard | Material hazards can probably be mitigated with proper packaging. |
| Temperature performance | Likely not resolvable with packaging or treatments of the system. This includes coupling with the moisture criteria in the form of freeze–thaw cycle performance. |
| UV sensitivity | Arrestor beds that use covering layers (cement board, plastic, other) inherently protect the arresting materials from UV exposure. Paint and dye for the covering layers must be selected for resistance. |
| Moisture performance | May be resolvable with proper packaging of materials used. |
| Jet Blast resistance | Cover layers tend to resolve jet blast issues. |
| Chemical resistance | May be resolvable with proper packaging of materials used. |
| Non-flammable | The materials involved, or their location, must be inherently non-flammable. |

**Table 7-3. Arrestor alternatives with evaluation comments.**

| Subcategory | Technology | Evaluation Comments | |
|---|---|---|---|
| **Crushable Foams** | Cellular cement | Current EMAS material. Baseline for passive system comparison.<br>Moisture and freeze–thaw related issues have been qualitatively observed, but not quantified. | |
| | Phenolic foam | Previously evaluated by FAA and since superseded by cellular cement (*5*).<br>Similar material properties as cellular cement, but with more material rebound (disadvantageous).<br>Flammability concerns. | |
| | Metal foam | Excellent mechanical properties for energy absorption.<br>Cost prohibitive.<br>Corrosion vulnerability. | |
| | Glass foam | Glass-based material that is chemically inert and has moisture-resistant properties.<br>Material generally stronger than required for an arrestor application, but can be modified.<br>Density for desired mechanical properties will require determination through experimentation. | C |
| | Depth-varying foam | Concept proposed by research team.<br>Depth-varying foam idea involves hardening material throughout the arrestor bed depth. This variant would be broadly applicable and not tied to a particular foam material.<br>(Depth-varying foam concept evaluated in a parallel graduate study research effort (*33*). Summary findings included in this report.) | C |
| **Loose Crushable Fill** | Crushable aggregate foam | Glass-based material that is chemically inert and has moisture-resistant properties.<br>Made of recycled glass, it offers potential cost savings over cellular glass foam.<br>Density for desired mechanical properties will require determination through experimentation. | C |
| **Crushable Aggregates with Binder** | Pumice aggregate | Novel concepts developed by research team, but deemed less viable than hollow microsphere concept. | |
| | Styrofoam aggregate | | |
| | Hollow microspheres | Novel concept developed by research team.<br>Hollow plastic or glass microspheres connected with a cementitious binder.<br>Offers potential immunity to moisture and freeze–thaw degradation and has pour-in-place simplicity.<br>Brief experiments indicated that obtaining the necessary 80% void ratios was infeasible. | |
| | Ceramic glass aggregate | Crushable ceramic glass aggregate connected with a phosphate cement binder.<br>This solution offered the possibility of a pour-in-place crushable material, which would reduce cost compared with prefabricated block installation.<br>Concerns regarding moisture penetration and subsequent freeze–thaw performance.<br>Eliminated from consideration due to lack of manufacturer interest. | |
| **Soil** | Clay | Previously evaluated by FAA (*2*). | |
| | Sand | Mechanical properties too dependent on moisture and temperature. | |
| **Loose Aggregates** | Gravel | Previously evaluated by FAA (*2*).<br>Gravel composed of angular pieces settles over time, altering bed response.<br>Loose gravel poses ingestion hazard for aircraft. | |

**Table 7-3. (Continued).**

| Subcategory | Technology | Evaluation Comments | |
|---|---|---|---|
| **Loose Aggregates** | Engineered aggregate | Aggregate used in the UK without covering layer, this poses a possible ingestion hazard.<br>Concept allows for one of several covering layers, potentially eliminating this problem.<br>Unlike normal gravel, engineered aggregate's spherical shape prevents settling of the bed over time.<br>Moist freezing conditions could potentially freeze particulates together.<br>Issue: deceleration loading expected to be speed-dependent, which is not a desired trait. | C |
| **Fluids** | Water or glycol pond | Previously evaluated by FAA (*2*).<br>Freezing in winter, contamination, and attracting animals made ponds impractical.<br>Emergency vehicle access and passenger evacuation hindered.<br>Loadings only suitable up to certain velocity thresholds (<50 knots). | |
| **Braking Devices** | Hydraulic brake<br>Water impeller<br>Textile | All three of these arresting brakes are commercially available at present and are typically used for military aircraft.<br>The hydraulic braking systems, such as those used for BAK-12 arrestors, are applicable and offer the feature of active servo-controlled loading, making them capable of the most idealized loading of the various arrestor options.<br>Coupling with an appropriate engagement device for civil applications remains the problem to be solved. | C |
| | Eddy-current brake | Typically used in roller-coaster applications.<br>While viable, no inherent advantage has been found when compared with the time-proven hydraulic friction brakes. | |
| **Engagement Devices** | Barrier nets | Long-standing design option, commercially available.<br>Must be erected to a height that interferes with normal flight path, requiring active deployment in an overrun event.<br>Imparts loading to the leading edge of the wings, with potential for entanglement with leading edge flaps.<br>Can wrap over emergency exits, hindering egress of passengers and crew. | |
| | Landing gear strut engagement | Long-standing design option.<br>Low-slung engine design on some current civil aircraft creates timing issues regarding deployment.<br>Range of landing gear dimensions and interfering landing gear features (gear doors, electrical/hydraulic features, etc.) creates further deployment complexities. | C |
| **Mechanical Surface** | Surface of spring-supported panels | Unique design approach that offers fully reversible system, which would not require repair after arresting events (*32*).<br>Pulsed loading on landing gear due to surface segmentation would reduce performance compared with monolithic foam beds. Reducing pulse strengths to avoid landing gear overloads would require discretization of surface into many small panels.<br>Number of mechanical components and degrees-of-freedom could be substantial, which creates concerns regarding maintenance, reliability, and cost. | |

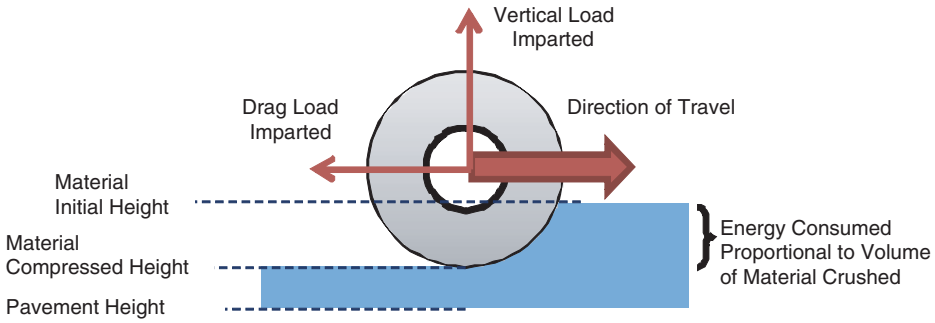


***Figure 7-1. Physical performance of crushable materials.***

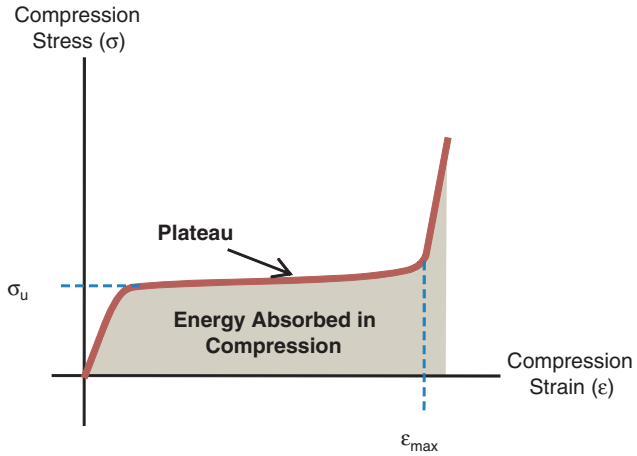


***Figure 7-2. Crushable foam stress-strain curve.***

surface. Tires with higher pneumatic pressures tend to penetrate more deeply; lower pressure tires tend to penetrate less.

Table 7-4 gives several sample pneumatic tire ground pressures, as well as the compressive strength of the current EMAS cellular cement. As may be seen, the internal pressure of the aircraft tire is greater than the strength of the EMAS material. A typical heavy truck with an 80-psi tire, however, has a pressure very close to that of the EMAS material, indicating a poor matchup in which the truck may or may not effectively crush the material. A reduction in the drag load would be expected in this case. Finally, the car's 35-psi ground pressure is lower than the compression strength of the arresting material.

Note that the EMAS material strengths cited in the table are based on a punch test methodology developed by the manufacturer that includes both compression and shear strength components together (*34*). The uniaxial compression strength of the EMAS material would actually be less than these values.

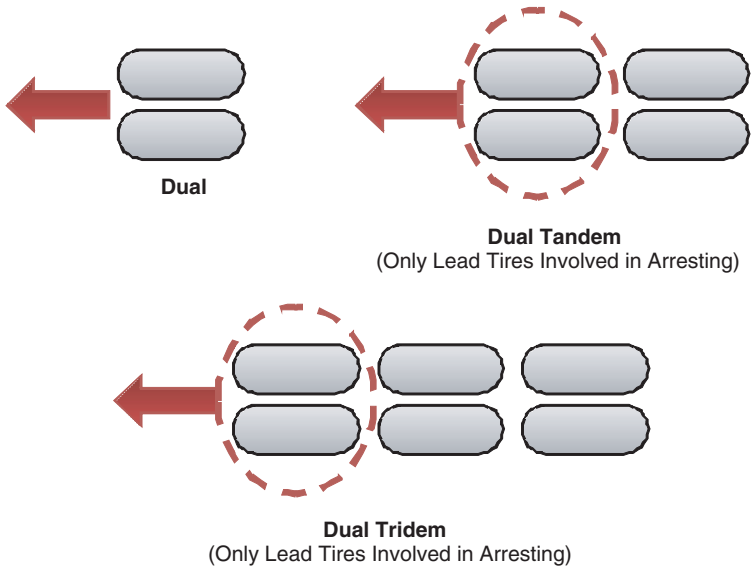


***Figure 7-3. Effect of inline tires on arresting loads.***

**Table 7-4. Sample pneumatic tire pressures.**

| Vehicle or Material | Ground/Pneumatic Pressure | EMAS Material Strength | Arresting Efficiency |
|---|---|---|---|
| **Typical Car** | 35 psi | 60 – 80 psi | Negligible |
| **Typical Work Truck** | 80 – 100 psi | 60 – 80 psi | Questionable |
| **B737-800** | 185 psi (nose gear)<br>205 psi (main gear) | 60 – 80 psi | High |

The simple tire comparison above has implications for the current research. There can be a substantial variation in pneumatic tire pressure for different types of planes. Aircraft with lower tire pressures will tend to skim the top of an arrestor bed, and those with higher pressures will dig in more deeply. Also, differences in pressure between the main- and nose-gear tires can affect the relative loading that each strut experiences.

The dependencies on landing gear configuration and pneumatic tire pressure are limitations of the crushable material approach.

### 7.5.4. Overall Aircraft Dynamics

When overrunning the arrestor bed, the nose gear and main gear of the aircraft experience vertical and drag loads (Figure 7-4). For the main gear, this is normal, as they have been designed for braking loads. In contrast, the nose gear is not normally fitted with brakes, and so is not typically designed to be subjected to the same rearward loading as the main gear. The drag load that the arrestor bed applies to the nose gear constitutes an unnatural way to slow the aircraft.

In addition, the deceleration of the aircraft generates a forward pitching motion that increases the vertical load on the nose gear. This in turn drives the nose gear deeper into the arrestor bed, generating additional drag loads on it.

A critical distinction must be made with regard to deceleration of the aircraft created by (1) a normal braking stop, and (2) an arrestor-bed stop: it is insufficient to compare the two stops using the gross aircraft g-loading. For example, let us assume a case of a 0.5 g deceleration created by normal braking or created by an arrestor bed (Table 7-5). The loading on the aircraft is similar in most respects. The 0.5 g deceleration in the braking case is entirely due to the drag load on the main-gear struts. The 0.5 g deceleration in the arrestor bed case is due to drag loads on all three struts: part of the 0.5 g is achieved by the main gear and part by the nose gear. The exact breakdown in percent contributions from the nose and main gear cannot be determined without an overall aircraft dynamics model, which will be developed in Phase 2 of this effort.

### 7.5.5. Summary of Mechanical Factors

To summarize the dynamics of crushable material arrestor beds, the following factors have a direct impact on the overall performance:

- Material properties
  - Compressive strength ($\sigma_u$)
  - Shear strength ($\tau$)
  - Maximum compressive strain ($\varepsilon_{max}$)
  - Volumetric energy absorption
- Material depth
- Landing gear configuration
- Pneumatic tire pressure
- Limiting landing gear design loads, with special consideration for the nose gear
  - Vertical limit load
  - Longitudinal (drag-direction) limit load

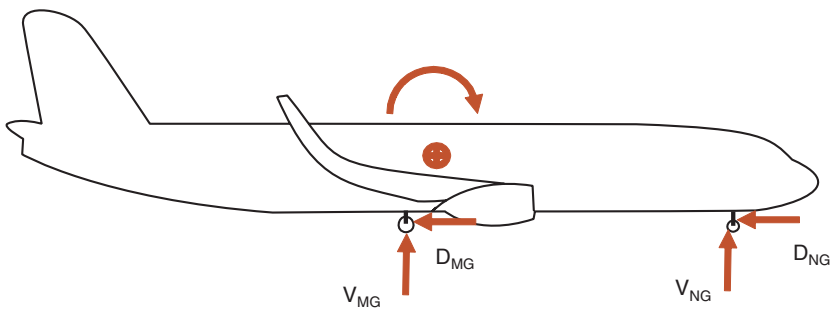


*Figure 7-4. Overall aircraft loading dynamics.*

**Table 7-5. Comparison of braking and arrestor bed deceleration.**

| Variable | Braking Deceleration | Arrestor Bed Deceleration |
|---|---|---|
| **Gross Deceleration** | 0.5 g | 0.5 g |
| **Braking Condition** | Typical | Reduced (due to arrestor material) |
| **Thrust Reverser** | Not used | Not used |
| **Main-Gear Vertical Loading** | Typical | Typical |
| **Main-Gear Drag Loading** | Typical (caused by braking) | Typical/reduced (caused by arrestor material) |
| **Nose-Gear Vertical Loading** | Typical | Typical |
| **Nose-Gear Drag Loading** | Near zero (rolling friction only) | High (drag loading due to arrestor material) |

When all of these factors are combined, the performance of an arrestor bed varies across a given fleet of aircraft. Figure 7-5 illustrates the spread in design speeds for a typical arrestor bed, where the dashed line shows the average exit speed. The spread in exit speeds (43 to 57 knots in this case) represents the non-ideal performance that naturally results from designing the bed for a mixture of aircraft. The illustrated bed is most efficient for a B737, which it can arrest at nearly 60-knots, and it is least efficient for the DC-10. The plot shows that the weight of the aircraft alone does not drive the stopping efficiency of the bed: the most efficient stops are achieved for aircraft between 150,000 and 200,000 lbs, with efficiency decreasing to the left and right. Thus, the aggregate combination of the listed mechanical factors produces the aircraft stopping efficiency on a case-by-case basis.

A similar performance variation is expected to persist for all surface-based arrestor beds, regardless of the crushable material chosen.

### 7.5.6. Candidate 1: Glass Foam

Cellular glass foam was proposed as a material and would be made as a modification of an existing insulating product (Figure 7-6). The material would be used in a large bed either composed of blocks akin to the current EMAS or constructed as a monolithic structure.

The chemical makeup and closed-cell properties of glass foam suggested good chemical resistance, excellent durability to the environment, and resistance to water absorption (*36*). The potential improvement in durability suggested the possibility of reduced maintenance and replacement needs for an arrestor using this material.

Chapter 9 discusses the glass foam concept evaluation in detail.

### 7.5.7. Candidate 2: Aggregate Foam

An aggregate foam arrestor concept has been proposed. The arrestor would use rough-broken foam aggregate made from recycled glass (Figure 7-7) (*37, 38*). The foamed, or aerated, glass material has nominally 80% void space by volume. Its closed-cell microstructure makes it resistant to water absorption and degradation.

An arrestor using this material would be created by filling a shallow basin with the loose material and covering it with a

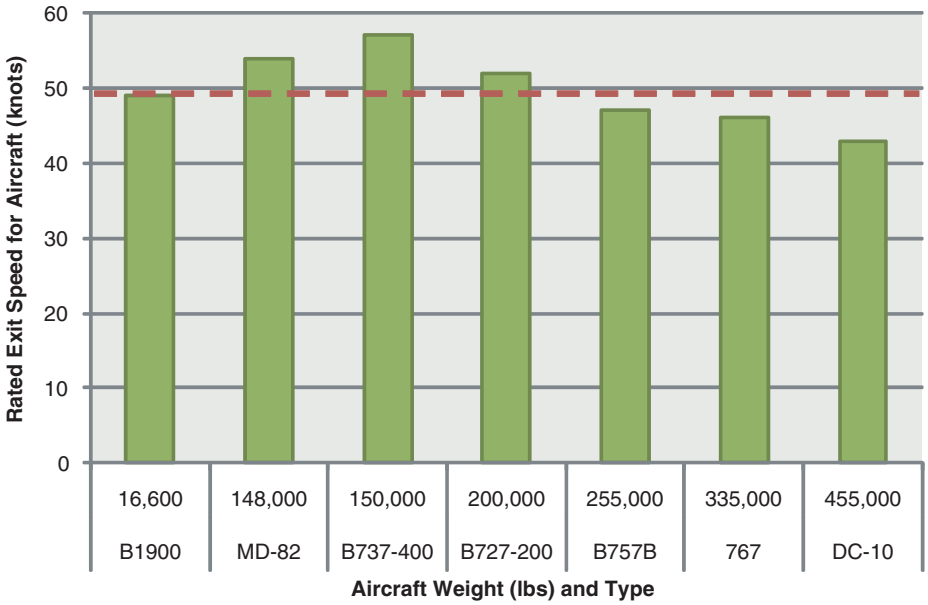


***Figure 7-5. Exit speeds for sample EMAS arrestor (35).***

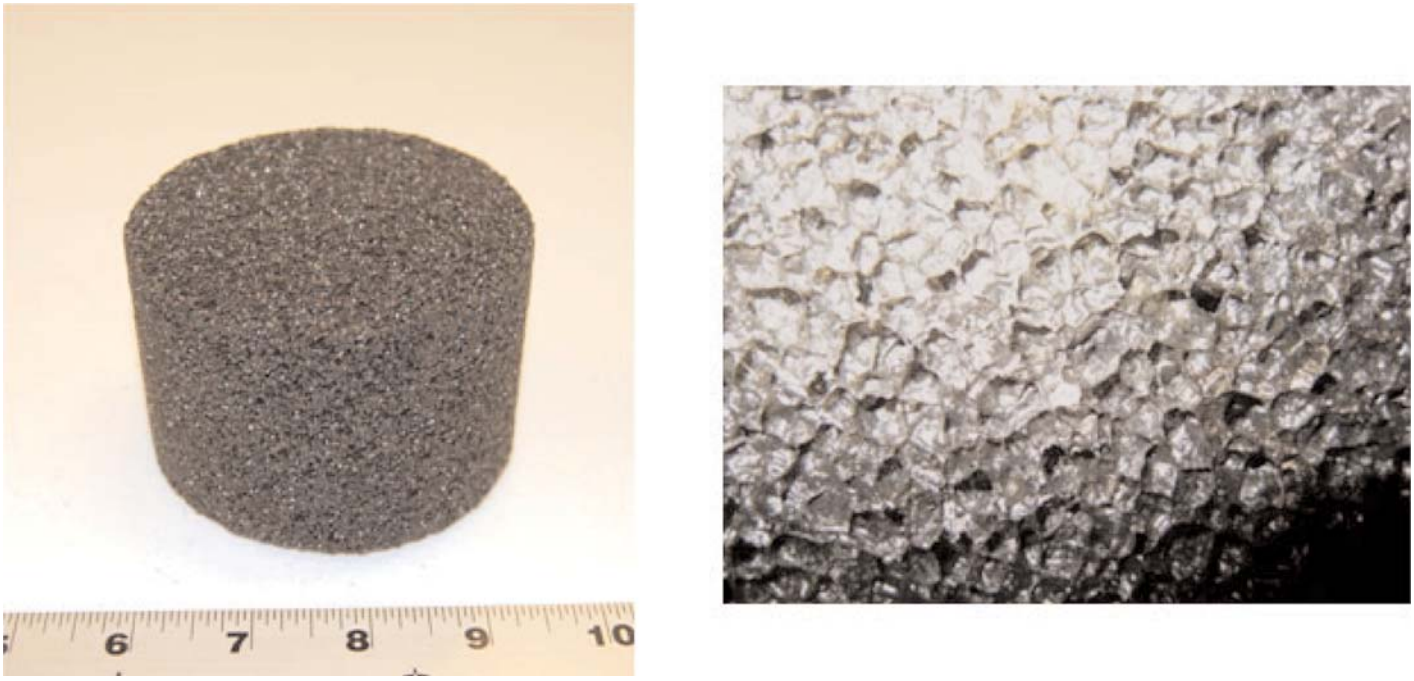


*Figure 7-6. Cellular glass foam material.*

reinforced turf layer. The loose fill approach offered the potential advantage of reduced manufacturing and installation cost, as compared with pre-fabricated foam blocks.

Chapter 11 discusses the aggregate foam concept evaluation in detail.

### 7.5.8. Additional Study: Depth-Varying Foam

The depth-varying foam concept was developed by the research team. It involves the use of non-homogeneous crushable foam that becomes firmer as the bed depth increases.

The cellular cement used in existing EMAS arrestors is homogeneous, having the same density and strength throughout each block of material. Changing the density and strength to become harder at deeper levels could achieve a degree of performance leveling between large and small aircraft (Figure 7-8). Further, this concept is fairly independent of the material chosen. Many crushable materials exist, and depth-varying layups for most could be achieved, including cellular cement.

This concept was evaluated as a parallel graduate-level research study; Chapter 12 summarizes the relevant findings from the study.

## 7.6. Displaceable Material Systems

Several displaceable material systems are listed in Table 7-3, but only one of these systems was selected for detailed evaluation: loose engineered aggregate. This material is much like normal gravel in that the individual aggregate pieces do not

*Figure 7-7. Aggregate foam: close-up of microstructure (left) and pile (right).*

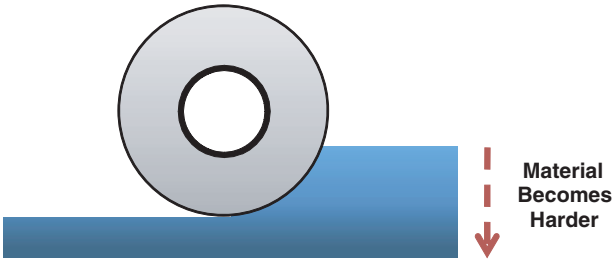


*Figure 7-8. Depth-varying material concept.*

(in general) break or compress. They can be compacted by removing the void spaces between them, or they can be displaced. However, after a tire overrun, they can simply be raked back into the ruts with little change in the effectiveness of the material. Gravel systems are most often used for arresting large trucks that lose effective braking on down-hill roads, but they have been used for aircraft in the U.K. (*4, 13*).

The engineered aggregate differs from normal gravel in that the particulates are all roughly spherical, instead of angular or elongated shapes. This has the principal advantage of preventing settling of the material over time, which is typical for normal gravels. Similarly, since the particulates are made of the same material, the friction between individual pieces is more consistent.

### 7.6.1. Drag Load Dynamics

Although a gravel-type arrestor bed appears to load the landing gear in a similar fashion as the current EMAS design, the dynamics involved are quite different. The tire–gravel interaction is highly complex because aggregates have more than one mode of behavior.

Consider a pile of sand or gravel, created by pouring the material from a spout above it. The pile forms in a cone shape whose sides are at an inclined "angle of repose." At an angle steeper than the angle of repose, the material runs freely, acting similarly to a fluid (*39*). The loose sand or gravel that pours on top slides down the surface, returning the sides once again to the angle of repose. At slopes shallower than the angle of repose, the material does not behave like a fluid, but a solid: a fluid would eventually flatten out into a pancake shape of uniform thickness, as a puddle. Mechanically, the angle of repose is determined by the internal angle of friction for the material. This angle of friction divides the different regimes of behavior.

For a tire rolling through an aggregate, the physical behavior follows the illustration of Figure 7-9. The material below a certain level behaves in a solid-like fashion and undergoes compaction beneath the weight of the tire. Above this level, fluid-like behavior dominates, and the material is pushed out of the way of the tire, similar to water being pushed by the hull of a boat. The uppermost part of the aggregate can spray to the sides at high speed when the tire cuts through the material quickly. In the "wake," a rut is left in the gravel.

Altogether, there are three major components to the energy dissipation:

1. Compaction of the lower layer,
2. Friction between pieces of aggregate moving around the tire, and
3. Momentum transfer in projecting the aggregate away from the tire.

Unlike the crushable material systems, the drag load from the aggregate is highly rate dependent. The momentum components are proportional to the tire speed squared (*2,* p. 8). This means that the drag load decreases as the aircraft slows, progressively exerting less stopping force. It has also been found that at higher rates, the tires skim the surface, not penetrating as deeply and generating lower drag loads (*2,* p. 16).

Low inter-particle friction allows for more fluid-like behavior and permits the tires to sink more deeply into the aggregate

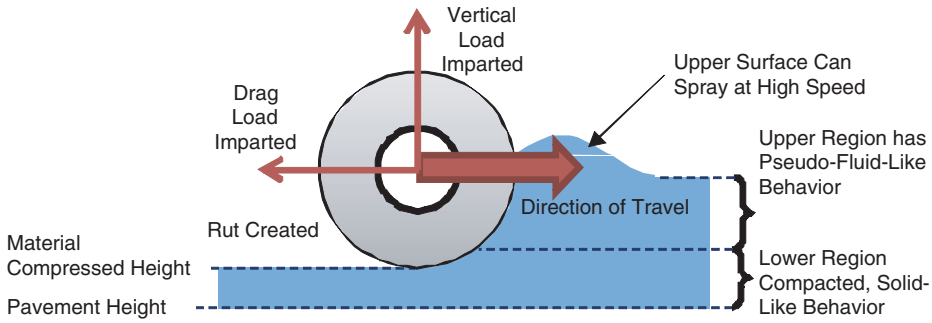


*Figure 7-9. Physical performance of gravel/aggregate materials.*

(*13*). This can be either desirable or undesirable, depending on the vehicle to be stopped. For truck arresting, allowing the vehicle to sink to the axles is positive, as the gravel also engages the undercarriage of the truck. For an airplane, however, there is no undercarriage to halt the descent into the medium, and sinking too deeply could result in drag loads high enough to cause landing gear to fail.

Another factor related to internal friction is the impact of environmental variables such as moisture, dust, or ice in the arrestor bed. Dry, clean gravel generally has lower inter-particle friction than damp, dusty gravel. Friction, or the resistance of sliding between the particles, is in contrast to cohesion, or the sticking of the particles together. Dust, moisture, and ice can all generate cohesion between the particles as well. In severe winter environments, testing has revealed that an open bed of gravel can form a deep ice crust layer, rendering it ineffective (*13*).

A variant to be considered in this research effort involves applying a protective cover layer to the aggregate bed (Figure 7-10). Open arrestor beds produce a spray from the uppermost layer of the aggregate, which could be ingested by an aircraft engine; this cover layer will protect against ingestion. It could also mitigate or eliminate the development of ice crusts in cold environments. However, the layer could alter the dynamic response of the aggregate bed because the aggregate would be confined. Thin protective cover layers added to crushable systems do not induce a fundamental change in dynamic behavior, so this effect (if it exists) would be unique to covered aggregate beds.

Altogether, the aggregate behavior is highly complex and must be treated as an entirely different dynamic response from that of the crushable material systems.

### 7.6.2. Effect of Landing Gear Configuration

The effect of the landing gear configuration is essentially the same as for the crushable system (Section 7.5.3).

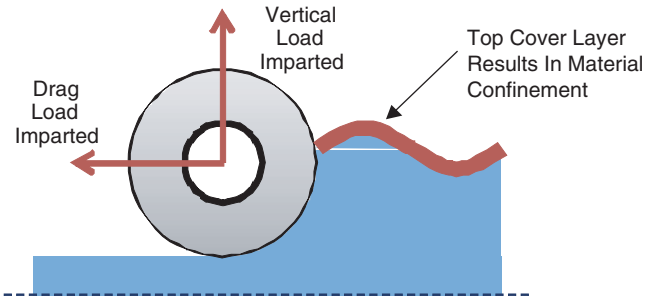


***Figure 7-10. Physical performance of gravel/aggregate materials with confining top layer.***

### 7.6.3. Overall Aircraft Dynamics

The overall aircraft dynamics are the same as for the crushable system (Section 7.5.4).

### 7.6.4. Summary of Mechanical Factors

To summarize the dynamics of aggregate/gravel arrestor beds, the following factors have a direct impact on the overall performance:

- Material properties
  - Particle size/gradation
  - Particle shape
  - Particle density
- Inter-particulate properties
  - Internal angle of friction
  - Inter-particle friction
  - Inter-particle cohesion
- Speed of travel
- Material depth
- Landing gear configuration
- Pneumatic tire pressure
- Limiting landing gear design loads, with special consideration for the nose gear
  - Vertical limit load
  - Longitudinal (drag-direction) limit load

### 7.6.5. Candidate 3: Engineered Aggregate

An engineered aggregate arrestor concept is called the Engineered Root-zone Arresting System (ERAS). It uses a manufactured aggregate composed of nearly spherical particles (Figure 7-11) and is topped with a reinforced turf cover layer.


***Figure 7-11. Engineered aggregate.***

The engineered aggregate solution offers the advantage of construct-in-place simplicity, requiring no fabrication of blocks or cure time. Repairs after overruns would essentially involve shoveling or scraping the material back into place, with little material replacement required.

Chapter 10 discusses the engineered aggregate concept evaluation in detail.

## 7.7. Cable/Net Active Systems

Active arresting systems have long been deployed to arrest military planes. Prior attempts have been made to adapt them for use with civil transport aircraft. To surpass these predecessors, any new attempts to adapt the active systems would require innovation and new sensor approaches. However, the active systems offer elegance and a decided performance advantage over passive systems. As such, they have been revisited in this effort and re-examined for feasibility.

### 7.7.1. Braking Devices

A wide range of braking technologies has been developed to arrest military aircraft, including hydraulic brakes, water impellers, and textiles. Hydraulic brakes function much like automobile disc brakes, where a caliper compresses to a rotating disc. Water impellers dissipate kinetic energy by generating turbulence in a reservoir of water. Finally, textile devices absorb kinetic energy by tearing fibers.

Of the three types of braking devices, the hydraulic brake, pictured in Figure 7-12, is the most precise. Because it features servo-controlled loading, it is capable of applying a consistent deceleration profile to a variety of aircraft. As a result, the hydraulic brake could be used to apply the ideal deceleration profile to a given aircraft, thus minimizing the stopping distance. For example, hydraulic brakes could be used to stop a B747-400 with a 1 g deceleration at 70 knots. Furthermore, the military hydraulic brakes have a minimum of 97.5% reliability. Therefore, if civil aircraft could be engaged with hydraulic brakes, the result would be a highly efficient and reliable arresting system.

*Figure 7-12. Hydraulic brake (servo controlled) (40).*

*Figure 7-13. Deployed barrier net (41).*

Figure 7-13 shows an active arrestor with a barrier net engagement. During aircraft engagement, the nose of the aircraft passes through the barrier net, and the net wraps over the aircraft wings. A braking device is then used to decelerate the aircraft. As Figure 7-13 suggests, over-wing barrier nets are a commercially available technology.

There are three issues that complicate use of barrier nets for civil aircraft. First, because the arrestor constitutes a vertical obstruction, it cannot remain erected at the runway end under normal conditions. Thus, in the event of an overrun, either the pilot or an air traffic controller would activate the arrestor. As discussed in Section 3.8, airport operators and pilots have expressed hesitancy about use of active arrestors for civil aircraft. Also, for most net-based arrestors, activation requires approximately two seconds. Thus, detection of an overrun and deployment of the arrestor may require more time than is available to engage the aircraft in an emergency.

Second, any net-based engagement of civil aircraft would subject the leading edge wing flaps to loads for which they were not designed. The flaps could either become entangled or suffer damage as a result.

Third, nets tend to envelope the fuselage of the aircraft. This result is problematic for civil aircraft because it could hinder emergency egress of occupants.

### 7.7.2. Candidate 4: Main-Gear Engagement System

Given the complications associated with barrier net engagement, a main-gear engagement approach was considered. For

this concept, a cable-based arrestor would pop up from underneath to engage the main landing gear and decelerate the aircraft. This approach to arresting the aircraft is illustrated in Figure 7-14.

One of the main advantages of the cable-based arrestor is that the nose gear would not be engaged. As shown in Figure 7-15, the nose gear would only be loaded vertically, due to the weight of the aircraft and pitching moment. This main-gear engagement approach circumvents the weakness of the crushable bed systems: it does not subject the nose gear to drag loads. Consequently, it would be possible to achieve higher decelerations and shorter stopping distances. Further, with automated servo control of the braking units, it could obtain uniform decelerations for a wide range of aircraft weights.

Chapter 14 discusses the active arrestor concept evaluation in detail.

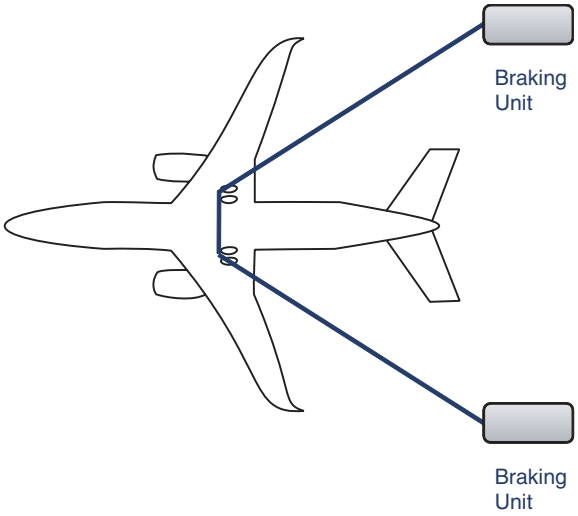


***Figure 7-14. Main-gear engagement active arrestor (42).***

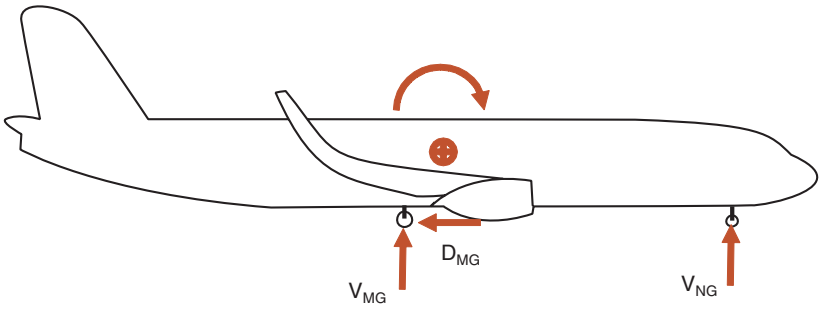


***Figure 7-15. Loads on aircraft subjected to active arrestor deceleration (42).***

CHAPTER 8

# Experimentation Overview

This chapter briefly summarizes the overall experimentation process followed for the candidate evaluations. It provides context for the interrelationships and commonalities of Chapters 9 through 14, which document the evaluations on a system-by-system basis.

## 8.1. Scope and Emphasis

The research funding did not support full-scale testing on a broad enough basis to be meaningful for the effort. Because the experimentation phase was intended to compare the most promising alternatives to the current system, and because there were several to evaluate, a modeling-centric approach was adopted. Within this approach, various physical tests were performed in order to characterize the materials involved and to provide a basis for calibrating high-fidelity computer models of the systems. The models were then used to assess the performance of the arrestor concepts in different configurations and for different aircraft.

The candidate systems and evaluation methods are given in Table 8-1. As the table indicates, the passive systems shared similar evaluation approaches, but the active system differed. The experimentation does not include the current ESCO cellular cement material. Comparisons between different candidates and the current EMAS technology were made based on overall aircraft deceleration.

The majority of the experimentation emphasis was placed on the passive systems (Candidates 1 through 3), which included testing and high-fidelity modeling. Figure 8-1 shows the relative emphasis given to each of the areas.

Crushable material technologies were emphasized most because they have a proven track record; finding a similar material solution with better life-cycle performance would provide a useful alternative in the near-term.

Aggregate systems have historically experienced a discrepancy of acceptance, seeing use in the UK but not within the U.S. The evaluation approach outlined herein offers the promise of resolving the question of predictable arresting performance.

The active system approach required a feasibility study to determine its merit. As such, a small 10% allotment was dedicated to completing a more detailed paper/analytical study.

## 8.2. Evaluation Process

The evaluation method for the passive systems was composed of (1) modeling and (2) physical testing. Figure 8-2 illustrates a simplified version of the modeling and testing approach.

The materials underwent laboratory testing and small-scale one-wheel bogey tests. The data was used to construct models and undertake a more substantial array of simulations for the tire–arrestor interface. These simulations provided data for a wide range of dynamic cases with various speeds of travel, tire sizes, and bed dimensions.

The simulation data was collected into databases, which were referenced by the APC (Appendix G). The APC was used to simulate the aircraft suspension response to different arrestor bed designs. It predicted landing gear loads, the effects of material property alterations, and overall arresting performance. The viability of each alternative was assessed based on the best-case performance obtained through the APC simulations.

Early in the research effort, best-case EMAS arrestment prediction data was provided for three aircraft from different size regimes: the CRJ-200, B737-800, and B747-400 (Figure 8-3). In order to compare the candidate systems' performance with these EMAS baseline cases, aircraft models for each were developed for use in the APC. These three aircraft are cited through the evaluation chapters.

## 8.3. Order of Discussion

The candidates were numbered per the sequence of discussion from Chapter 7, which was ordered in accordance with the mechanical classification of the arrestor systems. The

**Table 8-1. Summary of evaluation methods for candidates.**

| Category | System | Evaluation Approach |
|---|---|---|
| Crushable Material Systems | • Candidate 1: Glass foam<br>• Candidate 2: Aggregate foam | • Material testing<br>• One-wheel bogey testing<br>• Numerical modeling to develop tire/material response surfaces<br>• Overall aircraft response evaluation using an aircraft suspension model |
| Displaceable Material Systems | • Candidate 3: Engineered aggregate | |
| Active Systems | • Candidate 4: Main-gear engagement active system | • Extended paper study<br>• Analytical spreadsheet model |

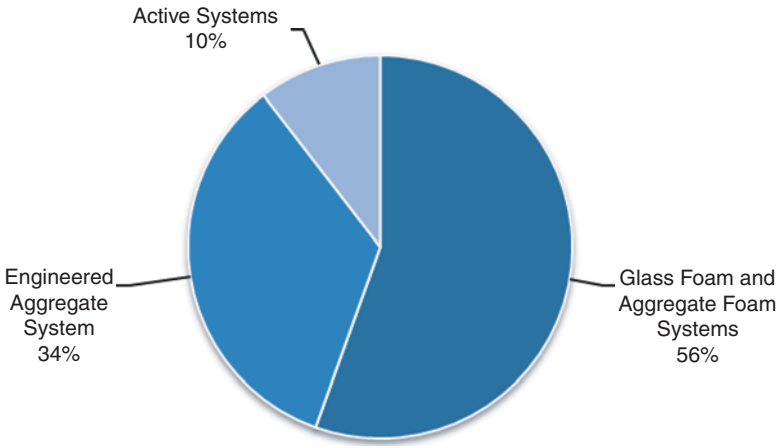


***Figure 8-1. Relative emphasis for different systems during experimentation phase.***

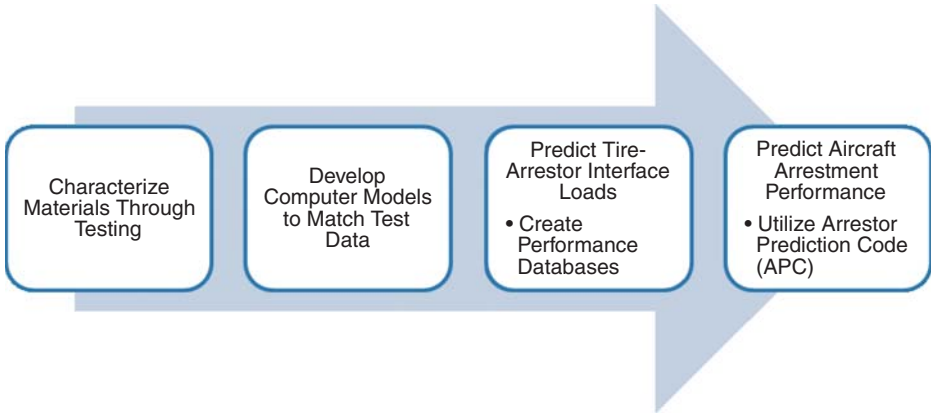


***Figure 8-2. Simplified diagram of modeling and testing approach.***

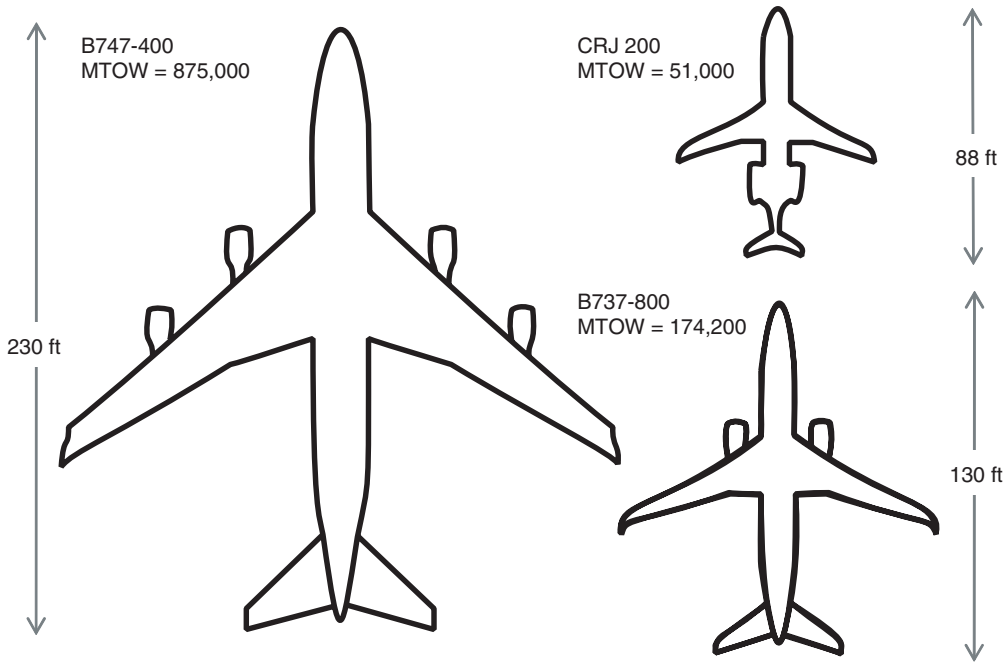


***Figure 8-3. Three evaluation aircraft for the effort. (MTOW = Minimum takeoff weight.)***

crushable concepts were discussed first, followed by the engineered aggregate and active systems.

However, in the detailed evaluation of the following chapters, the sequence is altered. The glass foam and engineered aggregate concepts are discussed first, in Chapters 9 and 10. These two candidates serve as bounding mechanical cases; prior discussion of these concepts simplifies the subsequent discussion of the aggregate foam concept. As such, aggregate foam is placed third (Chapter 11).

CHAPTER 9

# Glass Foam Arrestor Concept

## 9.1. Concept Description

### 9.1.1. System Overview

Glass foam is a crushable low-density material that has been proposed as an arrestor (Figure 9.1). The foam has a closed-cell microstructure that prevents water absorption and makes it an excellent thermal insulator. Glass foam has material properties that suggest excellent durability to the environment and good chemical resistance. Typically manufactured in solid blocks of various sizes, the foam can be cut into a variety of shapes for different applications.

Because both materials are low-density crushable foams, the glass foam material exhibited properties similar to cellular cement. However, glass foam in general appeared to be less fragile, easier to handle, and potentially more durable than the cellular cement. Additionally, adhesives and moisture sealants are available for glass foams that permit joining and weatherproofing.

Because the glass foam material is generally manufactured in blocks sized at approximately $24 \times 18 \times 6$ inches, two variants are possible (Figure 9-2):

1. **Block Method.** The block method would use 4-ft square blocks of the foam, analogous to the current EMAS construction approach. The blocks would be constructed by adhering multiple smaller blocks together, followed by the potential addition of top and/or bottom cap materials. The sides of the block could potentially be sprayed with a sealant to further weatherproof the blocks. These blocks would be transported to and installed at a runway in essentially the same manner as the current EMAS beds.
2. **Monolithic Method.** The monolithic method would be assembled on-site at the runway by stacking and gluing blocks into a single large structure. The final assembly would then be fitted with a continuous top cover layer composed of a roll/spray-on polymer. This layup would preclude the need for joint seams, sealants, and maintenance, which are required for the current EMAS design. Moisture sealing of the vertical sides of individual blocks would be unnecessary. Monolithic layups such as this have been used in building roof applications.

### 9.1.2. Performance Considerations

Because glass foam material is a lightweight crushable foam bearing many similarities to cellular cement, the list of performance considerations at the outset was relatively short. Issues for evaluation included:

- Compression performance of the material in terms of energy absorption and rebound characteristics,
- Required density/strength for effective arresting,
- Balance of compression and shear strengths of the material,
- Rate dependence of the material, and
- Durability to freeze–thaw exposure.

## 9.2. Testing and Modeling Approach

The goal for the performance evaluation was to perform testing that would allow calibration of high-accuracy computer models of the glass foam concept. The testing and modeling approach for the glass foam material was comprehensive in nature, and the final outcome was a well-calibrated numerical model for predicting arrestment loads.

The testing and modeling approach for the glass foam concept is illustrated by Figure 9-3. Five major stages are illustrated by the larger process bubbles of the chart:

1. **Arrestor Material Testing and Modeling.** Laboratory and pendulum testing generated test data, and computer models of the material were calibrated to match it.
2. **Tire Modeling.** Aircraft tire models for the three test aircraft were built and calibrated to match manufacturer performance specifications.

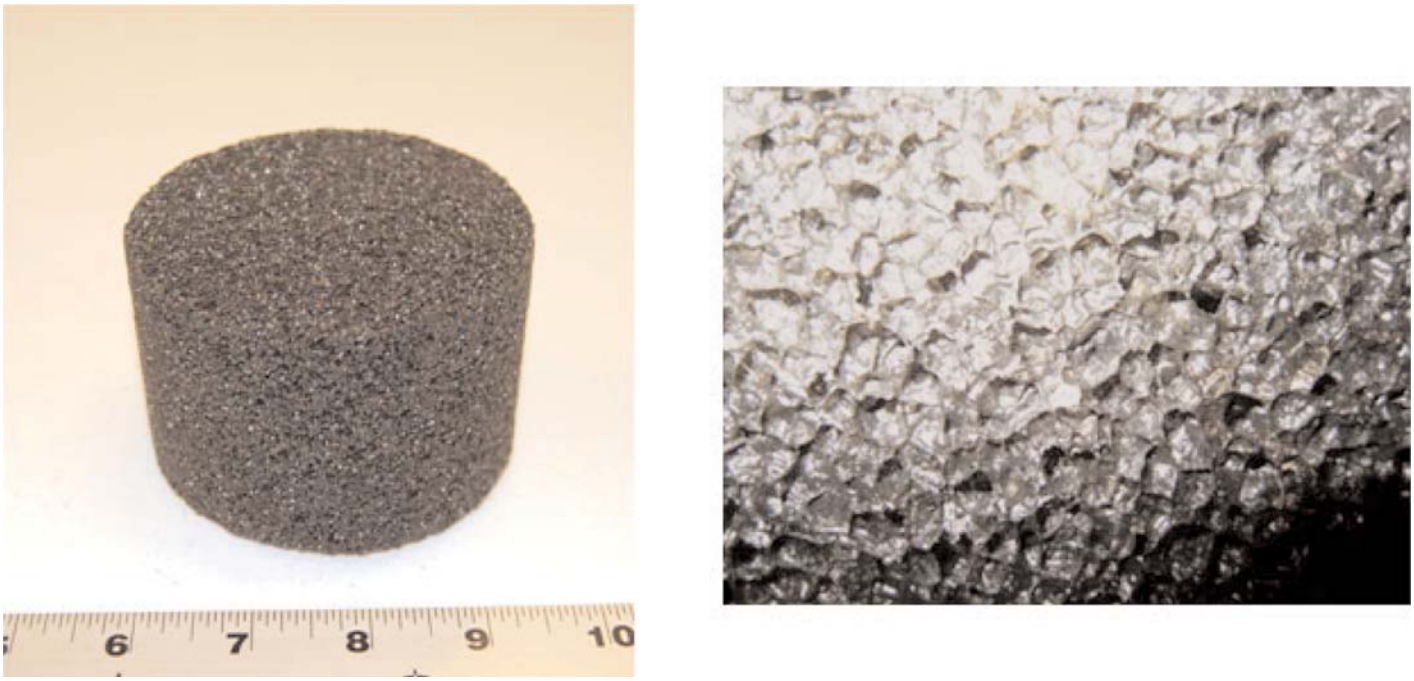


*Figure 9-1. Glass foam material: cylinder test specimen (left) and close-up of cellular microstructure (right).*

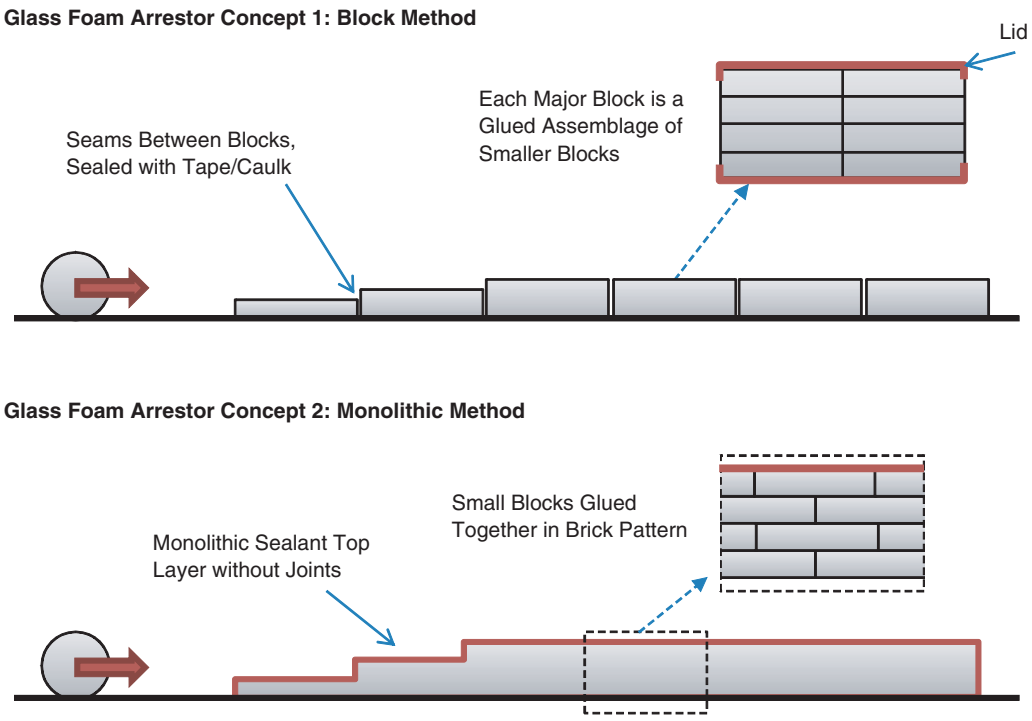


*Figure 9-2. Glass foam arrestor variants: block method (top) and monolithic method (bottom).*

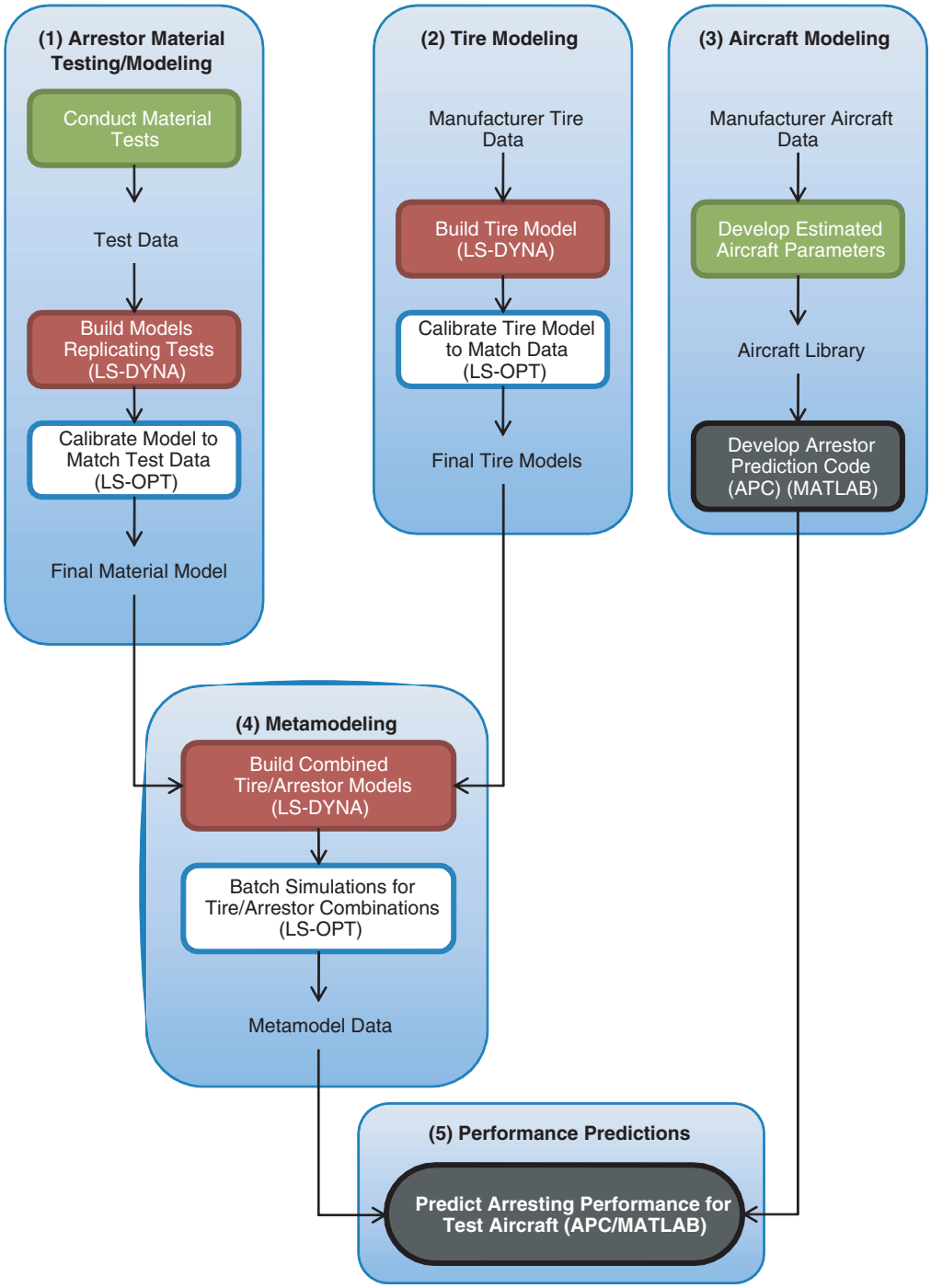


***Figure 9-3. Testing and modeling process for glass foam arrestor evaluation.***

3. **Aircraft Modeling.** A generalized aircraft model was developed to predict the suspension response of the plane and its deceleration during a ground roll. This model was then incorporated into an APC for determining stopping distances and landing gear loads when an aircraft is driven through an arrestor bed. A library of aircraft definitions was created to represent the three test aircraft.
4. **Metamodeling.** The arrestor material and tire models were combined to produce an overrun model for determining the loads exerted on the different aircraft tires by the arrestor bed. Large data sets were generated using simulation batches for each tire and arrestor combination. These data sets were then accessible by the arrestor prediction code (next step).
5. **Performance Predictions.** The preceding four development stages culminated in the final, bottom-most process on the figure. The APC was used to predict arresting distances, landing gear loads, and ideal arrestor bed designs for the different aircraft.

The subsequent sections of this chapter will focus on areas (1), (4), and (5). Specific attention will be given to the glass foam material testing that was conducted and the calibration of the computer models to match the tests. The development of the tire models (2) and aircraft model (3) will be reserved for Appendix F and Appendix G, respectively.

## 9.3. Testing Effort

The testing effort for the glass foam material involved an extensive battery of mechanical and environmental tests. Table 9-1 depicts the overall test matrix for the glass foam material.

All cylinder dimensions specify diameter followed by height. Conditioned specimens were environmental test specimens that were compression-tested following freeze–thaw exposure. These cylinders were only 2.5 in. tall to maintain the aspect ratio of prior "short" cylinder specimens. The specimen diameter was constrained by the environmental test apparatus.

### 9.3.1. Density and Dimension Measurements

Several densities of the glass foam material were examined. The higher density samples had higher compressive strengths. Preliminary screening indicated that the lowest density specimens, at nominally 6 pcf, were most promising for this application. The remainder of the testing discussion is confined to this density of the material. Specimens were obtained in cylindrical shapes with 3.65- and 5.625-in. diameters and larger $24 \times 18 \times 5$-in. blocks.

### 9.3.2. Platen Compression Tests

#### *9.3.2.1. Low Rate*

Platen compression tests were performed for the initial material density screening, enabling a rapid down-selection to the 6 pcf density as the most likely candidate. The platen compression tests further permitted the evaluation of the energy absorption capacity of the material and the effects of loading rate.

**Table 9-1. Test matrix for glass foam material.**

| Test | Properties Characterized | Detail | Number of Tests |
|---|---|---|---|
| **Laboratory Tests** | | | |
| Hydrostatic Triaxial Compression Test | • Compressive strength at failure ($\sigma_u$)<br>• Shear strength ($\tau_u$) | • Per ASTM D2850<br>• 3.65 x 8" cylinder<br>• 0.0592 in./min compression rate<br>• Maximum compression of 5 to 10%<br>• Confining pressures of 0, 5, 10, and 20 psi | 0 psi 1<br>5 psi 2<br>10 psi 2<br>20 psi 2<br>Total: 7 |
| Parallel Platen Compression Test | • Compressive strength at failure ($\sigma_u$)<br>• Compressive stress–strain curve<br>• Extrapolated: volumetric energy capacity<br>• Determined for different strain rates | • Version 1: low speed, tall<br>• Non-standard<br>• 3.65 x 8" cylinder<br>• 3 in./min compression rate<br>• Maximum compression of 85%<br>• Unconfined flat disk specimen compression | Fresh<br>Capped: 2<br>Uncapped: 3<br>Conditioned<br>Uncapped: 2 |
| | | • Version 2: low speed, short<br>• Non-standard<br>• 5.625 x 4" cylinder<br>• 3 in./min compression rate<br>• Maximum compression of 85% | Capped: 2<br>Uncapped: 3 |
| | | • Version 2: high speed, short<br>• Non-standard<br>• 5.625 x 4" cylinder<br>• 60 in./sec compression rate<br>• Maximum compression of 70% | Capped: 2<br>Uncapped: 3 |
| Punch Compression Test | • Combined compression and shear strain behavior<br>• Somewhat similar to EMAS material testing method | • Non-standard<br>• 5" thick material block<br>• 1.5" punch diameter<br>• 3 in./min compression rate<br>• Maximum compression of 70% | 5 |
| Environmental Chamber Tests | • Durability to freeze–thaw cycles<br>• Effectiveness of sealant treatments, where applicable | • Per ATSM C 666/C 666M-03 (modified)<br>• 3.65 x 2.5" cylinder<br>• 78 freeze-thaw cycles | 2 |
| **Pendulum Test** | | | |
| Pendulum One-Wheel Bogey Test | • Dynamic response for the material to a moderate-speed tire overrun characterized | • Non-standard<br>• 16.9 mph collision<br>• 24 x 18 x 5" blocks, glued into stacks | 2 |

*Figure 9-4. Low-rate uncapped platen test of glass foam pre-test (left) and post-test (right).*

Low-rate platen tests were conducted by placing a cylindrical specimen between two metal platens. The upper platen was then displaced downward at a fixed rate of 3 in. per minute until the specimen was fully compressed.

The platen tests were conducted with and without Sorbothane capping material on the top and bottom of the specimens to determine whether capping was beneficial or not. For the uncapped specimens, the material crushed in a localized failure zone immediately adjacent to the platen. These specimens maintained their shape throughout the duration of the loading up to the final 85% compression state, which aided in capturing the full energy absorption of the material (Figure 9-4).

When caps were used, the specimens tended to split along vertical planes, causing a shape change that often led to early terminations of the compression test (Figure 9-5). The uncapped approach was eventually favored due to its superior test repeatability and its ability to capture the full energy capacity of the material.

Tall and short cylinder specimens were tested for comparison with the hydrostatic triaxial tests, which used tall cylinders (3.65 × 8 in.), and the high-rate platen tests, which used short cylinders (5.625 × 4 in.).

The glass foam material exhibited a characteristic crushable foam load history that rose to a plateau value, where it remained until the material approached full compression (Figure 9-6). Near full compression, the material hardened and the loading increased. The stress–strain curve was integrated to produce the energy absorption curve shown in the figure. No measurable rebound occurred after compression.

#### *9.3.2.2. High Rate*

High-rate compression tests (60 in.-s) were conducted on short cylinders (5.625 × 4 in.) to evaluate the effects of rapid compression on the material. For a B747 main-gear tire travelling at 70 knots, the average vertical compression rate would be 40 in./(in.-s). The test produced an average strain rate of 150 in./(in.-s), which exceeds the overrun case by a substantial margin.

When comparing the high- and low-rate loading curves, only a minimal difference is observed, which could be due only to inertial effects of the material. Overall, the high-rate platen

***Figure 9-5. Mid-test splitting of low-rate capped platen test cylinder of glass foam.***

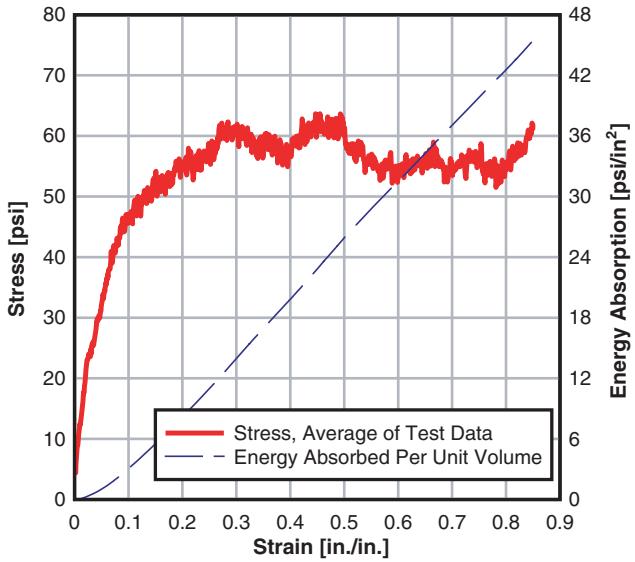


*Figure 9-6. Average load history for glass foam material from low-rate platen tests, tall specimen.*

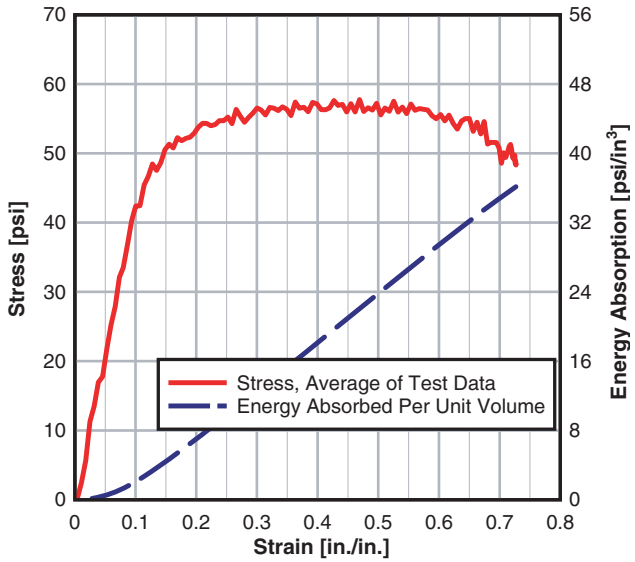


*Figure 9-7. Average load history for glass foam material from high-rate platen tests, short specimen.*

tests indicate that there is little to no practical rate effect in the material for the loading regimes of interest (Figure 9.7).

### 9.3.2.3. Hydrostatic Triaxial Tests

The hydrostatic triaxial tests evaluated the glass foam performance at different confining pressures to determine if any strength increase or bulking deformation took place. Neither was anticipated because the glass foam material behaved as a one-dimensional foam with little to no observed lateral bulking (low Poisson ratio).

The specimens were tall cylinders (3.65 × 8 in.) placed between platens using Sorbothane caps at the top and bottom (Figure 9-8, left). The specimens were fitted with flexible membrane sleeves before immersion in a pressurized vessel of water. While at this hydrostatic pressure, the specimens were compressed axially until failure.

As observed in the platen tests, the use of capping induced vertical failure plane formation in the specimen (Figure 9-8, right), which typically occurred at a compression displacement of about 5%. This failure load did show a mild dependence on

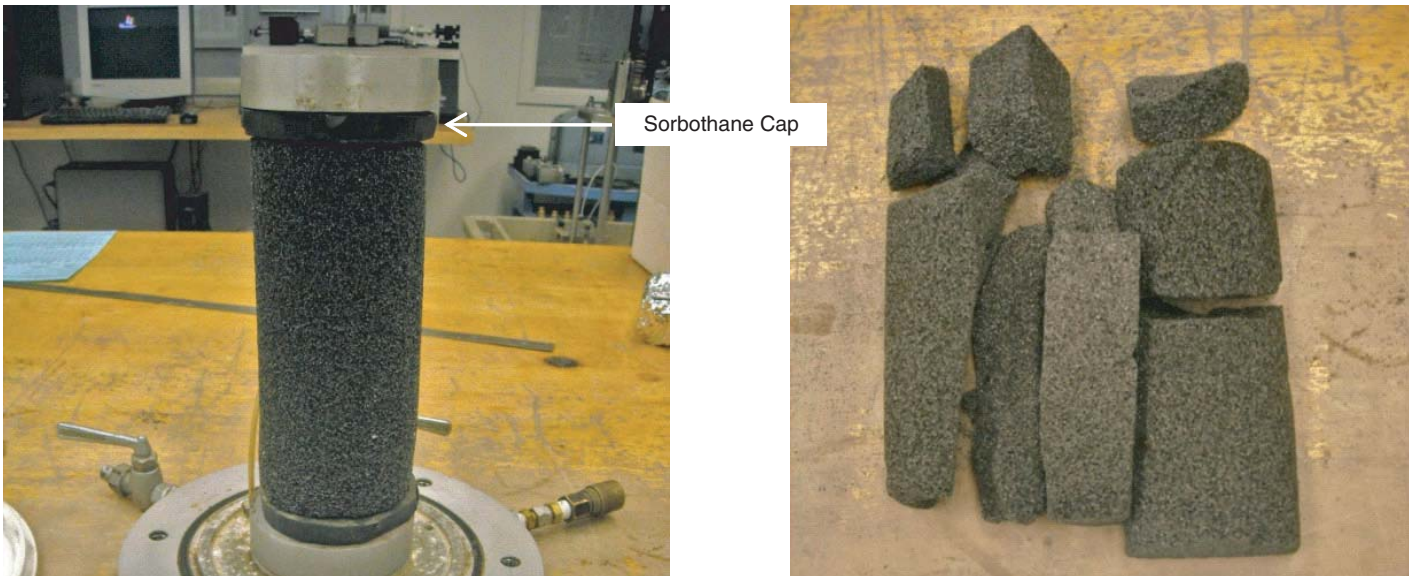


*Figure 9-8. Hydrostatic triaxial compression test of glass foam pre-test (left) and post-test (right).*

*Figure 9-9. Punch test of glass foam test specimen pre-test (left) and post-test (right).*

confinement pressure, though no bulking behaviors were observed.

### 9.3.3. Punch Tests

Punch tests were performed by pressing a 1.5-in. diameter, smooth-sided punch into a 5-in. thick block of the material (Figure 9-9). The glass foam material compressed cleanly, leaving a smooth-sided hole in the block. These tests were similar to the characterization tests performed by the current EMAS manufacturer (*34*). However, the tests differed with regard to the proportional aspect ratio of the punch, the punch shape, the specimen size, and the loading rate.

The resulting load was due to a combination of the compression strength of the material (area under the punch) and the shear strength of the material (circumferential edge of the punch). Figure 9-10 illustrates the averaged load history for the punch tests. As shown, the effective "pressure" on the

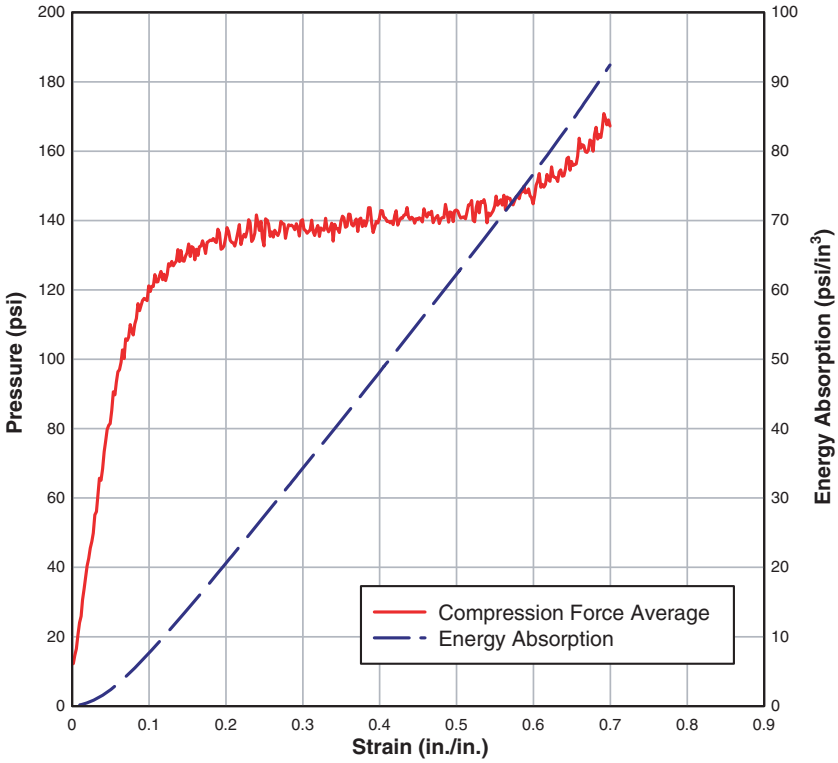


*Figure 9-10. Average load history for glass foam material from punch test with stress normalized for cross-sectional area of 1.5-in. diameter punch.*

punch was nominally 140 psi, which compares at 2.5 times the nominal 55 psi strength of the material exhibited in the platen tests (Figure 9-6). This increase in apparent strength is due to confinement and shear contributions. In arrestor applications, the shear strength of the material would be relevant along the vertical walls of the tire rut.

## 9.3.4. Pendulum Tests

### *9.3.4.1. Pendulum Apparatus*

In addition to the small-scale laboratory tests, a larger-scale one-wheel bogy test was conducted using a large pendulum test apparatus. The pendulum test apparatus featured a heavy 4,400-lb mass that hung from an overhead support frame, giving it a swing arc of 24.5 ft. The mass was hoisted to the desired height and then released; the speed of the mass was controlled by the release height.

The pendulum mass was fitted with a strut and wheel assembly, which Figure 9-11 illustrates in an exploded view. The strut was instrumented with three load cells that measured loads at the connections. These three connection loads were resolved into orthogonal vertical and drag loads on the strut and wheel assembly.

To reduce the number of variables in the design, a rigid aluminum wheel form was used rather than a pneumatic tire. The diameter and width were 14.8 and 5.5 in., respectively. These proportions were based on a nominal one-third scale B737-800 main-gear tire, which has a diameter and width of 44.5 and 16.5 in., respectively.

### *9.3.4.2. Glass foam retention box.*

Below the pendulum assembly, a box was constructed to retain larger blocks of the glass foam, which each measured $24 \times 18 \times 5$ in. The blocks were arranged in one row, 6 blocks long and 2 blocks in depth, for a total of 12 blocks. The overall dimensions were 9 ft in length, 2 ft in width, and 10 in. in height. The upper and lower blocks were glued in 6 pairs, which were placed in the retention box and held in place by an upper cap rail around the perimeter. The block pairs were not adhered to one another. Figure 9-12 shows the overall pendulum apparatus with the glass foam blocks beneath it.

### *9.3.4.3. Tests Executed*

For the tests, the pendulum was set to swing such that the wheel penetrated to a depth of nominally one-third diameter, or 5.0 in. One swing height was used to produce an average overrun speed of 16.9 mph. Due to the single-use nature of the material and the limited supply of evaluation samples, two tests were conducted for these conditions. Both tests gave consistent results.

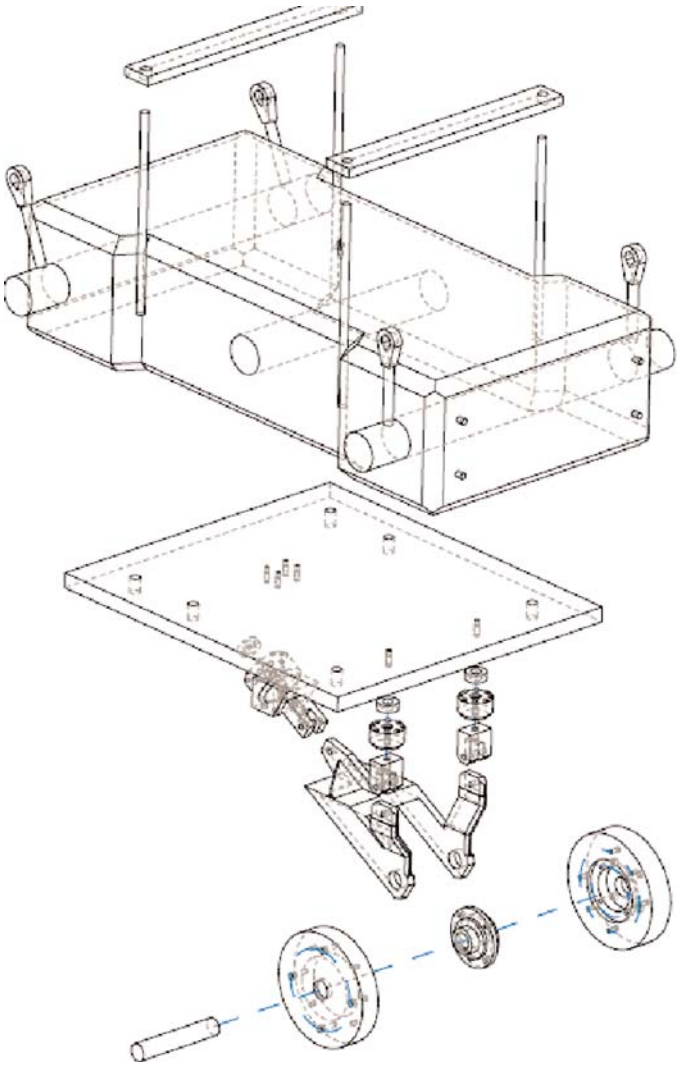

***Figure 9-11. Pendulum test device with one-wheel bogy.***

Figure 9-13 shows the rut created through the material by the strut and wheel of the pendulum; the wheel cut a clean path through the material, leaving the RG-1 material adjacent to the rut essentially undamaged. This behavior was consistent with expectations based on the small-scale testing.

### *9.3.4.4. Landing Gear Loads*

The loading history for the pendulum strut showed oscillations in both the drag and vertical loads (Figure 9-14). It is believed that these pulses were caused by the seams between the block pairs in the bed. As the wheel approached the end of a block, the load decreased; when the wheel began to overrun the next block, the load increased. Since the blocks were not glued at the seams, these joints presented a discontinuity in the material. The pulsing effect was further amplified by the


*Figure 9-12. Overview of pendulum test setup for glass foam.*

*Figure 9-13. Post-test results from pendulum test for glass foam.*

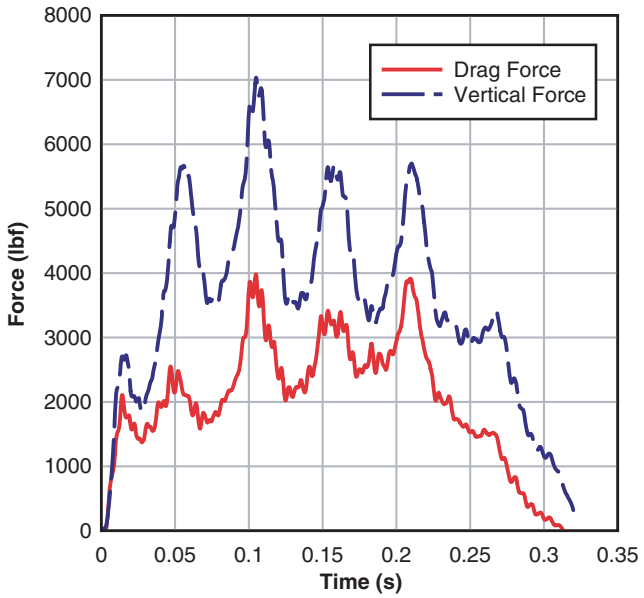


***Figure 9-14. Loading history for glass foam pendulum test.***

rigid wheel used in the strut assembly, which prevented natural smoothing that might result with a pneumatic tire.

In arrestor applications, the severity of the loading pulses depends on several variables:

- Relative compressive strength of the material,
- Flexibility of the pneumatic aircraft tire,
- Relative penetration depth of the tire, and
- Glued or non-glued approach to joints in the material.

In applications involving a flexible tire, or where the blocks are glued at all joints, the loading pulses are expected to smooth substantially. However, the appearance of these pulses generated questions regarding the feasibility of using separate blocks of the material in an analogous manner to the current approach for EMAS. Whether or not these pulses would occur during overruns into the existing EMAS beds is unclear. The nature of the pulses suggests that an arrestor design using a foam block material should explicitly include this seam effect; it is not sufficient to make a general assumption that separate blocks essentially give the same loading as a continuous bed of the material.

### 9.3.5. Environmental Tests

A basic set of environmental tests was conducted to determine the necessity for weatherproofing the glass foam material. Two 3.65 × 2.5-in. cylinders were subjected to fully immersed freeze–thaw testing, per ATSM C 666/C 666M-03. The specimens were subjected to 78 freeze–thaw cycles, during which they absorbed water and partially eroded (Figure 9-15).

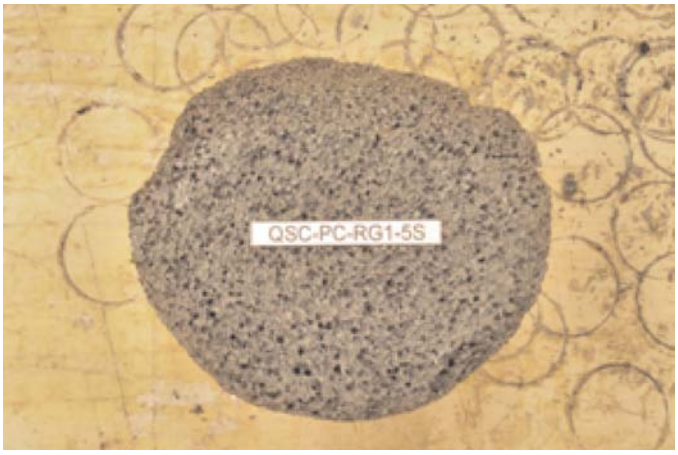


***Figure 9-15. Glass foam specimen after environmental freeze–thaw testing.***

(Standardized testing generally uses 300 freeze–thaw cycles. Due to the test duration required, this was abbreviated to a planned 50 cycles for this effort. An unplanned cycling overrun at the test facility resulted in a total of 78 cycles.)

Following the environmental tests, the specimens were subjected to a low-speed platen compression test (Figure 9-16) to determine the performance degradation. When compared with the fresh material, the samples exhibited a 60% decrease in energy absorption capacity and compression strength.

Mechanically, the closed cell foam limits water absorption, such that water penetrates only the outer-most open pores of the foam. Upon freezing, the expanding water cracks the cells, permitting progressively deeper penetration into the specimen as the cyclical testing proceeds. The degradation observed is, therefore, not surprising.

These environmental tests represent the most severe of circumstances, where the specimens are fully immersed in water, without normal countermeasures of drainage, protective packaging, or sealants. Information provided by the manufacturer indicates that cyclical temperature and humidity do not degrade the material over time, and a number of sealants are available to prevent water absorption, if required.

Overall, these tests indicate that the glass foam material should be protected from immersion conditions caused by standing water, as is done for the current cellular cement material. Additional testing could be conducted to characterize durability in non-immersion scenarios, or in immersion conditions where a sealant has been applied to the material.

## 9.4. Modeling Effort

The modeling effort involved several stages, as shown previously in the flowchart of Figure 9-3. A high-fidelity model for the glass foam material was calibrated to match the test data (Figure 9-3, block 1). Using this material model, an arrestor

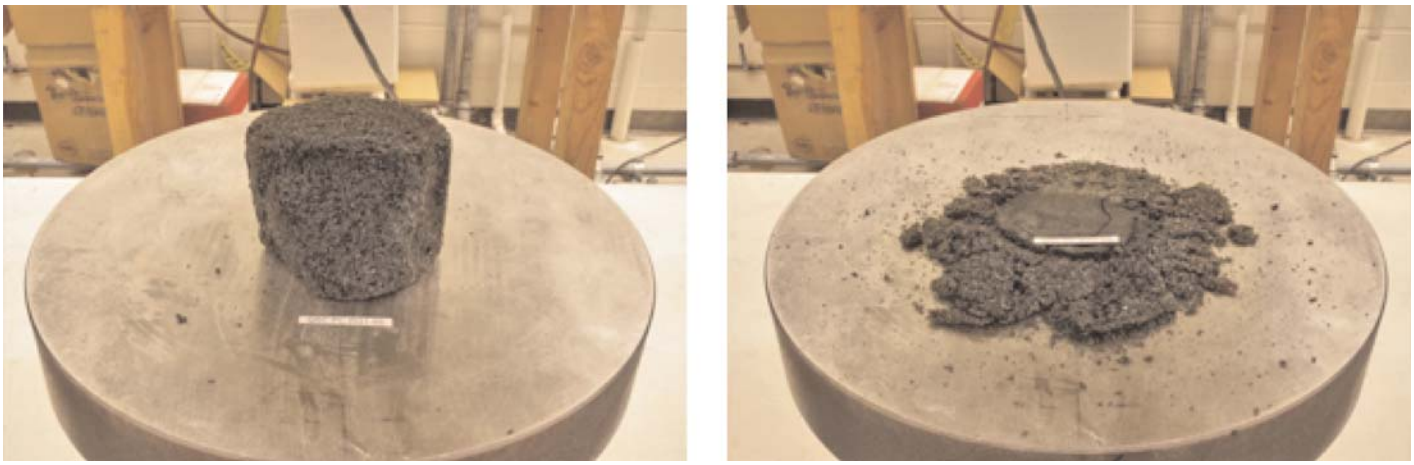

*Figure 9-16. Platen testing of glass foam environmental test specimen.*

bed model was constructed and coupled with tire models for the different aircraft (Figure 9-3, block 4). Finally, large batches of simulations were conducted using these paired models, which generated volumes of data for use by the APC (also block 4).

This section will discuss the arrestor model development and batch simulation process. Performance predictions for the glass foam arrestor concept are reserved for the following section (9.5).

### 9.4.1. Smoothed Particle Hydrodynamics (SPH) Formulation

The glass foam arrestor models were developed in LS-DYNA, a general-purpose finite element modeling code. Within LS-DYNA, a number of formulations exist for representing solids and fluids. Due to the high compressibility of the glass foam material, an SPH mesh-free formulation was employed. SPH offered the ability to represent high-dislocation solids with accuracy while maintaining time-efficient simulations.

Because SPH uses particles instead of the more typical finite elements, the illustrations in this section depict the material as a collection of small spheres. These particles are not disjointed pieces of aggregate, but are instead mathematically interconnected to represent a continuous solid material (Lagrangian formulation).

### 9.4.2. Calibration to Physical Tests

#### *9.4.2.1. Constitutive Model*

LS-DYNA currently offers about 200 constitutive models; of these, about 18 are applicable to various foams. Based on prior experience and on a review of the LS-DYNA keyword manual, several candidates were singled out for evaluation. After some experimentation, *MAT_CRUSHABLE_FOAM was selected as the best overall choice. This material model has parameters as given by Table 9-2. The calibration process required defining these material parameters such that the model performance matched that of the physical material tests.

#### *9.4.2.2. Multi-Tester Model*

A multi-tester model was constructed to simultaneously replicate the four laboratory material tests (Figure 9-17). The material parameters of the multi-tester model were optimized using LS-OPT, an optimization software package. LS-OPT ran the simulations in batches iteratively; after each iteration, it narrowed the region of interest, effectively zooming in closer to the predicted optimum calibration point. After 8 iterations of 12 simulations each, the design was optimized for a best-fit set of material parameters.

Table 9-3 gives a summary of the calibration process, including the final accuracy of the calibrated model. Test metrics marked with an asterisk were optimization criteria, which LS-OPT attempted to minimize. The remaining metrics were measured, but did not act as optimization criteria.

Of the various metrics given, the energy absorption values were the most critical to match accurately. As shown, all energy

**Table 9-2. Parameters for *MAT_063 or *MAT_CRUSHABLE_FOAM.**

| Parameter | Symbol | Description |
|---|---|---|
| **MID** | | Material ID number |
| **RO** | $\rho$ | Density |
| **E** | $E$ | Young's modulus |
| **PR** | $\nu$ | Poisson's ratio |
| **LCID** | | Load curve ID for nominal stress versus strain |
| **TSC** | | Tensile stress cutoff |
| **DAMP** | | Rate sensitivity via damping coefficient |

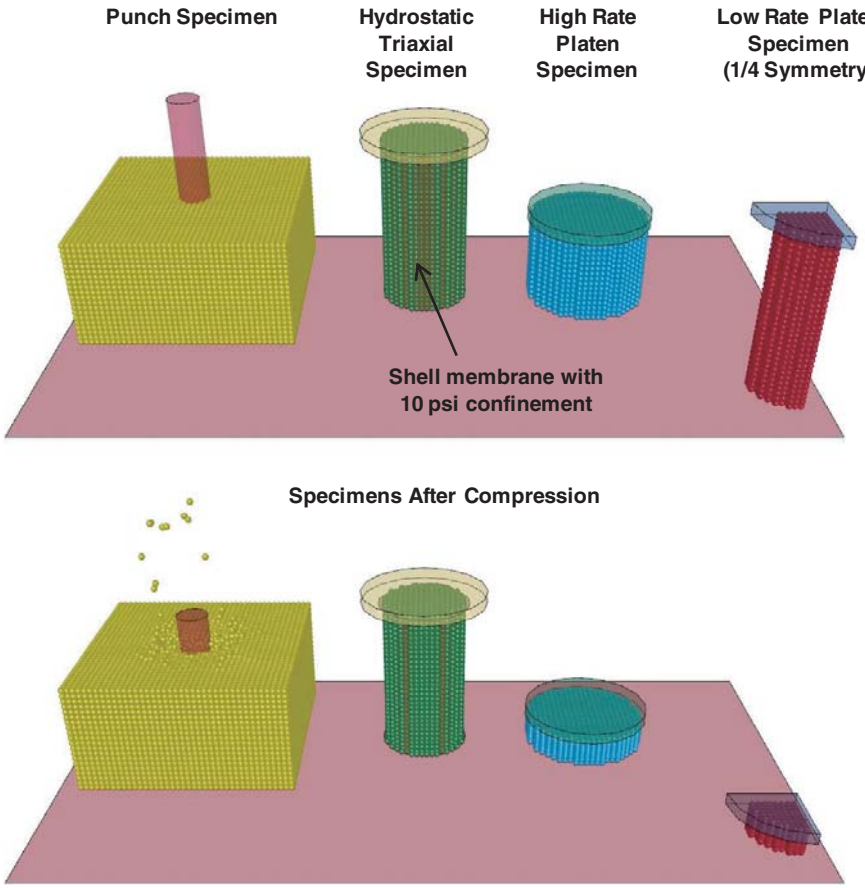


*Figure 9-17. Multi-tester model for glass foam material calibration.*

**Table 9-3. Multi-tester specifications for glass foam material calibration.**

| Test to Replicate | Description | Accuracy of Calibration |
|---|---|---|
| **Low-Speed Platen Test** | • 3.65 x 8-in. cylinder | |
| | • Match stress–strain load curve with root-mean-squared error (RMSE) to 85% compression* | *7.0%* |
| | • Match energy absorption at 85% compression* | **5.0%** |
| **High-Speed Platen Test** | • 5.625 x 4-in. cylinder | |
| | • Match stress–strain load curve with RMSE to 50% compression* | *17.7%* |
| | • Match energy absorption at 50% compression* | **2.9%** |
| **Hydrostatic Triaxial Test** | • 3.65 x 8-in. cylinder | |
| | • 10 psi hydrostatic pressure | |
| | • Match stress at 5% compression | *19%* |
| **Punch Test** | • Large block | |
| | • Match stress–strain load curve with RMSE to 70% compression | *8.4%* |
| | • Match energy absorption at 70% compression | **1.2%** |

metrics were within 5% of the actual test values. The matching of the stress–strain load curves proved less consistent, which was expected since those curves tended to vary among the test specimens as well.

The hydrostatic triaxial specimens proved somewhat difficult to calibrate due to a nuance of the SPH formulation, which proved challenging to fit with a hydrostatic membrane load. Since the glass foam material exhibited little pressure dependence in testing, this was deemed a low-priority calibration point.

#### *9.4.2.3. Pendulum Model*

Using LS-DYNA, a model was constructed to replicate the pendulum tests (Figure 9-18). Because the material had been well-calibrated via the multi-tester, the pendulum model was used for validation of the material model, rather than for calibration. The pendulum strut was omitted because the penetrate depth of the actual test only allowed the wheel to contact the glass foam material. The foam bed was constructed with half-symmetry, such that it measured 9 ft in length, 1 ft in width, and 10 in. in depth. The bottom and outer sides of the bed were constrained to simulate the presence of the confining box.

The wheel followed an arced path approximating that of the actual strut, with the same ⅓-diameter penetration depth into the arrestor bed. The wheel began with no rotation and was allowed to freely spin upon contact with the arrestor bed, just as in the actual test (Figure 9-19).

The SPH particles were sized to 0.75 in., which was based on particle size scaling relationships developed in other simulation sets to maintain reasonable accuracy. This provided four particles across the half-width of the wheel, which was the smallest characteristic length of the interface. A separate particle size convergence study was not undertaken for this model.

The resulting loads matched the test data well, though no pulses were observed due to the lack of material seams in the model (Figure 9-20). The average drag and vertical loads were within 6% and 1% of the average test results, respectively. Since the test data showed a 6 to 10% variation for these two metrics, the model is within the experimental data scatter.

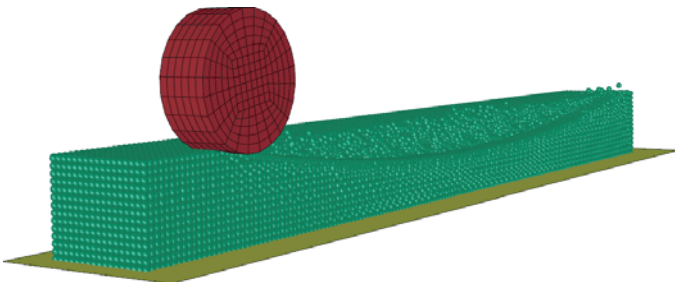

***Figure 9-18. Overview of glass foam pendulum model.***

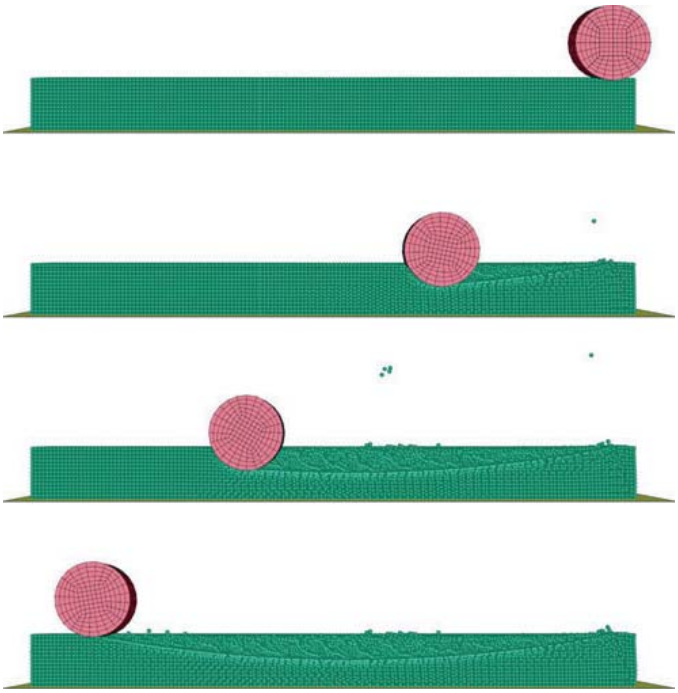

***Figure 9-19. Action sequence from glass foam pendulum model.***

Overall, the pendulum model validated that the glass foam material was well calibrated.

### 9.4.3. Tire and Arrestor Simulations

Using the calibrated glass foam material model previously described (Section 9.4.2), a large-scale arrestor model was created in LS-DYNA to simulate overruns by aircraft tires. No

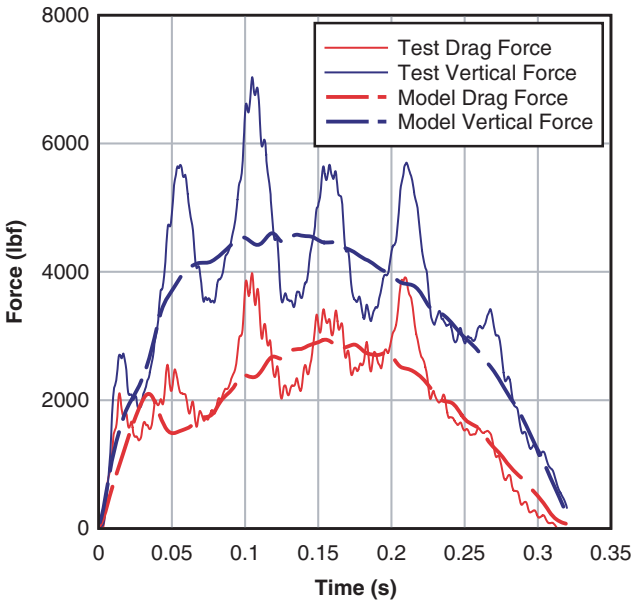


***Figure 9-20. Comparison of test and model load histories for glass foam pendulum test.***

protective cover layer for the bed was included in the model; it was assumed that a well-designed cover layer (likely made of thin plastic or a spray-on polymer) should have minimal impact on the mechanical response. The model further assumed a continuous material, and material seams were not included. Figure 9-21 illustrates the model with a 36-in. depth and a B737-800 main-gear tire (Goodyear H44.5 × 16.5) at 50% penetration depth.

### *9.4.3.1. Arrestor Bed Models*

The arrestor bed models were constructed using half-symmetry to reduce computation time. They varied in size depending on the aircraft tire being used. The bed length was determined by the distance required for the tire to make a certain number of rotations such that the loading settled to a steady-state condition. The bed width was determined by the tire width such that artificial boundary effects were minimal and the response approximated that of a wide bed of the material. The smallest bed, used for the 18-in. nose tire of the CRJ-200, was 120 in. long and 9 in. wide. The largest bed, used for the 49-in. main tire of the B747-400, was 225 in. long and 36 in. wide.

All beds were constructed with a 36-in. depth. However, the effective depth of the bed was adjusted by use of a movable rigid plane (Figure 9-22). Only the upper part of the material, above the rigid plane, was involved in the overrun compression. This approach enabled various depths to be rapidly configured within a single arrestor bed model.

SPH particle sizes were chosen based on the tire size. An error estimation process was undertaken to determine the required particle size to maintain an acceptably low discretization error. For the larger tires, a 2 in. particle size was found to have less than a 4% error for the predicted drag and vertical loads. For smaller tires, the particle size was reduced to 1 in. to maintain similar size proportionality. Based on the particle and bed size variations, a typical bed model had nominally 45K particles.

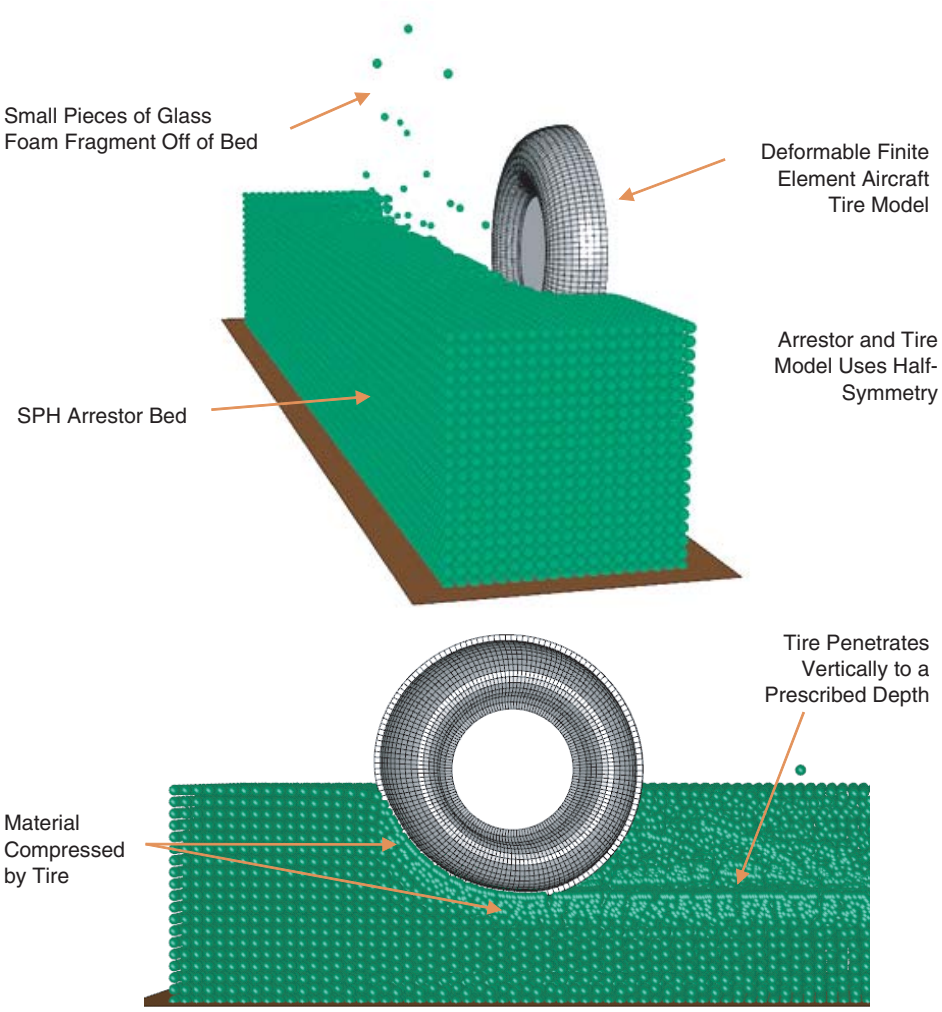


***Figure 9-21. Model of combined tire and glass foam arrestor system.***


***Figure 9-22. Adjustable height of glass foam arrestor bed.***

### *9.4.3.2. Tire Models*

The tire models were fully deformable finite element models (FEM), as discussed in Appendix F. Table 9-4 summarizes the tire models developed. Each tire model was calibrated to match the actual tire's load-deflection performance up to 80% of the maximum bottoming load. This 80% load became a limit criterion during the batch simulations.

The deformable nature of the tires produced an accurate representation of the interface between the tire and the arrestor material. As the load on the tire increased due to deeper bed penetration, the contact area became flatter with an increased surface area. This shape change created a corresponding increase in the load on the tire.

### *9.4.3.3. Sequencing of Simulations*

Because the tires in the LS-DYNA simulations were deformable and were allowed to spin freely, a sequencing method was required to create stable, fast-running simulations. These two factors were additional complications that were not present in the EDEM software package aggregate simulations. However, the inclusion of these factors led to higher-fidelity results.

From a mechanical standpoint, as the axle of the wheel penetrated the bed vertically, both the tire and the arrestor material underwent compression. The interplay of the tire and arrestor compression created oscillations in the measured loads. This oscillating behavior was further amplified by the free-spinning nature of the tire. Eventually the tire would settle to a constant rate of rotation, which proved to be a function of the forward speed, depth, and interface friction. It was found that a minimum forward travel distance was required for the loads and rotation to reach steady-state conditions before load measurements could be made.

Sequencing options included several factors:

- Prescribed vertical penetrations versus prescribed vertical loads,
- Applying the vertical penetration/load before or after beginning the forward motion, and
- Applying the forward motion before or after making contact with the bed.

Depending on the sequencing method used to accelerate the tire and set the penetration depth, the initial oscillations could be more or less severe. This in turn could require longer or shorter simulation times and longer or shorter arrestor beds. Because the arrestor–tire models were to be run repeatedly in large batches, it was important to develop a sequencing methodology that would produce efficient simulation run times.

Multiple methods were attempted through experimentation before settling on the approach illustrated by Figure 9-23. The tire was first pressed downward into the material to a prescribed depth. Then the tire was accelerated to the desired forward speed and spun-up to an initial rotation speed (typically about one-third of the ideal rotation rate expected on hard pavement). The prescribed spin rate was then released, allowing the tire to settle to a natural rotation rate, while the forward motion continued at a constant speed. After the oscillations settled out of the system, the steady-state vertical and drag loads were measured.

The final result was an accurate prediction of the loads on the tire under free-spinning un-braked conditions.

**Table 9-4. FEM tire library for glass foam arrestor models.**

| Aircraft | Landing Gear | Tire Designation |
|---|---|---|
| CRJ-200 | Main Gear | H29x9.0-15 |
| | Nose Gear | R18x4.4 |
| B737-800 | Main Gear | H44.5x16.5-21 |
| | Nose Gear | H27x7.7-15 |
| B747-400 | Main Gear | H49x19-22 |
| | Nose Gear | H49x19-22 |

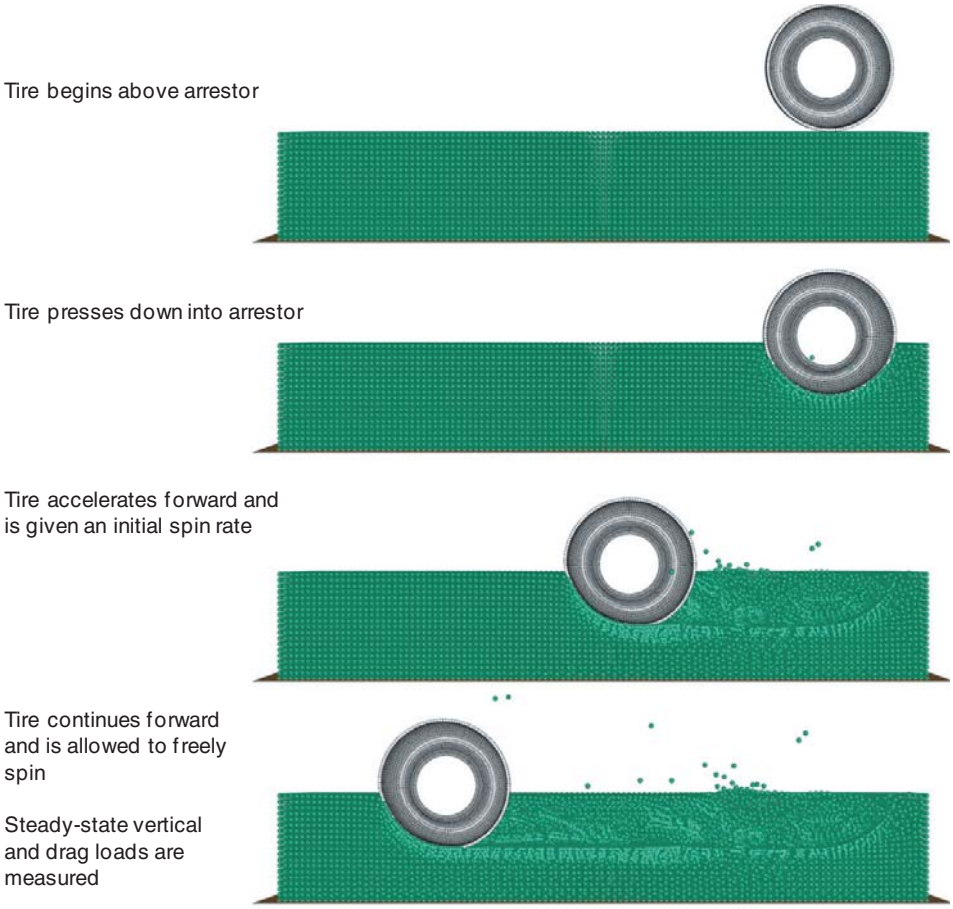


*Figure 9-23. Sequencing method for glass foam arrestor model.*

### 9.4.4. Batch Simulations

Using the arrestor bed model, large batches of simulations were conducted to generate substantial bodies of data for a wide range of overrun conditions. This data was then assembled into "metamodels" for uploading and use by the APC.

#### *9.4.4.1. Methodology*

Batch simulations were conducted for each tire with three open variables:

- **Speed,** from 10 to 70 knots (Speeds below 10 knots were impractical due to the long simulation times required for a tire to travel the required minimum distance. Loading at speeds below 10 knots was based on the extrapolated metamodel data fit.);
- **Bed depth,** in incremental depths from 3 to 36 in. (Figure 9-24); and
- **Penetration** into the bed, from 10% to 100% of maximum penetration depth.

Due to the two sources of compression (arrestor material and tire), the definition for penetration depth was more complex than for the rigid tire approach used for the aggregate arrestor models. Two conditions defined the maximum penetration depth:

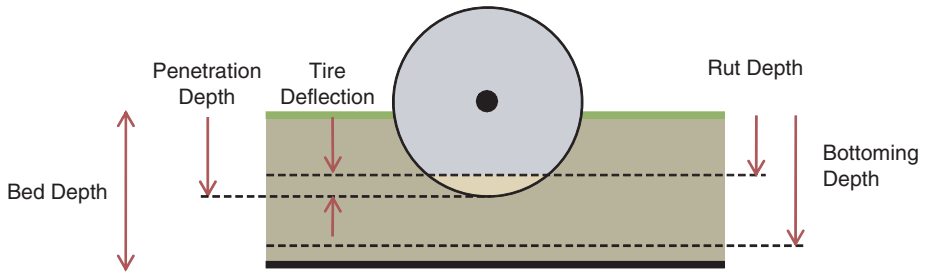


*Figure 9-24. Depth definitions for glass foam bed models.*

1. The maximum penetration depth was considered to be 85% of the bed depth (fully compressed material) plus the deflection of the tire at 80% of the bottoming load. Beyond this degree of penetration, the tire models were no longer accurate.
2. For small tires in deep beds, the maximum penetration was further limited to be no greater than the tire diameter. At depths beyond this, the simulations often did not settle to steady-state conditions. (This depth issue ultimately proved irrelevant, since most functional arrestor bed designs generated with the APC did not use bed depths that were greater than the tire diameter.)

The large batch simulations were conducted using LS-OPT. Based on the initial model files, LS-OPT generated permutations with various speeds, bed depths, and penetration levels. It sequentially executed the simulations and extracted the load data from them. Generally, the batches were conducted in multiple iterations of 10 simulations each. Additional iterations were added to improve accuracy as needed.

#### *9.4.4.2. Summary Tables of Metamodels*

The output from the batch simulations was extracted and assembled automatically by LS-OPT, where metamodels were constructed for the drag and vertical load forces. Metamodeling is analogous to fitting a curve through experimental data, except it is applied to multi-dimensional data sets. These data sets were four-dimensional, including speed, depth, penetration, and load (either vertical or drag). The metamodels were radial basis function (RBF) networks, which can effectively capture non-linear behaviors including multiple concavity changes across the data set.

Table 9-5 summarizes the fit quality for the metamodels. The root-mean-squared (RMS) error was typically below 5%, and the R-squared value was typically above 0.98, indicating good fit quality with minimal noise.

As the table shows, the points used in the metamodels were often less than the total number of simulations conducted. This discrepancy was caused by simulations that failed prior to termination due to tire overloading, or simulations that had not adequately settled to steady-state conditions for accurate load measurement. The smaller tires experienced a greater percentage of omitted runs than the larger tires due to the relative loading severity and greater proportional penetration depths.

#### *9.4.4.3. Parameter Sensitivities*

Using the metamodels, it is possible to review how sensitive the landing gear loads are to the different variables of speed, bed depth, and penetration percentage. Figure 9-25 shows a surface plot for the 44.5-in. main-gear tire of the B737 in an 18-in. deep glass foam arrestor bed.

Stronger drag loads (shown as the lower, more negative values) occur when the penetration ratio increases, up to the maximum of 1.0 (or 100%). The loading is, therefore, strongly dependent on the depth of penetration into the bed, as would be expected.

By contrast, the variation with speed shows very little change between 10 and 70 knots. The loading is fairly insensitive to speed, reflecting the low rate-sensitivity that was exhibited during the small-scale lab testing. Practically speaking, this means that the glass foam system will exert nearly the same deceleration load on an aircraft travelling at high or low speed. This behavior is desirable for an arrestor and is consistent with the general behavior of the current EMAS material.

#### *9.4.4.4. Data Transformation*

The final metamodel data for each tire was converted for use by the APC. LS-OPT was used to extract nominally 9,000 data points from each metamodel and export it into tabular form.

**Table 9-5. Metamodel accuracy summary for glass foam arrestor bed.**

| Tire | Simulations Conducted | Points Used | Response | RMS Error | $R^2$ |
|---|---|---|---|---|---|
| H49 | 49 | 49 | Drag | 2.35% | 0.999 |
| | | | Vertical | 5.25% | 0.988 |
| H44 | 70 | 67 | Drag | 2.78% | 0.999 |
| | | | Vertical | 1.08% | 0.999 |
| H29 | 60 | 60 | Drag | 2.78% | 0.998 |
| | | | Vertical | 4.88% | 0.986 |
| R27 | 60 | 47 | Drag | 3.21% | 0.998 |
| | | | Vertical | 5.06% | 0.982 |
| H18 | 100 | 86 | Drag | 3.74% | 0.995 |
| | | | Vertical | 5.83% | 0.969 |

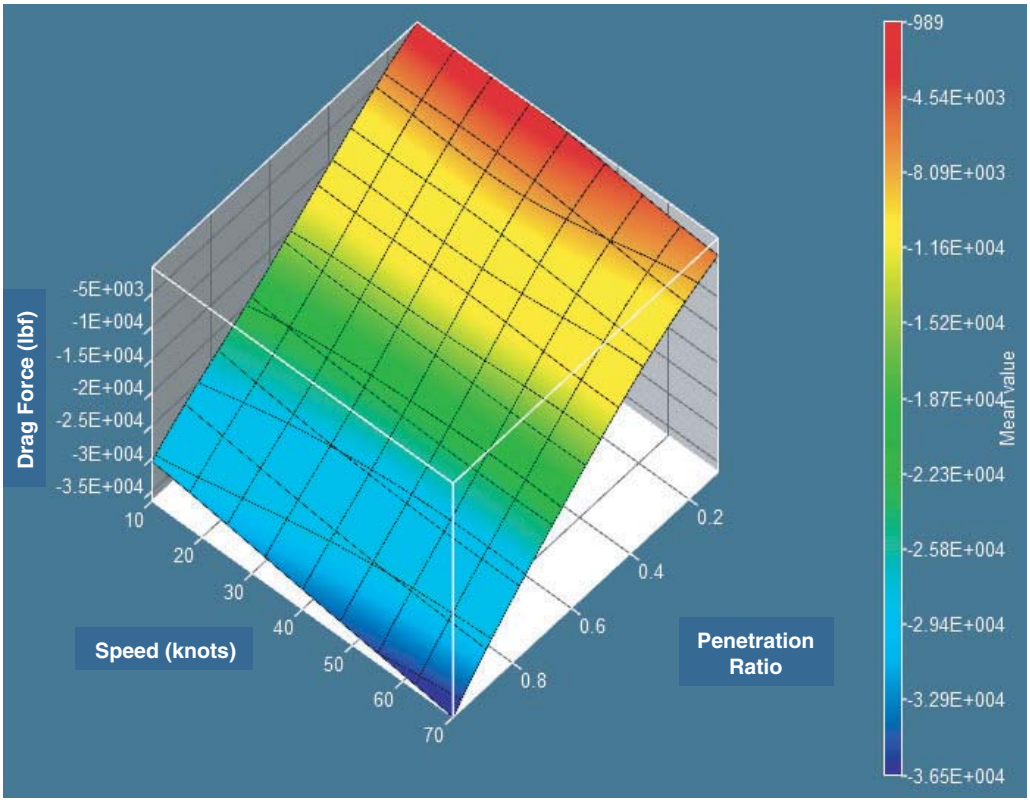


***Figure 9-25. Metamodel drag load surface plot for 44.5-in. tire in an 18-in. deep arrestor/turf bed.***

A MATLAB conversion program was written to map this data into multi-dimensional matrix form that could be quickly accessed by the APC.

## 9.5. Arrestor Performance Predictions

### 9.5.1. Scope of Simulations

Using the APC, a separate optimal arrestor was designed for each of the three trial aircraft: CRJ-200, B737-800, and B747-400. Subsequently, an optimal mixed-fleet arrestor was designed as a compromise best-fit for all three aircraft.

All arrestment predictions assumed the following:

- 50-ft setback distance,
- 50-ft gradual decline to the maximum bed depth,
- 70-knot starting speed for the aircraft,
- No reverse thrust,
- Braking factor of 0.25 before and within the bed,
- Cover layer had negligible effect,
- Material had no seams (Section 9.4.3), and
- Arrestor bed loads based on interaction with tires, neglecting strut and axle components.

Arrestor beds were designed for two different nose-gear loading criteria:

1. **Limit Load Criterion,** where the drag load applied to the nose strut cannot exceed the limit load for the nose gear (FAR Part 25.509);
2. **Ultimate Load Criterion,** where the drag load applied to the nose strut cannot exceed the ultimate load for the nose gear.

Since the ultimate loading criterion permits higher loads on the strut, deeper beds and shorter stopping distances resulted from those cases.

It was determined through experimentation that the glass foam arrestor design functioned best as a partially recessed bed, such that the fully crushed material depth was level with the runway. This left 85% of the bed thickness above grade, and 15% below grade. This approach produced the smoothest landing gear loads by limiting the effective step-up or step-down that the aircraft experienced upon entering the bed.

Two design variables were considered for the aircraft: the bed depth and the material strength. The material strength was adjusted by applying a scale factor to the metamodel loading data in the APC during a simulation. It was considered as an

**Table 9-6. Individual aircraft 70-knot arrestor beds for glass foam arrestor system.**

| | Nose-Gear Limit Load Criterion | | | Nose-Gear Ultimate Load Criterion | | | Current EMAS, Optimal Designs | |
|---|---|---|---|---|---|---|---|---|
| Aircraft | Strength (psi) | Depth (in.) | Bed Length (ft) | Strength (psi) | Depth (in.) | Bed Length (ft) | Depth (in.) | Bed Length (ft) |
| CRJ-200 | 17 | 20.0 | 294 | 25 | 19.9 | 243 | 22 | 258 |
| B737-800 | 15 | 25.6 | 388 | 20 | 30.0 | 302 | 22 | 287 |
| B747-400 | 47 | 36.0 | 409 | 53 | 36.0 | 406 | 28 | 495 |

open variable because the glass foam can be manufactured at a variety of strength levels (varying density).

## 9.5.2. Performance for Test Aircraft

Table 9-6 lists best-case arrestor designs for each aircraft taken individually. Each arrestor bed listed uses a different material strength and depth that are optimized for the design aircraft. Generally, a range of acceptable strength and depth combinations was available. Compared with the similar EMAS design cases on the right (provided by ESCO), the distances are comparable if the ultimate loading criterion is used.

Table 9-7 shows the compromise design case with the best arrestor design for all three aircraft. The CRJ-200 limits the bed depth in this case, while the B737 controls the bed length. With the material strength and depth as specified, the B747 would require 840 ft to decelerate from 70 knots. Since this is longer than a standard RSA, it is highly impractical. Per typical practice for EMAS design, the bed length may be specified such that all aircraft satisfy the minimum 40-knot exit speed requirement. The bed designs in the table assume a 400 ft length, which is sufficient to arrest the two smaller aircraft with 70-knot exit speeds. At this length, the B747-400 would have a maximum exit speed of approximately 46 knots, which satisfies the requirements of AC 150-5220-22a.

**Table 9-7. Fleet design arrestor bed for glass foam arrestor system.**

| | Nose-Gear Ultimate Load Criterion | |
|---|---|---|
| Bed Dimensions | 26 psi material<br>19.1 in. depth<br>400 ft long | |
| Aircraft | Exit Speed (knot) | Stopping Distance (ft) |
| CRJ-200 | 70+ | 244 |
| B737-800 | 70+ | 338 |
| B747-400 | 46 | 400 |

## 9.5.3. General Observations

The overall deceleration and loading trends on the three aircraft showed several common characteristics. Figure 9-26 and Figure 9-27 illustrate sample deceleration and nose-gear load plots generated by the APC for the B737 aircraft. Figure 9-26 represents the arrestor bed using the limit load design criterion, while Figure 9-27 is based on the ultimate load criterion. The overall bed lengths and depths reflect the values of Table 9-6.

The upper plot in each figure shows the aircraft speed decrease relative to the nose wheel location in the arrestor bed. The lower surface line of the arrestor is depressed by 15% of the bed thickness, as discussed in Section 9.5.1.

The middle plot in each figure shows the deceleration of the aircraft in g's. The deceleration first increases when the nose wheel penetrates the bed at zero feet, while the main-gear tires are still on pavement. The deceleration then increases strongly when the main-gear tires enter the arrestor, at a nose-wheel location of 50 to 70 feet. After the initial transition, the deceleration settles to a fairly constant value in both cases, at about 0.6 g for the limit design and about 0.8 g for the ultimate design. The relatively constant deceleration value is possible because the glass foam material shows only mild rate dependence. An ideal arrestor bed would provide a perfectly constant deceleration; the glass foam bed performance approximates the ideal bed fairly well.

The lower plot in each figure shows the nose-wheel drag loading, which proved to be the limiting load for the arrestor bed design. The loading is highest between 50 and 125 ft, which is after the main-gear tires have entered the bed. When the main-gear tires enter, the deceleration increases substantially, and this causes the aircraft to pitch forward and presses the nose wheel deeper into the material. The deeper penetrations lead to higher drag loads on the nose wheel.

## 9.5.4. Braking Effects

In the APC simulations, braking loads for the main-gear tires while in the arrestor bed were added to the drag loads of the tire–arrestor metamodel. Thus, the net drag load on the

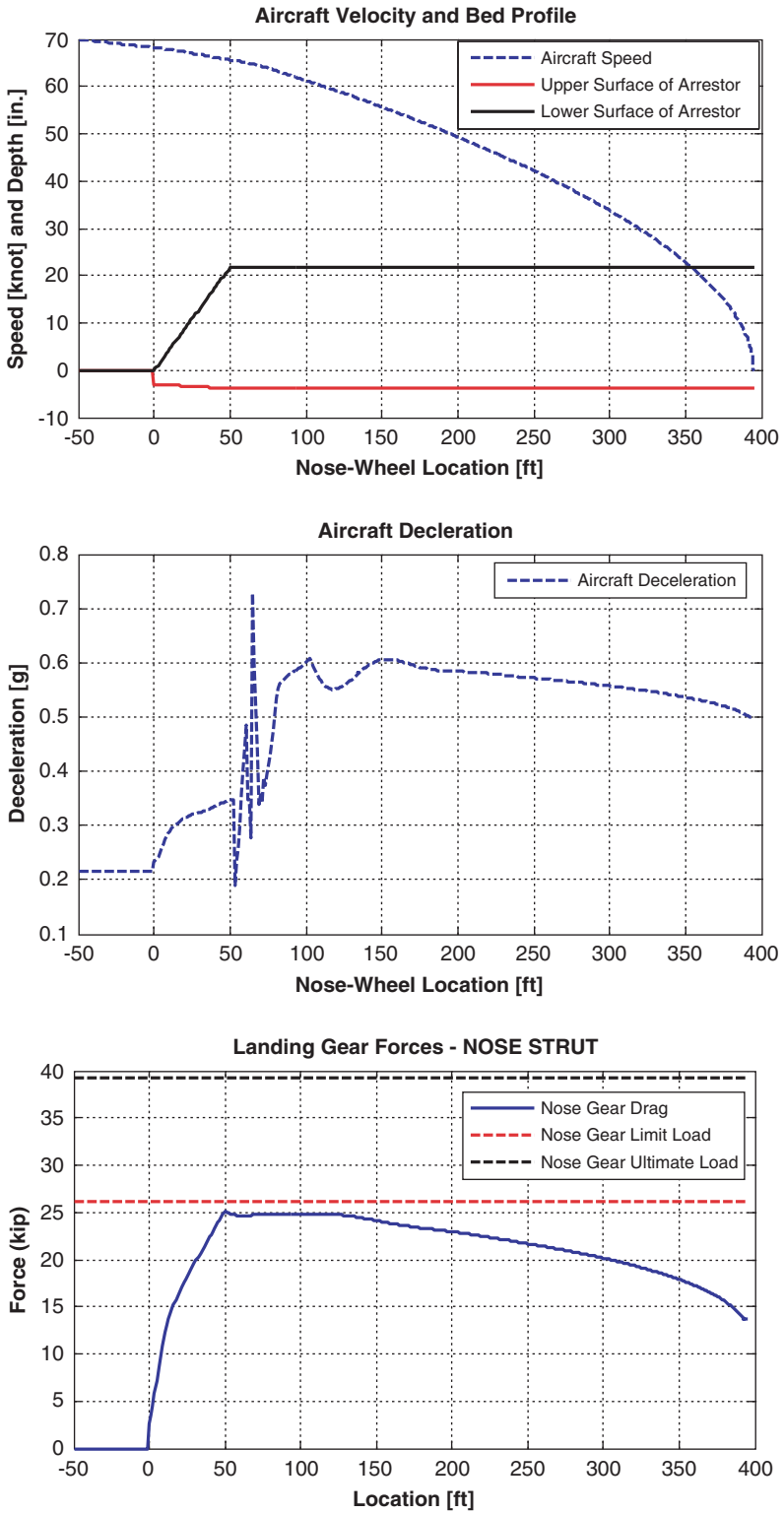


***Figure 9-26. Limit criterion glass foam arrestor design plots for B737-800 showing speed (top), deceleration (middle) and nose-gear drag load (bottom).***

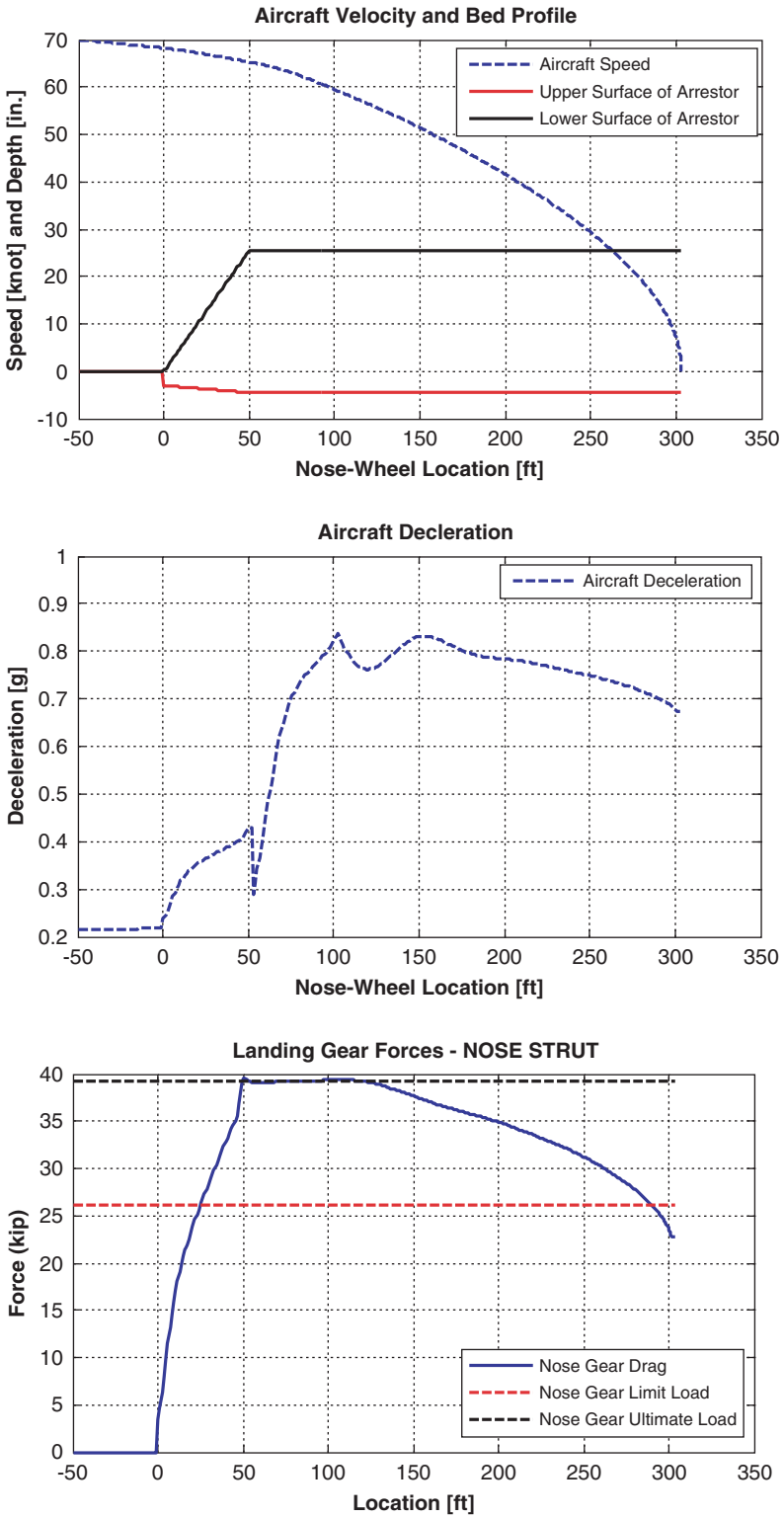


***Figure 9-27. Ultimate criterion glass foam arrestor design plots for B737-800 showing speed (top), deceleration (middle) and nose-gear drag load (bottom).***

main-gear tires was due to the braking plus the arrestor resistance. As an approximate solution, this approach worked well and was appropriate.

However, a small side study conducted during the metamodeling process indicated that braking applied to the main gear tires could cause the penetration depth to increase. Since the arrestor metamodel loads assumed a non-braked free-spinning wheel, this depth change would not be captured.

For a bottomed tire, little increase is feasible and this effect would likely not occur. For a non-bottomed tire, however, the tendency to penetrate deeper would lead to higher arrestor drag loads on the tire. Since this effect would only apply to the braked wheels of the main gear, it would benefit the deceleration process while not affecting the nose gear. Stopping distances could be somewhat reduced by this effect, though it is unclear by what amount or in what limited subset of arrestor design cases.

### 9.5.5. Effect of Material Seams

As previously discussed, seams in the glass foam material produced notable pulses in the pendulum test strut loading (Section 9.3.4.4). However, the metamodels for the material assume a monolithic arrestor bed without seams.

If seams were present in the material, such as in the design concept featuring separate blocks (Section 9.1.1), they could impart pulsed drag loads to the nose gear. Pulsed loads would require a reduction in the bed depth to ensure that the peak loads did not exceed the limit or ultimate thresholds for the nose gear. Consequently, the arrestment distances would increase.

Since the effect of the material seams in a fielded system has not been established, the caveats of Section 9.3.4.4 apply to these observations.

## 9.6. Estimated System Cost and Upkeep

### 9.6.1. Installation Process

The arrestor beds would likely use sloped entry and terraced sides regions, with a slight vertical depression below the runway level (described further in Section 9.5). For the block variant of the system, the glass foam would be manufactured and assembled into the larger blocks while at the production facility. These blocks would then be transported to the airport and laid in place in the RSA. Because of the lower density of the material (~6 pcf), a 4-ft block may only weigh 200 lbs; this could permit placement of the blocks using pallet jacks or dolly-type devices rather than forklifts. After placement, the seams would be sealed using joint tape or caulk.

For the monolithic variant, the glass foam would be shipped to the site without prior assembly. The small blocks would then be hand-laid in rows and layers, with glue applied in between. After the monolithic bed was completed, a roll-on or spray-on polymer would be applied to the surface to seal the bed. The hand-laying process would require more time than placing larger blocks; however, the final bed would have reduced maintenance needs thereafter due to the lack of joints.

### 9.6.2. Cost to Establish System

A preliminary estimate was made for the cost to establish a glass foam arrestor system. It must be noted that the cost estimate from this section is only a basic approximation for the purposes of comparing the different arrestor alternatives. The cost estimate is based on a mixture of information from the manufacturer, the airport survey, and FAA Order 5200.9. To develop a more accurate estimate of the costs to install such a system, it is recommended that a detailed cost quote be sought from a firm qualified to undertake an installation effort. Where possible, the methodologies used were consistent with the prior survey information collected regarding the existing EMAS (Section 3.5).

The glass foam arrestor concepts would require site preparation and paving similar to the current EMAS. It was assumed that the costs for this preparation would be identical to the site preparation cost for an EMAS.

In terms of manufacturing cost, lower density versions of the material are more expensive than the commercially available insulating product. To provide a conservative cost estimate, the upper bound for the possible cost range was assumed.

The installation cost estimate was separated into specific materials and general installation labor needs. Because these costs were specific to the glass foam arrestor concepts, they do not have a direct connection to any prior EMAS data. Discussions with a potential manufacturer produced cost estimates for the foam blocks, adhesive to join the blocks, and a polymer top coating material. The labor costs were estimated based on similar labor needs for installation of glass foam in roof applications.

Finally, the site preparation and estimated EMAS costs were computed in two ways: (1) assuming average survey costs from this research, and (2) assuming FAA Order 5200.9 costs. The final cost estimates for both options are given in Table 9-8 and Table 9-9, respectively.

Using the survey cost assumptions of Table 9-8, a 300-ft arrestor bed would cost approximately 7% less than the current EMAS design. If the Order 5200.9 costs are assumed, the glass foam system would be nominally 37% more expensive (Table 9-9). Due to the preliminary nature of the estimated system cost, it is feasible that actual costs for the system would be higher based on unforeseen elements. A conservative approach would conclude that the cost for this concept will probably be similar to that of EMAS.

In addition to the tables in this section, longer-term life-cycle issues could also be considered. FAA Order 5200.9 includes a

**Table 9-8. Estimated costs to establish glass foam arrestor, 150 x 300 ft, assuming survey average costs for current EMAS, units of millions USD.**

| Cost Category | Glass Foam System | Current EMAS |
|---|---|---|
| Site Preparation | $ 2.17 | $ 2.17 |
| Installation | $ 5.49 | $ 6.03 |
| Cost to Establish | $ 7.65 | $ 8.19 |
| Percent of EMAS | 93% | |

standard 10-year replacement interval for an EMAS, which translates into present-value life-cycle costs. Such a replacement could arguably be unnecessary for this arrestor concept (Section 10.6.4). Eliminating the assumed 10-year replacement could effectively trim about $2.6M of present-value life cycle costs (based on the EMAS replacement cost estimates of the survey).

### 9.6.3. Maintenance

The glass foam material is expected to have a superior durability when compared with cellular cement. Glass foam does not exhibit the tendency to crumble during handling that occurs with cellular cement, nor does it exhibit overt sensitivity to moisture due to its closed cell microstructure. Many industrial applications of glass foam materials indicate that long service life is possible with little degradation as long as mild protective measures are taken.

In the monolithic version of the concept, joint tape/caulk maintenance would not be required. Annual maintenance could be limited to upkeep of the required yellow chevron markings on the arrestor.

### 9.6.4. Replacement and Overhaul

It is not anticipated that replacement of the bed would be required after 10 years, as anticipated for an EMAS in FAA Order 5200.9. Based on other fielded applications for glass foam material, life cycles of 20 years should be realistic, with some past applications indicating that it can last as long as 50 years. This effectively reduces the life-cycle cost of the concept. Since the installation costs are expected to be similar to the existing EMAS, the elimination of a 10-year bed replacement would effectively trim $3.5M of present-value life-cycle costs.

However, the top cover layer applied to the material must also be considered. Polymer coatings and plastic lids can degrade when exposed to ultraviolet radiation and varying weather conditions. Overhaul may be required to replace or repair the top material periodically.

**Table 9-9. Estimated costs to establish glass foam arrestor, 150 x 300 ft, assuming Order 5200.9 costs for current EMAS, units of millions USD.**

| Cost Category | Glass Foam System | Current EMAS |
|---|---|---|
| Site Preparation | $ 0.68 | $ 0.68 |
| Installation | $ 5.49 | $ 3.83 |
| Cost to Establish | $ 6.17 | $ 4.50 |
| Percent of EMAS | 137% | |

### 9.6.5. Repair

Repairs after an overrun would parallel those of the current EMAS design. Damaged sections of glass foam material would require removal and replacement after aircraft extraction.

## 9.7. Transition to a Fielded System

In order to transition the glass foam concept to a fielded system, the following additional development steps may be advisable.

### 9.7.1. Low Material Density Calibration

As shown in the example arrestor beds of Table 9-6 and Table 9-7, the compressive strengths for optimal designs ranged from 17 to 53 psi. Since the material tested and calibrated during the research had a nominal strength of 55 psi with a 6-pcf density, the fielded material will be softer and lighter. To estimate the needed density and strength, the metamodel data was simply scaled, which was an appropriate simplification.

However, in migrating to a fielded system, several standard densities would probably be selected to provide flexibility during the design of actual arrestors (currently done with EMAS). For each density, some testing would be required to generate calibration data. The foam glass material model would require minor adjustments to compensate for the alterations. Fresh metamodel data should then be generated such that data scaling would no longer be required in the arrestor design process.

### 9.7.2. Cover Layer Design

Two major cover-layer design concepts are possible:

1. Plastic lids, applied to the block version of the concept, or
2. Spray-on or roll-on polymer coating, applied to the monolithic concept.

For either case, the material type and thickness of the layer must be established. The material should be selected based on ultraviolet and weather durability. A material that can be dyed to a pavement gray color would be preferable, such as is currently in use for plastic EMAS tops. Paint application for yellow chevron markers would be required.

After selection of a cover layer material that meets these general requirements, a moderate to full-scale test bed should be constructed for overrun testing by a one-wheel bogy apparatus or an aircraft. Such testing would ensure that the cover layer does not negatively impact the mechanical deceleration performance of the bed.

### 9.7.3. Seam Effect Characterization

The research performed to date has identified that seams between glass foam blocks should be investigated further. Seams in the material have been observed to generate pulsed loads on a rigid tire form during testing; it is not presently known how substantial such loading pulses might be on actual landing gear.

One evaluation method could involve using a one-wheel bogy apparatus fitted with a full-scale pneumatic tire that is towed through the material. Direct comparisons could be made between fully glued test beds and those having un-glued seams.

### 9.7.4. Braking Dynamics

The research performed has identified that braking in the glass foam material may require further study. The current modeling method of the APC makes simplifying assumptions regarding this phenomenon that are sufficient for a concept-level evaluation. However, to ensure accuracy of design predictions, some additional tests may be beneficial. One method would involve using a one-wheel bogy apparatus fitted with brakes and a load measurement system that is towed through the material.

### 9.7.5. Full-Scale Testing

A full-scale aircraft overrun test of the glass foam arrestor bed may or may not be critical to approve and field such a system. The mechanical nature of the system is very similar to that of the current EMAS, which leaves fewer unknown factors than for the other concepts evaluated. A one-wheel bogy test apparatus may prove sufficient to characterize the remaining unknown factors of the concept, such as the cover layer, seam effects, and braking dynamics.

## 9.8. Summary

Of the candidate systems evaluated, the glass foam arrestor concept is most similar to the current EMAS. It uses blocks of crushable foam material that are installed on a paved surface. While the mechanical properties differ somewhat from cellular cement, the overall dynamic behavior proves analogous. Consequently, the glass foam concept could be considered an equivalent to the existing EMAS technology, with the caveat that bed thicknesses and material properties would not be identical.

The material is closed-cell glass foam, which provides inherent moisture and chemical resistance and improved handling durability as compared with cellular cement. Manufacturer information regarding past use indicates that long service life is possible, potentially eliminating the standard 10-year replacement for an EMAS assumed in FAA Order 5200.9. Water immersion must be avoided, so drainage measures would still be required for the bed.

Installation of the system would rival the current EMAS design in terms of time and effort required. Repair of the bed after an overrun would be analogous to the current EMAS requirements. Preparatory paving requirements would be identical. The cost to establish such a system would be nominally equal to, or greater than, EMAS; however, life-cycle costs could be reduced due to longer bed life. Maintenance needs could be reduced for a monolithic version of the concept, which would have no joints to seal with tape or caulk.

The APC predictions for the glass foam arrestor show fairly constant deceleration throughout the arrestment with little speed dependence, which are desirable characteristics. Arresting distances were comparable to the current EMAS. Of the three candidates evaluated, the multi-aircraft design case for the glass foam concept showed moderate performance. Arresting distances varied with the aircraft size.

Transition to a fielded system would require selecting a covering material and finalizing a set of foam densities that could be used for different arrestor applications. Additional investigation would be advisable to determine the impact of material seams in producing pulsed landing gear loads.

CHAPTER 10

# Engineered Aggregate Arrestor Concept

## 10.1. Concept Description

### 10.1.1. System Overview

An engineered aggregate arrestor concept has been proposed. Its primary material is a spherical engineered aggregate that has excellent flow properties and resists settling and compaction that are more typical for angular gravels (Figure 10-1). This material would reside in a shallow bed and be covered with a reinforced turf layer. However, the engineered aggregate may also be used without a turf layer, which has been done at four airports in the UK. Other top layer materials are possible, such as a thin asphalt skim coat. Figure 10-2 illustrates the two major variants of the engineered aggregate arrestor concept.

The difference between the two concepts is the existence of a confining top layer, which can serve several purposes:

1. Prevent aggregate dispersion due to jet blast;
2. Mitigate aggregate spraying during overrun by aircraft tire, thus limiting engine ingestion hazard;
3. Regulate water drainage and potential ice crust formation in winter; and
4. Act as a structural component to prevent lightweight land vehicles from penetrating the arrestor bed.

Because the engineered aggregate materials are not greatly affected by water, the bed can be designed to handle precipitation in two different ways (Figure 10-3).

1. **Drainage Approach.** This approach would allow water drainage downward through the bed. In this case, the bed would be designed to prevent standing water within it using normal civil engineering design practices.
2. **Waterproof Approach.** In the second approach, a composite top layer could be employed to prevent water drainage through the bed. It would likely be composed of a channelized or cuspated plastic layer, overlaid with a geo-textile fabric layer, and finally topped with reinforced turf. Precipitation would not seep through the aggregate in this case, but would run off to the perimeter of the arrestor bed. Hence, the bed would be kept dry and the material response during an overrun would likely prove more consistent.

### 10.1.2. Performance Considerations

The dynamic performance issues for the engineered aggregate concept are different from those of the crushable material candidates. During the assessment process, the following aspects were considered:

- Dynamic behavior and energy absorption,
- The degree of non-linearity of the landing gear loading and danger of failing the nose gear,
- Performance in a short-landing situation that involves an aircraft touchdown inside the arrestor bed,
- Applicability to arresting a wide range of aircraft types,
- Vulnerability to ice crust formation in severe winter environments, and
- Effect of a cover layer on the performance of the aggregate system.

## 10.2. Modeling and Testing Approach

As with the crushable systems, the goal for the performance evaluation was to perform testing that would allow calibration of high-accuracy computer models of the engineered aggregate concept. Determining the necessary physical tests was driven by the requirements of the modeling software. Therefore, a modeling method capable of high-fidelity aggregate simulations was determined first, and the required tests for material characterization followed thereafter.


*Figure 10-1. Engineered aggregate.*

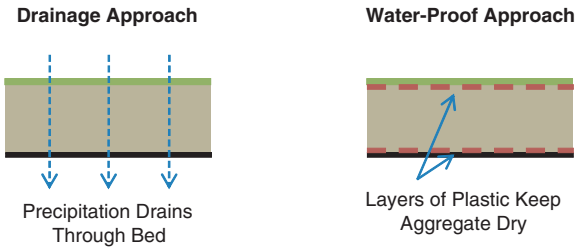


*Figure 10-3. Aggregate bed methods for handling precipitation and drainage.*

### 10.2.1. Discrete Element Modeling (DEM) Method

Modeling aggregates presents a number of complexities when compared with crushable materials because they have both solid-like and fluid-like regions of behavior. Bell et al. describe the complexities from a modeling and simulation standpoint: the fluid-like behaviors cannot be adequately simulated with solid material models (Lagrangian), nor can the solid-like behaviors be adequately simulated with a fluid material model (Eulerian) (*39*). LS-DYNA, which can simulate both Lagrangian and Eulerian behaviors, is still not adequate for modeling this particular material.

The current state of the art for modeling aggregate behavior involves the use of DEM codes, which model the aggregate on a particle-by-particle basis. The EDEM software package, produced by DEM Solutions, was selected from among the commercially available DEM codes. Using EDEM, the bed of aggregate was modeled using individual aggregate pieces. The particles move and interact with one another in fundamentally the same way that actual aggregate does, with friction between the particles, compaction, fluid-like spraying behavior, and momentum transfer.

### 10.2.2. Required Parameters for Material Models

EDEM defines aggregate pieces as rigid spheres, or lumps of rigid spheres grouped together to form irregular pieces. The rigid sphere assumption was valid here since the spheres behave as fairly incompressible particles with respect to the aircraft tire. Particle size, size variation, density, and so on were all defined as expected.

The main effort in characterizing the engineered aggregate behavior was in determining the particle interactions with each other and with solid surfaces (i.e., the aircraft tire, bed walls, etc.). This was a fundamental contrast to the crushable material modeling in LS-DYNA, where the main effort was expended in calibrating the material models.

Four interaction parameters required definition in EDEM, which are briefly described here:

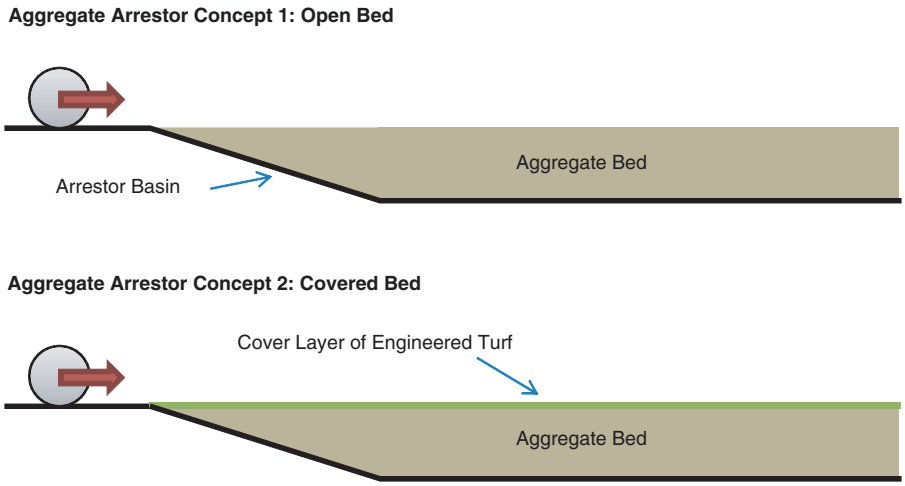


*Figure 10-2. Engineered aggregate arrestor concepts.*

1. **Coefficients of Static Friction** – a standard friction definition based on the contact force between particle/particle and particle/surface.
2. **Coefficients of Rolling Friction** – defines the resistance of the particles to tumbling/rolling past one another or over a surface, which could be due to shape irregularities (jaggedness) or other material properties.
3. **Coefficients of Restitution** – defines the degree of rebound that particles have following a collision.
4. **Particle Bond Strengths** – defines a bonding force between particles simulating glue or adhesion-type forces. Here this parameter was used to define the bonding of particles together for simulating a turf layer.

These parameters drove the selection of suitable physical tests of both the engineered aggregate and reinforced turf materials. Naturally, this collection of tests differed substantially from those of the crushable material candidates.

## 10.3. Testing Effort

### 10.3.1. Density and Dimension Measurements

The density and dimensions of the engineered aggregate were measured for several hundred randomly selected aggregate particles. The particle size was found to follow a bounded normal distribution, with a diameter mean and standard deviation of 0.348 and 0.047 in., respectively. The particles were essentially round, with an average max/min diameter ratio of 1.24.

The density of the actual material, on a per-particle basis, was 94.9 pcf, while the effective density of the continuum aggregate was 52.1 pcf. This leads to nominally 45% void space in the aggregate bed.

The high void percentage and sphericity of the particles lead to good drainage through the bed and effectively limit the settling of the material over time. The density is about three times greater than that of typical EMAS cellular cement (~18 pcf). The higher density leads to an increased sensitivity to speed in an arresting application; higher speeds will lead to higher loads on the landing gear.

### 10.3.2. Angle of Repose

Angle of repose measurements (Figure 10-4) were performed by overturning and raising a 5-gal bucket of the engineered aggregate material, allowing the material to spill and settle into a pile. The sides of the resulting heap settled to the aggregate's natural angle of repose. The test was repeated several times for the dry material, and again for wet material, which had been fully soaked and drained. The dry and wet angle of repose measurements averaged to 18.7 and 19.4 degrees, respectively.

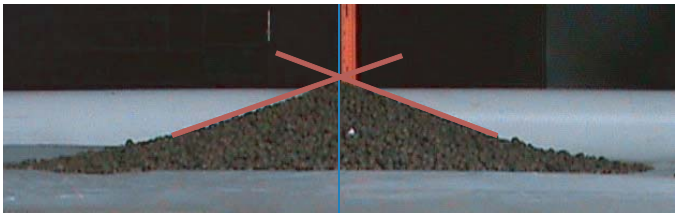

***Figure 10-4. Angle of repose test for engineered aggregate material.***

The higher angle of the wet samples results from increased wet particle adhesion.

This physical test eventually helped to calibrate the coefficient of rolling friction in the DEM model.

### 10.3.3. Hydrostatic Triaxial Tests

Standard hydrostatic triaxial compression tests (Figure 10-5) were performed on the engineered aggregate at various confining pressures in accordance with ASTM D2850. Cylindrical samples of the aggregate were enclosed in a flexible membrane and subjected to various hydrostatic confinement pressures. The specimens were then compressed uniaxially until the specimen bulged and deformed out of its original cylindrical shape.

The aggregate behaved much like a soil sample, which was in accordance with expectations. Values obtained from these tests included the elastic modulus of the material, the internal angle of friction, and the effective particle-to-particle cohesion. These tests further illustrated that the behavior of the material was consistent with essentially non-deforming particles and standard aggregate/soil behavior, thereby confirming that DEM modeling of the material was appropriate.

### 10.3.4. Pendulum Tests

#### *10.3.4.1. Test Apparatus*

In addition to the small-scale laboratory tests, a larger-scale one-wheel bogy test was conducted using a large pendulum test apparatus. The pendulum test apparatus featured a heavy 4,400-lb mass that hung from an overhead support frame, giving it a swing arc of 24.5 ft. The mass was hoisted to the desired height and then released; the speed of the mass was controlled by the release height.

The pendulum mass was fitted with a strut and wheel assembly, which Figure 10-6 illustrates in an exploded view. The strut was instrumented with three load cells that measured loads at the connections. These three connection loads were resolved into orthogonal vertical and drag loads on the strut and wheel assembly.

To reduce the number of variables in the design, a rigid aluminum wheel form was used rather than a pneumatic tire.

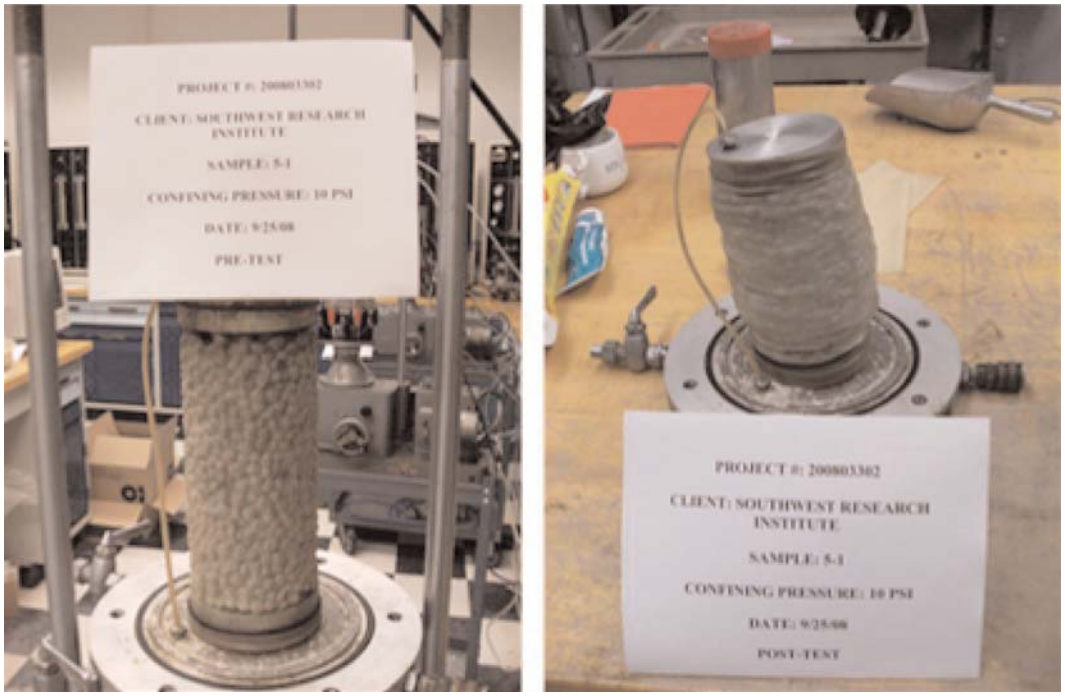


***Figure 10-5. Hydrostatic test specimen for engineered aggregate pre-test (left) and post-test (right), 10 psi confining pressure.***

The diameter and width were 14.8 and 5.5 in., respectively. These proportions were based on a nominally one-third scale B737-800 main-gear tire, which has a diameter and width of 44.5 and 16.5 in., respectively. Although this wheel size was smaller than full-scale, it was substantially larger than the typical particle size; this ensured the continuum-type behavior of the aggregate that was necessary for characterization.

Below the pendulum assembly, a bed of aggregate was constructed with a length of 22 ft, a width of 8 ft, and a depth of 22.5 in. Figure 10-7 shows the overall pendulum apparatus with the aggregate bed beneath it.

### *10.3.4.2. Test Matrix*

For the test series, the pendulum was set to swing such that the wheel penetrated to a depth of one-half diameter, or 7.4 in. Two swing heights were used to produce speeds of 17.2 and 8.5 mph. For the high speed tests, both wet and dry beds were used. The wet bed was well soaked with water and allowed to freely drain prior to every test. Three repetitions were conducted for each permutation tested, as shown in the test matrix of Table 10-1.

### *10.3.4.3. Test Results*

Figure 10-8 gives an action sequence of photos for the pendulum strut cutting a rut through the material.

After cutting the initial rut, the pendulum continued to swing back and forth until eventually coming to rest. Load measurements were only considered for the initial pass through the material. The final resting position and resulting rut are illustrated in Figure 10-9.

Figure 10-10 shows the average drag and vertical forces during the pendulum swing for the different permutations of the test matrix. The error markers atop the bars indicate a 90% confidence interval, as an indication of the spread in the test results for the three repetitions of each case. The drag force is defined as the rearward load on the strut, which would decelerate the aircraft (Figure 7.9). The vertical force is defined as the upward load, which would support the aircraft from sinking further into the aggregate.

Overall, both the speed and the moisture conditions affect the outcome, but speed has the greatest effect. Reducing the speed from 17.2 to 8.5 mph created a 65% reduction in the drag force. Wetting the aggregate increased the drag force by 26%.

These findings were consistent with initial observations and assumptions regarding the aggregate as an arrestor medium. The imparted landing gear load is highly dependent on the speed of the aircraft overrun and somewhat dependent on the moisture content of the aggregate.

The results of these tests were subsequently used to help calibrate the coefficients of static friction and restitution for the aggregate material.

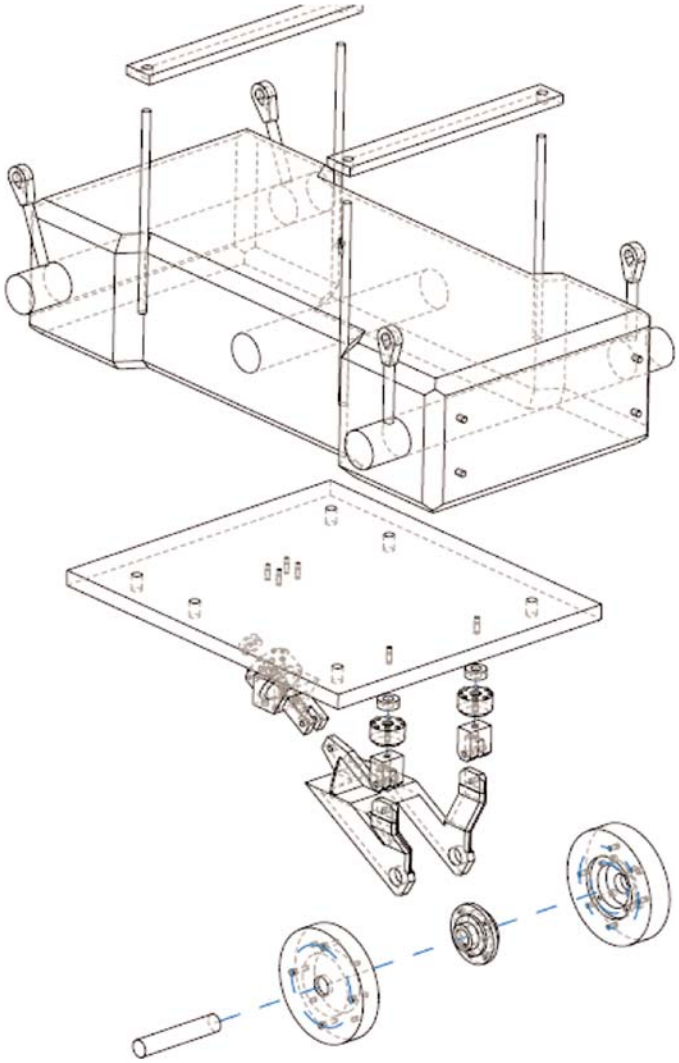

***Figure 10-6. Pendulum test device with one-wheel bogy.***

## 10.3.5. Tensile Turf Tests

### *10.3.5.1. Overview and Assumptions*

The reinforced turf material used a sandy soil mixed with small swatches of reinforcing material. Grass seed was planted in this soil base and grown to maturity. The resulting turf layer had changing properties through its thickness, with grass on top and sandy soil on the bottom.

Characterizing the reinforced turf required non-standard testing procedures. Several different test methodologies were considered, including punch tests, tensile tests, and tearing tests. At the small scale, the soil and reinforcement swatch mixture presented problems of heterogeneous properties, which eliminated some of the punch test concepts from consideration. To ensure a generally homogeneous behavior, the specimen size needed to be fairly large.

For tire overruns, it was assumed that the material would essentially act as a confining membrane layer atop the aggregate. It was further assumed that the through-thickness homogeneities could be neglected in the DEM models, where the turf layer would be represented using a homogeneous layer with equivalent membrane properties. This layer of particles would use defined particle bonds to create a membrane-type behavior.

With that end in mind, a simple tensile test was selected as the best all-around means of determining membrane performance. It produced results that could be transferred to bond strength values in the DEM modeling code.

While the tests sought to characterize the material properties for the turf layer, this was undertaken with fairly modest expectations for exactness. In actual application, the use of a turf layer presents several factors that could be difficult to control. The strength of the layer would be dependent on:

- Type of soil base used (sandy, clayey, etc.),
- Amount of reinforcement per unit area,
- Type of grass used (regionally dependent),
- Age/maturity of the grass, and
- Seasonal rainfall levels.

Therefore, the tests sought only to establish a nominal strength level for the turf layer, which in practice could either be stronger or weaker for different arrestor beds, at different times of the year, and at different ages.

### *10.3.5.2. Tests Conducted*

The turf specimens began as 4-ft square samples, which were 4.6 in. thick with a nominal areal density of 30 psf. From these squares, test specimens were cut out in dog-bone shapes, which narrowed to an 8-in. wide neck that was 8 in. long (Figure 10-11). The total specimen length was 14.25 in. These specimens were clamped in a special jig and attached to a tensile testing device. The specimens were then pulled apart axially, and the load history was recorded. Three specimens were tested overall, with a typical failure strength of 120 lbf at elongations of 4 in.

## 10.3.6. Environmental Tests

Environmental tests were considered for the engineered aggregate and turf materials. However, after consideration of the nature of both materials, as well as the body of existing research information, it was determined that such testing would not be included in the research effort. A simple set of environmental tests was not useful, and a comprehensive set of tests was not affordable within the current effort.

*Figure 10-7. Overview pictures of engineered aggregate pendulum test setup.*

Neither material degenerates under environmental conditions in a manner analogous to crushable materials, such as the currently used cellular cement. Both the turf and aggregate are durable to freeze–thaw, rain, and heat. Obviously, turf can degrade over time during periods of drought, which would lead to impacts on strength as discussed in Section 10.3.5. However, characterizing such impacts would require a very substantial body of tests using multiple hydration conditions, soil types, and grass types.

**Table 10-1. Pendulum test matrix for engineered aggregate.**

| | Number of Tests Conducted | |
|---|---|---|
| | High Speed | Low Speed |
| Dry Aggregate | 3 | 3 |
| Wet Aggregate | 3 | - |

Perhaps the most relevant issue is that of ice crust formation on an arrestor bed during winter conditions. Rainfall during freezing conditions could lead to water penetration and freezing in the upper layer of the aggregate and turf. However, freezing at deeper levels may be self-limiting due to insulating properties of the aggregate bed. Prior research by Rogers discusses cold-weather testing information that demonstrates the potential for aggregate arresting beds to freeze over and become ineffective in harsh winter environments (*13*).

In the event of such freezing, we can deduce several areas of performance impact. First, the particles would effectively be adhered to one another, which would create a solid block of material that an overrunning tire would likely break apart. After breakage of the ice bonds, however, the void spaces between particles would still be filled with ice and water, increasing the rolling friction of the particles and decreasing their effective flow around the tire. This would likely result in

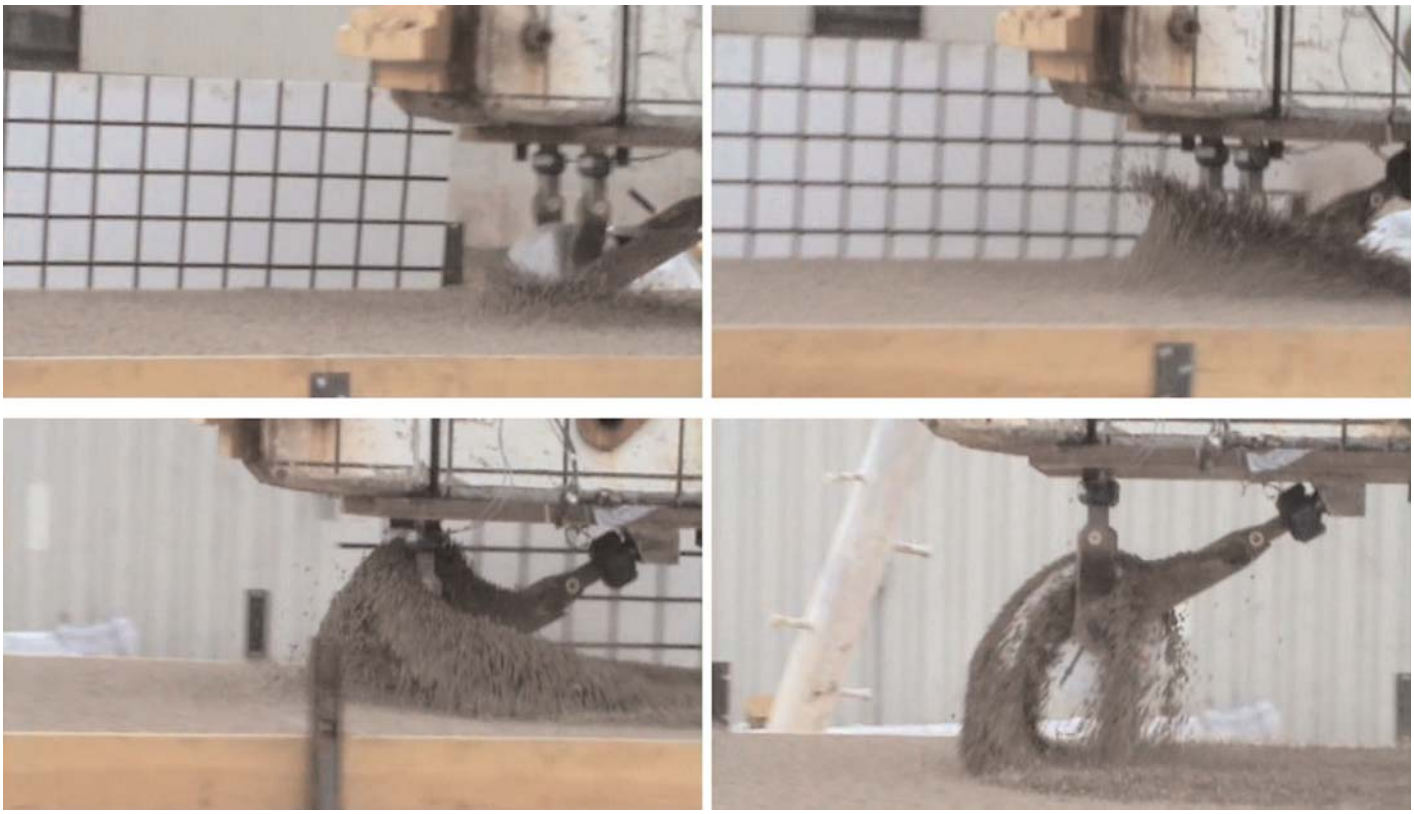

*Figure 10-8. Pendulum wheel passing through engineered aggregate material (upper left is first frame, lower right is last frame).*

increased drag and/or vertical loads on the tire. Overall penetration of the tire could prove similar to that in a normal bed, or it could be diminished. However, predictability of the total performance impact is difficult since the degree of such crusting would be variable.

To assess such effects on performance, a larger test bed would have to be constructed and subjected to artificial rain and freeze–thaw conditions. Further, this would need to be followed for the two different drainage and waterproofing approaches to the arrestor bed. In the former, the ice crust could penetrate below the turf layer; in the latter, it should be confined to the turf alone.

Larger testing as described above was beyond the scope of the current effort. However, it would be advisable if the

*Figure 10-9. Post-test view of rut in engineered aggregate created by pendulum wheel.*

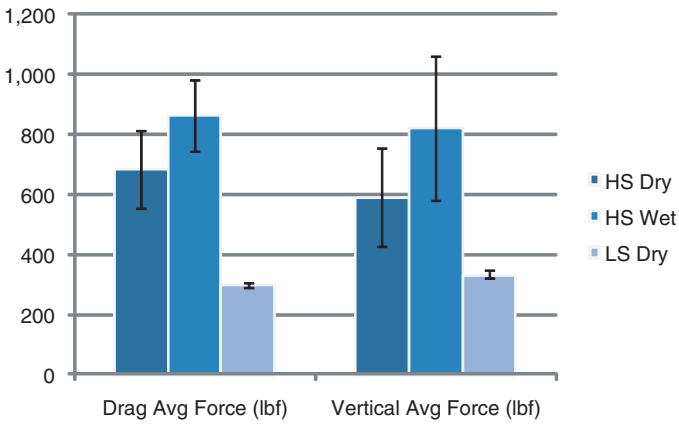


*Figure 10-10. Plot comparing strut forces for high-speed dry, high-speed wet, and low-speed dry conditions.*

*Figure 10-11. Reinforced turf material (left) and dog-bone specimen in tensile test jig (right).*

engineered aggregate concept is to be transitioned into a fieldable system.

## 10.4. Modeling Effort

The modeling effort sought to replicate the important behaviors of the engineered aggregate arrestor system concept. The aggregate and turf simulations were conducted using the EDEM software, which is a DEM code, as discussed in Section 10.2.1.

### 10.4.1. Particle Sizes and Shapes

#### *10.4.1.1. Size Selection*

In the DEM method, the model particles are often larger than the actual real-world particles. Because DEM modeling is a numerical method, various levels of fidelity are possible. High fidelity simulations will use a large number of smaller particles, while low fidelity simulations use a reduced number of larger particles. If the particles chosen are too large, accuracy suffers. Conversely, if the particles are too small, simulation times rapidly increase to impractical levels. The general goal for such models is to select a particle size that gives sufficient accuracy while keeping simulation times short.

During the course of the model development and calibration, care was taken to select particle sizes that struck the right balance of accuracy and time efficiency. For the aggregate models, particle diameters were as small as 0.348 in. (the actual aggregate size) and as large as 2 in. in diameter. The size required for good accuracy was highly dependent on the size of the tire or structure that was interacting with the material. Larger wheels passing through the material permitted larger particles to be used with negligible decrease in accuracy.

#### *10.4.1.2. Size Distributions*

Section 10.3.1 discussed the particle size variation of the engineered aggregate, which followed a bounded normal distribution. This normal distribution was important to replicate in EDEM because it affects the packing density and the void ratio of the particles. As such, all aggregate simulations used the same normal distribution regardless of size scaling.

The turf material was represented using uniformly sized particles in EDEM.

#### *10.4.1.3. Shapes*

The average maximum-to-minimum diameter ratio of the aggregate was 1.24, which is close to that of a perfect sphere (1.0). As such, all aggregate particles were modeled as simple spheres. The irregularities in shape were essentially accounted for through the coefficient of rolling friction for the aggregate, which is discussed further in Section 9.4.2.1.

### 10.4.2. Calibration to Physical Tests

The aggregate and turf models were calibrated to match the physical tests as closely as possible. Properties of density, particle size distribution, and so on were simply entered into the software. However, the particle interaction properties of the aggregate and particle bonding properties of the turf required iterative determination. This section briefly summarizes the outcome of the long calibration process.

#### 10.4.2.1. Angle of Repose

The angle of repose test was replicated in EDEM using a bucket of identical size, filled with particles. The bucket was then removed, and the particles were allowed to fall and settle into a heap (Figure 10-12). Simulations were conducted for several scaled particle sizes ranging from the actual size of 0.348 in. up to 1 in. in diameter. Each model had nominally 35K particles and 43K particle-to-particle contacts.

The coefficient of rolling friction for the aggregate was determined using this method, and it was found to be dependent on the particle diameter. Therefore, in all subsequent simulations, the coefficient of rolling friction was matched to the scaled particle size to ensure accurate results.

The overall accuracy of the predicted angle of repose was within ½ degree (Figure 10-13).

#### 10.4.2.2. Hydrostatic Triaxial Tests

The hydrostatic triaxial tests were not replicated in EDEM due to software limitations. EDEM does not support deformable structure modeling or pressure load applications. Both of these features would be required to replicate the elastic membrane that surrounded the triaxial test articles and the applied hydrostatic pressure.

The hydrostatic triaxial tests nevertheless revealed that the aggregate performed normally and had no unusual characteristics that might make the use of EDEM inappropriate. The tests also provided data for the shear modulus of the aggregate material, which was a parameter required in EDEM.

#### 10.4.2.3. Pendulum Tests

An EDEM model was constructed to replicate the pendulum tests and was used to calibrate the remaining aggregate material parameters (Figure 10-14). The pendulum strut was simplified in the model to include only the features that interacted with the aggregate in the actual test. The aggregate bed was 16 ft in length, 5 ft in width, and 22.5 in. in depth. The model bed width was less than the actual bed width (8 ft) in order to reduce the particle count, but was still wide enough to prevent substantial boundary effects.

The strut followed an arced path approximating that of the actual strut, with the same ½-diameter penetration depth into the arrestor bed. The wheel was set to a constant rotation rate approximating the observed rotation rate of the wheel on test video.

Several particle sizes were attempted, and an error convergence study was undertaken. It was determined that a 1.0-in. particle diameter was required for the relatively small pendulum strut/wheel assembly. The particle size error was estimated to be less than 6%. The model had a total of 315K particles and 781K particle contacts.

Figure 10-14 and Figure 10-15 show the pendulum model replicating the high-speed test. The shading indicates the relative particle speeds as the one-wheel bogy passes through the arrestor bed. Figure 10-16, by contrast, shows the compression force on the particles, indicating the region of high loading in front of and beneath the wheel.

The pendulum tests were used to calibrate two critical parameter sets for the aggregate: the coefficients of restitution and the coefficients of static friction. Both parameters must be defined for particle-to-particle and particle-to-surface interactions. These interactions had a substantial effect on the predicted loads for the pendulum strut as it passed through the aggregate bed.

After calibrating these parameters, the pendulum model matched the test results for both the high- and low-speed tests for the dry aggregate bed. Figure 10-17 shows a graphical comparison of the simulation and test data, where the error bars indicate the scatter of the actual test data. The deviations from the true test data for the low- and high-speed tests are 3.1% and 3.0%, respectively.

Recalling the speed dependence manifested during the physical tests (Figure 10-10), it was important that the aggregate model be capable of capturing this effect. It was clear from the calibration results in this section that the model did in fact do this with high accuracy. This lends confidence to the later predictions made for even faster overrun situations, at speeds as high as 70 knots (81 mph).

#### 10.4.2.4. Turf Tests

The turf tensile test was replicated in EDEM using a layer of particles joined together with a bond contact definition (Figure 10-18). The bonded layer was then pulled apart using simulated clamps at either end. The geometry of the tensile specimen is not an exact match to that of the physical tests due to the rigid geometry limitations of EDEM. However, the loaded area reflects the 8-in. wide region used in the physical test specimens. The model had a total of 946 particles, 2,126 contacts, and 1,937 bonds.

Figure 10-18 illustrates the tensile loading of the model turf. The failure of the specimen is progressive, and as the turf is stretched an increasing number of inter-particle bonds are broken. The bonds were defined in terms of stiffness and failure strength, in both normal and shear directions. Iterative combinations of these four parameters were tried until the overall turf strength and elongation at failure matched the actual test specimens. Other material properties (shear modulus, Poisson's ratio, etc.) were taken from nominal values for sand or the aggregate model, depending on appropriateness.

The tensile strength of the model turf was within 1% of the test data average, while the energy absorption was within 11% of the test data average. However, the spread in the test data itself was +/– 7% and 11% for these quantities, respectively.

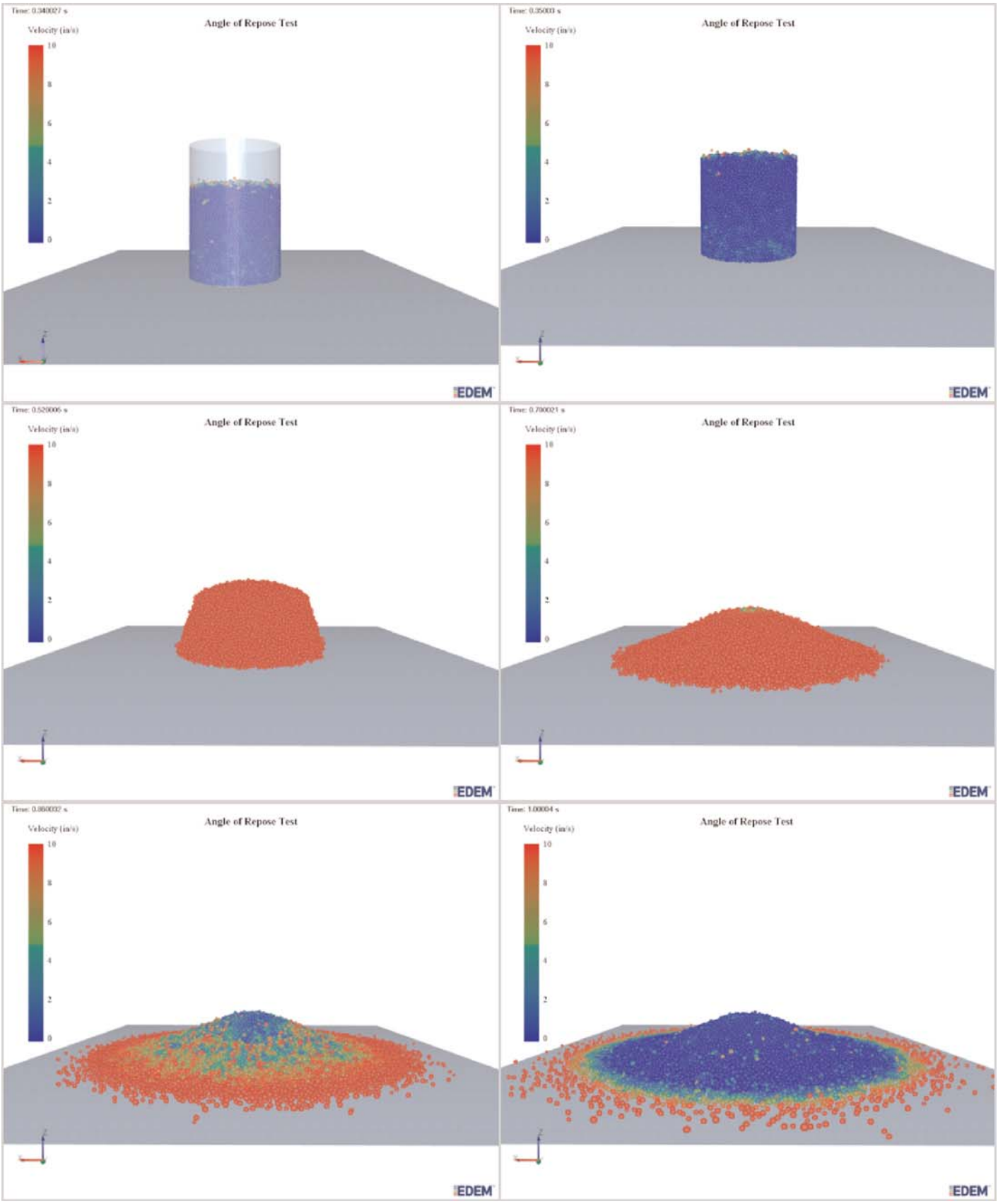


*Figure 10-12. Angle of repose simulation in EDEM.*

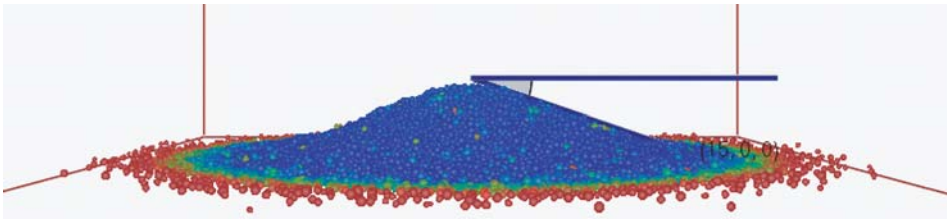

*Figure 10-13. Angle of repose measurement.*

Given the highly variable nature of the turf as a material, this accuracy was deemed sufficient for the needs of the evaluation.

## 10.4.3. Tire and Arrestor Simulations

Using the calibrated aggregate and turf material models previously described (Section 9.4.2), a large-scale arrestor model was created in EDEM to simulate overruns by aircraft tires. Figure 10-19 illustrates the model with a 36-in. depth and a B737-800 main-gear tire (Goodyear H44.5x16.5) at 50% penetration depth.

### *10.4.3.1. Arrestor Bed Models*

The arrestor bed models for the aircraft tire simulations were 8 ft wide and 25 ft long. Versions of the arrestor bed model were created with different depths in 6-in. increments, from 6 to 36 in. The deeper the bed, the more particles were included. However, the turf layer was always 4.6 in. deep, since this was a fixed layer thickness. All bed depths cited include the thickness of the turf layer.

Compared with the pendulum model, this new model was longer, wider, and deeper, giving a larger overall volume of aggregate. As such, larger particles became a practical necessity to keep simulation times efficient. A particle size convergence study using the B737 main-gear tire showed that a 2-in. diameter particle could be used with an estimated particle size error of less than 6%.

For the 36-in. depth, the model had a total of 149K particles, including 138K aggregate particles and 11K turf particles. The particles formed 372K contacts, and the turf layer had 15K inter-particle bonds.

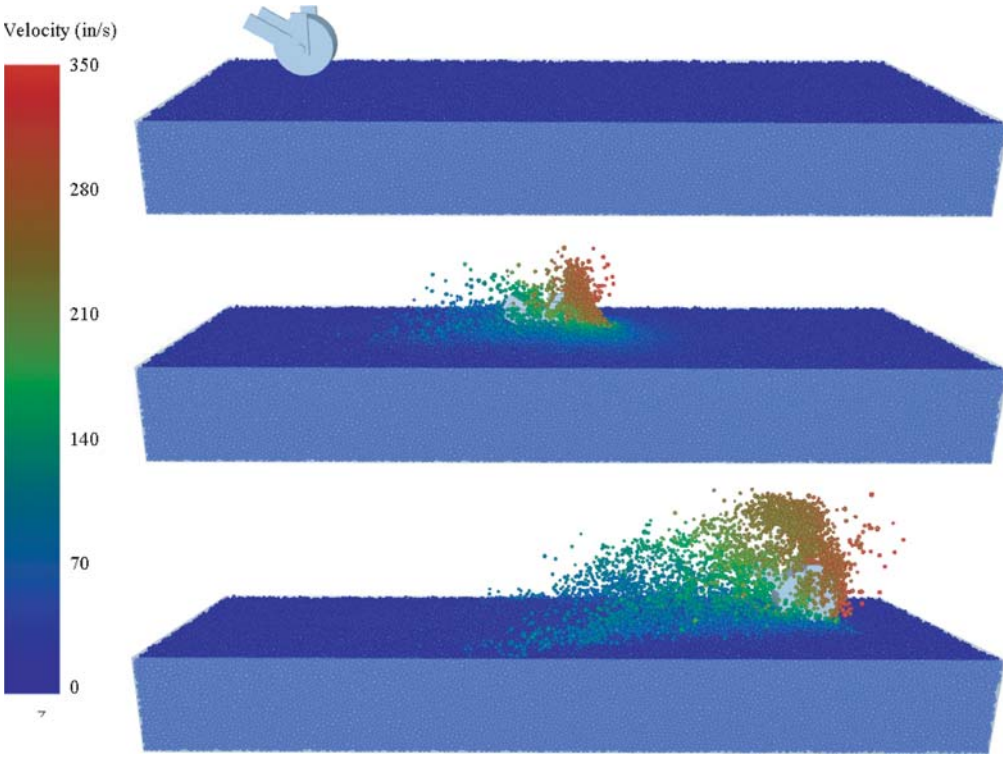


*Figure 10-14. Overall view of engineered aggregate pendulum model, velocity fringe plot.*

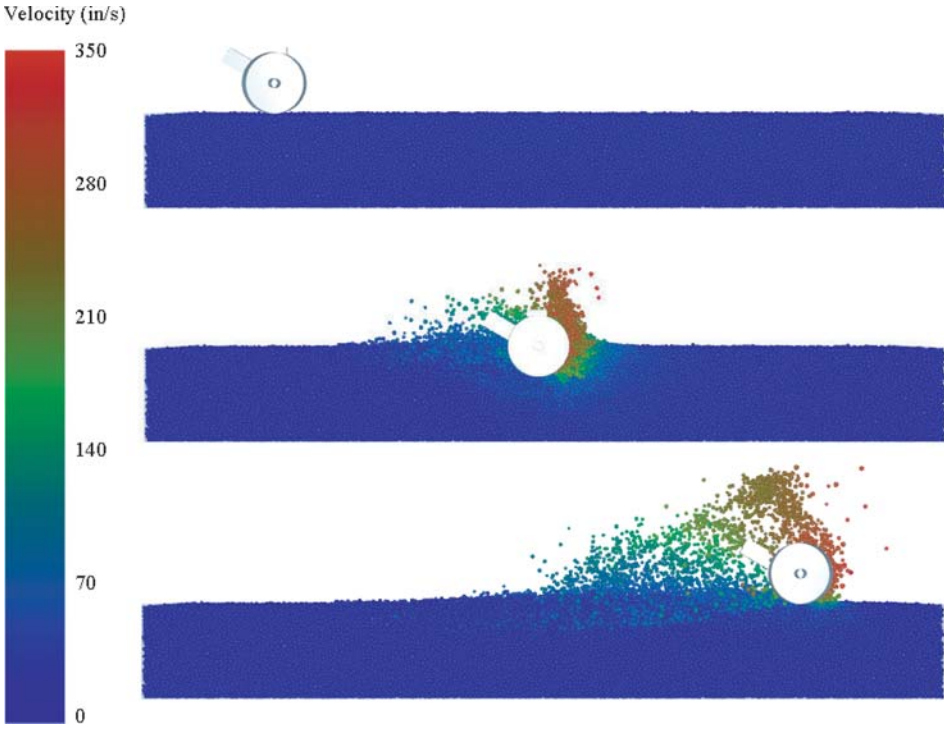


***Figure 10-15. Side cutaway view of engineered aggregate pendulum model, velocity fringe plot.***

While most simulations were conducted on a turf-covered bed, some were also run using an aggregate-only bed. The comparison of results is discussed in Section 10.4.4.4.

### *10.4.3.2. Tire Models*

EDEM does not inherently support deformable tire modeling, which necessitated a different approach be taken than that of the LS-DYNA crushable arrestor models. The model tires were rigid forms that matched the inflated dimensions of the respective tires. During overruns, the tires maintained this undeformed shape. In reality, the tires would form flat regions on the bottom and front faces, as is shown in the LS-DYNA crushable material models. To account for this discrepancy, a corrective calculation was undertaken in the MATLAB Arrestor Prediction Code. For the EDEM arrestor models, the important measured components were the depth and width of the rut created, and the corresponding loads that it produced.

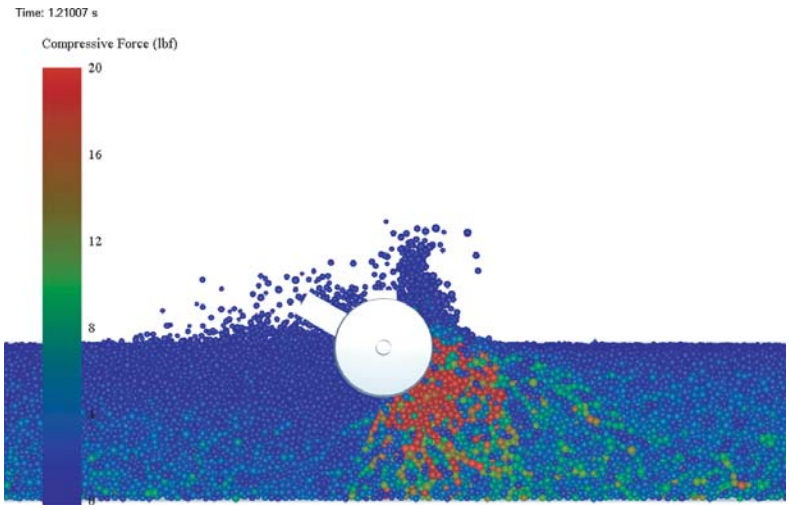


***Figure 10-16. Side cutaway view of engineered aggregate pendulum model, force fringe plot.***

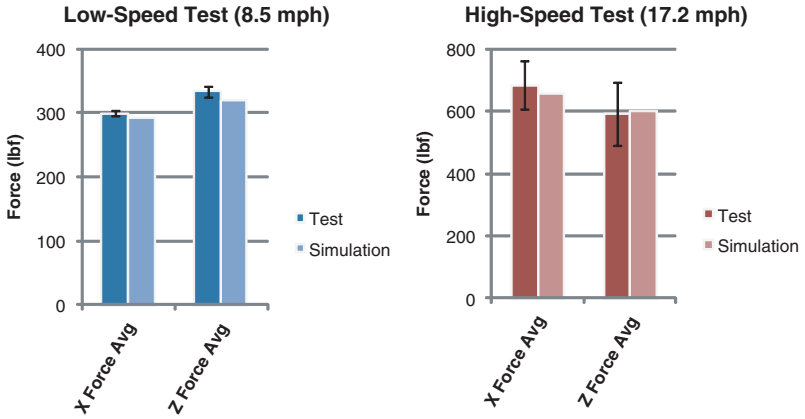


***Figure 10-17. Engineered aggregate pendulum model data comparison to test data.***

Because the tires were non-deforming, the tire library was simplified down to three tires instead of the five tires used in the crushable models (Table 10-2). The 44.5-in. and 49-in. main-gear tires of the B737 and B747 were very close to the same size. Similarly, the 29-in. main-gear CRJ-200 tire and 27-in. nose gear B737 tire were very close to the same size. The ruts each tire created would, therefore, be similar. As such, predictions for the 49-in. and 29-in. tires were scaled from the 44.5-in. and 27-in. tire models using width correction factors.

The tire path through the arrestors was based on a prescribed motion using a fixed forward speed and rotation rate. As the tire passed through the bed, a steady-state loading resulted. The vertical and horizontal loading at this state was measured.

Unlike the LS-DYNA arrestor models, the tire spin could not be released to settle at a steady self-rotation rate in EDEM,

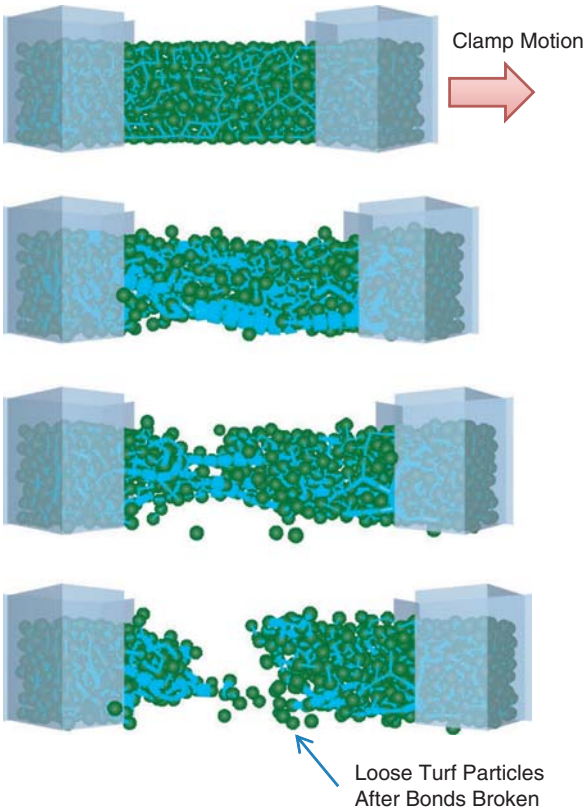


***Figure 10-18. Turf tensile test model showing turf particles (dark) and bonds (light).***

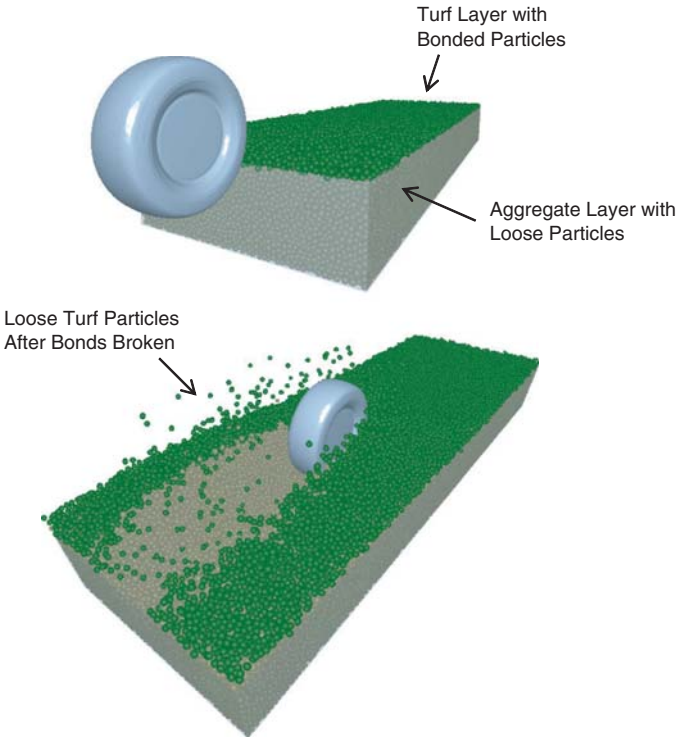


***Figure 10-19. Model of combined tire and engineered aggregate arrestor system showing aggregate (light) and turf (dark) particles.***

**Table 10-2. Tire library simplification for engineered aggregate arrestor models.**

| Aircraft | Landing Gear | Tire Designation | Modeling Method |
|---|---|---|---|
| CRJ-200 | Main Gear | H29x9.0-15 | Scaled from H27 Data |
| | Nose Gear | R18x4.4 | Modeled in EDEM |
| B737-800 | Main Gear | H44.5x16.5-21 | Modeled in EDEM |
| | Nose Gear | H27x7.7-15 | Modeled in EDEM |
| B747-400 | Main Gear | H49x19-22 | Scaled from H44.5 Data |
| | Nose Gear | H49x19-22 | Scaled from H44.5 Data |

since EDEM does not have inherent dynamics calculations for the rigid tire parts. Instead, it was held at a constant prescribed rate, assumed to be the ideal rate of spin that the tire would have on a hard surface with no slippage at the given forward speed. This unfortunate necessity affected the prediction accuracy because the tires can exert a forward "driving" type of torque due to their constant rotation rate. The impact of this effect was mitigated by prescribing a low tire-to-aggregate friction of 0.10, which limits any fictitious driving effects. The impact of such driving was deemed a second-order effect in the simulations.

Future simulations using the aggregate could potentially link EDEM with a dynamics code for improved accuracy; such enhancements were, however, outside the scope of the current effort.

## 10.4.4. Batch Simulations

Using the arrestor bed model, large batches of simulations were conducted to generate substantial bodies of data for a wide range of overrun conditions. This data was then assembled into "metamodels" for uploading and use by the APC.

### *10.4.4.1. Methodology*

Batch simulations were conducted for each tire with three open variables:

- **Speed,** from 10 to 70 knots (Speeds below 10 knots were impractical due to the long simulation times required for a tire to travel the required minimum distance. Loading at speeds below 10 knots was based on the extrapolated metamodel data fit.);
- **Bed depth,** from 6 to 36 inches (Figure 10-20); and
- **Penetration** into the bed, from 10% to 100% of bottoming depth.

Batch simulations for the EDEM arrestor models were more involved than for the LS-DYNA models because the optimization software, LS-OPT, could not automatically create parameterized variants of the models. Consequently, the input files were created manually prior to running, using experimental design points specified by LS-OPT. After the simulations were finished, the measured load data was then extracted manually and assembled into a form that could be read back into LS-OPT. The time-consuming nature of this manual approach led to a simplified process: simulations were done in batches of 50 for each tire in a single iteration. No additional add-on runs were undertaken, which was often done for the LS-DYNA batches in an attempt to increase the accuracy of the final data set.

### *10.4.4.2. Summary Tables of Metamodels*

The output from the batch simulations was assembled and uploaded into LS-OPT, where metamodels were constructed for the drag and vertical load forces. Metamodeling is analogous to fitting a curve through experimental data, except it is applied to multi-dimensional data sets. Here, the data sets are

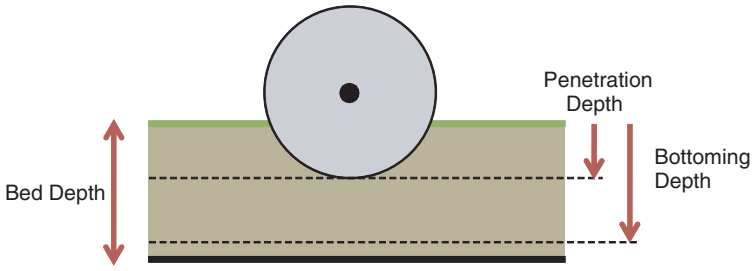


***Figure 10-20. Depth definitions for engineered aggregate bed models.***

**Table 10-3. Metamodel accuracy summary for engineered aggregate/turf arrestor bed.**

| Tire | Experimental Points | Points Used | Response | RMS Error | $R^2$ |
|---|---|---|---|---|---|
| H44 | 50 | 48 | Drag | 3.52% | 0.999 |
| | | | Vertical | 4.20% | 0.996 |
| H27 | 50 | 48 | Drag | 4.38% | 0.998 |
| | | | Vertical | 8.38% | 0.982 |
| R18 | 50 | 48 | Drag | 7.59% | 0.993 |
| | | | Vertical | 5.00% | 0.987 |

four-dimensional, including speed, depth, penetration, and load (either vertical or drag). The metamodels used for these responses were RBF networks, which can effectively capture non-linear behaviors including multiple concavity changes across the data set.

Table 10-3 summarizes the fit quality for the metamodels. The RMS error was typically below 5%, and the R-squared value was typically above 0.99, indicating good fit quality with minimal noise.

In the table, two outlier points were eliminated from each data set such that the metamodels were constructed using 48 of the 50 original experimental design points. Reasons for the outliers generally were data measurement issues arising from a failure of the run to reach steady-state conditions prior to the tire exiting the arrestor bed.

### *10.4.4.3. Parameter Sensitivities*

Using the metamodels, it is possible to review how sensitive the landing gear loads are to the different variables of speed, bed depth, and penetration percentage. The unusual feature for the engineered aggregate system is that the response is very sensitive to forward speed. Practically speaking, this means that the engineered aggregate system will exert more load on the landing gear when the aircraft is travelling at high speed, and less at low speed.

Figure 10-21 shows a surface plot for the metamodel. The drag force in this case becomes stronger (more negative) where the speed increases. For a deep penetration along the left-front edge of the plot, the loading at 70 knots is 34,700 lbf, and at 10 knots it is only 2,400 lbf—a factor of 14 difference.

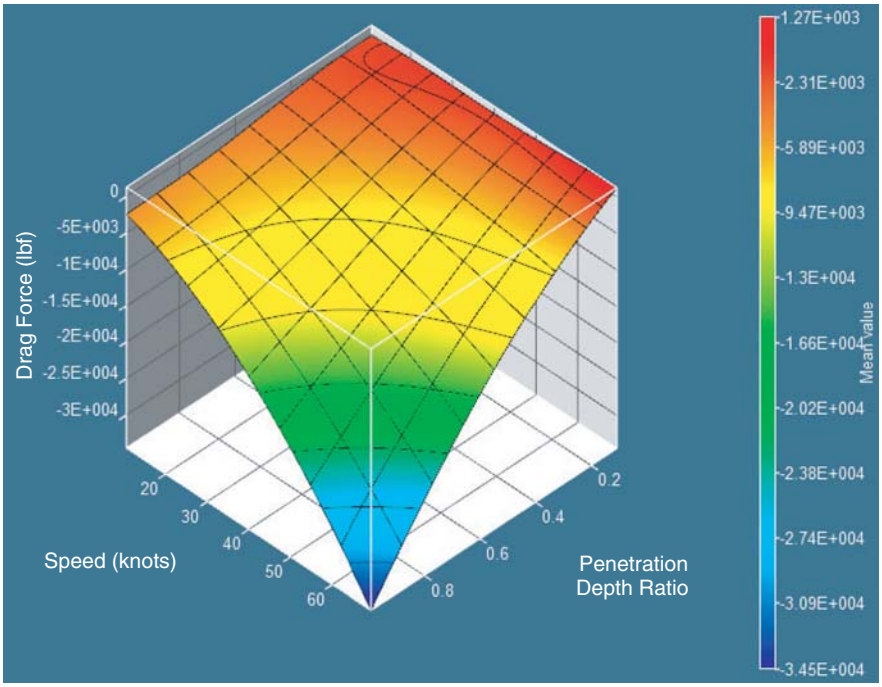


***Figure 10-21. Metamodel drag load surface plot for 44.5-in. tire in an 18-in. deep arrestor/turf bed.***

**Table 10-4. Comparison of speed sensitivities for engineered aggregate systems with and without turf cover layer.**

| System | Drag Force | Vertical Force |
|---|---|---|
| Aggregate/Turf | -14 | 20 |
| Aggregate Only | -20 | 23 |
| Percent Advantage for Aggregate/Turf | 30% | 13% |

The drag load was found to be dependent on speed and speed-squared terms:

$$Drag = A \cdot Speed^2 + B \cdot Speed + C$$

### 10.4.4.4. Effect of Turf Cover Layer

The presence of the turf cover layer produced a mild decrease in the rate sensitivity as compared with a bed of plain aggregate without a cover layer. Table 10-4 compares the relative sensitivities of the two systems to the aircraft speed (H44.5x16.5-22 tire). It may be possible to further enhance this mitigating effect with design improvements to the cover layer.

Another advantage of the turf layer is a predicted reduction in the aggregate ejecta thrown from the tire rut. Figure 10-22 shows a comparison for an 18-in. deep bed with a 44.5-in. tire at a deep penetration level (99%). In the left-hand illustration, the aggregate particle flyout is shown with the turf layer omitted. The right-hand image is the analogous case for a bed with no turf cover layer. The maximum aggregate particle velocities are similar in both cases (~1,000 in./s), but the volume of debris appears to be reduced where the turf layer is present.

If the ejecta plume is mitigated in this way, it could reduce the risk of ingesting aggregate particles in the aircraft engines. However, the reality of this predicted behavior requires confirmation through physical testing.

### 10.4.4.5. Effects of Penetration Depth

The bi-layer construction of the turf-covered aggregate bed can lead to situations where the tire creates a tunnel beneath the turf surface. Figure 10-23 illustrates such a situation, where the turf layer is stretched, but not broken, above the small 18-in. diameter tire. In actuality, the landing gear vertical strut member would sever the turf layer, preventing a complete tunnel. Additionally, bed designs of this relative depth would typically not be feasible because they would overload the landing gear.

### 10.4.4.6. Data Transformation

The final metamodel data for each tire was converted for use by the APC. LS-OPT was used to extract nominally 9,000 data points from each metamodel and export them into tabular form. A MATLAB matrix conversion program was written to map this data into multi-dimensional matrix form that could be quickly accessed by the APC.

For the two tires not explicitly modeled, the appropriate response surface data was scaled to produce an approximate metamodel (Section 10.4.3.2).

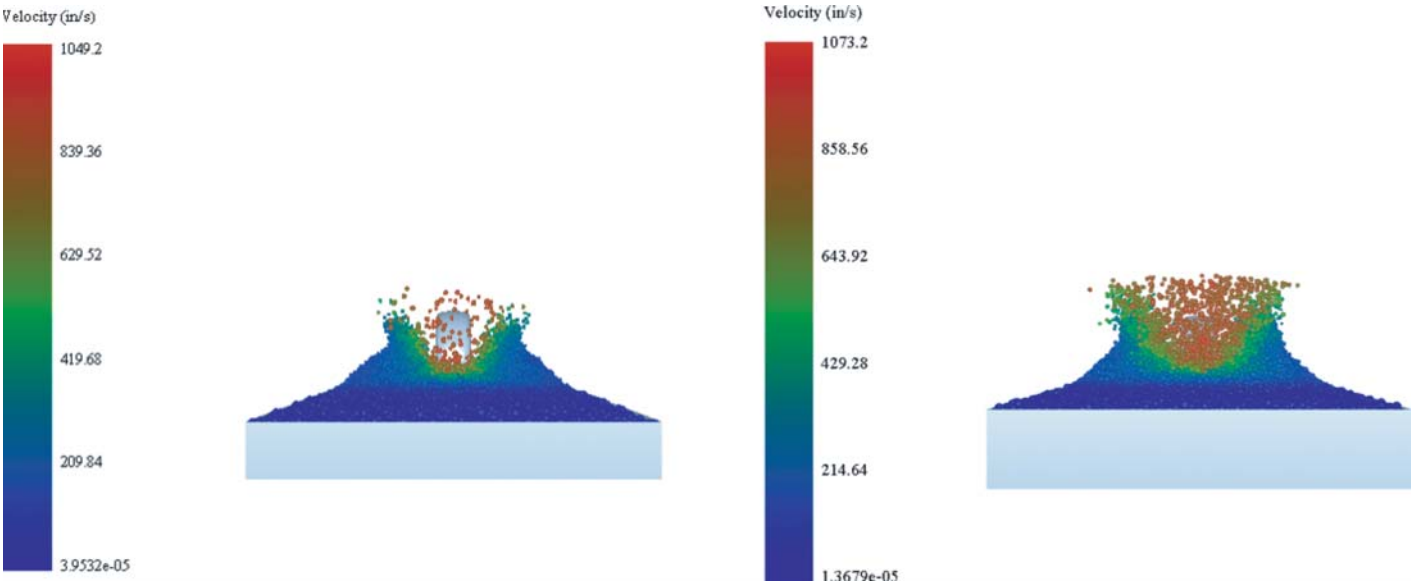


***Figure 10-22. Ejecta plumes of engineered aggregate for beds with (left) and without (right) turf cover layers.***

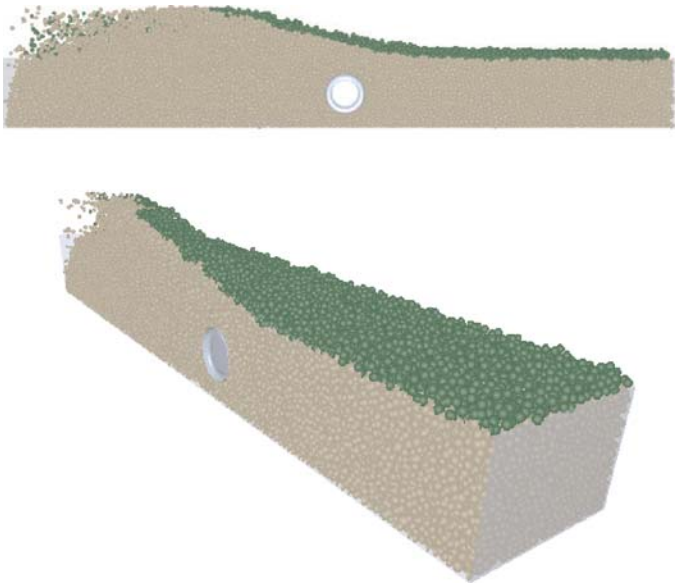

*Figure 10-23. Tunneling of tire below turf surface.*

## 10.5. Arrestor Performance Predictions

### 10.5.1. Scope of Simulations

Using the APC, a separate optimal arrestor was designed for each of the three trial aircraft: CRJ-200, B737-800, and B747-400. Subsequently, an optimal mixed-fleet arrestor was designed as a compromise best-fit for all three aircraft.

All simulations assumed a turf-covered arrestor bed with dry aggregate. If a drainage-type arrestor bed were used, the aggregate would be intermittently wet and dry, and longer arrestor designs would be required.

It was determined through experimentation that the aggregate arrestor design functioned best as a fully recessed bed, with the top of the turf level with the runway, and the remainder of the material placed in a basin below grade.

The predicted stopping distances for the three aircraft are given in Table 10-5. All arrestment predictions assumed the following:

- 50-ft setback distance;
- 50-ft gradual decline to the maximum bed depth;
- 70-knot starting speed for the aircraft;
- No reverse thrust;
- Braking factor of 0.25 before and within the bed; and
- Arrestor bed loads based on interaction with tires, neglecting strut and axle components.

Arrestor beds were designed for two different nose-gear loading criteria:

1. **Limit Load Criterion,** where the drag load applied to the nose strut cannot exceed the limit load for the nose gear (FAR Part 25.509);
2. **Ultimate Load Criterion,** where the drag load applied to the nose strut cannot exceed the ultimate load for the nose gear;

Since the ultimate loading criterion permits higher loads on the strut, deeper beds and shorter stopping distances resulted from those cases.

### 10.5.2. Performance for Test Aircraft

Table 10-5 lists best-case arrestor designs for each aircraft taken individually. Each arrestor bed listed uses a different material strength and depth that are optimized for the design aircraft. Generally, a range of acceptable strength and depth combinations was available. Compared with the similar EMAS design cases on the right (provided by ESCO), the distances are comparable if the ultimate loading criterion is used.

Table 10-6 shows the compromise design case with the best arrestor design for all three aircraft. The CRJ-200 controls the bed depth in this case, while the B737 controls the bed length. With the material strength and depth as specified, the B747

**Table 10-5. APC predicted 70-knot stopping distances for engineered aggregate arrestor system.**

| | Nose-Gear Limit Load Criterion | | Nose-Gear Ultimate Load Criterion | | Current EMAS, Optimal Designs | |
|---|---|---|---|---|---|---|
| **Arrestor Bed Design** | Depth (in.) | Bed Length (ft) | Depth (in.) | Bed Length (ft) | Depth (in.) | Bed Length (ft) |
| **Single Aircraft** | | | | | | |
| **CRJ-200** | 9.6 | 495 | 14.1 | 310 | 20 | 258 |
| **B737-800** | 13.5 | 462 | 19.5 | 361 | 20 | 287 |
| **B747-400** | 29.1 | 568 | 34.7 | 517 | 26 | 495 |

**Table 10-6. Fleet design arrestor bed for glass foam arrestor system.**

| | Nose-Gear Ultimate Load Criterion | |
|---|---|---|
| **Bed Dimensions** | 14.1-in. depth<br>400 ft long | |
| **Aircraft** | **Exit Speed (knots)** | **Stopping Distance (ft)** |
| **CRJ-200** | 70+ | 335 |
| **B737-800** | 63 | 400 |
| **B747-400** | 39 | 400 |

would require 922 feet to decelerate from 70 knots. Per typical design practice for an EMAS, the bed length may be specified such that all aircraft satisfy the minimum 40-knot exit speed requirement. For comparison with the other alternatives, the bed designs in the table assume a 400-ft length. At this length, the B737-800 and B747-400 would have maximum exit speeds of approximately 63 and 39 knots, respectively. The former satisfies the requirements of AC 150-5220-22a, while the latter is just below the 40-knot minimum.

### 10.5.3. General Observations

Figure 10-24 and Figure 10-25 give sample output plots from the APC for the B737 arrestor bed case for the limit and ultimate design cases, respectively. The setback for the bed is given in negative x-distance values, with the arrestor bed beginning at $x = 0$. As shown, the deceleration and nose gear drag loading are highest just after entry into the bed, when the nose wheel is located at 70 ft into the bed. Here the bed depth has increased to a maximum, but the forward velocity is still high. Due to the rate dependent nature of the loading, the drag load peaks here and tapers steadily as the aircraft decelerates.

From a standpoint of mechanical efficiency, this behavior is less desirable than an ideal constant deceleration rate. As the aircraft speed decreases, the arrestor becomes ever less efficient, stretching out the end of the arresting process.

From a standpoint of safety, this behavior requires a suitable design criterion to be developed with regard to design exit speeds. If, for example, a bed has been designed for a particular aircraft at a 70-knot overrun speed, the landing gear loading would reach a maximum redline value at about 70 knots. If that aircraft were to overrun the arrestor at 80-knots in an actual event, damage or failure of the landing gear could occur. A second possible scenario would involve a short landing, when the aircraft touches down in the arrestor bed. A suitable criterion could require higher design speeds to ensure a margin of safety; however, the current EMAS advisory circular does not specifically contain such a provision.

### 10.5.4. Braking Effects

The assumed braking factor of 0.25 is applied to the main gear as a coefficient of friction, which helps to slow the aircraft. However, this may not be a valid assumption for the engineered aggregate systems. Because the aggregate is loose and rolls easily over itself, it may not provide a good base beneath the tire for braking. This "bottoming" behavior, when the material is compacted in a thin layer beneath the tire, will require more experimentation to better understand and accurately represent within the APC. However, in the absence of data to the contrary, a braking factor of 0.25 is likely still a reasonable, conservative assumption.

### 10.5.5. Short Landings

Short landings involving an aircraft touch down inside the arrestor bed were not simulated. However, the potential for short landings presents an additional issue for consideration.

The basin geometry of the arrestor concept would force the aircraft to roll up the decline slope in the reverse direction from normal, acting as a ramp that would cause a strong load to the landing gear. This issue could be eliminated by only partially recessing the bed, as in the ideal EMAS design cases. Retaining walls or berms would be required for confining the aggregate and allowing the bed to maintain its shape in an above-grade orientation. With a nominal bed thickness of 20 in., it is unlikely that this would present a significant obstacle to implementation.

## 10.6. Estimated System Cost and Upkeep

### 10.6.1. Installation Process

The engineered aggregate concept would require excavation of an arrestor bed basin with a depth nominally equivalent to that of an EMAS bed. This basin may or may not require paving before being filled with aggregate. However, the below-grade nature of the basin would require drainage from the bed to be included in the design using standard roadway engineering practices. The basin would be filled with aggregate using earth-moving heavy equipment. If a reinforced turf layer is used, the turf would be grown ahead of time, then cut into segments and placed atop the bed with heavy equipment.

The loose aggregate solution offers the advantage of construct-in-place simplicity that could produce installation cost savings over a traditional EMAS. It reduces site preparation and eliminates block manufacturing, placement, and joint sealing. Additionally, the durable nature of the engineered aggregate means that the bed filling process will not require special care to be taken; this will further

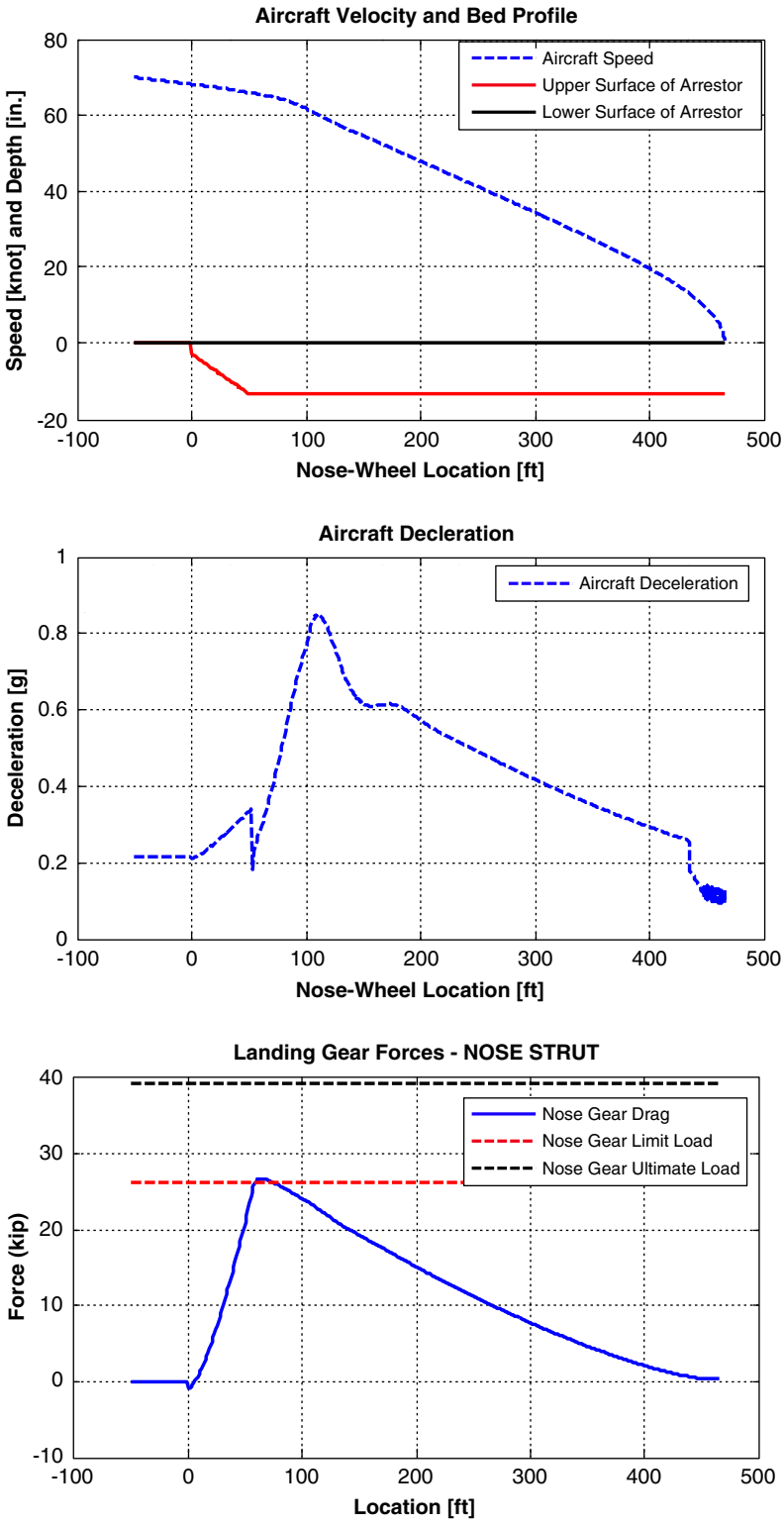


***Figure 10-24. Limit criterion engineered aggregate arrestor design plots for B737-800 showing speed (top), deceleration (middle), and nose-gear load (bottom).***

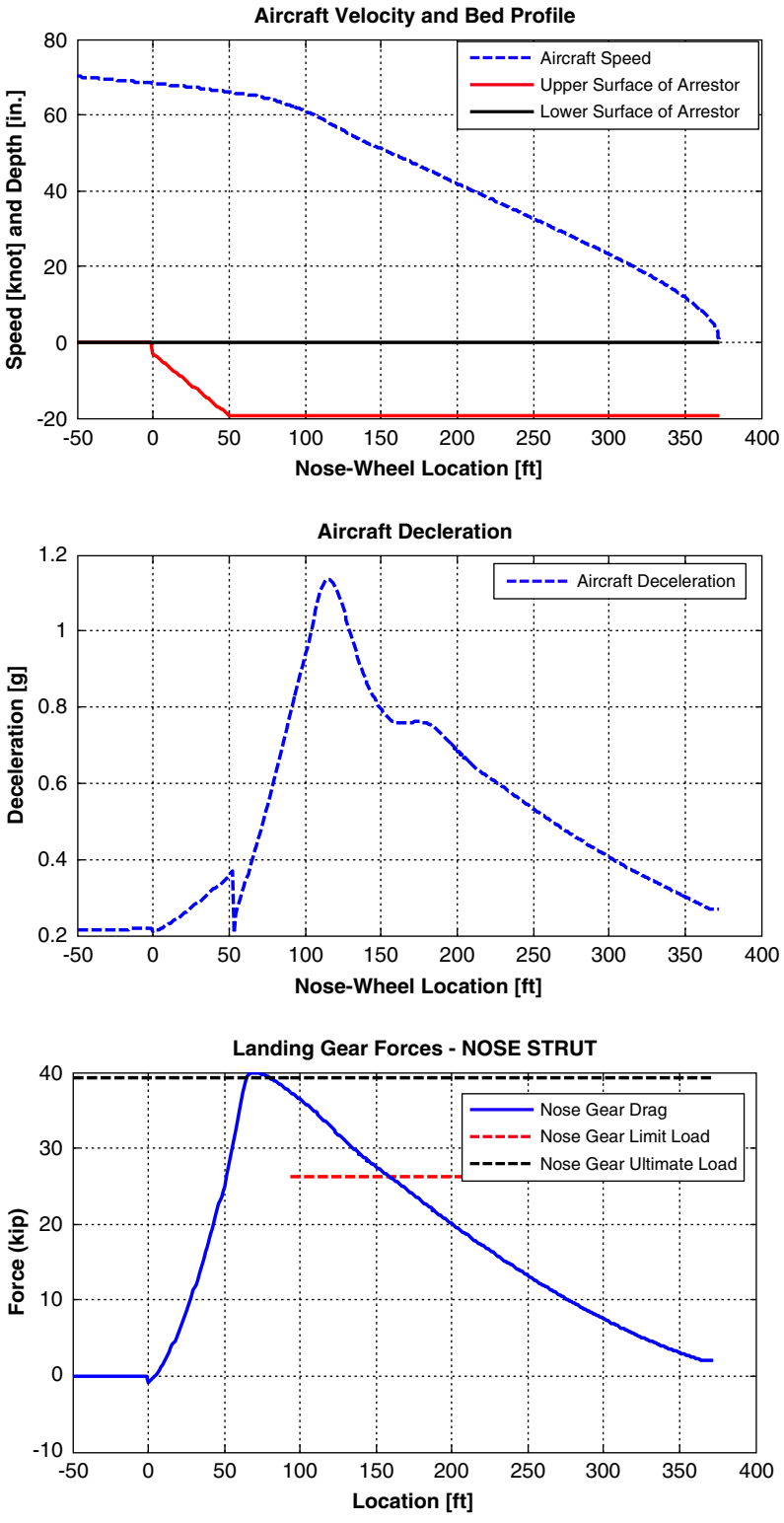


***Figure 10-25. Ultimate criterion engineered aggregate arrestor design plots for B737-800 showing speed (top), deceleration (middle), and nose-gear load (bottom).***

speed the installation process. However, turf preparation and placement would be additional tasks not required for the current EMAS design.

### 10.6.2. Cost to Establish System

A preliminary estimate was made for the cost to establish an engineered aggregate arrestor system. It must be noted that the cost estimate from this section is only a basic approximation for the purposes of comparing the different arrestor alternatives. The cost estimate is based on a mixture of information from the manufacturer, the airport survey, and FAA Order 5200.9. To develop a more accurate estimate of the costs to install such a system, it is recommended that a detailed cost quote be sought from a firm qualified to undertake an installation effort. Where possible, the methodologies used were consistent with the prior survey information collected regarding the existing EMAS (Section 3.5).

The costs may be broken into two major categories: site preparation and installation. The site preparation costs were estimated for two cases. The engineered aggregate arrestor would use a basin for the arresting materials rather than a flat runway-type surface as is used for the current EMAS. The bottom of the basin could either be paved or earthen. Drainage, excavation, and leveling would be required for either option. Assuming that a full-paved surface is not provided under the bed, the cost for site preparation was assumed to be reduced by half; this value was used for the lower-bound cost estimate for the system. If a full-paved surface is provided, identical to that of an EMAS, then the preparatory costs were assumed to be the same as for an EMAS; this provided the upper-bound cost estimate.

The installation cost estimate was separated into specific materials and general installation labor needs. Because these costs were specific to the engineered aggregate arrestor concept, they do not have a direct connection to any prior EMAS data. Discussions with the manufacturer produced cost estimates for the engineered aggregate, reinforced turf cover layer, and geo-textile/geo-plastic layers. Where applicable, materials included freight costs for trans-Atlantic shipping. The labor costs were based on estimates from the manufacturer established from similar installation efforts.

Finally, the site preparation and estimated EMAS costs were computed in two ways: (1) assuming average survey costs from this research, and (2) assuming FAA Order 5200.9 costs. The final cost estimates for both options are given in Table 10-7 and Table 10-8, respectively.

Using the survey cost assumptions of Table 10-7, a 300-ft arrestor bed would cost between 30% and 43% less than the current EMAS. If the Order 5200.9 costs are assumed, the cost advantage drops to between 5% and 12% (Table 10-8).

**Table 10-7. Estimated costs to establish engineered aggregate arrestor, 150 x 300 ft, assuming survey average costs for current EMAS, units of millions USD.**

| Cost Category | Engineered Aggregate System | | Current EMAS |
|---|---|---|---|
| | Lower Bound | Upper Bound | |
| Site Preparation | $ 1.08 | $ 2.16 | $ 2.17 |
| Installation | $ 3.61 | $ 3.61 | $ 6.03 |
| Cost to Establish | $ 4.69 | $ 5.77 | $ 8.19 |
| Percent of EMAS | 57% | 70% | |

In addition to the tables in this section, longer-term life-cycle issues could also be considered. FAA Order 5200.9 includes a standard 10-year replacement interval for an EMAS, which translates into present-value life-cycle costs. Such a replacement could arguably be unnecessary for this arrestor concept (Section 10.6.4). Eliminating the assumed 10-year replacement could effectively trim about $2.6M off present-value life-cycle costs (based on the EMAS replacement cost estimates of the survey).

### 10.6.3. Maintenance

Maintenance for the engineered aggregate concept would be relatively simple, and should be limited to standard groundskeeping measures for the protective turf layer. Drainage of the area to prevent standing water is required and periodic inspections would be advisable to ensure that no issues arise due to seasonal weather changes. Due to the lack of joints, blocks, and degradable materials, many protective measures used in current EMAS construction would not be necessary. Therefore, the predicted maintenance needs are lower than for that of the existing EMAS.

**Table 10-8. Estimated costs to establish engineered aggregate arrestor, 150 x 300 ft, assuming Order 5200.9 costs for current EMAS, units of millions USD.**

| Cost Category | Engineered Aggregate System | | Current EMAS |
|---|---|---|---|
| | Lower Bound | Upper Bound | |
| Site Preparation | $ 0.34 | $ 0.68 | $ 0.68 |
| Installation | $ 3.61 | $ 3.61 | $ 3.83 |
| Cost to Establish | $ 3.95 | $ 4.29 | $ 4.50 |
| Percent of EMAS | 88% | 95% | |

Compared with crushable materials, there are no material breakdown concerns regarding freeze–thaw exposure. However, it is presently unknown how substantially ice may affect the inter-particle friction of the aggregate; changes to the friction could alter the dynamic arresting response. Additionally, dirt entrainment over time could solidify the bed if the drainage approach is used for handling precipitation. Therefore, the waterproofed option is recommended to minimize the maintenance and performance impacts of water, soil, and ice.

### 10.6.4. Replacement

All materials included in the engineered aggregate concept are expected to last for the 20-year life cycle prescribed in the EMAS Advisory Circular, if not longer. It is not anticipated that replacement of the bed would be required after 10 years, as anticipated for an EMAS in FAA Order 5200.9.

### 10.6.5. Repair

After an overrun event, the rut areas would require repair. The aggregate remaining in the ruts would be reusable, and fresh aggregate would likely need to be added to bring the beds back to level condition. The damaged cover layer, if used, would need to be removed from the rut areas and replaced with fresh material. If the cover layer is turf, it is possible that replacement turf could be planted at another area of the facility on initial installation of the system. When replacement needs arise, this turf could be harvested for immediate use to prevent delays that would accompany growing fresh turf.

## 10.7. Transition to Fielded System

In order to transition the engineered aggregate concept to a fielded system, the following additional development steps may be advisable.

### 10.7.1. Cover-Layer Design

Several cover-layer design concepts are possible:

1. Thin sealant,
2. Asphalt skim coat,
3. Reinforced turf layer,
4. Reinforced turf with geo-textile fabric, and
5. Turf/geo-textile/plastic composite cover layer.

Only concept three was modeled during the research effort. Additional testing and modeling would be required for whichever method is selected since the membrane behavior of a cover layer will impact the dynamic mechanical performance of the arrestor bed. The cover layer performance should be further characterized under frozen conditions because it will be exposed to such conditions even where the aggregate layer of the system is waterproofed.

### 10.7.2. Bottoming and Braking Dynamics

The research performed has identified that tire bottoming and braking in the aggregate material require further study. The current modeling method of the APC makes simplifying assumptions regarding both phenomena sufficient for a concept-level evaluation. However, to ensure accuracy of design predictions, some additional tests would be required. One method could involve using a one-wheel bogy apparatus fitted with brakes and a load measurement system that is towed through the material.

### 10.7.3. Aggregate Ingestion

While the presence of a cover layer appears to offer mitigation of aggregate spray, it is unclear as to the level of residual hazard remaining. The spraying gravel from the nose-wheel may or may not pose an ingestion hazard for the aircraft engines. If an ingestion hazard is present, it is unclear what practical risk this presents with regard to engine damage, potential fire, and so on. A limited test series using a one-wheel bogy apparatus may be able to answer the issue of ingestion likelihood. Discussions with aircraft manufacturers or other FAA safety personnel should provide insight into the practical risks in the event that ingestion occurred.

### 10.7.4. Requirements and Standards

Due to the speed dependence issues, development of a practical design criterion for the design exit speed may be advisable to ensure a factor of safety for the landing gear.

### 10.7.5. Full-Scale Testing

A full-scale aircraft overrun test of an engineered aggregate arrestor bed is advisable because this concept represents a substantial departure from the current EMAS design in terms of mechanical loading and the materials used.

## 10.8. Summary

Of the candidate systems evaluated, the engineered aggregate arrestor concept is most dissimilar to the current EMAS technology. It uses a hard spherical aggregate that primarily undergoes displacement rather than the compaction that occurs with crushable foams like cellular cement. The arresting bed would be constructed with a shallow basin of the material topped with a reinforced turf cover layer.

Since the engineered aggregate material is not a porous foam, it is durable against moisture and other environmental factors,

including water immersion. However, while the material itself does not degrade with such exposures, the mechanical response changes, exhibiting an increase in arresting loads when wet. To maintain predictable arresting performance, the material would require the use of protective plastic geo-membranes and typical drainage provisions. The material characteristics indicate that long service life is possible, potentially eliminating the standard 10-year replacement interval assumed in FAA Order 5200.9.

Installation of the system would likely be simpler and less expensive than for the current EMAS since placement of blocks and sealing joints is unnecessary. Heavy equipment would place the material in the bed basin and top it with pre-grown reinforced turf segments. Geo-membrane and geo-textile layers, as applicable, would be placed and joined manually. The arrestor basin could be constructed with or without paving, which could result in preparatory cost reduction.

The cost to establish such a system would be nominally 57% to 70% of the survey cost of the existing EMAS. Life-cycle costs could be reduced due to longer bed life. Maintenance needs appear to be simplified, requiring standard grounds-keeping measures, but no block or joint repairs.

The APC predictions for the engineered aggregate arrestor show that the deceleration varies throughout the arrestment process, exhibiting a strong dependence on aircraft speed. This is not a preferable characteristic; however, functional arrestor designs are still feasible. Arrestor bed lengths for individual aircraft were nominally 15% longer than for the current EMAS technology due to the speed-dependent properties of the arrestor. Additionally, the multi-aircraft design case for the concept showed the weakest performance among the three candidate systems. Bed designs that were safe for the smallest aircraft did not exert a strong deceleration load on the largest aircraft.

The speed dependence of the engineered aggregate bed would require development of a new design criterion. Overruns exceeding the rated exit speed or short landings into the bed could result in overloads to the landing gear if the speed dependence is not considered in the design process. Arrestor designs that include provisions for these events would necessarily have gentler decelerations and longer arrestment distances than the design cases cited in this research.

Transition to a fielded system would require finalizing a composite turf cover-layer design and calibrating a predictive model to match the response. Characterization would be advisable for the soil layer under various freezing conditions to assess the impact on arresting dynamics. Additionally, investigation should be made regarding the basin geometry to determine whether above- or below-grade construction is preferable. Full-scale testing is advisable for evaluation of the complete system.

CHAPTER 11

# Aggregate Foam Arrestor Concept

## 11.1. Concept Description

### 11.1.1. System Overview

An aggregate foam arrestor concept has been proposed. The arrestor would use rough-broken foam aggregate made from recycled glass (Figure 11-1). The foamed, or aerated, glass material has nominally 80% void space by volume. Its closed-cell microstructure makes it resistant to water absorption and degradation. The aggregate comes in a variety of gradations and is currently used in different civil engineering applications for light fill construction, insulation, and frost protection of road foundations and terraces (*43*). For the evaluation effort, fragments were graded to fall between 0.4 and 2.4 in., with a loose fill density of 11.2 pcf (Figure 11-2).

An arrestor using the aggregate foam would be constructed by creating a basin and filling it with the material (Figure 11-3). An engineered turf would serve as a top cover layer for the bed, which can serve several purposes:

1. Prevent material dispersion due to jet blast;
2. Mitigate material spraying during overrun by an aircraft tire, thus limiting engine ingestion hazard;
3. Regulate water drainage and potential ice crust formation in winter; and
4. Act as a structural component to prevent lightweight land vehicles from penetrating the arrestor bed.

This simple fill-and-cover construction would likely produce lower manufacturing and installation costs than the block construction methods used at present. This potential advantage is offset by the possibility that the material could settle over time and result in altered arresting performance; potential mechanisms of settling could include:

1. Consolidation, and
2. Mechanical/chemical degradation and shrinkage/breaking of aggregate pieces.

Because the aggregate foam material has a closed-cell microstructure, it has an inherent resistance to moisture. However, the presence of water during freeze–thaw cycling could present a more aggressive erosion hazard for the material. Two potential methods have been identified to handle precipitation (Figure 11-4).

1. **Drainage Approach.** This approach would allow water drainage downward through the bed. The bed would be designed to prevent standing water within it using normal civil engineering design practices.
2. **Waterproof Approach.** In this approach, layers of geoplastic and geo-textile materials would be employed at the top and bottom of the bed. The upper and lower plastic layers would be sealed at the edges to produce a watertight envelope around the fill material (a practice currently in use at some landfills). Precipitation in this design would run off to the perimeter of the arrestor bed.

### 11.1.2. Performance Considerations

Mechanically, each piece of material is composed of crushable glass foam, which has fairly conventional properties. However, when acting as a continuum, many irregular and loose-fitting pieces would exhibit flowing aggregate behavior. While the material would have compressive and shear strength properties, the loose aggregate would not exhibit tensile strength because nothing binds the loose pieces together. Overall, the aggregate foam concept falls somewhere in between a conventional foam block system and a conventional hard aggregate system.

Falling between these two different material categories, the aggregate foam concept presented multiple issues for evaluation:

- Overall dynamic response characteristics,
- Required density/strength for effective arresting,

*Figure 11-1. Aggregate foam material: pile of aggregate (left) and close-up of microstructure (right) (43).*

*Figure 11-2. Typical aggregate foam fragments.*

- Effect of aggregate size,
- Rate dependence of the material, and
- Durability to freeze–thaw exposure.

## 11.2. Testing and Modeling Approach

### 11.2.1. Overview

The goal for the performance evaluation was to undertake testing that would allow calibration of high-accuracy computer models of the aggregate foam concept. The testing approach evaluated several characteristics of the material, which was sufficient for a concept-level evaluation. The subsequent modeling approach for the aggregate foam material was comprehensive in nature, and the outcome was a calibrated numerical model for predicting arrestment loads.

The testing and modeling approach for the aggregate foam concept is illustrated by Figure 11-5. Five major stages are illustrated by the larger process bubbles of the chart:

1. **Arrestor Material Testing and Modeling.** Laboratory testing generated test data, and computer models of the material were calibrated to match it.
2. **Tire Modeling.** Aircraft tire models for the three test aircraft were built and calibrated to match manufacturer performance specifications.
3. **Aircraft Modeling.** A generalized aircraft model was developed to predict the suspension response of the plane and its deceleration during a ground roll. This model was then incorporated into an APC for determining stopping distances and landing gear loads when an aircraft is driven through an arrestor bed. A library of aircraft definitions was created to represent the three test aircraft.
4. **Metamodeling.** The arrestor material and tire models were combined to produce an overrun model for determining the loads exerted on the different aircraft tires by the arrestor bed. Large data sets were generated using simulation batches for each tire and arrestor combination. These data sets were then accessible by the arrestor prediction code (next step).
5. **Performance Predictions.** The preceding four development stages culminated in the final, bottom-most process

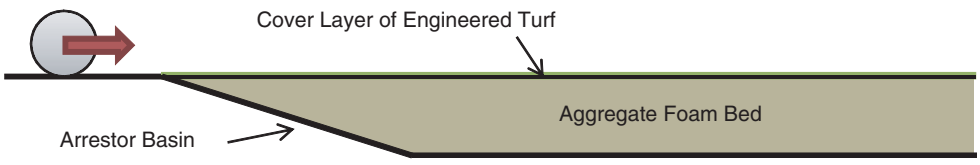


*Figure 11-3. Aggregate foam arrestor concept.*

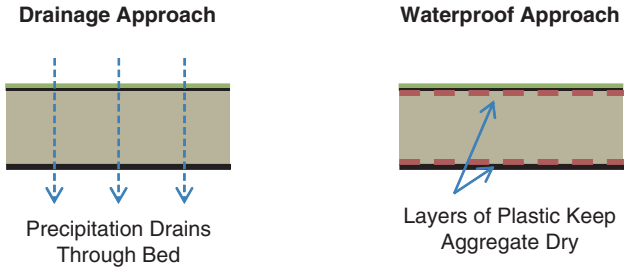


***Figure 11-4. Aggregate bed methods for handling precipitation and drainage.***

on the figure. The APC was used to predict arresting distances, landing gear loads, and ideal arrestor bed designs for the different aircraft.

The subsequent sections of this chapter will focus on areas (1), (4), and (5). Special attention will be given to the aggregate foam material testing that was conducted and the calibration of the computer models to match the tests. The development of the tire models (2) and aircraft model (3) will be reserved for Appendix F and Appendix G, respectively.

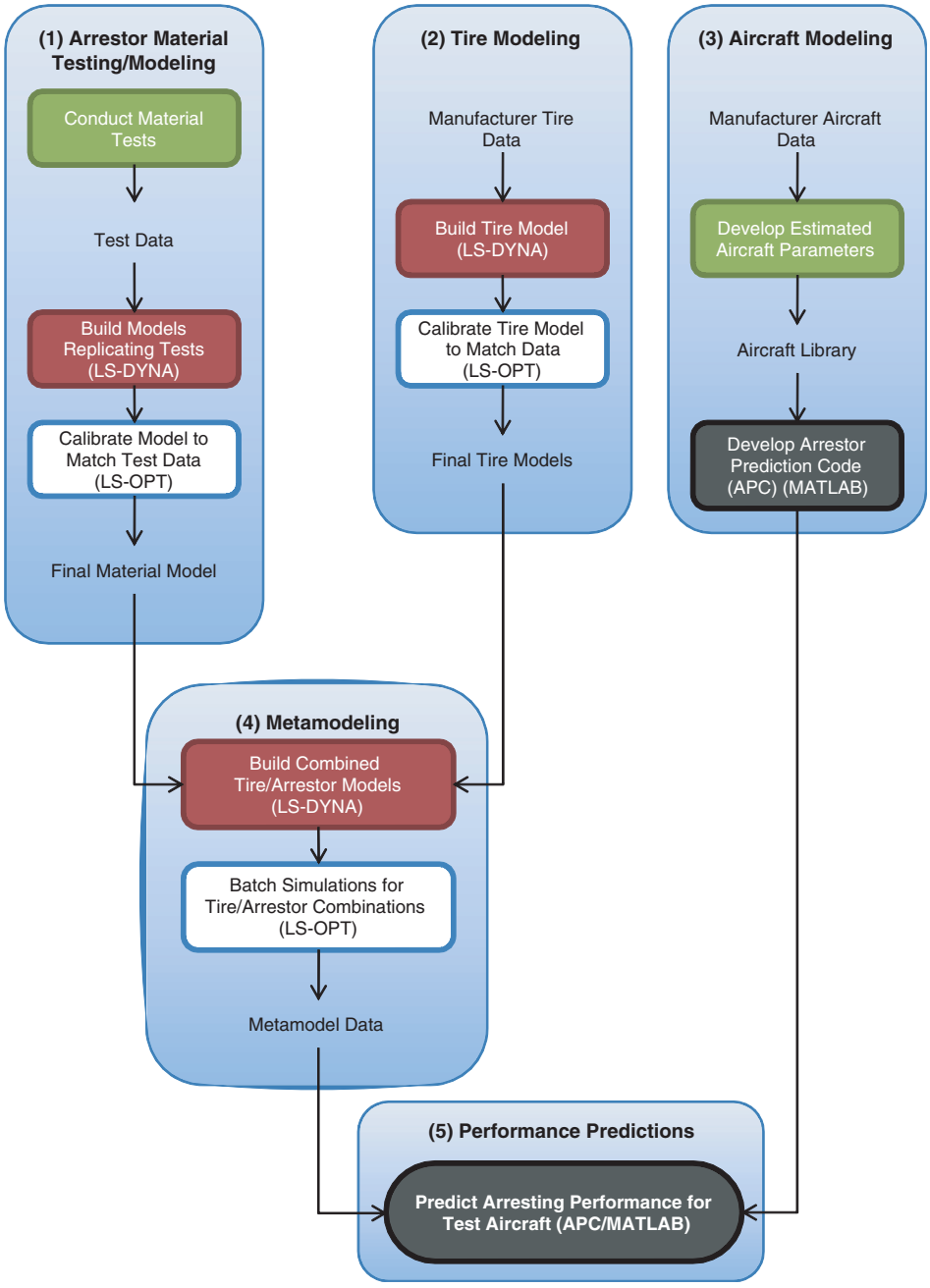


***Figure 11-5. Testing and modeling process for aggregate foam arrestor evaluation.***

### 11.2.2. Special Considerations

Overall, testing the aggregate foam proved challenging for three reasons:

1. The combined crushable and aggregate properties of the material did not readily fit into standardized test methods.
2. The large size of the foam pieces required large test fixtures to capture continuum-type properties of the loose fill; this precluded the use of some desirable tests.
3. The dual-mode material behavior did not allow comprehensive definition by the material models of the available modeling software.

## 11.3. Testing Effort

The testing effort for the aggregate foam material involved several mechanical and environmental tests. Table 11-1 depicts the overall test matrix for the aggregate foam material. All cylinder dimensions specify diameter followed by height.

### 11.3.1. Density and Dimension Measurements

The original, as-received aggregate foam material had pieces graded to between 0.4 and 2.4 in., with a loose fill density of 11.2 pcf. For a small sample of pieces measured, the average size was 1.9 in.

As previously discussed (Section 11.2.2), the as-received aggregate size precluded some testing that might otherwise have been conducted. For other tests, the aggregate was broken down into smaller pieces and sifted through a 1-in. grid, giving it a gradation of 0.4 to 1.0 inches.

All tests, therefore, were conducted on either the original 2.4-in. material, or on the reduced 1.0-in. material.

**Table 11-1. Test matrix for aggregate foam material.**

| Test | Properties Characterized | Detail | Number of Tests | |
|---|---|---|---|---|
| **Laboratory Tests** | | | | |
| Hydrostatic Triaxial Compression Test | • Compressive strength ($\sigma_u$)<br>• Shear strength ($\tau_u$)<br>• Effects of confining pressure on strength | • Per ASTM D2850<br>• 6 x 10.5" cylinder<br>• Reduced aggregate size<br>• Pieces graded for 0.4" to 1.0"<br>• 0.24%/min compression rate<br>• Maximum compression of 15 to 25%<br>• Confining pressures of 5, 10, 20, 60, and 100 psi | 5 psi<br>10 psi<br>20 psi<br>60 psi<br>100 psi<br>Total: | 1<br>2<br>2<br>2<br>2<br>9 |
| Confined Cylinder Compression Test | • Compressive strength ($\sigma_u$)<br>• Compressive stress–strain curve<br>• Extrapolated: volumetric energy capacity | • Version 1: Original Aggregate Size<br>• Non-standard<br>• Pieces graded for 0.4" to 2.4"<br>• 12.375 x 9.5" confining cylinder<br>• 3 in./min compression rate<br>• Maximum compression of 75% | | 2 |
| | | • Version 2: Reduced Aggregate Size<br>• Non-standard<br>• Pieces graded for 0.4" to 1.0"<br>• 12.375 x 7.5" confining cylinder<br>• 3 in./min compression rate<br>• Maximum compression of 45% | Fresh<br>Conditioned | 1<br>2 |
| Environmental Chamber Tests | • Durability to freeze–thaw cycles in fully immersed conditions | • Version 1: Per ATSM C 666/C 666M-03 (modified)<br>• Trays of material, 10 gallons total<br>• 50 freeze–thaw cycles<br>• Material compression tested thereafter | 2 | |
| | | • Version 2: Per AASHTO T 103<br>• Particles separated by gradation into different sieve sizes<br>• Particle size distribution changes measured<br>• 50 freeze–thaw cycles | 2 | |

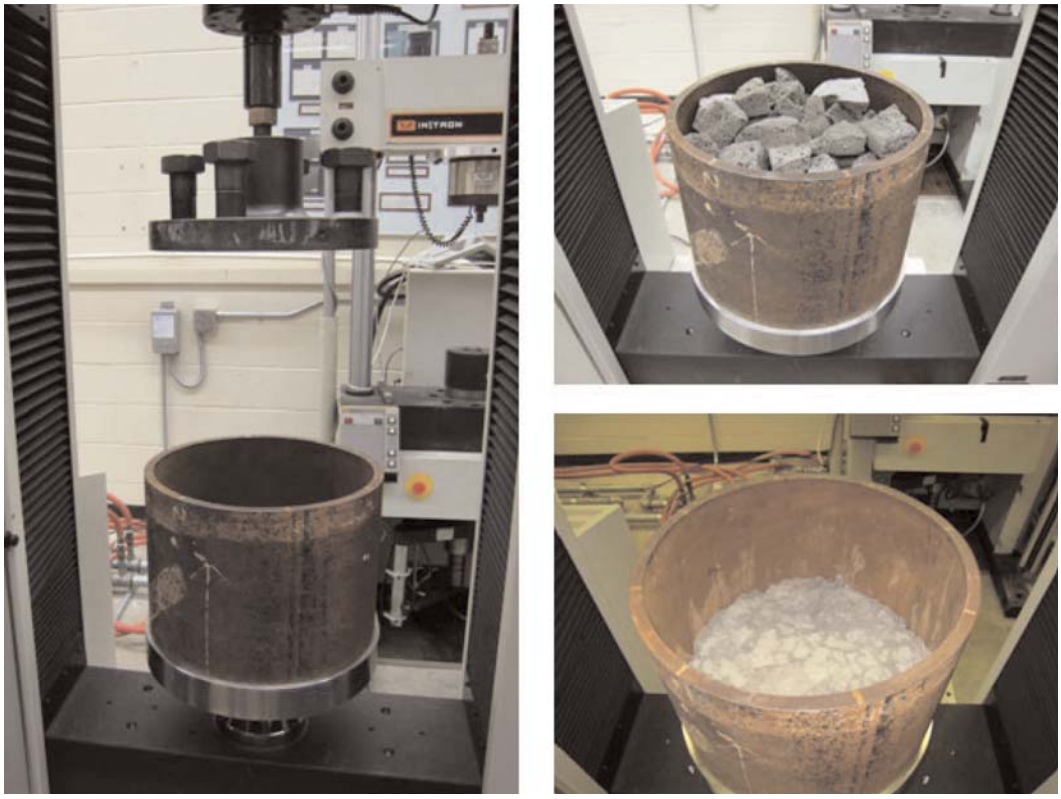

*Figure 11-6. Confined cylinder test for aggregate foam showing the test fixture (left), pre-test specimen (top) and post-test specimen (bottom).*

### 11.3.2. Confined Cylinder Compression Tests

Confined cylinder compression tests were performed on both the original and the reduced size aggregate foam. The tests were conducted by pressing a 12-in. diameter platen into a 12.375-in. diameter cylinder at a fixed rate of 3 in./min (Figure 11-6). The 12-in. diameter was chosen as being greater than six times the characteristic dimension of the material, which as a rule of thumb helps to ensure continuum material behavior. The material was poured loosely into the cylinder without packing. Due to the irregular nature of the aggregate, initial depth measurements were approximate.

The load data for replicate tests was remarkably consistent, despite the random nature of the selected aggregate pieces for each test. However, the gradation size of the aggregate appeared to have a substantial effect on the loading and the energy absorption.

Figure 11-7 illustrates the load history for both gradations. The general load curve shape followed an exponential form; as a result, the energy absorption also followed an exponential trend (Figure 11-8). As shown, the reduced gradation material only obtained a compression of about 45%, whereas the original larger gradation reached 75% at the same load. This led

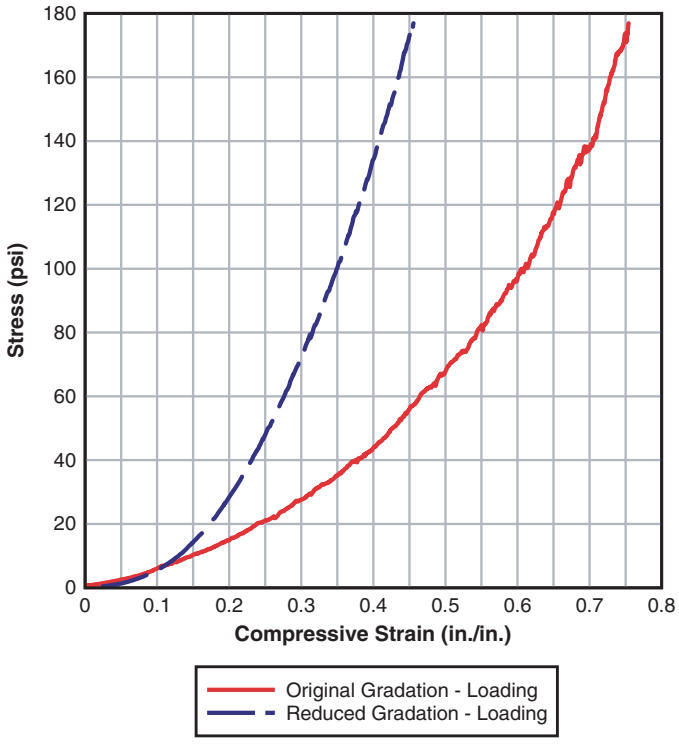


*Figure 11-7. Confined cylinder test average load histories for aggregate foam material.*

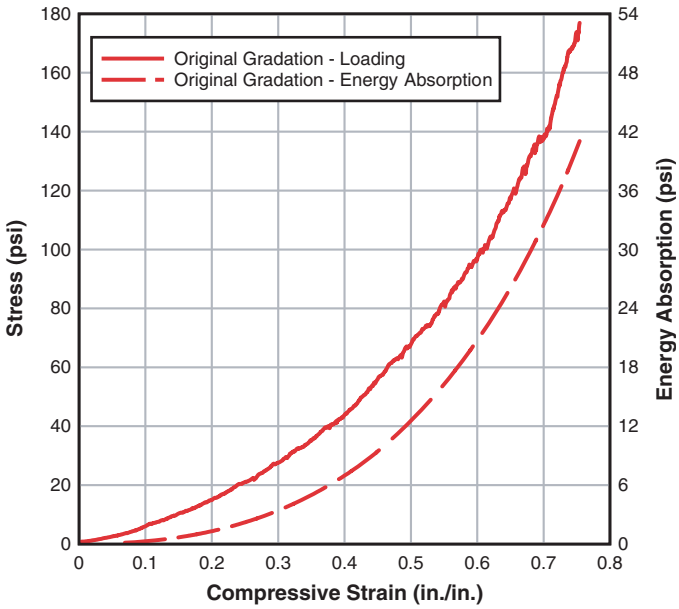


***Figure 11-8. Confined cylinder test stress and energy absorption for original gradation aggregate foam material.***

to a 39% decrease in energy absorption for the reduced gradation material.

The gradation effect may be due to two geometric differences between the specimens. First, in the larger gradation material, the particles may simply have more size variation. If the reduced gradation sizing was more uniform (smaller size range), then the packing ratio may have been higher, leading to less empty space between the particles. Second, some of the larger pieces had concave surface features that may have bolstered the void percentage of the original gradation material. Once broken into smaller 1-in. pieces, the particles may have become rounder, which would, again, reduce the empty space between the particles. In either case, or in a combined case, a reduction in the void space between pieces would lead to earlier compaction of the material and less energy absorption.

It is clear from these tests that the aggregate foam gradation would need to be chosen carefully for an arrestor application. Further, the intended gradation would need to be protected during the installation process and over the life of the bed. Repetitive vehicle overruns, jet blast, or other physical loads that might induce compaction or fragmentation of the pieces would need to be avoided. If gradation shifts occurred over time, the bed properties could change and lead to unanticipated mechanical performance.

Another important observation from the confined cylinder tests is that the material would, in effect, act as a depth-varying compressible material. Deeper tire penetrations would lead to an increase in vertical load, not simply because a larger surface area comes into contact with the material, but because the material continually hardens as the compression increases. This trend is dissimilar from a typical block of crushable foam, which reaches a fairly constant plateau strength for the majority of the compression range. The energy absorption for a crushable block increases linearly with compression; for the aggregate foam, the increase is exponential. This depth-varying property posed an interesting alternative for arrestor applications.

### 11.3.3. Hydrostatic Triaxial Tests

The hydrostatic triaxial tests evaluated the aggregate foam performance at different confining pressures to determine if any strength increase or bulking deformation took place. Due to the aggregate mode of behavior, lateral bulging of the specimens was anticipated.

The largest practical specimen size for testing was a 6-in. diameter cylinder. The reduced gradation material was developed to satisfy the rule of thumb for six times the nominal particle dimension across this width. All hydrostatic triaxial specimens used the 1-in. graded material.

The specimens were cylinders (6 × 10.5-in.) placed between platens using Sorbothane caps at the top and bottom (Figure 11-9, left). The specimens were fitted with flexible membrane sleeves before immersion in a pressurized vessel of water. While at this hydrostatic pressure, the specimens were compressed axially until reaching 15 to 25% compression. As shown on the right in Figure 11-9, the specimens bulked laterally as anticipated.

A wide range of hydrostatic pressures was explored in order to determine the overall effects on the material. The upper range was chosen as 100 psi because little was observed in the way of new trends by that pressure. Because the hydrostatic specimen data had more scatter than the confined cylinder data, a total of nine tests were conducted.

Figure 11-10 compares the hydrostatic triaxial data for the three main material candidates: glass foam block, aggregate glass foam, and hard engineered aggregate. The data points in the figure represent the top center for the Mohr's circles at the different confining pressure conditions. Of the three materials, the only material exhibiting a change in behavior is the aggregate foam, which has a distinct transition occurring at compressive stress of 20 psi. This 20-psi stress value would occur for a test specimen at a confinement pressure of about 15 psi.

Prior to the transition point, the trend-line fit to the aggregate foam has a steep slope and a very low initial value (near zero); these characteristics are analogous to the hard aggregate material. As the compressive stress drops to zero, so does the shear strength of the material. This is consistent with intuitive observations since lower confinement pressures allow the material pieces to roll and flow past one another more readily.


***Figure 11-9. Hydrostatic triaxial compression test of aggregate foam pre-test (left) and post-test (right), 100 psi confining pressure.***

After the transition point, the trend-line fit to the aggregate foam has a shallow slope and a much higher initial value (~6 psi); these characteristics are analogous to the foam block material, albeit with lower values. The pressure dependence of the material decreases substantially, producing solid-like behavior, where the individual pieces are compressed together too much to permit flow.

Because the transition point occurred at a fairly low confinement pressure (~15 psi), an important simplification became possible. By observing the confined cylinder load data from Figure 11-8, only about 3 to 5% of the total material energy absorption would occur by this point. Figure 11-11 illustrates the relative energy capacity of the material, divided by behavioral regime. The clear dominance of the solid regime from an

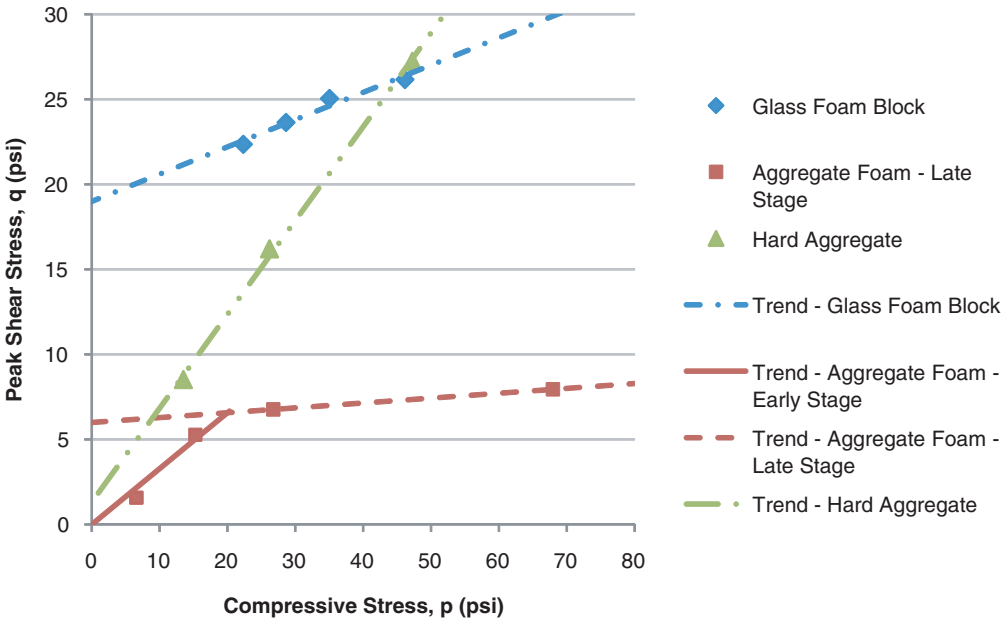


***Figure 11-10. Comparison of hydrostatic triaxial data for three primary material candidates.***

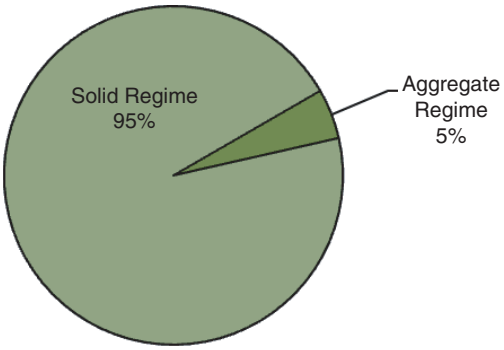


*Figure 11-11. Approximate compaction-based energy dissipation in aggregate foam, divided by behavioral regime.*

energy absorption standpoint eventually led to a modeling decision to use a solid crushable foam model to simulate the material.

### 11.3.4. Pendulum Tests

The pendulum tests that were conducted for the other candidate arrestor concepts were omitted for the aggregate foam material. It was determined that the ungraded material would be required for such tests. Having a nominal 2-in. particle size, this presented substantial scaling issues for the pendulum's ⅓-scale tire form. The wheel form was only 5 in. in width, leaving it at just over two particles wide.

Further, the effective penetration depth of the wheel would likely have been about 7.5 in., or half the diameter. This would likely have created a spraying of the upper surface particles, but minimum compression of the material. As such, minimal energy dissipation would have occurred.

Finally, the turf cover layer of the concept could not be scaled in thickness, mass, or strength, which would have made it disproportionate to the small wheel.

Making a larger wheel and strut assembly for the pendulum was considered, but ultimately not feasible. Larger wheels would produce more significant loads on the pendulum mass; the wheel size for the pendulum was chosen as the upper feasible limit without causing bouncing or path deviation of the mass.

### 11.3.5. Environmental Tests

Two sets of environmental tests were conducted to determine the necessity for weatherproofing the aggregate foam material.

The first test involved subjecting 10 gal of 1-in. graded material to freeze–thaw testing in various sized sieves, per AASHTO T103. The particles were fully immersed in water and subjected to 75 freeze–thaw cycles. The relative degradation of the different sized pieces was recorded. It was concluded that the particles generally eroded in size during the course of the testing. However, this test did not ultimately provide a great deal of insight regarding the performance impact of the degradation.

The second test also subjected 10 gal of 1-in. graded material to freeze–thaw testing. The test methodology was nonstandard, but similar in nature to ATSM C 666/C 666M-03. The aggregate foam was placed in two open plastic tubs and fully immersed in water (Figure 11-12). The specimens were then subjected to 50 freeze–thaw cycles. After the test, the

*Figure 11-12. Aggregate foam environmental test specimens before (left) and during (right) test.*


*Figure 11-13. Aggregate foam material environmental test specimens pre-test (left) and post-test (right).*

specimens were oven dried to eliminate the absorbed water mass (Figure 11-13).

Following the environmental tests, the specimens were subjected to a confined cylinder compression test (Figure 11-14) to determine the performance degradation. When compared with the fresh material, the samples exhibited a 47% decrease in energy absorption capacity.

Mechanically, the closed-cell microstructure of the foam limits water absorption such that water penetrates only the outer-most open pores of the foam. Upon freezing, the expanding water cracks the cells, permitting progressively deeper penetration into the specimen as the cyclical testing proceeds. The degradation observed is, therefore, not surprising.

These environmental tests represent the most severe of circumstances, where the specimens were fully immersed in water, without normal countermeasures of drainage or a protective plastic envelope. Information provided by the manufacturer indicates that cyclical temperature and humidity alone do not degrade the material over time. The presence of water immersion, therefore, is the cause for the observed degradation.

*Figure 11-14. Confined cylinder testing of aggregate foam environmental test specimen (post-test).*

Overall, these tests indicate that the aggregate foam material should be protected from immersion conditions caused by standing water. Additional testing could be conducted to characterize durability in non-immersion scenarios where a drainage bed approach is used. For the waterproof bed approach using a fully sealed plastic envelope, degradation over time is not anticipated.

## 11.4. Modeling Effort

The modeling effort involved several stages, as shown previously in the flowchart of Figure 11-5. A high-fidelity model for the aggregate foam material was calibrated to match the test data (Figure 11-5, block 1). Using this material model, an arrestor bed model was constructed and coupled with tire models for the different aircraft (Figure 11-5, block 4). Finally, large batches of simulations were conducted using these paired models, which generated volumes of data for use by the APC (also block 4).

This section will discuss the arrestor model development and batch simulation process. Performance predictions for the aggregate foam arrestor concept are reserved for the following section (Section 11.5).

### 11.4.1. Selection of Modeling Approach

Of the three candidate systems evaluated, the aggregate foam concept was the most difficult to represent with a robust high-fidelity computer model. Because it had both loose aggregate and crushable foam properties, it did not readily fit into existing material models.

Two modeling code choices were available:

1. **LS-DYNA** is a general purpose FEM code that supports multiple numerical methods. LS-DYNA could readily sup-

port crushable material models. However, loose aggregates could only be represented by defining many separate pieces of material and allowing them to interact on the basis of defined contacts between the pieces. This approach represented a computationally expensive path that would have required infeasible simulation times.
2. **EDEM** is a DEM code that supports the modeling of hard aggregates. EDEM could readily model massive beds of aggregate pieces while maintaining efficient simulation times. However, EDEM did not support crushable material modeling of any kind.

In light of these considerations, some simplifying assumptions were made, and LS-DYNA was selected to model the material using a crushable foam model. The model represented the aggregate foam as a continuum of material (Lagrangian), rather than representing individual pieces of crushable foam. Because the material definition did not discretely represent the separate pieces of the material, the aggregate mode of behavior was not captured by the model. This was deemed an acceptable loss in fidelity based on several assumptions:

1. **Dominant Mode of Energy Absorption.** As the hydrostatic compression tests showed, the majority of the energy absorption for the material takes place in the solid regime of behavior, rather than the aggregate regime (Section 11.3.3). About 95% of the energy absorption capacity of the material exists when the material behaves in a solid-like fashion.
2. **Cover Layer Effect.** In arrestor applications, the aggregate-type behavior would appear in the uppermost portion of the arrestor bed, where the confinement pressures are low and the pieces are allowed to flow past and roll over one another. This upper portion of the aggregate would likely spray forward and away from the tire, as with solid aggregate arrestor beds. Material projected away from the tire would not participate significantly in the arresting process, decreasing the effective thickness of the arrestor bed. However, the design concept includes a cover layer that would attenuate or prevent this spray from occurring. The aggregate at the top would presumably be held in place until overrun by the tire and preserve the effective bed thickness.
3. **Material Density.** Unlike a hard aggregate arrestor bed, the foam aggregate has a low density (11 pcf). This leads to minimal mass-based momentum transfer effects, which can occur when an aggregate is projected, or sprayed, at high speed. Because the material is light, the momentum effects would be much less significant than the energy absorbed by material compaction.
4. **SPH Formulation.** Within LS-DYNA, the material was represented using an SPH formulation. While this formulation does not represent aggregate particles, it does represent solids in a way that allows large dislocations, permitting the material to move over and past itself. The SPH methodology enhanced the continuum representation of the material. Additionally, because the material acted as a continuum, this was assumed to at least partially represent the turf layer's mild confinement effects on the bed.

## 11.4.2. Smoothed Particle Hydrodynamics Formulation

The aggregate foam arrestor models were developed in LS-DYNA, a general-purpose finite element modeling code. Within LS-DYNA, a number of formulations exist for representing solids and fluids. Due to the high compressibility of the aggregate foam material and its loose fill properties, an SPH mesh-free formulation was employed. SPH offered the ability to represent high-dislocation solids with accuracy while maintaining time-efficient simulations.

Because SPH uses particles instead of the more typical finite elements, the illustrations in this section depict the material as a collection of small spheres. Although it would be desirable given the nature of the aggregate foam material, these particles do not represent disjointed pieces of aggregate. Rather, they are mathematically interconnected to represent a continuous solid material (Lagrangian formulation).

## 11.4.3. Calibration to Physical Tests

### *11.4.3.1. Constitutive Model*

LS-DYNA currently offers about 200 constitutive models; of these, about 18 are applicable to various foams. Based on prior experience and on a review of the LS-DYNA keyword manual, several candidates were singled out for evaluation. After some experimentation, *MAT_CRUSHABLE_FOAM was selected as the best overall choice. This material model has parameters as given by Table 11-2. The calibration process required defining these material parameters such that the model performance matched that of the physical material tests.

**Table 11-2. Parameters for *MAT_063 or *MAT_CRUSHABLE_FOAM.**

| Parameter | Symbol | Description |
|---|---|---|
| **MID** | | Material ID number |
| **RO** | $\rho$ | Density |
| **E** | $E$ | Young's modulus |
| **PR** | $\nu$ | Poisson's ratio |
| **LCID** | | Load curve ID for nominal stress versus strain |
| **TSC** | | Tensile stress cutoff |
| **DAMP** | | Rate sensitivity via damping coefficient |

The constitutive model assumes a normal homogeneous crushable foam material. In a typical foam, the compressibility derives from the presence of voids within the cells of the foam microstructure. However, the aggregate foam includes not only these microstructure void spaces (in each aggregate piece) but also larger voids between the aggregate pieces.

The approach taken for applying this material model was to match the overall net behavior of the material. The load curve definition (LCID) was therefore defined per the confined cylinder test data, with an exponential shape. In testing, this shape was produced by the sum of the microstructure compression and inter-particle void space compaction. Using this material model, the same summed behavior was assumed.

#### *11.4.3.2. Material Calibration Model*

A confined cylinder calibration model (Figure 11-15) was developed to determine the best-fit properties for the constitutive model. The material parameters of the model were optimized using LS-OPT, an optimization software package developed by LSTC, the makers of LS-DYNA. LS-OPT ran the simulations in batches iteratively. After each iteration, it narrowed the region of interest, effectively zooming in closer to the predicted optimum calibration point. After 5 iterations of 18 simulations each, the design was optimized for a best-fit set of material parameters.

Table 11-3 gives a summary of the calibration process, including the final accuracy of the calibrated model.

Attempts were made to calibrate the model to also match the hydrostatic triaxial specimens. These specimens were somewhat difficult to model due to a nuance of the SPH formulation, which proved challenging to fit with a hydrostatic membrane load. Application of high confinement pressures led to instabilities due to the low initial slope of the material compression curve. Since the aggregate foam material exhibited minimal pressure dependence for the higher confinement pressures (Figure 11-10), this was deemed a low-priority calibration point.

### 11.4.4. Tire and Arrestor Simulations

Using the calibrated aggregate foam material model previously described (Section 11.4.3), a large-scale arrestor model was created in LS-DYNA to simulate overruns by aircraft tires. Figure 11-16 illustrates the model with a 36-in. depth and a B737-800 main-gear tire (Goodyear H44.5x16.5) at 50% penetration depth.

No turf cover layer for the bed was included in the model. Several possible turf layer designs were feasible, each with different thicknesses and material properties. It was assumed that, while a turf layer would confine the top layer of aggregate foam to prevent spraying, it would optimally not affect the mechanical response substantially. Because the spraying behavior was inherently mitigated by the continuum representation of the material, a discrete top layer was not necessary to determine the characteristic arrestor response.

As Figure 11-17 shows, the compressed material area extended all the way to the bottom of the arrestor bed, which was in con-

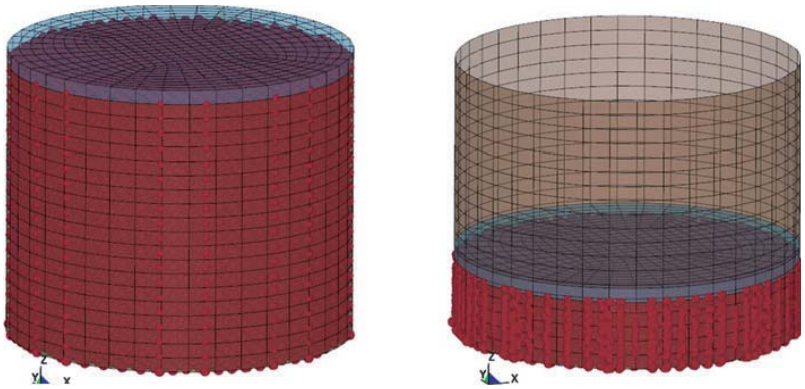

***Figure 11-15. confined cylinder model for aggregate foam material calibration.***

**Table 11-3. Specifications for aggregate foam material calibration.**

| Test to Replicate | Description | Error of Calibration |
|---|---|---|
| **Confined Cylinder Compression Test** | • 12.375 x 9.5-in cylinder<br>• Match stress–strain load curve with RMSE to 75% compression | *<2.0%* |

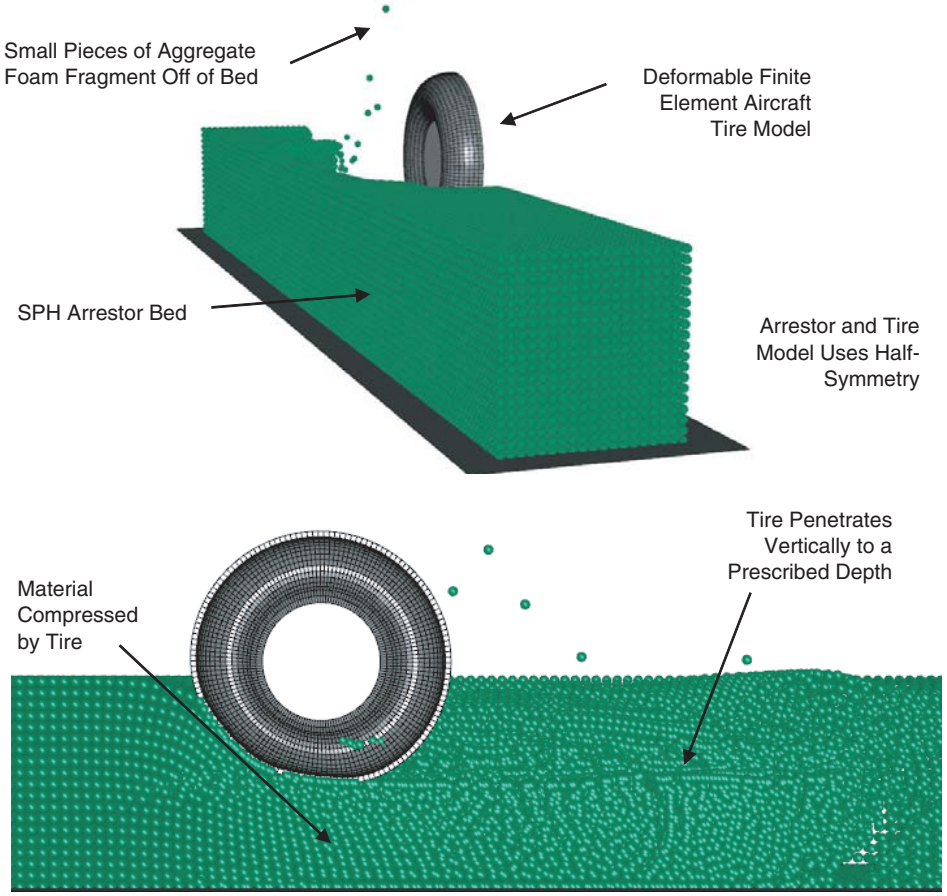


***Figure 11-16. Model of combined tire and aggregate foam arrestor system.***

trast to the localized compression region for the solid foam block candidate (Section 9.4.3). Waviness in the rut sidewalls and a longer compression region in front of the tire were also manifest. Figure 11-17 shows that under a static downward load, the material exhibited a pyramid-shaped compression zone. These behaviors are consistent with the anticipated mechanical response of the aggregate foam material.

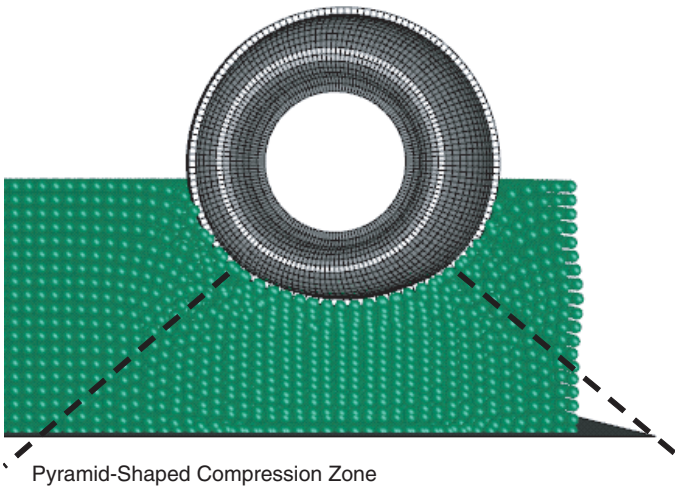


***Figure 11-17. Compression zone under tire without forward motion.***

### *11.4.4.1. Arrestor Bed Models*

The arrestor bed models were constructed using half-symmetry to reduce computation time. They varied in size depending on the aircraft tire being used. The bed length was determined by the distance required for the tire to make a certain number of rotations, such that the loading settled to a steady-state condition. The bed width was determined by the tire width, such that artificial boundary effects were minimal and the response approximated that of a wide bed of the material. The smallest bed, used for the 18-in. nose tire of the CRJ-200, was 120 in. long and 9 in. wide. The largest bed, used for the 49-in. main tire of the B747-400, was 300 in. long and 36 in. wide.

All beds were constructed with a 36-in. depth. However, the effective depth of the bed was adjusted by use of a movable rigid plane (Figure 11-18). Only the upper part of the material, above the rigid plane, was involved in the overrun compression. This approach enabled various depths to be rapidly configured within a single arrestor bed model.

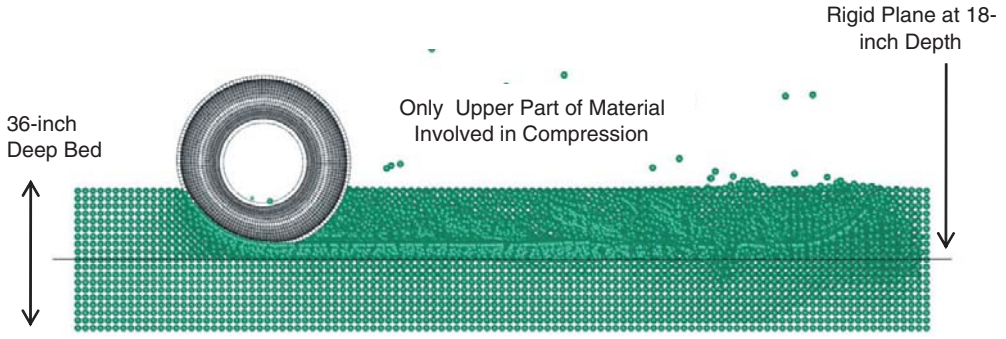


***Figure 11-18. Adjustable height of aggregate foam arrestor bed.***

SPH particle sizes were chosen based on the tire size. An error estimation process was undertaken to determine the required particle size to maintain an acceptably low discretization error. For the larger tires, a 2-in. particle size was found to have less than a 4% error for the predicted drag and vertical loads. For smaller tires, the particle size was reduced to 1 in. to maintain similar size proportionality. Based on the particle and bed size variations, a typical bed model had nominally 45K particles.

### *11.4.4.2. Tire Models*

The tire models were fully deformable FEM, as discussed in Appendix F. Table 11-4 summarizes the tire models developed. Each tire model was calibrated to match the actual tire's load-deflection performance up to 80% of the maximum bottoming load. This 80% load became a limit criterion during the batch simulations.

The deformable nature of the tires produced an accurate representation of the interface between the tire and the arrestor material. As the load on the tire increased due to deeper bed penetration, the contact area became flatter with an increased surface area. This shape change created a corresponding increase in the load on the tire.

### *11.4.4.3. Sequencing of Simulations*

Because the tires in the LS-DYNA simulations were deformable and were allowed to spin freely, a sequencing method was required to create stable, fast-running simulations. These two factors were additional complications that were not present in the EDEM aggregate simulations. However, the inclusion of these factors led to higher-fidelity results.

**Table 11-4. FEM tire library for aggregate foam arrestor models.**

| Aircraft | Landing Gear | Tire Designation |
|---|---|---|
| CRJ-200 | Main Gear | H29x9.0-15 |
| | Nose Gear | R18x4.4 |
| B737-800 | Main Gear | H44.5x16.5-21 |
| | Nose Gear | H27x7.7-15 |
| B747-400 | Main Gear | H49x19-22 |
| | Nose Gear | H49x19-22 |

From a mechanical standpoint, as the axle of the wheel penetrated the bed vertically, both the tire and the arrestor material underwent compression. The interplay of the tire and arrestor compression created oscillations in the measured loads. This oscillating behavior was further amplified by the free-spinning nature of the tire. Eventually the tire would settle to a constant rate of rotation, which proved to be a function of the forward speed, depth, and interface friction. It was found that a minimum forward travel distance was required for the loads and rotation to reach steady-state conditions before load measurements could be made.

Sequencing options included several factors:

- Prescribed vertical penetrations versus prescribed vertical loads;
- Applying the vertical penetration/load before or after beginning the forward motion; and
- Applying the forward motion before or after making contact with the bed

Depending on the sequencing method used to accelerate the tire and set the penetration depth, the initial oscillations could be more or less severe. This in turn could require longer or shorter simulation times, and longer or shorter arrestor beds. Because the arrestor–tire models were to be run repeatedly in large batches, it was important to develop a sequencing methodology that would produce efficient simulation run times.

Multiple methods were attempted through experimentation before settling on the approach illustrated by Figure 11-19. The tire was first pressed downward into the material to a prescribed depth. Then the tire was accelerated to the desired forward speed and spun-up to an initial rotation speed (typically about one-third of the ideal rotation rate expected on hard pavement). The prescribed spin rate was then released, allow-

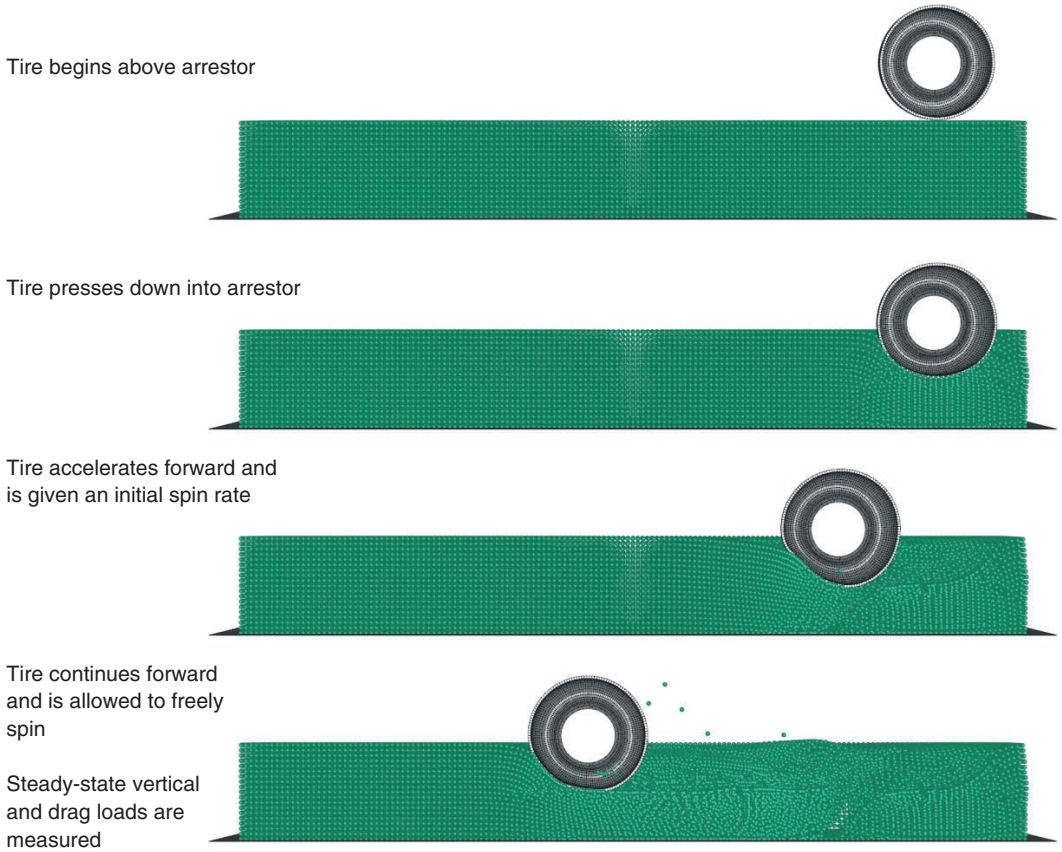


***Figure 11-19. Sequencing method for aggregate foam arrestor model.***

ing the tire to settle to a natural rotation rate, while the forward motion continued at a constant speed. After the oscillations settled out of the system, the steady-state vertical and drag loads were measured.

The final result was an accurate prediction of the loads on the tire under free-spinning un-braked conditions.

## 11.4.5. Batch Simulations

Using the arrestor bed model, large batches of simulations were conducted to generate substantial bodies of data for a wide range of overrun conditions. This data was then assembled into "metamodels" for uploading and use by the APC.

### *11.4.5.1. Methodology*

Batch simulations were conducted for each tire with three open variables:

- **Speed,** from 10 to 70 knots (Speeds below 10 knots were impractical due to the long simulation times required for a tire to travel the required minimum distance. Loading at speeds below 10 knots was based on the extrapolated metamodel data fit.);
- **Bed depth,** in incremental depths from 3 to 36 in. (Figure 11-20); and
- **Penetration** into the bed, from 10% to 100% of maximum penetration depth.

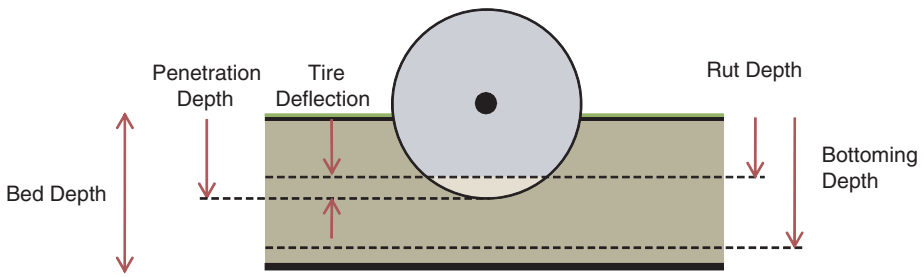


***Figure 11-20. Depth definitions for aggregate foam bed models.***

Due to the two sources of compression (arrestor material and tire), the definition for penetration depth was more complex than for the rigid tire approach used for the aggregate arrestor models. Two conditions defined the maximum penetration depth:

1. The maximum penetration depth was considered to be 85% of the bed depth (fully compressed material) plus the deflection of the tire at 80% of the bottoming load. Beyond this degree of penetration, the tire models were no longer accurate.
2. For small tires in deep beds, the maximum penetration was further limited to be no greater than the tire diameter. At depths beyond this, the simulations often did not settle to steady-state conditions.

The large batch simulations were conducted using LS-OPT. Based on the initial model files, LS-OPT generated permutations with various speeds, bed depths, and penetration levels. It sequentially executed the simulations and extracted the load data from them. Generally, the batches were conducted in multiple iterations of 10 simulations each. Additional iterations were added to improve accuracy as needed.

### *11.4.5.2. Summary Tables of Metamodels*

The output from the batch simulations was extracted and assembled automatically by LS-OPT, where metamodels were constructed for the drag and vertical load forces. Metamodeling is analogous to fitting a curve through experimental data, except it is applied to multi-dimensional data sets. These data sets were four-dimensional, including speed, depth, penetration, and load (either vertical or drag). The metamodels were RBF networks, which can effectively capture non-linear behaviors including multiple concavity changes across the data set.

Table 11-5 summarizes the fit quality for the metamodels. The RMS error showed the highest variation among the three candidates simulated, which was typically below 7%, but had three instances of higher values for the 29-in. and 18-in. tires. The R-squared value was typically above 0.97, but again dropped below 0.95 for the 18-in. tire. Typically, these problems would be resolved by adding additional simulation points. In this case, however, the scatter in the data persisted even when more simulations were conducted.

A closer examination of the batch simulation output reveals that the cases most responsible for the scatter involve deeper arrestor beds. Because the material essentially has a depth-varying quality to it, with an exponentially shaped load curve, it tended to exhibit slip–stick behavior under the tire. The material would compact into a clump until enough force was built up for a section to break free, forming a fissure. Two potential solutions to this data scatter would have involved (1) longer rolling distances in the simulations with correspondingly increased run times, and (2) revisions to the constitutive model for the aggregate foam material. Project time and budget constraints prohibited further pursuit of improvements, so the existing metamodels were used.

As the table shows, the points used in the metamodels were often less than the total number of simulations conducted. This discrepancy was caused by simulations that failed prior to termination due to tire overloading, or simulations that had not adequately settled to steady-state conditions for accurate load measurement. The smaller tires experienced a greater percentage of omitted runs than the larger tires due to the relative loading severity and greater proportional penetration depths.

**Table 11-5. Metamodel accuracy summary for aggregate foam arrestor bed.**

| Tire | Simulations Conducted | Points Used | Response | RMS Error | $R^2$ |
|---|---|---|---|---|---|
| H49 | 50 | 50 | Drag | 7.10% | 0.995 |
| | | | Vertical | 5.96% | 0.994 |
| H44 | 60 | 58 | Drag | 3.57% | 0.999 |
| | | | Vertical | 3.05% | 0.998 |
| H29 | 60 | 47 | Drag | 16.70% | 0.971 |
| | | | Vertical | 7.70% | 0.986 |
| R27 | 40 | 40 | Drag | 3.39% | 0.998 |
| | | | Vertical | 3.78% | 0.997 |
| H18 | 80 | 73 | Drag | 23.80% | 0.948 |
| | | | Vertical | 21.40% | 0.943 |

#### 11.4.5.3. Parameter Sensitivities

Using the metamodels, it is possible to review how sensitive the landing gear loads are to the different variables of speed, bed depth, and penetration percentage. Figure 11-21 shows a surface plot for the 44.5-in. main-gear tire of the B737 in an 18-in. deep aggregate foam arrestor bed.

Stronger drag loads (shown as the lower, more negative values) occur when the penetration ratio increases, up to the maximum of 1.0 (or 100%). The loading is, therefore, strongly dependent on the depth of penetration into the bed, as would be expected. However, unlike with crushable block foam, the increase is non-linear, as shown by the downward concavity of the surface.

By contrast, the variation with speed shows very little change between 10 and 70 knots. The loading is fairly insensitive to speed, reflecting the low rate-sensitivity that would be expected from crushable glass foam. Practically speaking, this means that the aggregate foam system will exert nearly the same deceleration load on an aircraft travelling at high or low speed. This behavior is desirable for an arrestor and is consistent with the general behavior of the current cellular cement material.

While overall rate insensitivity is expected for a glass foam material, the aggregate foam glass presents an additional layer of complexity. The inter-particle void compaction may not be a rate-independent process, and that could affect the overall rate sensitivity of the medium. This trait requires confirmation through larger-scale testing.

#### 11.4.5.4. Data Transformation

The final metamodel data for each tire was converted for use by the APC. LS-OPT was used to extract nominally 9,000 data points from each metamodel and export it into tabular form. A MATLAB conversion program was written to map this data into multi-dimensional matrix form that could be quickly accessed by the APC.

## 11.5. Arrestor Performance Predictions

### 11.5.1. Scope of Simulations

Using the APC, a separate optimal arrestor was designed for each of the three trial aircraft: CRJ-200, B737-800, and B747-400. Subsequently, an optimal mixed-fleet arrestor was designed as a compromise best-fit for all three aircraft.

All arrestment predictions assumed the following:

- 50-ft setback distance;
- 50-ft gradual decline to the maximum bed depth;

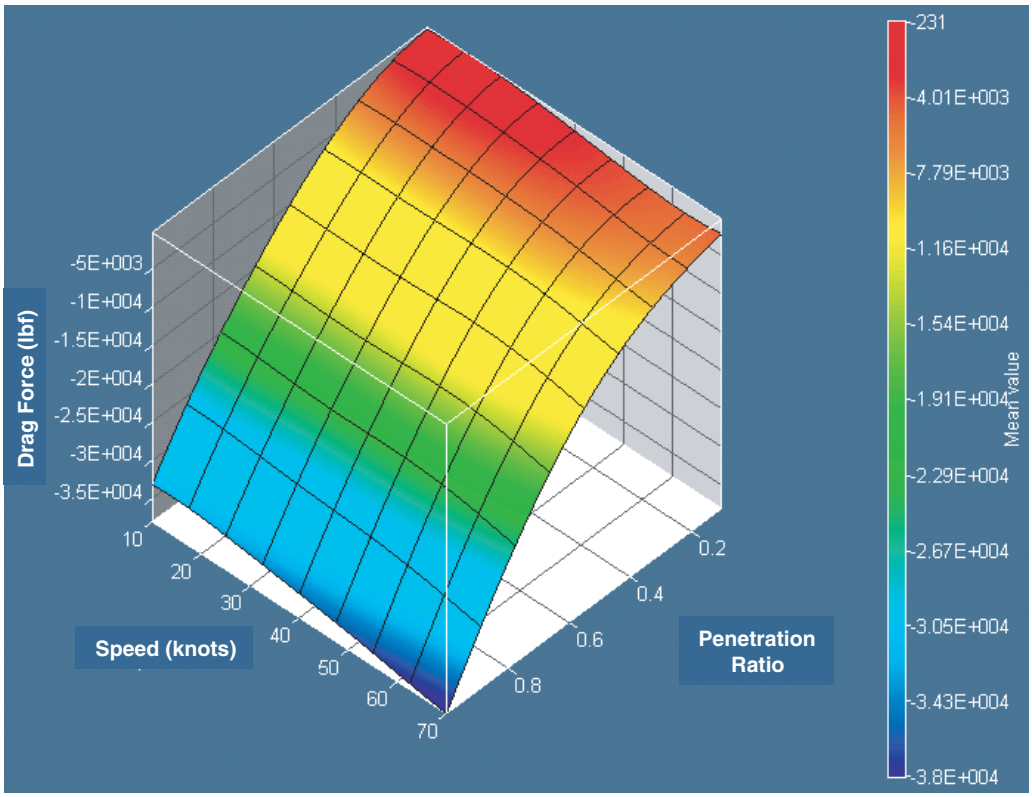


***Figure 11-21. Metamodel drag load surface plot for 44.5-in. tire in an 18-in. deep aggregate foam bed.***

**Table 11-6. Individual aircraft 70-knot arrestor beds for aggregate foam arrestor system.**

| | Nose-Gear Limit Load Criterion | | | Nose-Gear Ultimate Load Criterion | | | Current EMAS, Optimal Designs | |
|---|---|---|---|---|---|---|---|---|
| Aircraft | Strength (%) | Depth (in.) | Bed Length (ft) | Strength (%) | Depth (in.) | Bed Length (ft) | Depth (in.) | Bed Length (ft) |
| **CRJ-200** | 68% | 19.0 | 326 | 59% | 21.1 | 309 | 22 | 258 |
| **B737-800** | 103% | 29.3 | 356 | 72% | 36.0 | 315 | 22 | 287 |
| **B747-400** | 61% | 36.0 | 580 | 61% | 36.0 | 580 | 28 | 495 |

- 70-knot starting speed for the aircraft;
- No reverse thrust;
- Braking factor of 0.25 before and within the bed; and
- Arrestor bed loads based on interaction with tires, neglecting strut and axle components.

Arrestor beds were designed for two different nose-gear loading criteria:

1. **Limit Load Criterion,** where the drag load applied to the nose strut cannot exceed the limit load for the nose gear (FAR Part 25.509);
2. **Ultimate Load Criterion,** where the drag load applied to the nose strut cannot exceed the ultimate load for the nose gear;

Since the ultimate loading criterion permits higher loads on the strut, deeper beds and shorter stopping distances resulted from those cases.

It was determined through experimentation that the aggregate foam arrestor design functioned equally well for a partially or fully recessed bed. In practice, a partially recessed bed would require a shallow basin, and a raised, flat mound of arrestor material covered with turf. The simulations conducted in this section, however, assume a simpler, fully recessed bed, where the top of the arrestor is level with the runway (Figure 11-3).

Two design variables were considered for the arrestor: the bed thickness and the material strength. The material strength was adjusted by applying a scale factor to the metamodel loading data in the APC during a simulation. It was considered an open variable because the aggregate foam can be manufactured at a variety of strength levels (varying density).

## 11.5.2. Performance for Test Aircraft

Table 11-6 lists best-case arrestor designs for each aircraft taken individually. Each arrestor bed listed uses a different material strength and depth optimized for the design aircraft. Compared with the similar EMAS design cases on the right, the distances are all somewhat longer.

Material strength in the table is given as a percentage of the tested material (original gradation) since there is not a simple plateau strength as with normal crushable foams. The scaling assumes that a 75% maximum compression is retained and that the gradation remains the same. However, the composition of the aggregate foam material itself is altered in density to effect a stronger or weaker foam aggregate. Generally, a range of acceptable strength and depth combinations was available, so a different material strength could be chosen than the one given.

Table 11-7 shows the compromise design case with the best arrestor design for all three aircraft. With the material strength and depth as specified, the B747 would require 592 feet to decelerate from 70 knots. Per typical practice for EMAS design, the bed length may be specified such that all aircraft satisfy the minimum 40-knot exit speed requirement. The bed designs in the table are fixed with a 400-ft length for comparison with the other alternatives. At this length, the B747-400 would have a maximum exit speed of approximately 56 knots, which satisfies the requirements of AC 150-5220-22a.

Interestingly, this multi-aircraft design is the best one-size-fits-all arrestor bed from among the three candidate systems. Some of the other candidate design cases provided better single-plane performance, but they lagged comparatively

**Table 11-7. Fleet design arrestor bed for aggregate foam arrestor system.**

| | Nose-Gear Ultimate Load Criterion | |
|---|---|---|
| **Bed Dimensions** | Bed Depth: 36.0 in.<br>Bed Length: 400 ft<br>Material Strength Scaling: 86% | |
| **Aircraft** | **Exit Speed (knot)** | **Stopping Distance (ft)** |
| **CRJ-200** | 70+ | 367 |
| **B737-800** | 70+ | 327 |
| **B747-400** | 56 | 400 |

with respect to the multi-plane case. The reason for the superior performance appears to be the depth-varying nature of the material. Deeper beds were feasible for the aggregate foam, which performed better in arresting the B747, with its large-diameter tires. Yet, because of the depth-varying properties, the smaller aircraft each found their own equilibrium rut depths without being overloaded. The equilibrium depth effect is further discussed in Section 11.5.3.2.

## 11.5.3. General Observations

### *11.5.3.1. Deceleration and Nose-Gear Loading*

The overall deceleration and loading trends on the three aircraft showed several common characteristics. Figure 11-22 and Figure 11-23 illustrate sample deceleration and nose-gear load plots generated by the APC for the B737 aircraft. Figure 11-22 represents the arrestor bed using the limit load design criterion, while Figure 11-23 is based on the ultimate load criterion. The overall bed lengths and depths reflect the values of Table 11-6.

The upper plot in each figure shows the aircraft speed decrease relative to the nose wheel location in the arrestor bed. The lower surface line of the arrestor is depressed by the bed thickness, as discussed in Section 11.5.1.

The middle plot in each figure shows the deceleration of the aircraft in g's. The deceleration first increases when the nose wheel penetrates the bed at zero feet, while the main-gear tires are still on pavement. The deceleration then increases strongly when the main-gear tires enter the arrestor, at a nose-wheel location of 50 to 100 ft. After the initial transition, the deceleration oscillates in both cases, at about 0.65 g for the limit design and about 0.8 g for the ultimate design. The oscillations are substantially more severe in the ultimate design case due to the combined effects of the deeper bed and the depth-varying material properties. Among the three arrestor candidates, this oscillatory tendency is unique to the foam aggregate concept. The reason for the oscillations becomes clearer when analyzing the wheel rut characteristics in the next section.

The lower plot in each figure shows the nose-wheel drag loading, which proved to be the limiting load for the arrestor bed design. The loading is highest between 100 and 120 ft, which is after the main-gear tires have entered the bed. When the main-gear tires enter, the deceleration increases substantially, and this causes the aircraft to pitch forward and presses the nose wheel deeper into the material. The deeper penetrations lead to higher drag loads on the nose wheel.

### *11.5.3.2. Rut Depth Effects*

Figure 11-24 gives the corresponding main and nose-wheel rut depths for the limit case of Figure 11-22. As shown by the lower dashed line in each figure, the rut is only about 10 to 12 in. deep in the material. For a normal crushable block foam system, the rut would tend to cut near the bottom of the bed at the bottoming compression depth of the material. In this case, however, the depth-varying properties of the foam aggregate (exponential curve of Figure 11-7) allow the tires to find their own natural equilibrium depth in the material, which is at a much shallower penetration. The tires are, in a sense, floating atop a layer of partially compacted material. Because the material has not been fully compressed, oscillations can result as the tire bounces above and below the equilibrium rut depth.

Because of the rut depth effect, large oscillations were observed in a number of design cases attempted. New design practices were required to stabilize the ruts. In general, two main principles emerged:

1. Oscillations are more likely for beds that are deep relative to the tire diameter, and
2. Oscillations are more likely where the decline distance is not substantially longer than the wheel base of the aircraft (discussed further in the next section).

The B747 was not observed to form any lasting oscillations in any design case. Any bouncing quickly settled to a steady-state condition. It was determined that this was because all tires on the B747 are 49-in. diameter, which is substantially larger than the maximum 36-in. bed depth.

### *11.5.3.3. Decline Distance Effects*

The decline distance is the length of the depth-tapering region of the arrestor bed. For the two other candidate systems, a 50-ft decline distance was sufficient to produce stable arrestors. However, it was found that a 100-ft decline was considerably more stable for the aggregate foam concept due to its relative size with respect to the aircraft wheelbase.

A shorter 50-ft decline produced sometimes drastic oscillations, as shown in Figure 11-25 and Figure 11-26. This design case for the B737 is identical to that of Figure 11-22 except for the decline distance, which was 100 ft. The cause of the oscillations appears to be the initial pitch rate caused by the sudden drop of the nose wheel, which set up a "porpoising" behavior in the aircraft. Since the rut bottom was floating, rather than bottomed, the motion damped out slowly.

## 11.5.4. Braking Effects

In the APC simulations, braking loads for the main-gear tires while in the arrestor bed were added to the drag loads of the tire–arrestor metamodel. Thus, the net drag load on the main-gear tires was due to the braking plus the arrestor

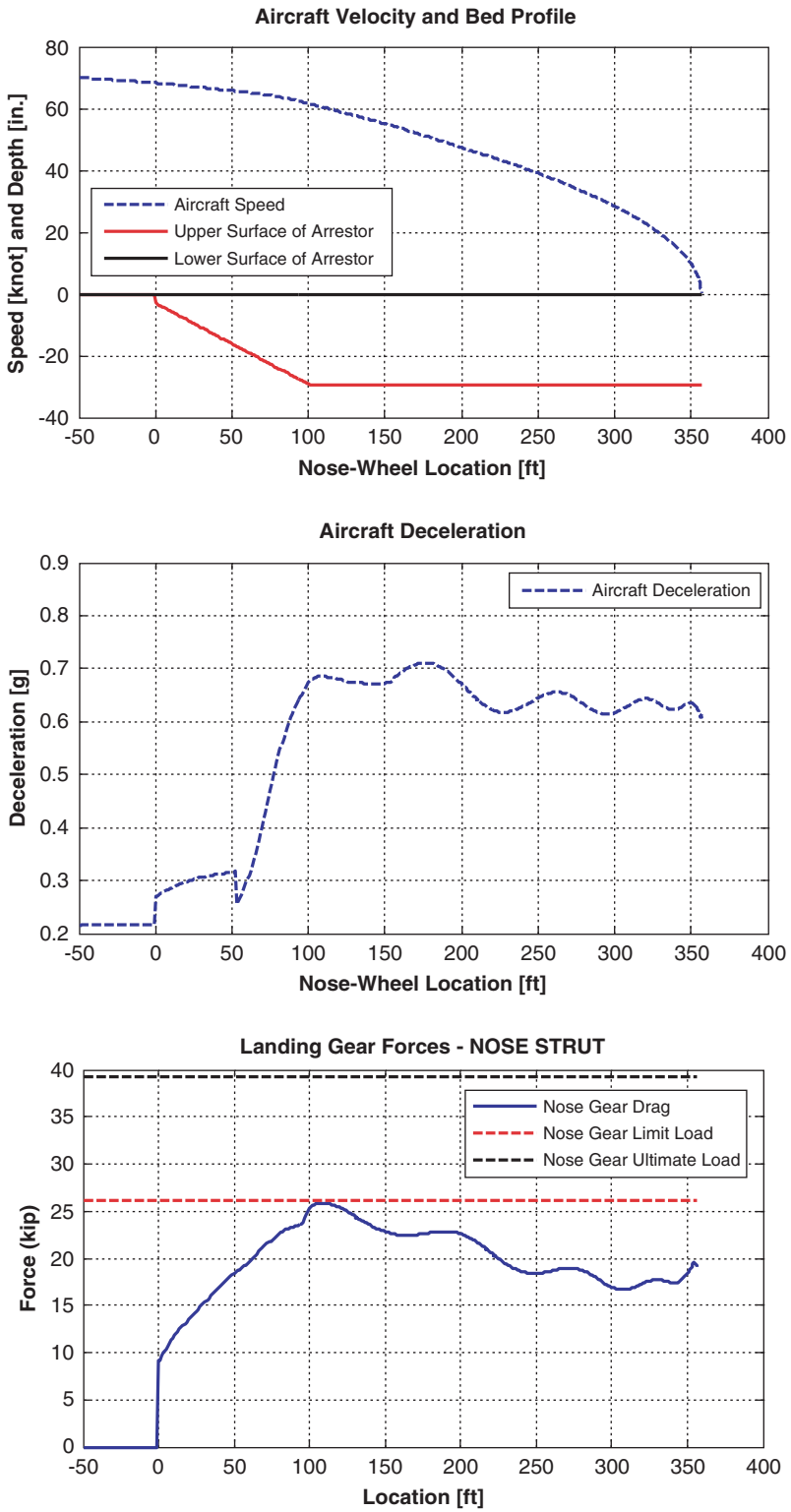


***Figure 11-22. Limit criterion aggregate foam arrestor design plots for B737-800 showing speed (top), deceleration (middle) and nose-gear drag load (bottom).***

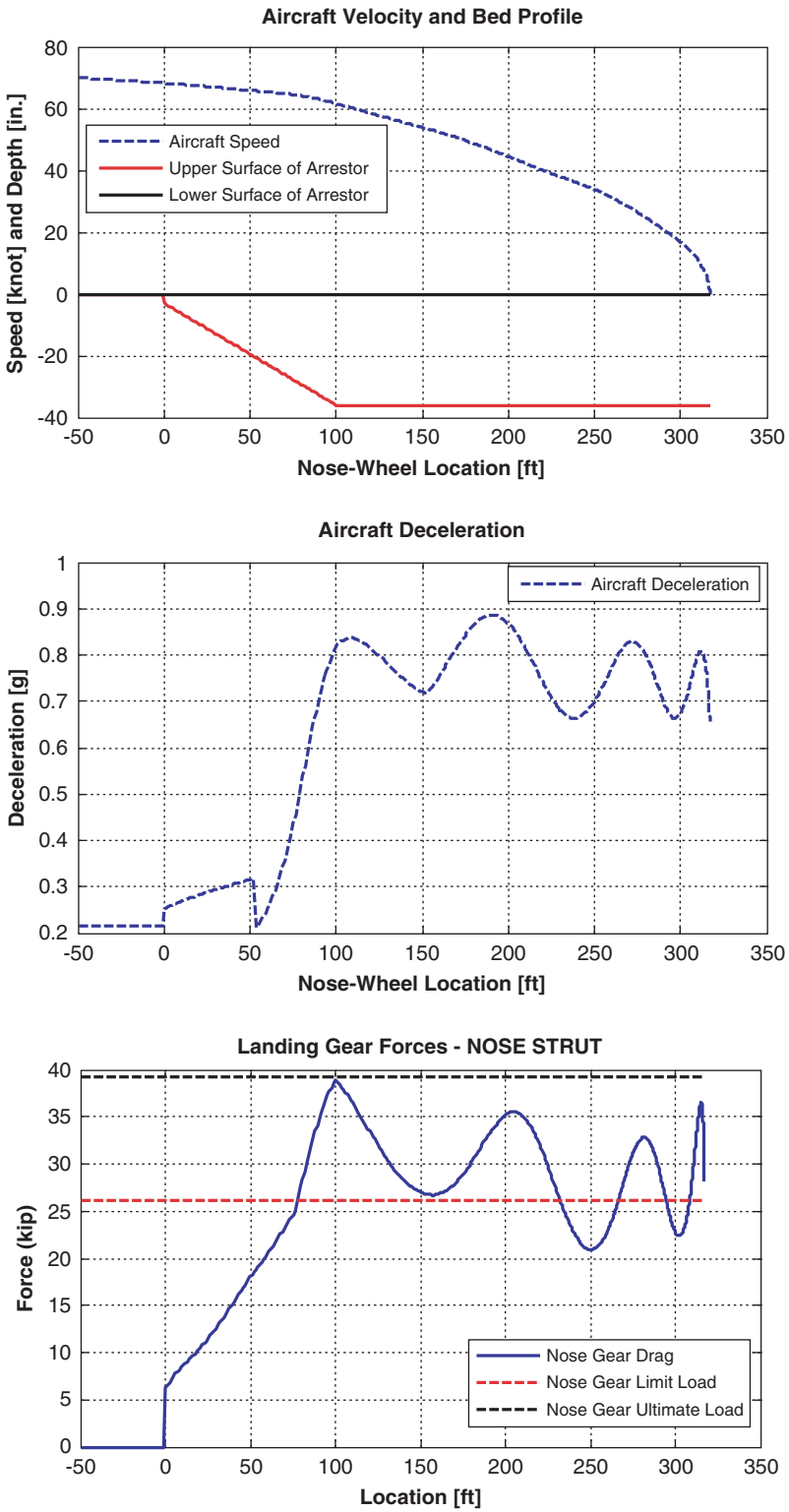


***Figure 11-23. Ultimate criterion aggregate foam arrestor design plots for B737-800 showing speed (top), deceleration (middle) and nose-gear drag load (bottom).***

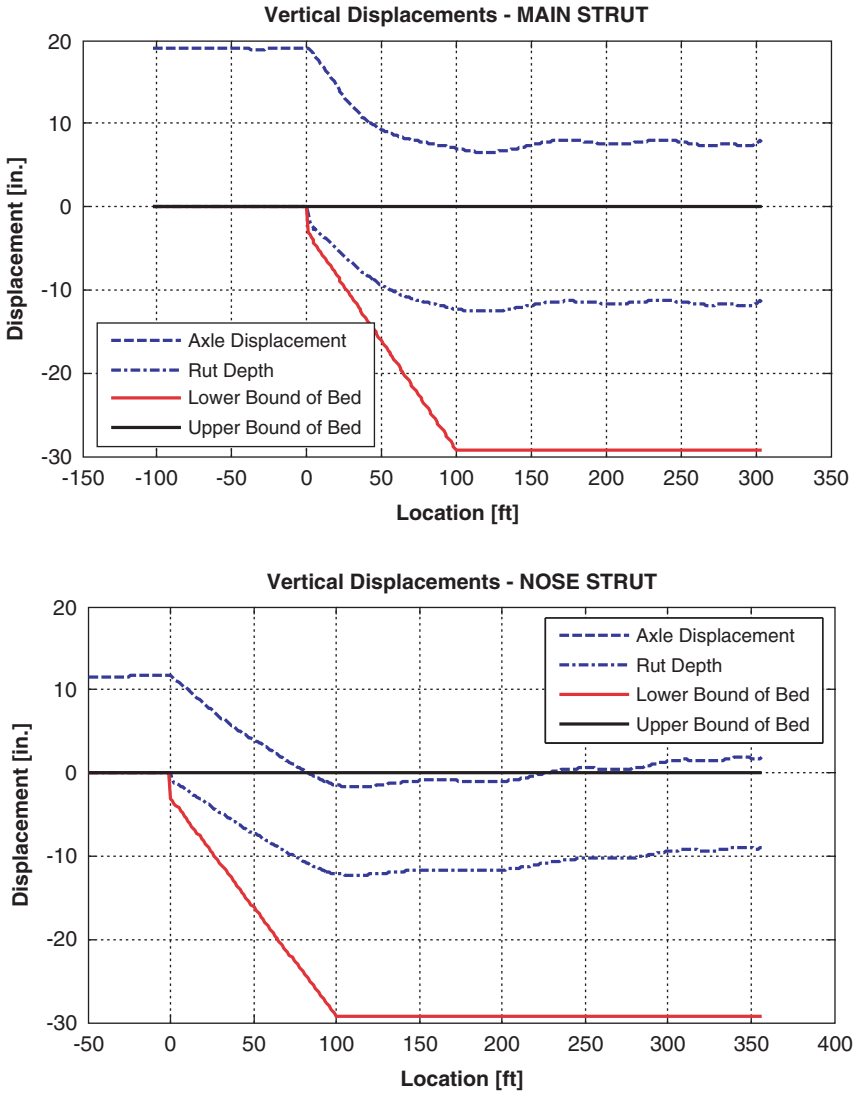


***Figure 11-24. Limit criterion aggregate foam arrestor design plots for B737-800 showing axle and rut depth for the main strut (top) and nose strut (bottom).***

resistance. As an approximate solution, this approach worked well and was appropriate.

However, a small side study conducted during the metamodeling process indicated that braking applied to the main-gear tires could cause the penetration depth to increase. Since the arrestor metamodel loads assumed a non-braked free-spinning wheel, this depth change was not captured in the predictions.

For a bottomed tire, little depth change is feasible and this effect would likely not occur. For a non-bottomed tire, however, the tendency to penetrate deeper would lead to higher arrestor drag loads on the tire. Since this effect would only apply to the braked wheels of the main gear, it would benefit the deceleration process while not affecting the nose gear. Stopping distances could be somewhat reduced by this effect, though it is unclear by what amount or in what limited subset of arrestor design cases.

Additionally, the sudden application of, or increase in, aircraft braking could induce a porpoising behavior similar to the short decline distance effects of Section 11.5.3.3. This brake-induced oscillatory behavior could be studied using the APC, but such an investigation fell outside the scope of the current effort. In actual practice, it seems doubtful that pilots in overrun situations would release and re-apply the brakes of the aircraft. It may prove most useful to characterize the torsional forces associated with a fully applied brake and assume those loads throughout the simulations.

## 11.5.5. Short Landings

Short landings involving an aircraft touch down inside the arrestor bed were not simulated. However, the potential for short landings presents two possible issues.

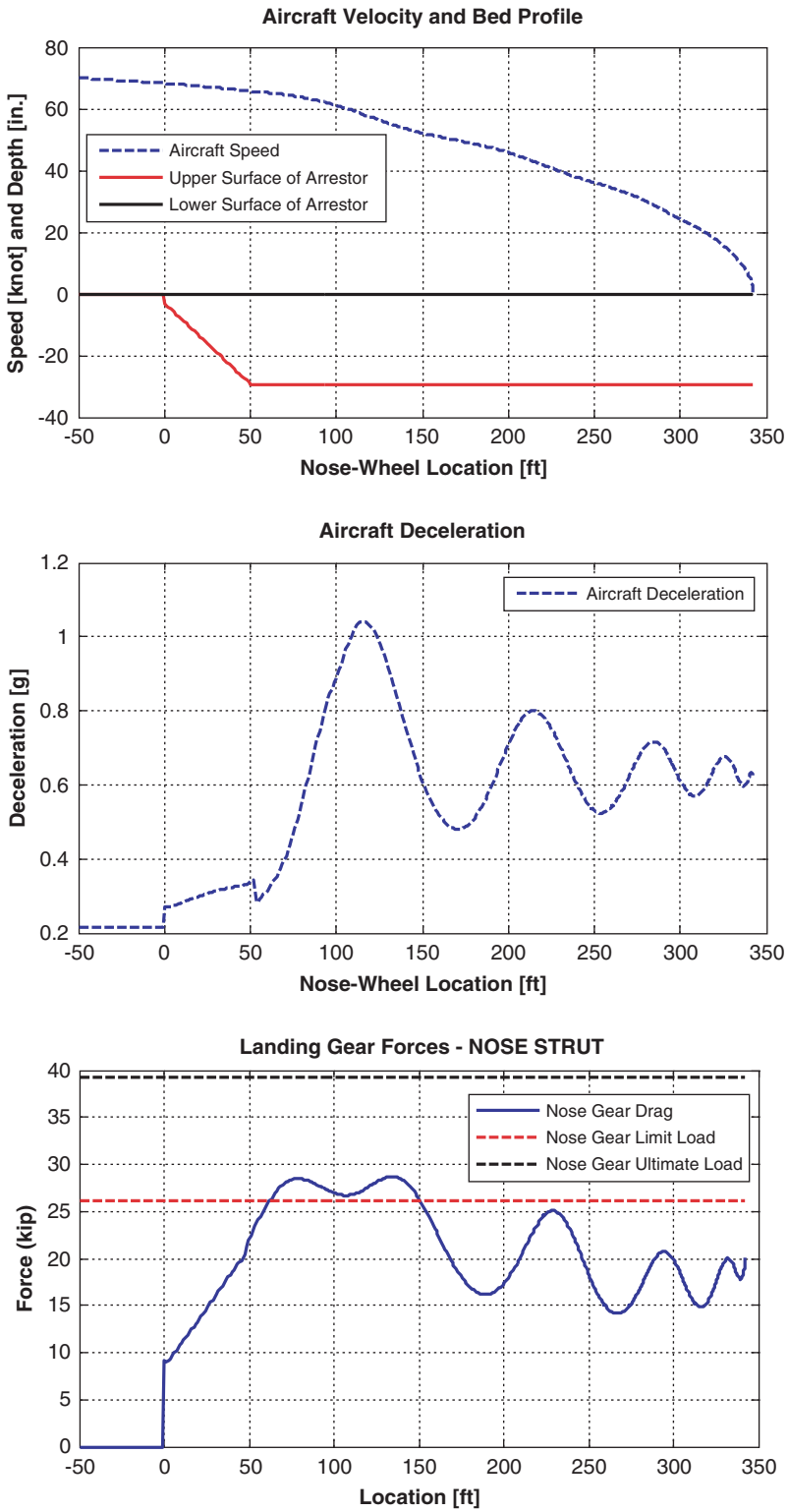


***Figure 11-25. Limit criterion aggregate foam arrestor—50-ft ramp—design plots for B737-800 showing speed (top), deceleration (middle) and nose-gear drag load (bottom).***

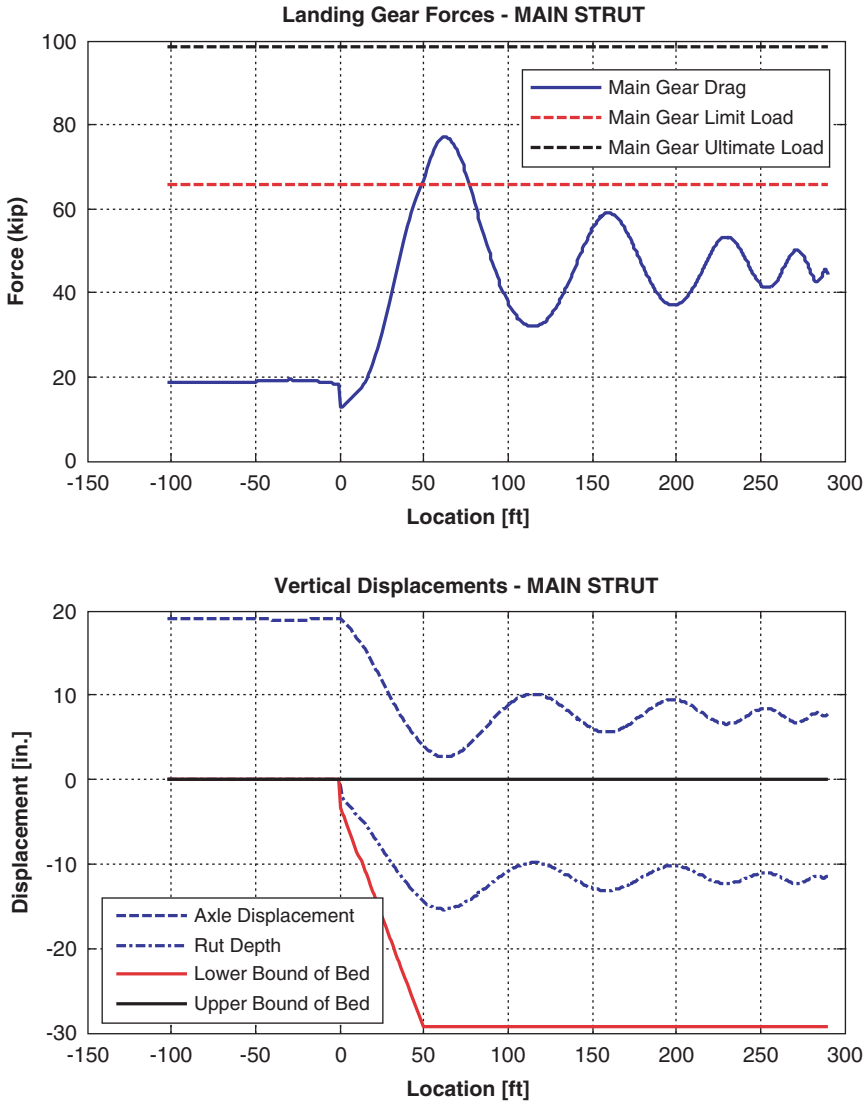


***Figure 11-26. Limit criterion aggregate foam arrestor—50-ft ramp—design plots for B737-800 showing main-gear strut loading (top) and main strut axle and rut depth (bottom).***

First, the aggregate foam arrestor exhibits a depth-varying strength property that is advantageous for arresting varied aircraft fleets. However, during a landing in an arrestor, the initial downward loads would be high, and this could cause a deep penetration and a corresponding drag-force overload to the landing gear.

Second, the basin geometry of the arrestor concept would force the aircraft to roll up the decline slope in the reverse direction from normal, acting as a ramp that would cause a strong load to the landing gear. This issue could be eliminated by only partially recessing the bed, as in the ideal EMAS design cases. Mechanical performance was found to be nearly equivalent with either version. However, the turf covering of the arrestor would be above grade in such cases, presenting some construction and aesthetic complications.

## 11.6. Estimated System Cost and Upkeep

### 11.6.1. Installation Process

The loose aggregate solution offers the advantage of construct-in-place simplicity, which could produce installation cost savings over a traditional EMAS. It reduces site preparation and eliminates block manufacturing, placement, and joint sealing. However, turf preparation and placement would be additional tasks not required for the current EMAS.

The foam aggregate concept would require excavation of an arrestor bed basin with a depth nominally equivalent to that of an EMAS bed. This basin may or may not require paving before being filled with foam aggregate. However, the below-grade nature of the basin would require drainage from

the bed to be included in the design using standard roadway engineering practices.

The basin would be filled with foam aggregate using earth-moving equipment. Due to the crushability of the material and the importance of maintaining the original gradation and density (Section 11.3.2), the foam aggregate would require care during installation. Bulldozers, or an equivalent, would reverse fill the bed starting from the distal end and working backwards, such that they did not overrun previously deposited material. Only vehicles with low ground pressure would be permissible on top of the bed material, such that the material was not compacted beyond design specifications. If a roller was to be used for creating a level surface on top of the bed before applying the turf cover layer, a prescribed degree of compaction would need to be pre-defined (Figure 11-27). However, grading the bed could require a fairly manual process to obtain the desired results.

Depending on the design of the reinforced turf layer, it could be grown in place, or it could be grown in advance, then cut into segments and placed atop the bed. The latter alternative would require the use of a front-end loader equipped to provide low ground pressure.

Once completed, the bed would permit normal traffic from grounds keeping vehicles and pedestrians. Vehicles with high tire pressures, such as emergency vehicles and aircraft, would be restricted from driving on top of the bed.

### 11.6.2. Cost to Establish System

A preliminary estimate was made for the cost to establish an aggregate foam arrestor system. It must be noted that the cost estimate from this section is only a basic approximation for the purposes of comparing the different arrestor alternatives. The cost estimate is based on a mixture of information from the manufacturer, the airport survey, and FAA Order 5200.9. To develop a more accurate estimate of the costs to install such a system, it is recommended that a detailed cost quote be sought from a firm qualified to undertake an installation effort. Where possible, the methodologies used were consistent with the prior survey information collected regarding the existing EMAS (Section 3.5).

The costs may be broken into two major categories: site preparation and installation. The site preparation costs were estimated for two cases. The aggregate foam arrestor would use a basin for the arresting materials rather than a flat runway-type surface as is used for the current EMAS design. The bottom of the basin could either be paved or earthen. Drainage, excavation, and leveling would be required for either option. Assuming that a full paved surface is not provided under the bed, the cost for site preparation was assumed to be reduced by half; this value was used for the lower-bound cost estimate for the system. If a full paved surface is provided, then the preparatory costs were assumed to be the same as for the current EMAS; this provided the upper-bound cost estimate.

The installation cost estimate was separated into specific materials and general installation labor needs. Because these costs were specific to the aggregate foam arrestor concept, they do not have a direct connection to any prior EMAS data. Discussions with the manufacturer produced cost estimates for the aggregate foam, reinforced turf cover layer, and geo-textile/geo-plastic layers. Where applicable, materials included freight costs for trans-Atlantic shipping. The labor costs were based on estimates from the manufacturer established from similar installation efforts.

Finally, the site preparation and estimated EMAS costs were computed in two ways: (1) assuming average survey costs from this research, and (2) assuming FAA Order 5200.9 costs. The final cost estimates for both options are given in Table 11-8 and Table 11-9, respectively.

Using the survey cost assumptions of Table 11-8, a 300-ft arrestor bed would cost between 47% and 60% less than the current EMAS. If the Order 5200.9 costs are assumed, the cost advantage drops to between 37% and 44% (Table 11-9).

*Figure 11-27. Roller compaction of aggregate foam material during typical installation (43).*

**Table 11-8. Estimated costs to establish aggregate foam arrestor, 150 x 300 ft, assuming survey average costs for current EMAS, units of millions USD.**

| Cost Category | Aggregate Foam System | | Current EMAS |
|---|---|---|---|
| | Lower Bound | Upper Bound | |
| Site Preparation | $ 1.08 | $ 2.17 | $ 2.17 |
| Installation | $ 2.16 | $ 2.16 | $ 6.03 |
| Cost to Establish | $ 3.24 | $ 4.32 | $ 8.19 |
| Percent of EMAS | 40% | 53% | |

**Table 11-9. Estimated costs to establish aggregate foam arrestor, 150 x 300 ft, assuming Order 5200.9 costs for current EMAS, units of millions USD.**

| Cost Category | Aggregate Foam System | | Current EMAS |
|---|---|---|---|
| | Lower Bound | Upper Bound | |
| Site Preparation | $ 0.34 | $ 0.68 | $ 0.68 |
| Installation | $ 2.16 | $ 2.16 | $ 3.83 |
| Cost to Establish | $ 2.50 | $ 2.84 | $ 4.50 |
| Percent of EMAS | 56% | 63% | |

In addition to the tables in this section, longer-term life-cycle issues could also be considered. FAA Order 5200.9 includes a standard 10-year replacement interval for an EMAS, which translates into present-value life-cycle costs. Such a replacement could arguably be unnecessary for this arrestor concept (Section 11.6.4). Eliminating the assumed 10-year replacement could effectively trim about $2.6M of present-value life-cycle costs (based on the EMAS replacement cost estimates of the survey).

### 11.6.3. Maintenance

Maintenance for the aggregate foam concept would be relatively simple, and should be limited to standard groundskeeping measures for the protective turf layer. Drainage of the area to prevent standing water is required, and periodic inspections would be advisable to ensure that no issues arise due to seasonal weather changes. Due to the lack of joints and blocks, many protective measures used in current EMAS construction would not be necessary.

The aggregate foam material is expected to have a superior durability when compared with cellular cement. Aggregate foam does not exhibit the tendency to crumble during handling as occurs with cellular cement, nor does it exhibit overt sensitivity to moisture due to its closed cell microstructure. Many industrial applications of glass foam materials indicate long service life is possible with little degradation, as long as mild protective measures are taken.

However, the aggregate foam carries some maintenance issues not present for solid foam block material. The loose aggregate could settle over time, or the aggregate pieces could eventually break down into smaller pieces, changing the gradation of the material. These are both issues to address through inspections. Plate-shaped dimensional markers could be inserted below the turf layer and checked periodically using surveying equipment for changes in height, and aggregate samples could be tested periodically (discussed further in the next section).

### 11.6.4. Replacement and Overhaul

FAA Order 5200.9 plans a full replacement for an EMAS after 10 years. Following this schedule for replacement may be required for the drainage version of the concept, but this would probably not be required for the sealed watertight bed. Given the minimal cost increase, adding the watertight membrane around the foam aggregate would likely afford considerable long-term savings. Eliminating the 10-year replacement could effectively trim about $3.5M of present-value life-cycle costs, based on the replacement cost estimates of the survey.

Rather than a scheduled replacement, periodic bed material sampling could be undertaken, perhaps in 3- to 5-year intervals. Small areas of the cover layer could be removed, and a sample of the aggregate foam could be extracted and tested. The removal area would then require refilling and repair of the top layer. These periodic small-scale tests would provide assurance that the bed has not degraded and still meets performance specifications.

### 11.6.5. Repair

After an overrun event, the rut areas would require repair. The foam aggregate remaining in the ruts would require removal and replacement. The damaged cover layer would also require removal from the rut areas and subsequent replacement. Geo-textile and geo-plastic layers would also require repair and fusing with the existing material to ensure continued waterproofing, as applicable.

## 11.7. Transition to a Fielded System

In order to transition the aggregate foam concept to a fielded system, the following additional development steps may be advisable.

### 11.7.1. Material Density and Compaction Calibration

As shown in the example arrestor beds of Table 11-6 and Table 11-7, the compressive strengths for optimal designs ranged from 59% to 103% of the tested material. To estimate the needed strength in the arrestment predictions, the meta-model data was simply scaled, which was an appropriate simplification.

However, in migrating to a fielded system, several standard densities and gradations would probably be selected to provide flexibility during the design of actual arrestors. For each density and gradation, some testing would be required to generate calibration data.

The installation process will likely affect the performance properties of the material because compaction by construction equipment and foot traffic will take place. Since this process is inevitable, it would be advisable to create several larger-scale testbeds using the anticipated installation process and equipment. Tests could then be conducted on these small beds using larger test apparatuses than those of the current research. From the results, a revised material model could be calibrated, and the arresting performance reassessed. In this manner, a calibrated prediction capability would exist for the as-installed material. Thereafter, installation of actual arrestor beds could proceed per the developed methodology with high confidence of the final system performance.

Such tests could be conducted in conjunction with the cover layer design (next section).

### 11.7.2. Cover Layer Design

The cover layer options that have been discussed include reinforced turf with or without additional geo-textile/geo-plastic layers. Additional testing and modeling would be required for whichever method is selected since the membrane behavior of a cover layer will affect the dynamic mechanical performance of the arrestor bed. The cover layer performance should be further characterized under frozen conditions since it will be exposed to such conditions even where the foam aggregate layer of the system is waterproofed.

### 11.7.3. Braking Dynamics

The research performed has identified that braking in the aggregate foam material may require further study. Of the three major concepts evaluated, braking dynamics appear likely to affect the aggregate foam concept the most. Because the depth-varying properties of the material have demonstrated tire "flotation" at mid-depth bed penetrations, there is room for potential depth shifts of the tires due to braking. If they occurred, such shifts could lead to excessive landing gear loads.

The current modeling method of the APC makes simplifying assumptions regarding this phenomenon that are sufficient for a concept-level evaluation. However, to ensure accuracy of design predictions, some additional tests would be beneficial. One method would involve using a one-wheel bogy apparatus fitted with brakes and a load measurement system that is towed through the material.

### 11.7.4. Full-Scale Testing

A full-scale aircraft overrun test of a foam aggregate arrestor bed is advisable because this concept represents a substantial departure from the current EMAS design in terms of mechanical loading and the materials used.

## 11.8. Summary

The aggregate foam arrestor concept was found to have a mechanical response similar to a crushable foam material, except with depth-varying properties. It would absorb energy from the aircraft primarily though material compaction rather than through displacement. An aggregate foam arresting bed would be constructed using a shallow basin of the material topped with a reinforced turf cover layer.

The material is closed-cell glass foam that provides inherent moisture and chemical resistance, and improved handling durability as compared with cellular cement. Manufacturer information indicates that long service life is possible, potentially eliminating the standard 10-year replacement assumed in FAA Order 5200.9. Water immersion must still be avoided, so the preferred design approach would use a sealed plastic geo-membrane envelope coupled with standard drainage provisions.

Installation of the system would likely be simpler and less expensive than the current EMAS since placement of blocks and sealing joints are both unnecessary. Heavy equipment would place the material in the bed basin and top it with reinforced turf. Geo-membrane and geo-textile layers, as applicable, would be placed and joined manually. The arrestor basin could be constructed with or without paving, which could provide for preparatory cost reduction. In order to preserve material gradation and prevent over-compaction during installation, an appropriate installation process would be required.

The cost to establish such a system would be nominally 40% to 53% of the survey cost of the existing EMAS, which provides the most substantial estimated cost reduction of the candidates evaluated; much of the cost reduction is due to the markedly less expensive aggregate foam material. Life-cycle costs could be further reduced due to longer bed life. Maintenance needs appear to be simplified, requiring standard grounds-keeping measures, but no block or joint repairs.

The APC predictions for the aggregate foam arrestor show fairly constant deceleration throughout the arrestment with little speed dependence, which are desirable characteristics. The depth-varying material characteristic produced a unique "floating" rut depth that was not observed for the other materials evaluated. This characteristic allowed each tire to settle to its own natural depth in the material, creating more even load distribution among tires of different sizes.

Bed lengths on a per-plane basis were nominally 15% longer than for the current EMAS. However, the multi-aircraft design case demonstrated the best one-size-fits-all performance from among the three candidate systems. A 400-ft

arrestor bed demonstrated 70+ knot exit speeds for the B737-400 and CRJ-200 and a 56-knot exit speed for the B747. The reason for the superior performance appears to be the depth-varying nature of the material.

The floating rut characteristic also gave rise to oscillating tendencies in which the plane could exhibit porpoising behavior. This was mitigated through appropriate bed geometry design. However, additional investigation would be required to establish the effects during short landings and in cases where the pilot applies intermittent braking.

Transition to a fielded system would require finalizing a composite turf cover-layer design and calibrating a predictive model to match the response. Characterization would be advisable for the soil layer under various freezing conditions to assess the impact on arresting dynamics. Additionally, investigation should be made regarding the basin geometry to determine whether above- or below-grade construction is preferable. Because the material performance can be affected by size gradation and compaction, development of a suitable installation process would be required. This installation process would be coupled with a predictive model matching the as-installed material characteristics. Finally, full-scale testing is advisable for evaluation of the complete system.

CHAPTER 12

# Depth-Varying Foam Material

As a companion effort to the ACRP research, additional graduate-level research was undertaken to explore a depth-varying foam material concept. A summary of that research is given in this chapter. For an in-depth examination, the original research document should be consulted (*33*).

The goal of the study was different from that of the full system concept evaluations in Chapters 9 through 11. The evaluation of the depth-varying concept did not include full aircraft arrestment simulations. Instead, it was confined to a narrower study of the effects of the material on two different tires: the main-gear tires of the CRJ-200 and the B737-800. While the likely arresting performance can be inferred based on the results, APC simulations were not conducted.

## 12.1. Depth-Varying Foam Concept

By its nature, an arrestor bed installed at an airport is a single, static system. It must arrest any and all aircraft that could overrun the runway end, from large B747s down to small regional jets. Problematically, these aircraft differ in ways that have a significant effect on arresting efficiency; the arrestor slows some aircraft more quickly than others.

To improve the one-size-fits-all performance of an arrestor bed, a depth-varying foam arrestor material was investigated. The cellular cement used in existing EMAS arrestors is homogeneous, having the same density and strength throughout each block of material. Changing the density and strength to become harder at deeper levels could potentially achieve a degree of performance leveling between large and small aircraft (Figure 12-1).

This concept was evaluated using an idealized foam material model rather than a particular type of crushable foam (cement, polymer, glass, etc.). Many crushable foam options exist, and depth-varying layups for many could be achieved.

## 12.2. Depth-Varying Profiles Considered

Multiple depth profiles for the material were possible. Figure 12-2 illustrates three simple profile types that were considered, as well as a depth-invariant material, which represents the current homogeneous arrestors. The curves have been normalized to compare overall trends.

Viewing the profiles shows that the linear and quadratic cases sit astride the exponential function, given the same starting and ending points. As such, the exponential case did not seem to offer novel content, and the evaluation was narrowed to include three profiles:

1. Constant (baseline),
2. Linear profile, and
3. Quadratic profile.

## 12.3. Modeling Approach

The modeling approach for the depth-varying material evaluation was essentially the same as for the glass foam material (Section 9.4). Only points of contrast in the methods will be discussed in this section.

### 12.3.1. Calibration of Material Model

Material calibration was not undertaken because the evaluation involved idealized materials. All three material options assumed zero Poisson ratios, which is consistent with typical crushable foam behaviors. Figure 12-3 illustrates the idealized compression load curve for the material model.

### 12.3.2. Tire and Arrestor Simulations

As with the glass foam material evaluation, the arrestor models were constructed in LS-DYNA using the deformable FEM tire models and SPH arrestor beds (Figure 12-4).

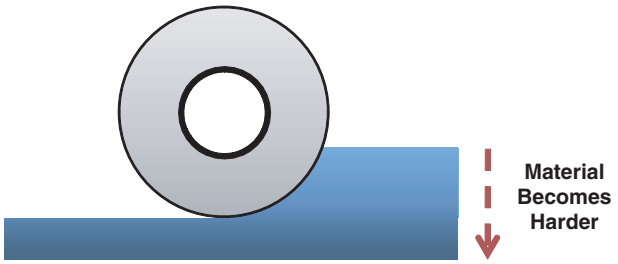


*Figure 12-1. Depth-varying material concept.*

A large-scale arrestor model was created in LS-DYNA to simulate overruns by aircraft tires. No protective cover layer for the bed was included in the model, and it assumed a continuous material without seams.

### 12.3.2.1. Arrestor Bed Models

The arrestor bed models were constructed using half-symmetry to reduce computation time. They varied in size depending on the aircraft tire being used. The bed length was determined by the distance required for the tire to make a certain number of rotations such that the loading settled to a steady-state condition. The bed width was determined by the tire width such that artificial boundary effects were minimal and the response approximated that of a wide bed of the material. The beds were 36 in. wide, 300 in. long, and 30 in. deep. However, the effective depth of the bed was adjusted by use of a movable rigid plane.

For the 44.5-in. tire, the SPH particles were sized at 2 in., but the smaller 29-in. tire used a bed with 1.5-in. particles to maintain a low discretization error.

The depth-varying arrestor bed featured a division of the SPH material into several parts, forming stratified layers.

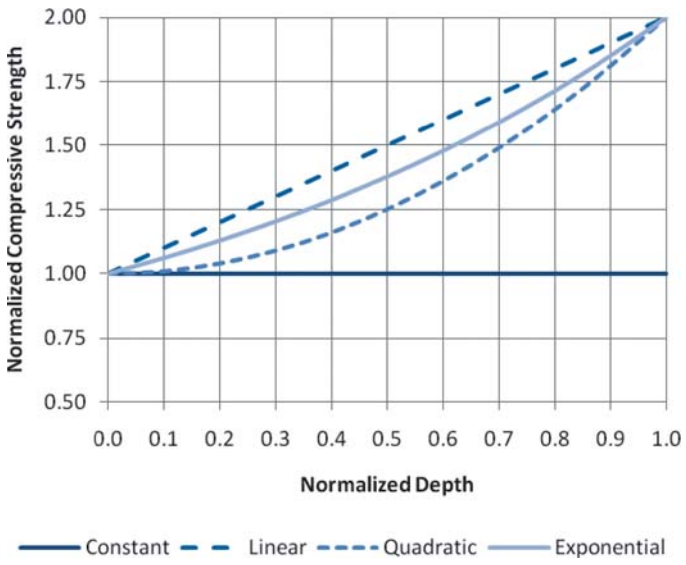


*Figure 12-2. Depth-varying profiles considered.*

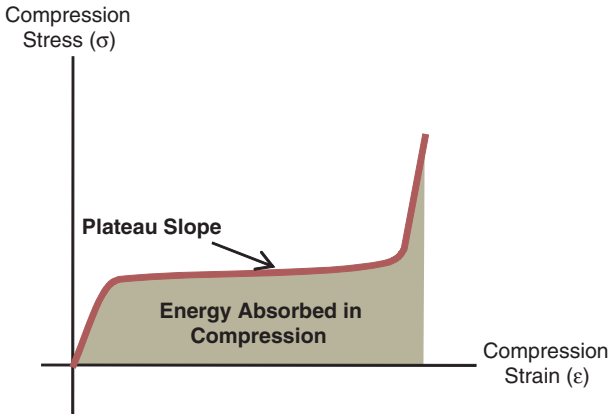


*Figure 12-3. Idealized crushable foam stress–strain compression curve.*

Each part/layer had its own material definition based on its depth. Experiments showed that each layer required at least two rows of SPH particles in order to initialize properly. The 30-in. deep arrestor, with 2-in. particles, had eight separate layers (Figure 12-5).

### 12.3.2.2. Tire Models

The tire models were fully deformable FEM, as discussed in Appendix F. However, for this limited study, only the main-gear tires for the B737 and CRJ-200 were used. The goal was to observe the behavioral trends, from which likely arresting performance was inferred. Table 12-1 summarizes the tires that were used in the evaluation.

### 12.3.2.3. Sequencing of Simulations

The sequencing method for this evaluation differed from that of the foam glass evaluation. Because a full metamodel of the design space was not required, the simulations were conducted using a constant vertical load rather than a prescribed vertical penetration depth. The load for each tire was chosen as the static vertical load when the aircraft was decelerating at 10 ft/s$^2$. Because the load was prescribed, the tire penetrated to a steady-state depth that varied depending on the arrestor bed material properties.

After experimenting with several methods, the sequence illustrated by Figure 12-6 proved superior on the basis of providing the most consistent results with the shortest settling time. The settling time refers to the second time stage, leading up to the steady-state rolling behavior when the load measurements on the tire are recorded.

Motion damping became one of the main problems with the combined model, tending to control how long the simulation had to run before the model approached steady-state. Two types of motion required damping: (1) oscillations in the

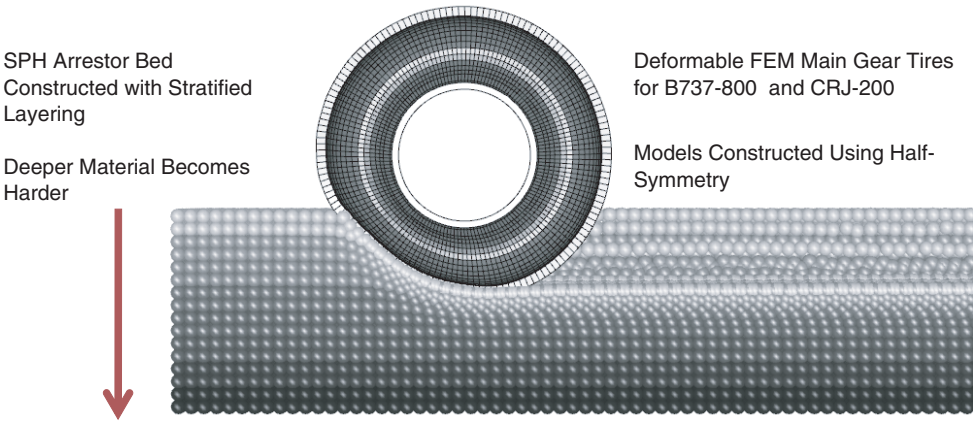


*Figure 12-4. Depth-varying arrestor and tire model.*

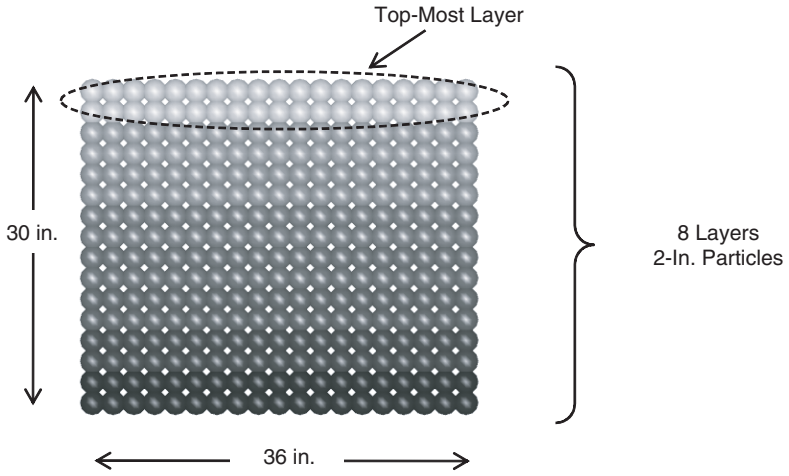


*Figure 12-5. Sectional view of eight-layer arrestor bed model.*

tire itself as it rebounded outward and inward from the axle line, and (2) vertical oscillation of the axle. Properly implemented damping prevented over- and under-damping the solution, leading to the shortest available run time while not altering the overall response of the system.

The final method involved a vertical damping value that produced slight overshoot behavior. Using this approach ensured that the full depth had been reached, while keeping simulation times short. Depending on the strength of the arrestor material, the simulation time required for settling could still vary considerably.

**Table 12-1. FEM tire library for glass foam arrestor models.**

| Aircraft | Landing Gear | Tire Designation | Included in Evaluation |
|---|---|---|---|
| CRJ-200 | Main Gear | H29x9.0-15 | Included |
| | Nose Gear | R18x4.4 | - |
| B737-800 | Main Gear | H44.5x16.5-21 | Included |
| | Nose Gear | H27x7.7-15 | - |
| B747-400 | Main Gear | H49x19-22 | - |
| | Nose Gear | H49x19-22 | - |

## 12.3.3. Batch Simulations

Using the arrestor bed model, large batches of simulations were conducted to generate metamodels for studying the effects of depth-varying material properties. For each tire, the run sets had three open variables:

- **Bed depth,** in incremental depths from 18 to 30 in.;
- **Material Initial Strength,** which defined the compressive strength at the surface of the bed; and
- **Material Strength Gradient,** which defined how rapidly the strength of the material increased with depth (the quadratic or linear coefficient of the material profile curve).

The large batch simulations were conducted using LS-OPT. Based on the initial model files, LS-OPT generated

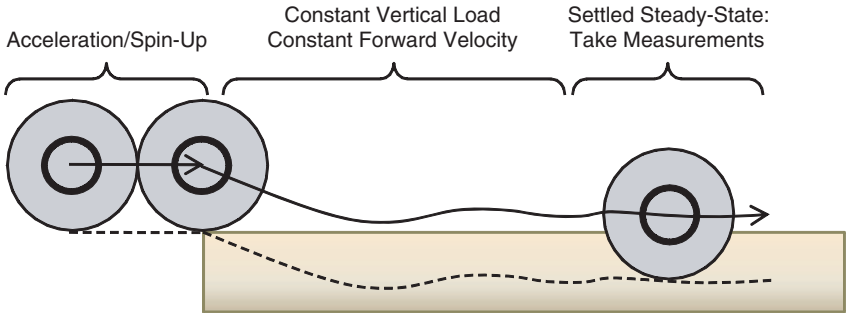


*Figure 12-6. Sequencing method for depth-varying simulations.*

permutations with various bed depths, strengths, and strength gradients. It sequentially executed the simulations and extracted the load data from them. Generally, the batches were conducted with one iteration of 50 simulations.

## 12.4. Metamodel Analysis

### 12.4.1. Metamodel Method

The output from the batch simulations was extracted and assembled automatically by LS-OPT, where metamodels were constructed for the drag and vertical load forces. Metamodeling is analogous to fitting a curve through experimental data except that it is applied to multi-dimensional data sets. These data sets were four-dimensional, including depth, strength, strength gradient, and load (either vertical or drag). The metamodels were RBF networks, which can effectively capture non-linear behaviors including multiple concavity changes across the data set.

### 12.4.2. Optimization Criteria and Constraints

The LS-OPT simulation sought to maximize the deceleration for both aircraft simultaneously, assuming that the main gear were responsible for the deceleration. Therefore, the drag load on both tires was maximized.

Landing gear loading limits constrained the optimization. From the tire drag load, multiplied by two tires per strut, the overall rearward strut loading was calculated. This loading was then limited to be no greater than acceptable horizontal loadings as defined by the FAR.

The loading requirements of the FAR define two types of criteria: (1) limit, which the gear should withstand without suffering damage, and (2) ultimate, which the gear should withstand without collapsing. For the evaluation, the limit strength criterion was used. FAR Section 25.493 requires horizontal main-gear strength equivalent to a 0.8 braking factor, applied to the maximum taxi weight on the strut. Therefore, the 0.8 factor became the optimization criterion; an optimal design would achieve a main-gear drag loading factor of 0.8 for both aircraft.

All nose-wheel loading was neglected, although in practice it typically limits the arrestor bed design. Since the results of the analysis would not be integrated with the APC, it was feasible to make this simplification.

### 12.4.3. Metamodel Interpretation

A visual review of the metamodel proved informative for comparing the material performance. Because this optimization study had two simultaneous constraints, one for each tire, the surface plots show two constraint curves and three shaded regions. As a key for understanding the other plots in this section, Figure 12-7 gives an example of such a surface.

Two curves are drawn across the surface as boundaries to the shaded regions. One curve indicates the constraint boundary for the 29.0-in. tire. The other curve indicates the constraint boundary for the 44.5-in. tire. For each case, the curve indicates the ideal case of a 0.8 strut load factor.

The darkest region violates the constraints for both tires (strut overload). The two medium-shaded regions violate the constraints for one tire or the other. The light-shaded region is acceptable for both constraints.

Where the region boundary curves intersect, a dual-case optimum occurs, providing an ideal load for both aircraft struts. The strut load factor would be 0.8 for both aircraft in this case. If the material was designed with the depth, strength, and strength gradient from this intersection point, the struts would be ideally loaded for maximum deceleration.

### 12.4.4. Linear and Quadratic Profile Comparison

For either the linear or quadratic depth-varying material, the performance for the 29.0-in. tire improved. In the homogeneous material, drastic overloading could occur if the bed

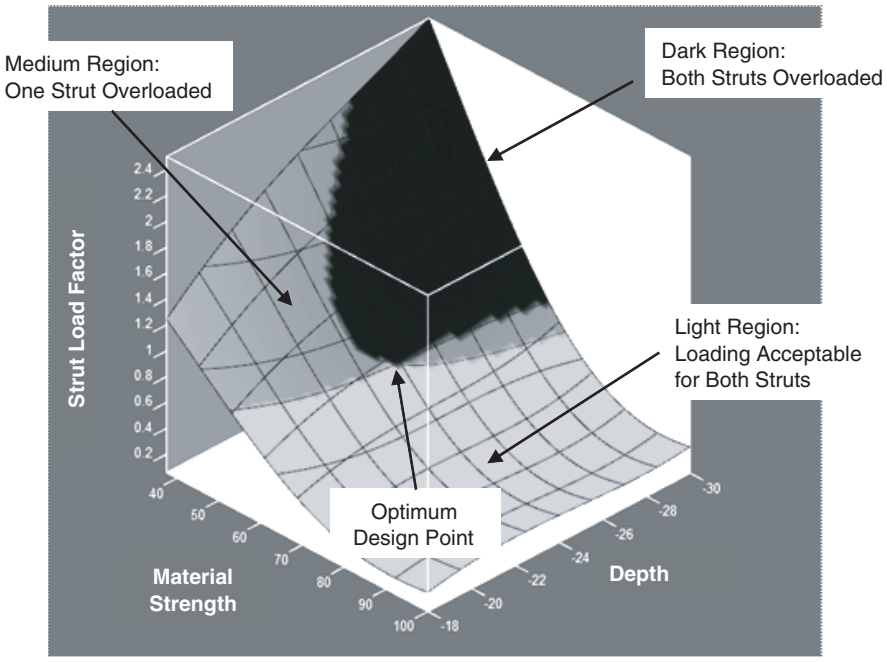


*Figure 12-7. Example figure for dual-constraint surface plot.*

was too deep; both depth-varying methods eliminated this drastic overloading regime.

Both methods also reduced the sensitivity to the material strength. This provided a serendipitous advantage, since crushable foam materials can have a degree of scatter in their strength values based on manufacturing variation. The sensitivity reduction implied that a robust design can be achieved with less dependence on precision materials.

The linear depth-varying approach seemed slightly better than the quadratic. While the qualitative trends are similar, the linear method appeared to offer simultaneous optimal conditions for both large and small tires. Hence, the linear profile was chosen for advancement to the final optimization stage.

### 12.4.5. Linear Gradient Material Optimum

Figure 12-8 and Figure 12-9 compare 29-in. tire metamodel surfaces for homogeneous (left images) and linear (right images) depth gradient materials. Figure 12-8 compares the penetration depth of the tires, while Figure 12-9 compares the strut loading ratios. The surfaces for the 44.5-in. tire (not shown) reflected similar trends.

The right hand image of Figure 12-8 shows an interesting behavior: for the linear gradient material, the response becomes insensitive to the arrestor bed depth, becoming essentially flat in the depth-wise direction. The tires settled to their own natural depth in the material and were no longer prone to

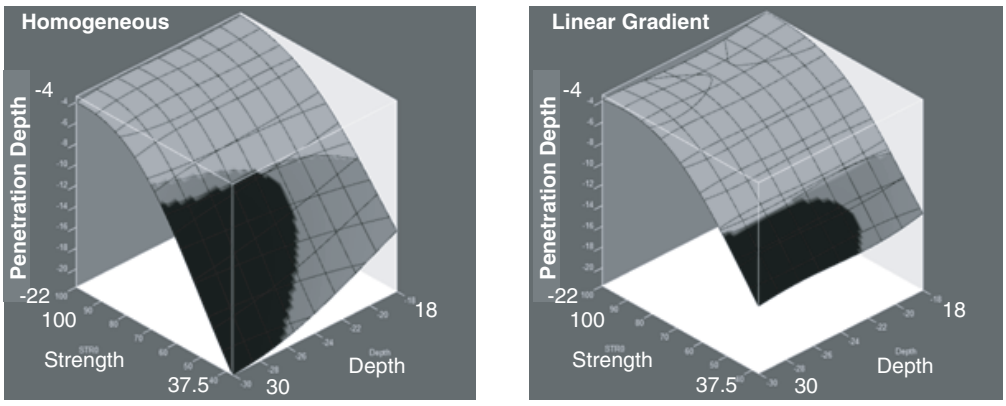


*Figure 12-8. Penetration depth trends for 29.0-in. tire with homogeneous (left) and linear (right) depth gradient.*

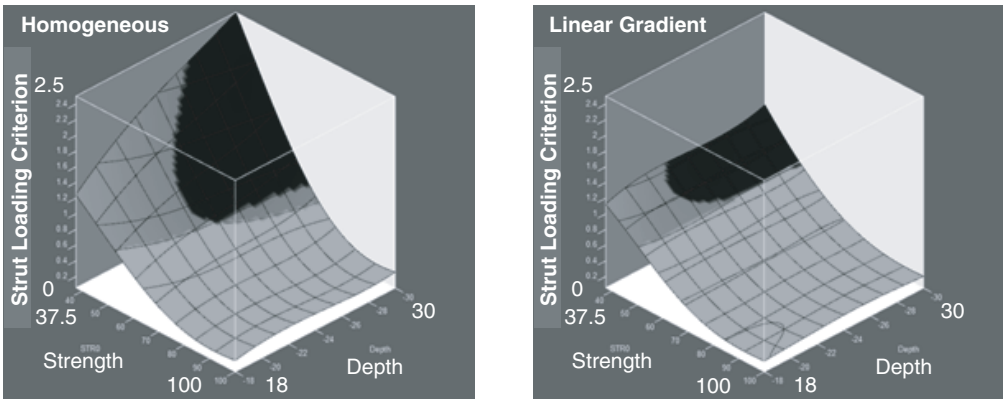


***Figure 12-9. Strut loading trends for 29.0-in. tire with homogeneous (left) and linear (right) depth gradient.***

over-penetration and the resulting overload behavior. This trend was not true for the homogeneous material shown on the left. This contrast implies a superior geometric coupling of the depth-varying material with the tire size and load.

The strut loading plot on the right side of Figure 12-9 shows a long, dual-tire optimal region where the boundary curves overlap one another at between 24 and 30 in. of bed depth. In that region, both aircraft struts are ideally loaded at a factor of 0.8.

This long overlap is superior to the crisscross intersection of the homogeneous material plot on the left. It implies that additional tires, either larger or smaller than the two subject tires, could also find optimal responses with such a design. After all, a larger tire would generally require a deeper bed; such a bed would not disturb the response of either existing tire, since neither feels the effects of the additional depth. The tires would tend to settle to their own equilibrium levels. This behavior contrasts with the homogeneous material, where the only dual-tire optimum point was a chance intersection of the two tire curves. The likelihood of a third tire happening to intersect those two curves at the same junction point is minimal.

Therefore, three behaviors emerge in the optimal design region of the linear depth gradient material:

1. Each tire ignores unneeded depth, and "sees" the bed as tailor-fit to its dimensions;
2. The strength sensitivity of the smaller tire is reduced, moving closer to that of the larger tire; and
3. The behavior suggests the feasibility of multi-tire simultaneous optimization due to the depth insensitivity.

### 12.4.6. Summary of Metamodel Analysis

The metamodel analysis explored linear, quadratic, and exponential depth-varying material profiles using stratified arrestor bed models. These profiles were compared with one another and with the currently used homogeneous material approach.

An initial down-selection eliminated the exponential profile from consideration; subsequent analysis eliminated the quadratic profile. The final analysis compared the linear profile material with the homogeneous approach.

A dual-tire optimum design can be obtained with either homogeneous or linear depth-varying arrestor beds. However, the optimum designs for each differ in several substantial ways:

- The homogeneous material strut-loading metamodels for the two tires had different shapes and magnitudes; the depth-varying material did much to bridge the response chasm, resulting in similar surfaces for the two tires.
- The optimal design for the homogeneous material exhibited high sensitivity to changes in the arrestor material strength for the smaller tire; the depth-varying system reduced the sensitivity difference between the tires by 50%.
- The homogeneous material did not lend itself to multiple simultaneous aircraft optimizations; the depth-varying system offered a dual-tire optimized region rather than a single intersection point, and likely could support multiple simultaneous aircraft optimizations.
- With the depth-varying material, each tire ignored unneeded bed depth, settling to its own natural equilibrium depth.

## 12.5. Transition to Fielded System

### 12.5.1. Comparison with Other Candidate Evaluations

The depth-varying foam material was assessed as part of a parallel study to the overall research effort. The focal point of the investigation differed from that of the other candidate arrestor concepts, and the final evaluation is less mature.

In order to bring the depth-varying concept evaluation to the maturity point of the other candidates, metamodel data would need to be created for the full suite of aircraft tires. Subsequent arrestment simulations could then be conducted with the APC to quantify the overall improvements to the arrestor bed lengths and aircraft exit speeds.

### 12.5.2. Transition to Glass Foam System

The depth-varying evaluation was carried out using a generalized ideal crushable foam material. Before conducting the metamodel generation recommended in the preceding section, it would be beneficial to link the concept with actual materials and calibrate to match them.

The glass foam material appears to be a strong candidate for implementing this concept (Chapter 9). It can be produced in a variety of strengths, is manufactured in relatively thin blocks, and can be adhered to itself in stratified layers matching the concept layup. It also has fairly ideal crushable foam characteristics that would lead to a good performance match with the idealized material predictions.

### 12.5.3. Comparison with Aggregate Foam System

The aggregate foam material manifested a depth-varying material property (Section 11.3.2), which should be compared with the concept investigations of this section.

The aggregate foam material exhibited the best overall fleet-wide performance of the three candidate systems evaluated (Section 11.5). The fleet design arrestor bed produced the closest overall exit speed rating for the three test aircraft, showing strong improvements in performance for the B747, which typically lagged in the one-size-fits-all beds. This improvement was possible because the foam aggregate essentially had an exponential depth-varying strength profile.

During the depth-varying profile investigation, it was determined that the linear strength profile offered more advantageous behavior than the quadratic or exponential profiles. If this observation holds true during a broader assessment involving the three test aircraft, it is possible that a stratified glass foam bed could perform even better than the foam aggregate. However, there are several design coefficients for either depth-varying profile, and a more extensive examination would be required to firmly establish the best fleet-wide approach.

The rut depths previously shown for the aggregate foam bed tended to be fairly shallow. The penetration depth into the linear gradient arrestor bed would likely be deeper, which could reduce the amount of unused material. Yet, for the same reason, loading oscillations could potentially be more severe in the linear case since it might not prove as robust for preventing over-penetration. The loading oscillations with the aggregate foam system required control through the bed geometry design. Similar control would probably be required for a stratified glass foam arrestor bed as well.

### 12.5.4. Estimated System Cost and Maintenance

If the depth-varying crushable foam concept were to be implemented using a glass foam material, the system cost and maintenance issues would be the same as discussed in Section 9.6.2. The nature of the glass foam concept's layup and construction would readily permit the use of several strengths of foam material in stratified layers without altering the construction methodology.

## 12.6. Summary

The depth-varying foam material concept was assessed as part of a parallel study to the overall research effort. The focal point of the investigation differed from the other arrestor concepts investigated, and the final concept evaluation is less mature than for the three primary arrestor candidate systems.

The comparative optimization study involved a protracted set of tire and arrestor simulations, which investigated linear, quadratic, and exponential material hardening profiles. A down-selection of these alternatives found that the linear strength increase profile was the most promising, and it was compared with the incumbent homogeneous material.

The results for this investigation proved positive: a linear depth-varying material offers several advantages over the current homogeneous material. The depth-varying approach helped bridge the geometry and loading gaps between large and small tires, reducing the performance disparities between them. A bed constructed using the linear depth-varying material could produce shorter arrestment distances and/or higher design exit speeds for the aircraft fleet.

In practice, this methodology could be readily implemented using a glass foam block material, with minimal impact on anticipated cost, construction methods, or maintenance needs.

Finally, Chapter 11 demonstrated that the exponentially depth-varying aggregate foam material could achieve performance leveling between aircraft. Although the exponential profile was not ideal per the findings of this study, the aggregate foam concept illustrates the potential results when extrapolated through full aircraft arrestment simulations.

CHAPTER 13

# Summary of Passive System Candidates

Chapters 9 through 12 examined the passive system candidates on an individual basis. This brief chapter summarizes key findings for performance and cost on a side-by-side basis.

## 13.1. Overview

The experimentation phase evaluated three passive arrestor candidate systems:

1. Glass foam arrestor
2. Aggregate foam arrestor
3. Engineered aggregate arrestor

Each demonstrated relative strengths and weaknesses. All three options provide concepts with increased material durability over cellular cement, which would likely result in longer life cycles and decreased maintenance requirements.

## 13.2. Performance Comparison

The performance of the different candidates can be compared in two primary ways: based on (1) single-plane or (2) multi-aircraft bed designs. When comparing single-aircraft bed designs, the thickness of each bed and its material properties are optimized for the plane of interest. However, the bed designs for the different aircraft may not be compatible with one another. For example, a best-case design for the B747-400 was typically found to overload the landing gear of the CRJ-200.

When comparing multi-aircraft bed designs, a single bed is designed for best-case performance with all three of the subject aircraft simultaneously. A single bed thickness and material property are determined such that the overall performance is optimized for all three aircraft.

The single-aircraft comparisons always produce the shortest feasible stopping distances. However, the multi-aircraft comparisons are more relevant to actual applications at airports, in which arrestor beds are designed as a compromise between the different aircraft serviced.

Figure 13-1 compares the best single-aircraft bed designs for the three alternatives and compares them to the current EMAS technology. The four sets of bars show very similar trends in terms of relative stopping lengths for the different aircraft. The glass foam stopping distances are slightly shorter than those of the current EMAS, while the other two concepts would require slightly longer beds. The performance similarity of glass foam and the current EMAS is not surprising because both designs use crushable foam block material with similar mechanical behavior. However, this comparison of single-aircraft performance is ultimately less relevant to real applications than the multi-aircraft comparisons that follow.

Figure 13-2 compares the best multi-aircraft arrestor bed designs for the three alternatives. In each case, the B747-400 required the longest bed for arrestment from a 70-knot exit speed. It should be noted that performance predictions for the existing EMAS have not been included in the figure because the design cases did not apply to multi-aircraft bed designs. In general, the material could be assumed to follow a similar trend to glass foam, owing to the mechanical similarities just discussed.

In comparing Figure 13-1 with Figure 13-2, the trend for leading and trailing concepts shifts considerably. The differences illustrate how substantially the multi-aircraft performance deviates from aircraft considered individually. For the multi-aircraft case, bars of similar height indicate improved equality in the treatment of the three aircraft. Of the three concepts, the aggregate foam shows the most consistent performance, with dramatic reduction in the stopping distance for the B747-400.

As an example, for a bed with a practical 400-ft length, the exit speeds for each aircraft are as shown in Table 13-1. The 400-ft bed would obtain a full 70-knot exit speed rating for the CRJ-200 with all arrestor concepts. Both the glass foam

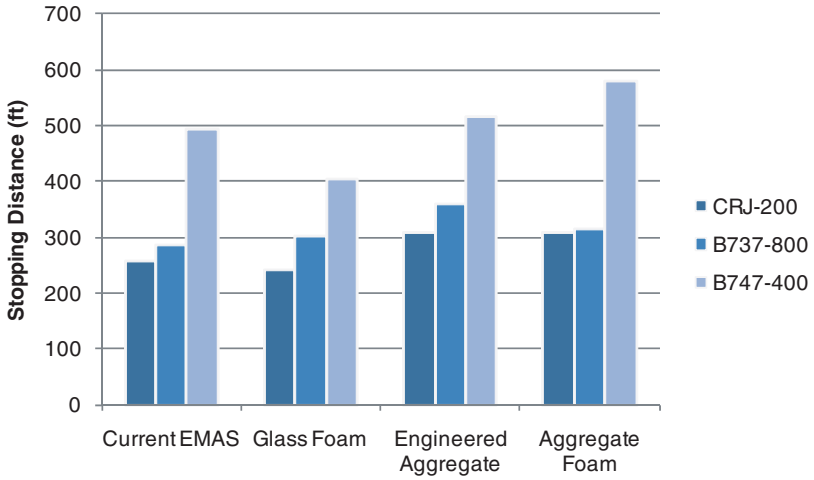


***Figure 13-1. Comparison of single-aircraft bed performance for all candidates: distance travelled in bed for full arrest assuming 70-knot exit speed.***

and aggregate foam beds would further obtain a 70-knot rating for the B737-800, while the engineered aggregate falls behind at only 63 knots. For the B747-400, none of the beds obtain a full 70-knot rating; the aggregate foam leads at 56 knots and the engineered aggregate falls to below the minimum allowable speed at 39 knots.

Overall, the performance of the three concepts can be summarized as:

- The aggregate foam concept provided the best overall mixed-fleet bed performance, showing the smallest spread in arrestor performance for the three aircraft. However, the bed design must be correctly specified to prevent oscillatory porpoising behavior.
- The engineered aggregate produced speed-dependent landing gear loads. This would typically require designs to hedge against overloading by under-designing them, resulting in longer arrests than illustrated above.
- The glass foam beds produced the most predictable and constant decelerations without speed dependence or porpoising effects.

## 13.3. Environmental Performance Comparison

From an environmental performance standpoint, all three alternatives appear likely to offer superior performance to the current EMAS technology. The environmental perfor-

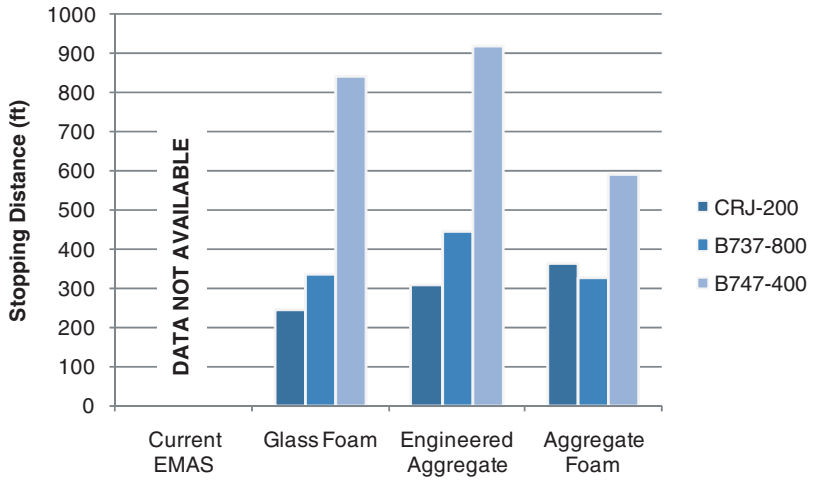


***Figure 13-2. Comparison of multi-aircraft bed performance for all candidates: distance travelled in bed for full arrest assuming 70-knot exit speed.***

**Table 13-1. Comparison of multi-aircraft bed performance: exit speeds for full arrest in 400-ft bed.**

| Aircraft | Glass Foam | Engineered Aggregate | Aggregate Foam |
|---|---|---|---|
| **CRJ-200** | 70+ | 70+ | 70+ |
| **B737-800** | 70+ | 63 | 70+ |
| **B747-400** | 46 | 39 | 56 |

mance estimates are based on some test data, historical use of the materials, and engineering judgment. An exhaustive environmental test program has not been undertaken as part of this program.

Life-cycle performance has been assumed to result from a combination of the core materials used and the protective measures taken to shield those materials from the elements.

From a materials standpoint, the glass foam and aggregate foam concepts both use closed-cell glass foams that inherently resist water penetration. The engineered aggregate is composed of hard spherical pellets. All three of these materials appear to offer superior inherent resistance to general handling and moisture/chemical exposure when compared to cellular cement.

Of the three, the engineered aggregate is the most durable material because it is not a crushable low-density foam. However, the arresting properties of engineered aggregate can be affected by the dampness of the material in a manner that is unlikely to affect the glass and aggregate foams.

The glass and aggregate foam materials showed degradation if subjected to fully immersed freeze–thaw cycling conditions. Protection from standing water conditions would be required in all three cases, which is feasible using the proposed protective measures. Where such measures are taken, the materials have demonstrated a long service life.

With regard to protective measures, methods for covering and sealing the three candidate materials against moisture, standing water, jet blast, and freezing conditions have been examined (see respective chapters). For the aggregate foam and engineered aggregate approaches, the use of geo-plastics and geo-textiles could render the beds essentially isolated from water entrainment and freeze–thaw damage. The glass foam material could be packaged in a manner similar to that of the current EMAS cellular cement or equipped with an alternative monolithic sealed top layer.

Both the aggregate foam and engineered aggregate concepts propose using a turf layer atop the beds, which is novel for arrestor beds. While modeling predictions indicate that this is feasible, additional testing in wet and freezing conditions would be required to characterize that facet of environmental performance. Alternative cover layers are possible in the event of adverse performance.

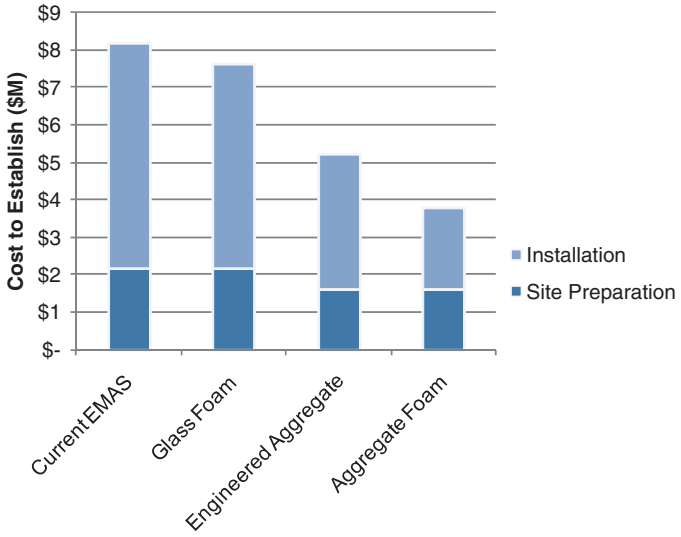


***Figure 13-3. Relative estimated cost comparison assuming survey costs (150 ft x 300 ft bed).***

In all three cases, the proposed designs offer life-cycle potential beyond the 10-year bed replacement interval that is assumed necessary for the current EMAS technology (*29*).

## 13.4. Cost Comparison

The relative costs for the current EMAS and the candidate systems are compared in Figure 13-3 and Figure 13-4 using survey cost assumptions and estimates from FAA Order 5200.9, respectively. The general trends appear similar in either case, with the aggregate foam concept providing the least expensive alternative, and the glass foam

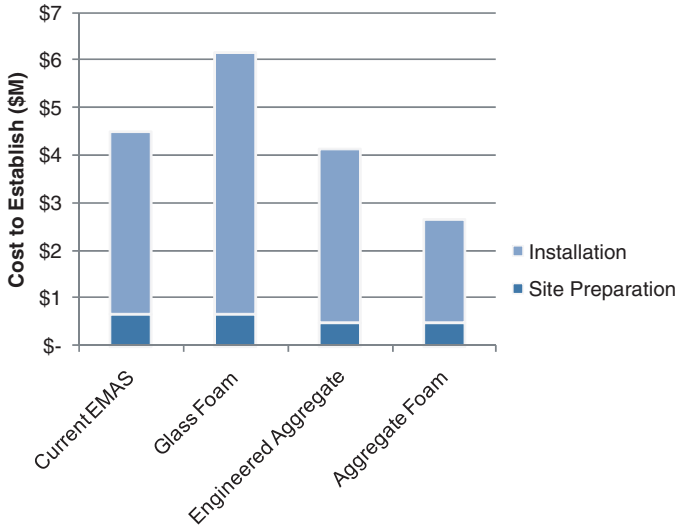


***Figure 13-4. Relative estimated cost comparison assuming FAA Order 5200.9 costs (150 ft x 300 ft bed).***

providing the most expensive alternative. The costs in the figures denote the total cost to establish such a system and do not include life-cycle costs of bed replacement and maintenance.

## 13.5. Summary Comparison

Glass foam provided equivalent dynamic behavior to the currently approved EMAS system. Its performance, cost, and construction are also similar to the current EMAS. However, use of glass foam with a monolithic construction offers reduced maintenance and a longer service life. Additionally, glass foam could be constructed using a stratified depth-varying layup, which would likely improve multi-aircraft bed performance (Chapter 12).

Aggregate foam provided a novel approach that featured excellent multi-aircraft bed performance due to its depth-varying crushable material; this would effectively lead to shorter arrestor beds. Its cost was the lowest of the alternatives, combining an inexpensive material with a simple installation process.

Engineered aggregate features the most durable candidate arrestor material, much of which could be reused after an arresting event. It has a cost that falls between the other concepts. Its speed-dependent nature produces weaker multi-aircraft performance, which would require longer arrestor beds to obtain the same exit speed ratings.

CHAPTER 14

# Main-Gear Engagement Active System Concept

The main-gear engagement active arresting system concept was evaluated in two major respects. First, a loading model was developed to determine the decelerations possible and the load effects on the landing gear. This model assumed that a cable-based arrestor system had successfully engaged the main-gear struts of the aircraft. The second part of the evaluation assessed the performance requirements to successfully engage the landing gear of a fast-moving aircraft.

## 14.1. Overview of Active System Deployment

Three issues complicate the deployment of a cable-based arrestor: aircraft identification, overrun event detection, and timing of deployment. First, the type of aircraft must be determined prior to the arrest. Civil aircraft in service at U.S. airports have a variety of main landing gear geometries. Therefore, the type of aircraft would have to be known prior to deployment. This issue could be resolved with a dedicated transponder or a video-based recognition system.

Second, unlike an EMAS, which passively arrests aircraft, the net or cable that engages the main gear must be activated to be erected in the event of an overrun. Under normal circumstances, the net or cable will be retracted and level with the runway. Activation depends on detection of an overrun. This issue could be addressed by locating sensors at or near the threshold of a runway. When the aircraft crosses the threshold, the system could automatically arm itself. With the correct detection sensors, the need for a ground operator to manually activate the system could be eliminated.

The third issue is the timing of deployment. Erecting an engagement device to capture the main gear must be done while avoiding contact with the aircraft engines. As shown in Figure 14-1, the main landing gear and the engines are in similar longitudinal positions on the aircraft. Consequently, any device that would propel the arresting cable up to engage the main landing gear would have to be timed to activate after the nose gear and engine nacelles had passed by.

## 14.2. Prediction of Arresting Loads

### 14.2.1. Predictive Tool

An analytical spreadsheet model was developed to calculate a time-marching aircraft deceleration. The mechanical input variables and output responses included in the model are shown in Table 14-1.

The predictive tool assumed the geometry shown in Figure 14-1. Figure 14-2 is a detail of the main landing gear engaged by the cable with tension. As shown, the initial deceleration tension in the cables, which the brake units create, produces a secondary tension between the main-gear struts.

The primary and secondary cable tensions produce a rearward deceleration load on the struts and an inward lateral load. The lateral load depends on the coefficient of friction between the cable and the strut. As the plane rolls further past the arresting engines, the angle $\theta$ decreases, which increases the lateral load on the struts.

The limiting lateral and longitudinal loads were determined from FAR part 25 for a Boeing 737-800.

### 14.2.2. Arrestment Simulations

Arrestment simulations were made for a B737-800 that was initially travelling at 70 knots. The aircraft was assumed to have a 0.25 braking coefficient during the arrest.

During the simulation, the cable tension was set to maximize the deceleration without exceeding the main-gear limit loads. The total load on the strut due to the cable force and the braking force summed to equal the longitudinal limit load. Due to the angle change for the cable, the tension was

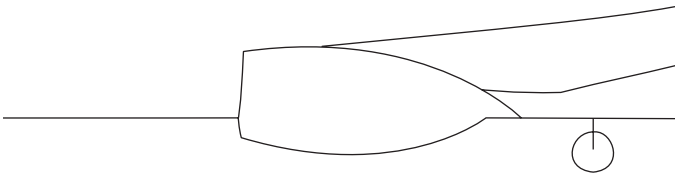

*Figure 14-1. B737-800 main landing gear and aircraft engine (42).*

continually adjusted to maintain the total overall load. This was done dynamically during an arrest to simulate an active feedback control for the arrestor system.

Because the deceleration was designed to maximize the drag loading on the main gear, a fairly low coefficient of friction ($\mu = 0.3$) was used between the main strut and the cable. With this configuration, the strut loads were calculated to be as shown in Figure 14-4. The struts are loaded maximally in the longitudinal (drag) direction, and the lateral strut loads climb steadily until the end of the arrestment. If the friction between the strut and the cable is higher, the lateral load becomes the limiting factor, and the cable tension must be reduced, lengthening the stopping process.

For the B737-800, the cable tensions are given by Figure 14-5. For the 140 kip tension shown, the cable would need to be composed of high-strength steel with a diameter of 1.4 in. or more, depending on strength. This cable size presents complications, especially when dealing with large and small aircraft. Strong decelerations of a large aircraft will require a thick, heavy cable. When a small aircraft is arrested by such a system, the weight of the cable itself could be sufficient to cause damage to the landing gear.

The aircraft speed and deceleration are shown in Figure 14-6 and Figure 14-7, respectively. This deceleration essentially represents a best-case solution for the aircraft, assuming the longitudinal FAR limit load criterion for the main gear. As Figure 14-7 shows, the system concept is capable of providing ideal constant decelerations.

**Table 14-1. Cable-based arrestor model parameters.**

| Input Variables | Output Responses |
|---|---|
| Geometry<br>• Distance between brake units<br>• Slack in cable<br>Maximum tension in cable<br>Coefficient of friction between strut and cable<br>Aircraft type (B737-800)<br>• Limiting lateral load<br>• Limiting longitudinal load<br>Aircraft braking condition<br>• Braking<br>• Free-rolling | Stopping distance<br>Max lateral load<br>Max longitudinal load |

### 14.2.3. Additional Friction Study

Simulations were conducted to determine whether, for a typical arrest case, the lateral load on the landing gear would reach a limiting value. Preliminary simulations showed that if the maximum tension in the cable were kept below a critical value, the lateral load on the landing gear remained below the limiting lateral load implied by FAR Section 25.485.

For a braking coefficient of 0.25 and no reverse thrust, simulations were run for a B737-800 in which the strut-cable coefficient of friction was varied and the maximum lateral load on the landing gear was recorded. These maximum lateral loads were normalized by the limiting lateral load. As shown in Figure 14-8, the maximum lateral load nearly reached 90%

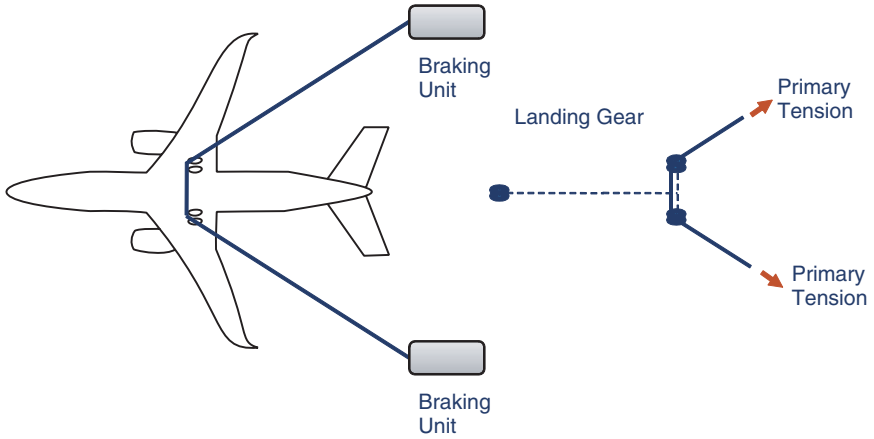


*Figure 14-2. Cable-based aircraft arrestment.*

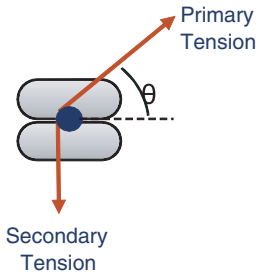


***Figure 14-3. Detail of cable tensions at main-gear strut.***

of the limiting lateral load for a strut-cable coefficient of friction of approximately 0.7. Therefore, on the basis of preliminary investigation, if the maximum tension in the cable is limited to the critical value, lateral collapse of the landing gear can be prevented.

## 14.3. Landing Gear Engagement

Arguably the most challenging aspect of the main-gear engagement active arrestor concept is "catching" the aircraft and establishing a solid connection with the landing gear. If the cable or net system misses the landing gear strut, or bounces off and is overrun by the plane, the braking devices will not be able to stop the aircraft.

### 14.3.1. Deployment Path

Assuming that the netting or cable system starts from an initially flat configuration, flush with the runway surface, it would require rapid vertical deployment to catch the strut above the top of the tires. For an aircraft with low-slung engines, the cable/net would have to elevate after the engine nacelles have passed by but in time to catch the strut (Figure 14-9).

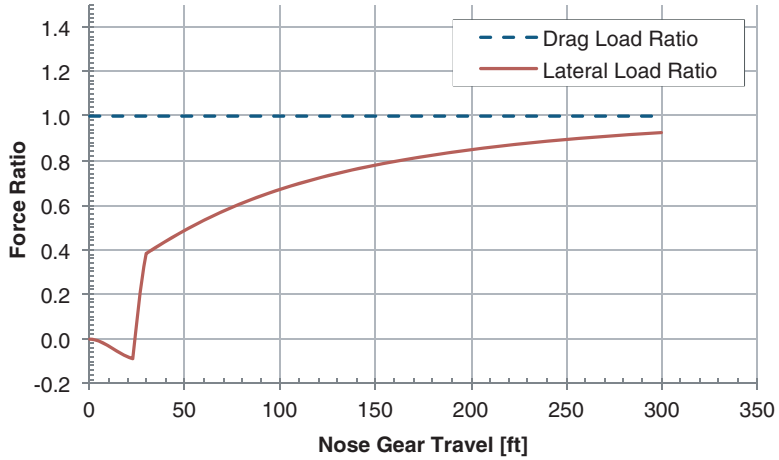


***Figure 14-4. Main-gear strut loads during active system arrestment for B737-800, normalized by FAR strut limit values.***

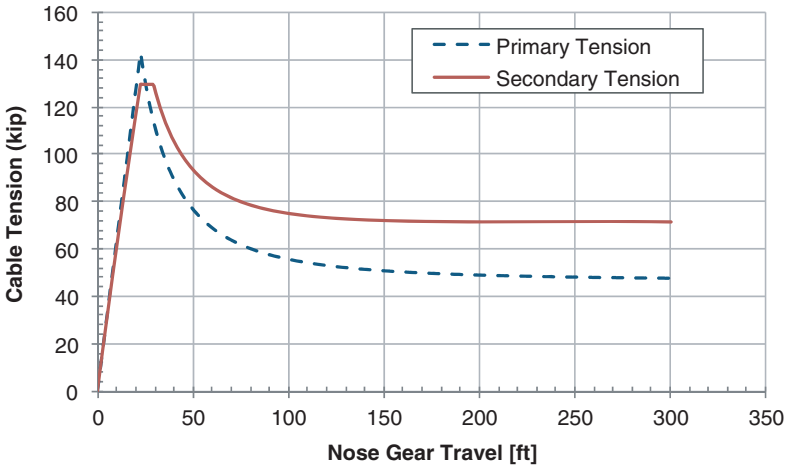


***Figure 14-5. Cable loads during active system arrestment for B737-800.***

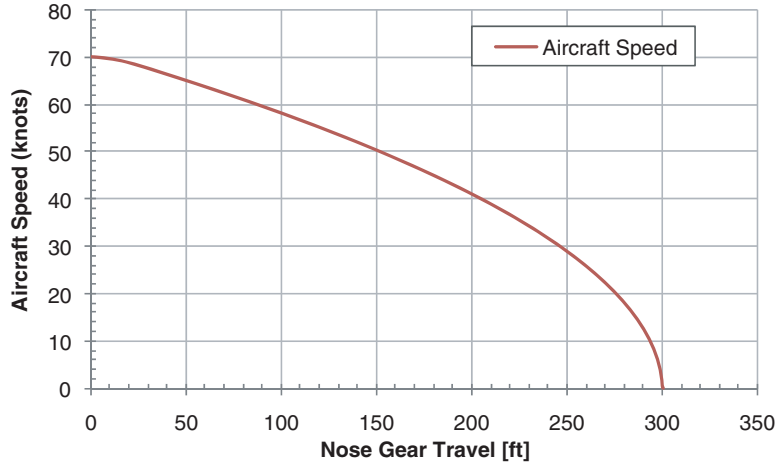


***Figure 14-6. Aircraft speed during active system arrestment for B737-800.***

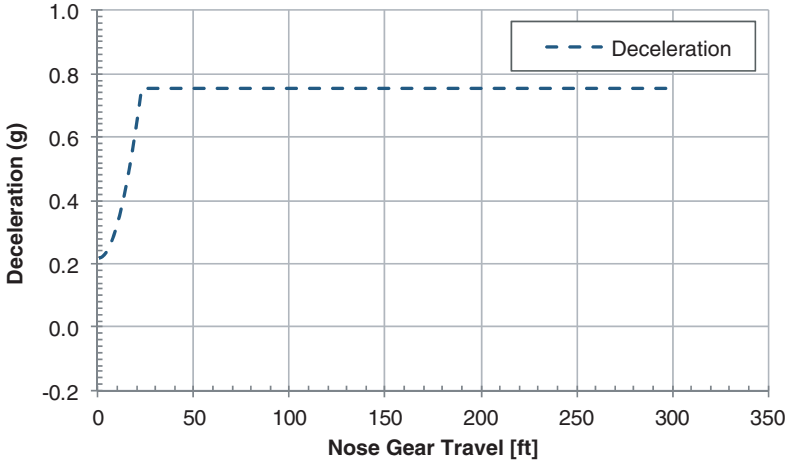


***Figure 14-7. Deceleration during active system arrestment for B737-800.***

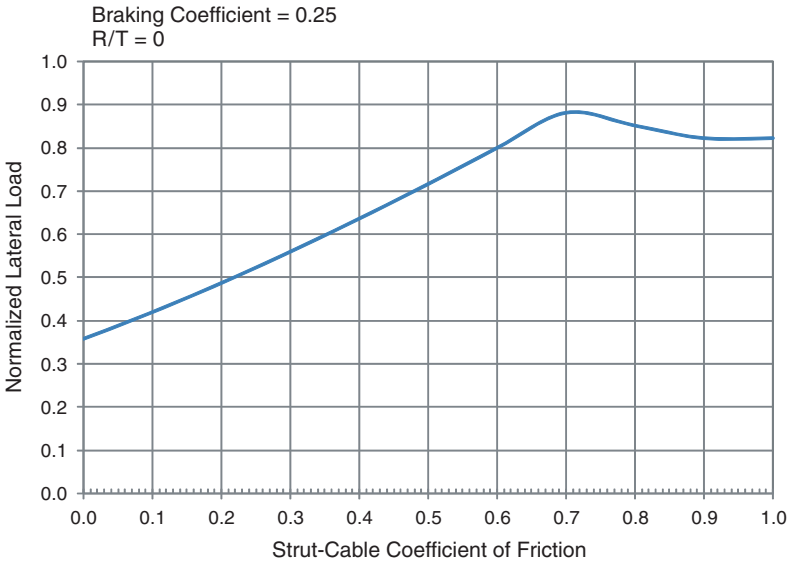


***Figure 14-8. Dependence of lateral load on strut-cable coefficient of friction.***

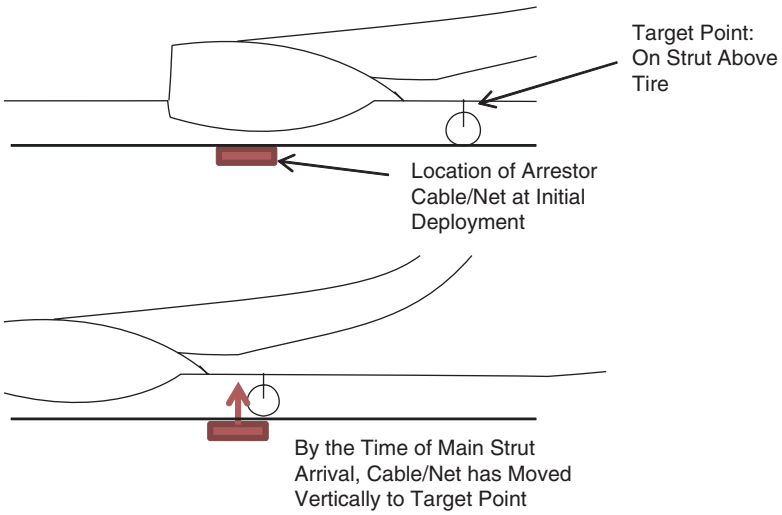


*Figure 14-9. Cable deployment concept (42).*

Assuming that the aircraft would be rolling forward at 70 knots, the necessary deployment timing was calculated. Because the aircraft's lateral location with respect to the runway centerline could vary, it was assumed that the cable for the system would be elevated uniformly across the entire runway width.

The test aircraft in this case was a B737-800. Using manufacturer-published dimensions, the required cable path is given in Figure 14-10. The illustration gives an upper and lower boundary to the cable path, as well as an optimal path. The path appears sloped because the aircraft is moving forward relative to the cable location. However, the calculations assume that the cable moves directly upward from its location on the runway.

## 14.3.2. Deployment Timing

Table 14-2 summarizes the timing and speed requirements for the deployment. The time to launch is essentially the delay in deployment after the nose wheel passes the arrestor cable. The tolerance shows that the initialization of the deployment must take place within about 8 milliseconds of the targeted time.

Overall, the velocities and timing tolerances in this example are feasible for a mechanical design. For each aircraft, these values would be different, which would require that a deployment system be capable of identifying the aircraft type. It would then need to make a timing determination based on a database of aircraft information.

One important feature of these calculations is the upward velocity, which would be nominally 40 ft/sec (27 mph) on initialization, and nearly that fast on contact with the strut. This means that the cable would still be moving upward. Depending on the nature of the mechanical deployment system, slack in the cable combined with the upward motion could cause it to slap against the bottom of the aircraft and the landing gear bay doors.

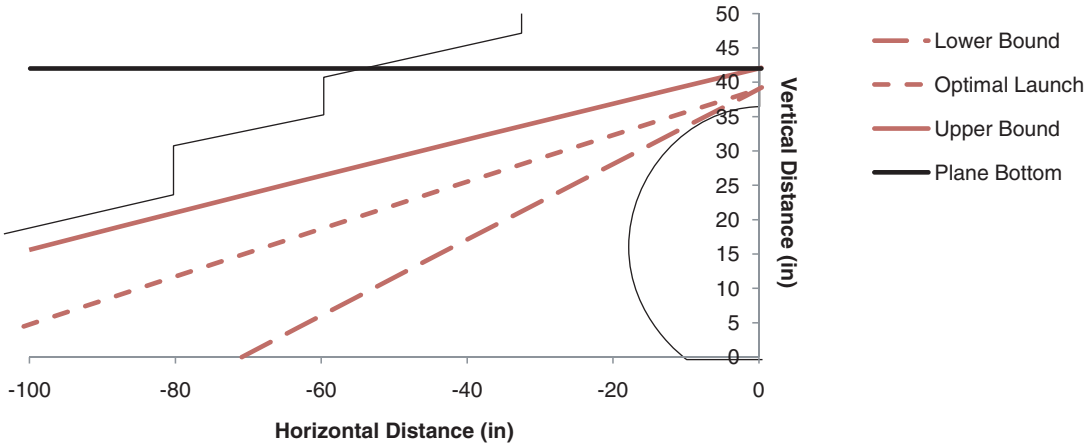


*Figure 14-10. Path calculation plot for active system B737 landing gear capture.*

**Table 14-2. Path calculation data for active system B737-800 landing gear capture.**

| | Lower Bound | Optimal Launch | Upper Bound |
|---|---|---|---|
| Time to Launch | 50 ms | 80 ms | 110 ms |
| Tolerance | ±4.78 ms | ±7.80 ms | ±11.03 ms |
| Initial Velocity | 67.73 ft/s | 42.33 ft/s | 31.36 ft/s |
| Tolerance | ±3.08 ft/s | ±2.71 ft/s | ±2.22 ft/s |
| Terminal Velocity | 66.12 ft/s | 39.75 ft/s | 27.82 ft/s |

### 14.3.3. Landing Gear Features

One of the more problematic issues with this concept is the varied nature of main landing gear features for different aircraft. On the main struts of many passenger aircraft, a variety of smaller hydraulic, electrical, and mechanical components are exposed on the front and outboard sides of the struts. If the struts of these aircraft were engaged with a cable or net and subjected to substantial load, these components would likely be damaged. In the case of some aircraft, such as the A380, which has a secondary strut forward of the main-gear strut, cable engagement could result in structural failure of the main-gear assembly. Although it is possible that engagement geometries could be developed that reduce the risk of structural damage to the landing gear, some degree of damage to the gear is likely under any arresting conditions.

### 14.3.4. Infeasible Aircraft

During the investigation, it became apparent that some aircraft would not have a deployment path solution as that discussed in Section 14.3.1. Figure 14-11 shows that the shorter B737-200 has engine locations that preclude engaging the target point on the strut. Although a broad survey of infeasible aircraft was not undertaken, this case illustrates that there would be at least some aircraft for which this arrestor concept would not work.

## 14.4. Summary

The main-gear engagement active system concept offered multiple advantages not available in surface-based arrestor beds. Feedback control offered the potential for ideal deceleration of aircraft. The friction brakes could adjust automatically to apply less load on a small plane than a large one, enabling one arrestor to treat all aircraft equally. The overall effect of these advantages would be shorter arresting distances for the entire design fleet of aircraft.

The load calculations undertaken confirm that the essential mechanics for the arrestor system would function as anticipated. Tension regulation in the cable would be essential to prevent lateral overloading of the landing gear toward the end of the arrestment.

Despite these promising features, a number of complicating issues remain for the active system concept:

- Aircraft identification and speed calculation would be required for the system to function correctly. Systems to accomplish both could likely be developed, although research of such facets has not yet been undertaken.
- Cable sizes are of concern because the thicker cables required for rapidly arresting large planes could be heavy enough to damage smaller ones.
- The cable engagement process would likely result in damage to landing gear doors, actuators, wiring, and hydraulic features on the front side of the main struts.
- The window of time for deploying the system could be narrow when the aircraft has low-slung engines because the vertical path of the cable or net must miss the engine nacelles yet engage the main strut above the tires.
- Due to the longitudinal overlap of the engines and main struts, some aircraft would not have a feasible solution

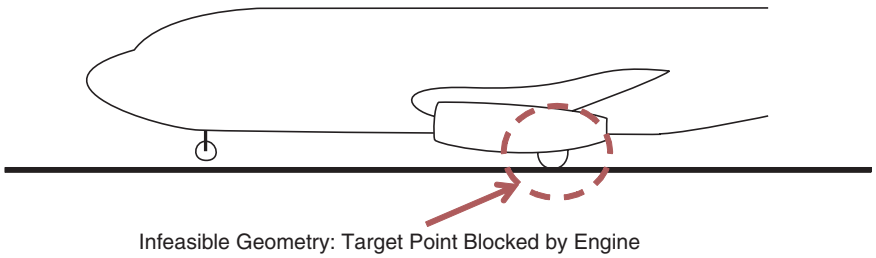


***Figure 14-11. Infeasible geometry for landing gear engagement: B737-200.***

path for cable deployment. These aircraft could not be engaged and arrested by a main-gear cable/net system.

For these reasons, the active system approach is feasible for stopping aircraft, but the main-gear engagement concept should perhaps be eliminated from consideration. Barrier net systems have been developed in the past, and they may still offer the best overall engagement approach. Past activation issues for the nets could be resolved using automation concepts as discussed, thereby eliminating the need for direct triggering by airport personnel. However, potential obstruction of aircraft exits and damage to the aircraft continue to remain obstacles to implementation.

CHAPTER 15

# Conclusions

The first research phase engaged in multiple studies of different topics relevant to developing arrestor alternatives. After identifying promising alternatives, several candidate concepts were selected for detailed evaluation in the second experimentation phase. In the second phase, testing and modeling were used to evaluate the performance of the candidates. This chapter summarizes important conclusions from both phases of research.

## 15.1. Study Phase

The survey of U.S. airport operators revealed that actual EMAS costs appear to exceed the predicted values contained in FAA Order 5200.9 in terms of preparatory paving, installation, and maintenance (Chapter 3). While the survey included more airports than the original data set used to create Order 5200.9, it did not include all EMAS systems installed at U.S. airports. It is possible that the average costs could shift once the remaining airports were included. However, since the survey data for the CTEE was 1.8 times higher than the predicted value, an update to the guidance document may be advisable.

A review of aircraft overrun data led to a revised probability curve for aircraft overrun exit speeds (Chapter 5). This revised curve indicated that 90% of aircraft overruns may no longer take place at or below an exit speed of 70 knots. The new curve suggests that the 90% threshold may have shifted to just above 80 knots. This could impact the design speeds for aircraft arrestors if a 90% criterion is to be maintained. Additional investigation may be warranted regarding the accuracy of the reported data that was used in the assessment.

The sensitivity analysis showed that the relative length of an arrestor bed will tend to vary with the aircraft exit speed squared (Chapter 5). Increasing the 70-knot standard exit speed or the 40-knot minimum exit speed requirements would have a notable impact on the size and cost of arrestor systems, irrespective of which passive arrestor technology is used.

The FAA EMAS design requirements currently prohibit damage to the aircraft, which typically results in arrestor bed designs constrained by the rearward nose-gear loads. More aggressive decelerations would be possible if the designs were permitted to collapse the nose gear as long as the main gear remained intact. Prior EMAS testing suggests that this may pose minimal hazards to aircraft occupants. However, aircraft with low-slung engines could potentially be damaged and/or ingest arrestor material in such cases, and the risks of these effects have not been quantified. Additional concerns would apply to turbo-prop aircraft, where propeller damage could present additional hazards. It may be advantageous to revisit the requirements regarding landing gear loading in order to determine if case-by-case exceptions may be permissible. In some circumstances, the benefits of aggressive arrestor performance may outweigh the risks of failing to stop an overrun.

The approval and commercialization study determined that the current lack of a general predictive software tool presents a barrier for new entrants to the arrestor system field (Chapter 6). Development of such a tool, or an update of the older ARRESTOR code, could be considered as part of any new approval process.

Although based on anecdotal experience, the researchers have noted a seeming lack of awareness regarding the existence, usage, and function of EMAS among airline pilots. This lack of awareness has been observed in both newer and seasoned pilots. It is unclear whether awareness is greater among pilots that typically land at airports with EMAS. Unfortunately, response from the pilot community was limited during the survey process. Nevertheless, it may be beneficial to consider pursuit of an educational effort to increase awareness of the existence and function of EMAS within the pilot community.

## 15.2. Experimentation Phase

The experimentation phase of the effort involved an extensive evaluation of four arrestor candidates:

1. Glass foam arrestor (passive)
2. Aggregate foam arrestor (passive)
3. Engineered aggregate arrestor (passive)
4. Main-gear engagement active arrestor (active)

A combined modeling and simulation effort successfully replicated each candidate in order to evaluate its merit and compare it with the existing EMAS performance.

### 15.2.1. Passive System Evaluation

Chapter 9 through Chapter 11 gave specific recommendations and guidance for transitioning the three passive candidates into fielded systems. The findings of this research indicate that a fieldable system is feasible for all three candidates.

The aggregate foam concept offers superior multi-aircraft performance due to its depth-varying material properties. This multi-aircraft performance is arguably the most important factor for keeping arrestor beds short, reducing land requirements, and increasing the rated aircraft exit speeds. Additionally, it provides a substantially lower estimated cost per square foot. However, because the aggregate foam concept uses a novel crushable material and cover layer, the number of unknowns is greater. The arrestor materials require additional evaluation in order to produce high-confidence performance estimations. Overall, the combination of unknown factors and anticipated cost and performance improvements make it a moderate-risk/high-payoff concept.

Conversely, the glass foam concept is the most conservative of the three alternatives in terms of development risk and payoff. Glass foam provides an alternative to the current EMAS technology with promising improvements regarding service life and maintenance, but at equivalent cost and performance. The mechanics of the material are predictable with relatively few unknown factors. Fielding such a system would be more straightforward than with aggregate foam, and the approval process could arguably follow the shorter "equivalent" path (Section 6.3). Overall, the combination of unknown factors and anticipated cost and performance improvements make it a low-risk/moderate-payoff concept.

Finally, the engineered aggregate concept provides a feasible alternative, but one without a particular distinguishing advantage. It provides cost savings and increased material durability over the current EMAS technology. However, the speed-dependent arrestor performance generally requires longer arrestor beds and diminishes the multi-aircraft performance. As with the aggregate foam, the materials to be used will require additional characterization in order to make high-confidence performance estimations. Overall, the combination of unknown factors and anticipated cost and performance improvements make it a moderate-risk/low-payoff concept.

The selection of one or more of these alternatives for fielding and approval is a task that requires consideration by the relevant stakeholders, which includes the government, airport community and manufacturers. Each candidate offers different advantages, risk levels, and payoff potential. Depending on the development track that is pursued, manufacturer investment may be required. The extensiveness of subsequent development plans and the associated costs may determine the feasibility of such participation. As a precursor to any such development, it is recommended that the concepts for pursuit be determined and that the relevant manufacturers be contacted for preliminary discussions of development scope and participation.

New arrestor and cover-layer materials will be used for any candidate that is pursued. It would be advisable to pursue full-scale tests for these alternatives, which would allow:

- Assurance of performance and safety,
- Characterization of the full arrestor layups,
- Down-selection of final cover layer alternatives, and
- Model calibration to match final configuration performance.

As part of future research, it would be advisable to test cellular cement specimens and incorporate a cellular cement arrestor into the APC. Inclusion of cellular cement was omitted during the current research. However, such a model could be developed in approximate form by testing a generic cellular cement material of nominally the same density. The incorporation of a cellular cement option in the APC would help to establish equivalency of various systems and provide additional comparison of performance between the arrestor options.

### 15.2.2. Active System Evaluation

The main-gear engagement active system candidate is not recommended for additional pursuit. While stopping the aircraft proved mechanically feasible, engaging the main-gear struts involved multiple complexities, including damage to landing gear features, damage to landing gear bay doors, and timing and deployment complexity. Additionally, some aircraft geometries made capture infeasible altogether.

Nevertheless, active systems remain feasible if barrier nets are used for engagement. Using the suggested sensor and activation methods, an automated system could be developed that would eliminate the need for manual triggering, but permit pilot overrides. The active system approach offers the highest theoretical deceleration limits, which could produce substantially shorter arrestment distances than any passive system alternative.

The survey findings indicate that endeavors to implement an active civil aircraft arresting system would meet with resistance by the aviation community. If pursued, it is recommended that an educational component be included to increase awareness and reduce misconceptions regarding such systems.

## 15.3. Final Conclusions

The research effort achieved its stated objective, which was to advance the development of alternative civil aircraft arresting systems. The research evaluated four alternatives to the current cellular cement EMAS technology, and successfully identified options that can provide improved performance, lower cost, and/or higher durability.

Pursuing full development and testing of one or more of these candidate systems would be the next step toward obtaining requisite FAA approval. Once fielded, the new arrestor system would provide additional options to airport operators for achieving RSA compliance. Increasing the choices available would allow decision makers to select the arrestor option that best fits with the budgetary, climate, and space constraints of the facility.

# References


1. FAA. *Engineered Materials Arresting Systems (EMAS) for Aircraft Overruns.* Washington, D.C.: Federal Aviation Administration, 2005. AC 150-5220-22a.
2. Cook, R. F. *Soft-Ground Aircraft Arresting Systems, Final Report.* Washington, D.C.: Federal Aviation Administration, 1987. FAA/PM-87-27.
3. Cook, R. F. *Evaluation of a Foam Arrestor Bed for Aircraft Safety Overrun Areas.* Dayton: University of Dayton Research Institute, 1988. UDR-TR-88-07.
4. Bade, E., C. Eng, and E. M. Minter. *Soft Ground Arresting of Civil Aircraft: Scaled Model VC 10 Tests in Gravel and Sintered Fuel Ash Pellets.* Farnborough, UK: Royal Aircraft Establishment, 1971. RAE Technical Report 71015.
5. White, J. C. and S. K. Agrawal. *Soft Ground Arresting System for Airports, Final Report.* Washington, D.C.: Federal Aviation Administration, 1993. CT-93-80.
6. Dole, G. R. "A Review of Computer Simulations for Aircraft-Surface Dynamics." *Journal of Aircraft*, Vol. 23, No. 4, 1986, pp. 257–265.
7. Cook, R., C. A. Teubert, and G. Hayhoe. *Soft Ground Arrestor Design Program.* Washington, D.C.: Federal Aviation Administration, 1995. DOT/FAA/CT-95.
8. Heymsfield, E., W. M. Hale, and T. L. Halsey. *A Parametric Sensitivity Analysis of Soft Ground Arrestor Systems.* American Society of Civil Engineers, 2007.
9. Stouffer, S. *A Study of the Pressure and Moisture in the ESCO Arrestor Bed at Minneapolis–St. Paul Airport.* Dayton, OH: University of Dayton Research Institute, 2000.
10. Stehly, R. *Report of Concrete Testing, Project: Engineered Material Arresting System Minneapolis–St. Paul Airport.* American Engineering Testing, Inc., 2007.
11. Zodiac ESCO. *EMAS MAX: Preliminary Design Report for EMAS Systems at the Runway 14 and 32 Departure Ends at St. Paul Downtown Airport in St. Paul, Minnesota, Revision B 8-7-07.* Logan Township, NJ: Zodiac ESCO, 2007. Revision B 8-7-07.
12. Minneapolis–St. Paul Airport. *Minneapolis–St. Paul International Airport Certification Manual.* Minneapolis–St. Paul, MN: 2004. pp. Section 11, 139.309 Safety Areas:11-1-11-5.
13. Rogers, C. *Aggregate for Truck Arrestor Beds.* Downsview, Ontario: Ministry of Transportation of Ontario, 2006.
14. Currey, N. *Aircraft Landing Gear Design: Principles and Practices.* Washington, D.C.: American Institute of Aeronautics and Astronautics, Inc., 1988.
15. Pritchard, J. "Overview of Landing Gear Dynamics." *Journal of Aircraft*, Vol. 38, No. 1, 2001, pp. 130–137.
16. Chester, D. H. "Aircraft Landing Impact Parametric Study with Emphasis on Nose Gear Landing Conditions." *Journal of Aircraft*, Vol. 39, No. 3, 2002, pp. 394–403.
17. Micklos, R. P. and T. Defiore. *Methods for Experimentally Determining Commercial Jet Aircraft Landing Parameters From Video Image Data, Final Report.* Washington, D.C.: Federal Aviation Administration, U.S. Department of Transportation, 1993. DOT-FAA-CT-93-7.
18. Tipps, D. O. et al. *Side Load Factor Statistics From Commercial Aircraft Ground Operations.* Washington, D.C.: Federal Aviation Administration, U.S. Department of Transportation, 2003. DOT/FAA/AR-02/129.
19. FAA. *Objects Affecting Navigable Airspace.* Washington, D.C.: Federal Aviation Administration, 1993. CFR 14 Part 77.
20. FAA. *Certification and Operations: Land Airports Serving Certain Air Carriers.* Washington, D.C.: Federal Aviation Administration, 1996. CFR 14 Part 139.
21. FAA. *Runway Safety Area Program.* Washington, D.C.: Federal Aviation Administration, 1999. Order 5200.8.
22. FAA. *Runway Safety Area Status Database.* Washington, D.C.: Federal Aviation Administration, 2007.
23. David, R. E. *Location of Commercial Aircraft Accidents/Incidents Relative to Runways.* Washington, D.C.: Federal Aviation Administration, 1990. DOT/FAA/AOV 90-1.
24. Hall, J., M. Ayres, Jr., D. Wong, A. Appleyard, M. Eddowes, H. Shirazi, R. Speir, D. Pitfield, R. Caves, O. Selezneva, and T. Puzin. *ACRP Report 3: Analysis of Aircraft Overruns and Undershoots for Runway Safety Areas.* Washington, D.C.: TRB, National Research Council, 2008.
25. FAA. *Introduction to Safety Management Systems (SMS) for Airport Operators.* Washington, D.C.: Federal Aviation Administration, 2007. AC 150/5200-37.
26. NTSB. *Report ATL06IA108.* Washington, D.C.: National Transportation Safety Board, 2006.
27. NTSB. *Report NYC03IA117.* Washington, D.C.: National Transportation Safety Board, 2003.
28. NTSB. *Report NYC99FA110.* Washington, D.C.: National Transportation Safety Board, 2000.
29. Aeronautical Information Services. Find an Airport. *AirportIQ 5010: Airport Master Records and Reports.* http://www.gcr1.com/5010web/.
30. FAA. *Financial Feasibility and Equivalency of Runway Safety Area Improvements and Engineered Material Arresting Systems.* Washington, D.C.: Federal Aviation Administration, 2004. Order 5200.9.

31. San Filippo, W. K. and H. DeLong. *Engineered Materials Arresting System (EMAS): An Alternative Solution to Runway Overruns.* American Society of Civil Engineers, 2004.
32. Rastegar, J. S. and J. G. Qiaode. Roadway for Decelerating and/or Accelerating a Vehicle Including an Aircraft. U.S. Patent 6,969,213, 2005.
33. Barsotti, M. A. *Optimization of a Passive Aircraft Arrestor with a Depth-Varying Crushable Material Using a Smoothed Particle Hydrodynamics (SPH) Model.* Graduate Thesis, University of Texas at San Antonio, 2008.
34. Angley, R. D. et al. Arresting Material Test Apparatus and Methods. U.S. Patent 5,789,681, August 4, 1998.
35. Zodiac ESCO. *EMAS: Design Report for Fort Lauderdale–Hollywood Airport R/W 9L.* Logan Township, NJ: Zodiac ESCO, 2005.
36. Pittsburgh Corning. Brochure: FOAMGLAS Insulation. Pittsburgh Corning, 2005. Number FG-3 20M. Rev 11/05.
37. Norsk Glassgjenvinning AS. Brochure: Glasopor, Konstruksjonspellets for framtiden, Produktinfo. Norsk Glassgjenvinning AS, 2006.
38. Norsk Glassgjenvinning AS. *Glasopor Product Specification. 180107.* Norsk Glassgjenvinning AS, n.d.
39. Bell, N., Y. Yu, and P. J. Mucha. *Particle-Based Simulation of Granular Materials.* Eurographics/ACM SIGGRAPH Symposium on Computer Animation, 2005.
40. Zodiac ESCO. Energy Absorbers. *Zodiac ESCO.* http://www.esco.zodiac.com/index.cfm/navid-30. Accessed July 1, 2009.
41. Zodiac ESCO. Barrier Nets. *Zodiac ESCO.* http://www.esco.zodiac.com/index.cfm/navid-98. Accessed July 1, 2009.
42. Boeing. *737 Airplane Characteristics for Airport Planning.* Renton, WA: The Boeing Company, 2005.
43. Norsk Glassgjenvinning AS. *Glasopor*. http://www.glasopor.no.
44. FAA. *Airworthiness Standards: Transport Category Airplanes.* Washington, D.C.: Federal Aviation Administration, 1997. CFR 14 Part 25.
45. Stapp, J. P. "Human Tolerance to Deceleration." *American Journal of Surgery*, 93(4), April 1957, pp. 734–40.
46. Latham, F. "Linear Deceleration Studies and Human Tolerance." *Clin. Sci. (Lond.)*, 17(1), February 1958, pp. 121–35.
47. Lewis, S. T. and J. P. Stapp. "Human Tolerance to Aircraft Seat Belt Restraint." *J. Aviat. Med.*, 29(3), March 1958, pp. 187–96.
48. Hendler, E. "Linear Acceleration as a Survivable Hazard in Aviation." *J. Aviat. Med.*, 27(6), December 1956, pp. 495–501.
49. DeWeese, R. L. and D. M. Moorcraft. *Evaluation of a Head Injury Criteria Component Test Device.* Washington, D.C.: Office of Aerospace Medicine, 2004. DOT/FAA/AM-04/18.
50. Moseley, H. G. and A. F. Zeller. "Relation of Injury to Forces and Direction of Deceleration in Aircraft Accidents." *J. Aviat. Med.*, 2(10), October 1958, pp. 739–49.
51. NHTSA. *Federal Motor Vehicle Safety Standards: Occupant Crash Protection.* Washington, D.C.: National Highway Transportation Safety Administration, Undated. 49 CFR Part 571.208.
52. FAA. *Federal Aviation Regulation, Airworthiness Standards: Transport Category Airplanes.* Washington, D.C.: Federal Aviation Administration, Undated. CFR 14 Section 25.662.
53. Zuidema, G. D. et al. "Human Tolerance to Prolonged Acceleration." *J. Aviat. Med.*, 27(6), December 1956, pp. 469–481.
54. U.S. National Library of Medicine. Ventricular Tachycardia. *Medline Plus.* http://www.nlm.nih.gov/medlineplus/ency/article/000187.htm.
55. Stapp, J. P. "Human Tolerance to Deceleration: Summary of 166 Runs." *J. Aviat. Med.*, 22(1), February 1951, pp. 42–5.
56. Stapp, J. P. "Effects of Mechanical Force on Living Tissue." *J. Aviat. Med.*, 26(4), August 1955, pp. 268–88.
57. Krishnamurthy, A. Current Concepts in Acceleration Physiology. *India Society of Aerospace Medicine.* www.isam-india.org.
58. Preston-Thomas, H. et al. "Human Tolerance to Multistage Rocket Acceleration Curves." *J. Aviat. Med.*, 26(5), October 1955, pp. 390–98.
59. Zuidema, G. D. et al. "*Human Tolerance to Prolonged Acceleration.*" *J. Aviat. Med.*, 27(6), December 1956, pp. 469–481.
60. Goodyear. *Aircraft Tire Data Book.* Akron, OH: Goodyear Tire & Rubber Company, 2007.
61. Brockman, R. A. and W. R. Braisted. "Critical Speed Estimation for Aircraft Tires." *Tire Science and Technology*, Vol. 22, No. 2, 1994, pp. 121–144.
62. Stander, N. and W. Roux. *LS-OPT Training Class, Optimization and Robust Design Using LS-OPT and LS-DYNA.* Detroit, MI: Livermore Software Technology Corporation, 2008.
63. Cook, R., C. A. Teubert, and G. Hayhoe. *Soft Ground Arrestor Design Program.* Washington, D.C.: Federal Aviation Administration, 1995.

APPENDIX A

# Bibliography

## A.1. Accidents and Incidents

David, R. E. *Location of Commercial Aircraft Accidents/Incidents Relative to Runways.* Washington, D.C.: Federal Aviation Administration, 1990. DOT/FAA/AOV 90-1.

Hall, J., M. Ayres, Jr., D. Wong, A. Appleyard, M. Eddowes, H. Shirazi, R. Speir, D. Pitfield, R. Caves, O. Selezneva, and T. Puzin. *ACRP Report 3: Analysis of Aircraft Overruns and Undershoots for Runway Safety Areas.* Washington, D.C.: TRB, National Research Council, 2008.

NTSB. *Hard Landing, Gear Collapse Federal Express Flight 647 Boeing Md-10-10f, N364fe Memphis, Tennessee, December 18, 2003:* National Transportation Safety Board, 2003.

## A.2. Aircraft

Boeing. *737 Airplane Characteristics for Airport Planning.* Renton, WA: The Boeing Company, 2005.

Boeing. *Minimizing the Impact of Runway Arresting Systems on Commercial Airplane Operations.,* ed. Brad Bachtel: Renton, WA: The Boeing Company.

Bruhn, E. F. *Analysis and Design of Flight Vehicle Structures.* ed. R. J. H. Bollard, L. E. Hackman, G. Lianis, W. F. McCombs, A. F. Schmitt, C. R. Smith, and J. A. Wolf: S. R. Jacobs & Associates, Inc., 1973.

Spieck, M. *Simulation of Aircraft Landing Impact Under Consideration of Aerodynamic Forces on the Flexible Structure.* Paper presented at the 10th AIAA/ISSMO Multidisciplinary Analysis and Optimization Conference, Albany, New York 2004.

## A.3. Arrestors

Cook, R. F. *Soft-Ground Aircraft Arresting Systems, Final Report.* Washington, D.C.: Federal Aviation Administration, 1987. FAA/PM-87-27.

Cook, R. F. *Evaluation of a Foam Arrestor Bed for Aircraft Safety Overrun Areas.* Dayton: University of Dayton Research Institute, 1988. UDR-TR-88-07.

Heymsfield, E., W. M. Hale. and T. L. Halsey. *A Parametric Sensitivity Analysis of Soft Ground Arrestor Systems.* 2007.

Rogers, C. *Aggregate for Truck Arrestor Beds.* Downsview, Ontario: Ministry of Transportation of Ontario, 2006. ISBN 1424959152.

San Filippo, W. K. and H. DeLong. *Engineered Materials Arresting System (EMAS): An Alternative Solution to Runway Overruns.* 2004, ASCE/Air Transport.

White, J. C. and S. K. Agrawal. *Soft Ground Arresting System for Airports, Final Report.* Washington, D.C.: Federal Aviation Administration, 1993. CT-93-80.

## A.4. FAA Documents

*Aircraft Arresting Systems on Civil Airports.* Washington, D.C.: Federal Aviation Administration, 2006. AC 150/5220-9a.

*Engineered Materials Arresting Systems (EMAS) for Aircraft Overruns.* Washington, D.C.: Federal Aviation Administration, 2005. AC 150-5220-22a.

*Financial Feasibility and Equivalency of Runway Safety Area Improvements and Engineered Material Arresting Systems.* Washington, D.C.: Federal Aviation Administration, 2004. Order 5200.9.

*Runway Safety Area Program.* Washington, D.C.: Federal Aviation Administration, 1999. Order 5200.8.

*Certification and Operations: Land Airports Serving Certain Air Carriers:* Washington, D.C.: Federal Aviation Administration, 1996. CFR 14 Part 139.

*Objects Affecting Navigable Airspace:* Washington, D.C.: Federal Aviation Administration, 1993. CFR 14 Part 77.

*Airport Design:* Washington, D.C.: Federal Aviation Administration, 1989. AC 150/5300-13.

*Introduction to Safety Management Systems (SMS) for Airport Operators.* Washington, D.C.: Federal Aviation Administration, 2007. AC 150/5200-37.

*Runway Safety Area Status Database.* Washington, D.C.: Federal Aviation Administration, 2007.

## A.5. Human Injury

DeWeese, R. L. and D. M. Moorcraft. *Evaluation of a Head Injury Criteria Component Test Device.* Washington, D.C.: Office of Aerospace Medicine, 2004. DOT/FAA/AM-04/18.

Hendler, E. Linear Acceleration as a Survivable Hazard in Aviation. 27(6), December 1956, *J. Aviat. Med.,* pp. 495–501.

Latham, F. Linear Deceleration Studies and Human Tolerance. 17(1), Feb 1958, *Clin Sci* (Lond), pp. 121–35.

Lewis, S. T. and J. P. Stapp. Human Tolerance to Aircraft Seat Belt Restraint. 29(3), March 1958, *J. Aviat. Med.,* pp. 187–96.

Moseley, H. G. and A. F. Zeller. Relation of Injury to Forces and Direction of Deceleration in Aircraft Accidents. 2(10), Oct 1958, *J. Aviat. Med.,* pp. 739–49.

Preston-Thomas, H. et al. Human Tolerance to Multistage Rocket Acceleration Curves. 26(5), October 1955, *J. Aviat. Med.,* pp. 390–98.

Stapp, J. P. Human Tolerance to Deceleration. 93(4), April 1957, *American Journal of Surgery,* pp. 734–40.

Stapp, J. P. Human Tolerance to Deceleration: Summary of 166 Runs. 22(1), February 1951, *J. Aviat. Med.,* pp. 42–5.

Stapp, J. P. Effects of Mechanical Force on Living Tissue. 26(4), August 1955, *J. Aviat. Med.,* pp. 268–88.

Zuidema, G. D. et al. Human Tolerance to Prolonged Acceleration. 27(6), December 1956, *J. Aviat. Med.,* pp. 469–481.

Zuidema, G. D. et al. Human Tolerance to Prolonged Acceleration. 27(6), December 1956, *J. Aviat. Med.,* pp. 469–481.

## A.6. Landing Gear

Batill, S. M., and J. M. Bacarro. *Modeling and Identification of Nonlinear Dynamic Systems With Application to Aircraft Landing Gear.* AIAA (1988).

Chester, D. H. Aircraft Landing Impact Parametric Study With Emphasis on Nose Gear Landing Conditions. *Journal of Aircraft* 39, no. 3 (2002): 394–403.

Collins, R. L. Theories on the Mechanics of Tires and Their Applications to Shimmy Analysis. *Journal of Aircraft* 8, no. 4 (1971): 271–277.

Currey, N. S. *Aircraft Landing Gear Design: Principles and Practice* AIAA Education Series. ed. J. S. Przemieniecki: American Institute of Aeronautics and Astronautics, 1988.

Holzapfel, F., R. Leitner and G. Sachs. *High Fidelity Landing Gear Modeling for Real-Time Simulation.* Paper presented at the AIAA Modeling and Simulation Technologies Conference and Exhibit, Keystone, Colorado 2006.

Kilner, J. R. Pneumatic Tire Model for Aircraft Simulation. *Journal of Aircraft* 19, no. 10 (1982): 851–857.

Lee, C. R., J.-W. Kim, J. O. Hallquist, Y. Zhang, and A. D. Farahani. *Validation of a FEA Tire Model for Vehicle Dynamic Analysis and Full Vehicle Real Time Proving Ground Simulations.* SAE Paper Number 971100 (2005).

Pacejka, H. B. *Tire and Vehicle Dynamics.* 2nd ed.: Society of Automotive Engineers, 2006.

Pritchard, J. Overview of Landing Gear Dynamics. *Journal of Aircraft* 38, no. 1 (2001): 130–37.

Wahi, M. K. *Oleopneumatic Shock Strut Dynamic Analysis and Its Real-Time Simulation.* Journal of Aircraft 13, no. 4 (1976): 303–8.

Wong, J. Y. *Theory of Ground Vehicles.* 3rd ed. New York, NY: John Wiley and Sons, Inc., 2001.

York, B. W. and O. Alaverdi. *A Physically Representative Aircraft Landing Gear Model for Real-Time Simulation A96-35001 09-01.* Paper presented at the AIAA Flight Simulation Technologies Conference, San Diego, CA 1996.

## A.7. Material Science

Stehly, R. D. *Report of Concrete Testing, Project: Engineered Material Arresting System Minneapolis/St. Paul Airport.:* American Engineering Testing, Inc., 2007, 05-03306.

Stouffer, S. *A Study of the Pressure and Moisture in the ESCO Arrestor Bed at Minneapolis–St. Paul Airport on June 22, 2000; Interim Data Report.:* University of Dayton Research Institute, 2000.

## A.8. Modeling and Simulation

Bell, N., Y. Yu and P. J. Mucha. *Particle-Based Simulation of Granular Materials.* Paper presented at the Eurographics/ACM SIGGRAPH Symposium on Computer Animation, 2005.

Cook, R., C. A. Teubert, and G. Hayhoe. *Soft Ground Arrestor Design Program:* FAA, U.S. Department of Transportation, 1995.

Dole, G. R., Jr. A Review of Computer Simulations for Aircraft-Surface Dynamics. *Journal of Aircraft* 23, no. 4 (1986): 257–265.

Nezami, E. G., Y. M. A. Hashash, D. Zhao, and J. Ghaboussi. *Simulation of Front End Loader Bucket–soil Interaction Using Discrete Element Method.* International Journal for Numerical and Analytical Methods in Geomechanics, no. 31 (2007): 1147–62.

Pi, W. S. Dynamic Tire/soil Contact Surface Interaction Model for Aircraft Ground Operations. *Journal of Aircraft* 25, no. 11 (1987): 1038–44.

## A.9. Patents

Allen, G., R. D. Angley, J. L. Gordon, P. T. Mahal, and S. C. Valentini. Jet Blast Resistant Vehicle Arresting Blocks, Beds and Methods. United States Patent 6,971,817, 2005.

Angley, R. D., M. S. Ciesielski, C. T. Dial, P. T. Mahal, and R. F. Cook. Vehicle Arresting Bed Systems. United States Patent 6,726,400, 2004.

Angley, R. D., M. S. Ciesielski, C. T. Dial, P. T. Mahal, and R. F. Cook. Arresting Material Test Apparatus and Methods. United States Patent 5,789,681, 1998.

Cobb, L. C. and T. J. Hirsch. Roadway Barrier. United States Patent 5,054,954, 1991.

Larratt, D. R. et al., Aircraft Arresting System, United States Patent 5,193,764, 1993.

Ogden, D. H. Vehicle Deceleration Means, United States Patent 3,967,704, 1976.

Rastegar, J. S. and J. Qiaode. Roadway for Decelerating and/or Accelerating a Vehicle Including an Aircraft. United States Patent 6,969,213, 2005.

Schirtzinger, J. F. Method and Means for Decelerating Aircraft on Runways. United States Patent 3,066,896, 1962.

APPENDIX B

# Survey Details

## B.1. Survey of U.S. Airport Operators

A copy of the survey submitted to the sixteen airports that participated in the Survey of U.S. Airport Operators, discussed in Chapter 3, is provided in this section. Furthermore, the responses of the airports are given in summary form. In some cases, the fields from the surveys contained sparse or unusable information. In other cases, fields included lengthy verbal commentary that could not be included in the tabular form. In both cases, such fields were not included in the tables summarizing the response of the airports. Cost information was omitted.

### B.1.1. Copy of Survey

Given in pages following.

# Airport Information

1. Facility name _____ 2. Location ID _____

3. Facility Address (City, State, Zip) _____

4. ARFF Index ☐ A ☐ B ☐ C ☐ D ☐ E

5. Number of annual operations _____

6. Approach ☐ Precision ☐ Non-precision

7. Navaids (ILS) ☐ CAT I ☐ CAT II and above

# Point of Contact Information

## *Point of Contact 1*

1. Name: _____
2. Telephone: _____
3. Email: _____
4. What is your position/job title? _____

5. List the areas of airport management you are involved with: ☐ Maintenance ☐ Airport operations ☐ Engineering ☐ General Management

6. How long have you worked in this position? _____ (yr) _____ (mo)

7. How long have you worked in this industry? _____ (yr) _____ (mo)

## *Point of Contact 2*

1. Name: _____
2. Telephone: _____
3. Email: _____
4. What is your position/job title? _____

5. List the areas of airport management you are involved with: ☐ Maintenance ☐ Airport operations ☐ Engineering ☐ General Management

6. How long have you worked in this position? (yr) (mo) _____

7. How long have you worked in this industry? (yr) (mo) _____

### *Point of Contact 3*

1. Name: _____
2. Telephone: _____
3. Email: _____
4. What is your position/job title? _____

5. List the areas of airport management you are involved with: ☐ Maintenance ☐ Airport operations ☐ Engineering ☐ General Management

6. How long have you worked in this position? (yr) (mo) _____

7. How long have you worked in this industry? (yr) (mo) _____

## Facility Questions

1. Is the airport land-locked by bodies of water, drop offs, highways, railroads, or buildings, which would prevent extension of the runway safety areas to satisfy FAA RSA requirements? ☐ Yes ☐ No

2. If yes to previous, how many runways ends are affected? _____

3. Does the airport have declared distances? ☐ Yes ☐ No

4. If yes to previous, which runways? _____

# Questions for Facilities with EMAS Arrestors

## *General*

1. How many EMAS arrestors are at the facility? _____

2. What are the EMAS arrestors dimensions and performance levels?

| | Runway Designation | Set Back from Runway End (ft) | Bed Dimensions (ft) | Aircraft Exit Speed |
|---|---|---|---|---|
| EMAS Arrestor 1 | | | Length:<br>Width: | ☐ 70 knots (standard)<br>☐ Less than 70 knots |
| EMAS Arrestor 2 | | | Length:<br>Width: | ☐ 70 knots (standard)<br>☐ Less than 70 knots |
| EMAS Arrestor 3 | | | Length:<br>Width: | ☐ 70 knots (standard)<br>☐ Less than 70 knots |

3. What is it about this facility that makes EMAS necessary? _____

4. Were alternatives to the EMAS arrestor considered? ☐ Yes ☐ No
(Declared Distances, shortening runways, etc)

5. If yes to previous, why was the EMAS approach chosen? _____

6. What are the negative traits of the EMAS arrestor? _____

7. What are the positive aspects of the EMAS arrestor? _____

8. If there were one thing that could be changed about the EMAS arrestor, what would it be?
_____

### *Installation*

1. What was the time and cost associated with installing each of the EMAS arrestors at your facility? (estimates are sufficient)

| | Year Installed | Per Runway End Cost ($M) | Preparatory Paving Cost ($M) | Time to Install (days) |
|---|---|---|---|---|
| EMAS Arrestor 1 | | $0.00 | $0.00 | |
| EMAS Arrestor 2 | | $0.00 | $0.00 | |
| EMAS Arrestor 3 | | $0.00 | $0.00 | |

2. Were there any special installation conditions (night-only, limited hours per day, etc)? _____

3. Installation inconvenience:

| ☐ 1 | ☐ 2 | ☐ 3 | ☐ 4 | ☐ 5 |
|---|---|---|---|---|
| (None) | | | | (Severe) |

### *Maintenance & Repair*

Which of the following maintenance issues have the EMAS arrestors experienced and to what degree?

1. Peeling paint

| ☐ 1 | ☐ 2 | ☐ 3 | ☐ 4 | ☐ 5 |
|---|---|---|---|---|
| (None) | | | | (Severe) |

2. Leaching of the material (chalky white)

| ☐ 1 | ☐ 2 | ☐ 3 | ☐ 4 | ☐ 5 |
|---|---|---|---|---|
| (None) | | | | (Severe) |

3. Caulking failure

| ☐ 1 | ☐ 2 | ☐ 3 | ☐ 4 | ☐ 5 |
|---|---|---|---|---|
| (None) | | | | (Severe) |

4. Joint tape debonding

| ☐ 1 | ☐ 2 | ☐ 3 | ☐ 4 | ☐ 5 |
|---|---|---|---|---|
| (None) | | | | (Severe) |

5. Soft tops

| ☐ 1 | ☐ 2 | ☐ 3 | ☐ 4 | ☐ 5 |
|---|---|---|---|---|
| (None) | | | | (Severe) |

6. Drainage problems

☐ 1 (None) ☐ 2 ☐ 3 ☐ 4 ☐ 5 (Severe)

7. Has your facility undertaken substantial repairs beyond scheduled maintenance?

☐ Replacement of blocks ☐ Substantial joint re-sealing/replacement
☐ Substantial repainting ☐ Other ☐ None

8. If yes to previous, have the repairs conducted been due to a deficiency in scheduled/expected maintenance? ☐ Yes ☐ No

9. Has the EMAS arrestor been out of service (NOTAM) due to damage from an overrun by aircraft or ground vehicle? ☐ Yes ☐ No

10. If yes to previous, how long did it take to repair the EMAS arrestor to service condition? _____ (mos)

11. What type of maintenance agreement/approach is the facility using for the EMAS arrestor?
☐ Maintenance contract with ESCO
☐ Use of local contractors
☐ Use of facility maintenance personnel

12. What do you estimate is the annual maintenance and repair cost for the EMAS arrestor (including maintenance agreement, if applicable)? _____ $0.00

### *Performance*

1. Perception: do you believe your current EMAS arrestor will likely perform to original specifications if it arrested an aircraft today? ☐ Yes ☐ No ☐ No Opinion

2. What aircraft type and speed is the EMAS arrestor system designed to arrest?

| | |
|---|---|
| Aircraft 1 | Speed (knots) |
| Aircraft 2 | Speed (knots) |
| Aircraft 3 | Speed (knots) |
| Aircraft 4 | Speed (knots) |

## Questions for Facilities without EMAS Arrestors

1. Do all of your runways meet the FAA's RSA requirements (e.g., nominal 1000' length and 500' width)? ☐ Yes ☐ No

2. Is your facility planning to install an EMAS arrestor in the future? ☐ Yes ☐ No
   If yes, how soon? _____ (mo) How many? _____ (qty)

3. Is the cost of an EMAS arrestor ($2M to $5M per runway end) too high for your facility to reasonably afford to install arrestors? ☐ Yes ☐ No ☐ N/A

4. What factors have prevented your facility from installing an EMAS arrestor?
   ☐ Cost ☐ Maintenance ☐ Other construction projects ☐ Lack of need ☐ Other

## Questions for All Facilities

1. How would you rate the need of your facility for an arrestor system: ☐ Low ☐ Moderate ☐ High
2. Has your facility experienced overruns in the past 5 years?

   Low risk, slight overrun QTY: _____

   High risk, substantial overrun QTY: _____

3. If a new system could be developed for the future, would lower cost or better stopping performance be more important to your facility?
   ☐ Lower Cost ☐ Improved Performance ☐ Both
   ☐ Neither would matter

4. Does your facility use active arrestor systems for military aircraft? ☐ Yes ☐ No
5. Would you feel comfortable with a net-based or cable-based arrestor system for civil aircraft?
   ☐ Not Comfortable ☐ Low ☐ Moderate ☐ Highly Comfortable

6. If yes to question 4, what comments do you have regarding: Cost, Performance, Reliability, and Maintenance? _____

7. Do you consider the FAA requirements for airports regarding RSA dimensions too rigid? ☐ Yes ☐ No ☐ No Opinion

8. Do you consider the FAA requirements for airports regarding arrestor bed performance too rigid? ☐ Yes ☐ No ☐ No Opinion

9. If yes to previous, what changes should be made to existing requirements? _____

10. Do you have any other comments? _____

**Table B-1. Selected data from survey of U.S. airport operators.**

| Airport Name | Location ID | City | ARFF Index | Annual Operations | Precision | Non-precision |
|---|---|---|---|---|---|---|
| **Anchorage International** | ANC | Anchorage, AK | E | 289,472 | Yes | Yes |
| **Baton Rouge Metropolitan** | BTR | Baton Rouge, LA | C | 94,852 | Yes | No |
| **Boston Logan International** | BOS | East Boston, MA | E | 409,066 | No | No |
| **Denver International** | DEN | Denver, CO | E | 586,151 | Yes | No |
| **Minneapolis–St. Paul International** | MSP | Minneapolis, MN | E | 475,000 | Yes | No |
| **Nashville International** | BNA | Nashville, TN | C | 215,830 | Yes | No |
| **New York Kennedy International** | JFK | New York, NY | E | 411,145 | Yes | No |
| **New York La Guardia Airport** | LGA | New York, NY | D | 404,990 | Yes | No |
| **Pittsburgh International** | PIT | Pittsburgh, PA | D | 237,696 | Yes | No |
| **Roanoke Regional** | ROA | Roanoke, VA | B | 86,091 | Yes | Yes |
| **San Diego International** | SAN | San Diego, CA | D | 220,485 | Yes | Yes |
| **Seattle Tacoma International** | SEA | Seattle, WA | E | 340,058 | Yes | No |
| **Teterboro** | TEB | Teterboro, NJ | E | 250,000 | Yes | No |
| **Washington National** | DCA | Washington, D.C. | C | 278,151 | Yes | No |

*(continued on next page)*

**Table B-1. (Continued).**

| Airport Name | CAT I only | CAT II and above | Land-locked runways | No. land-locked runway ends | Declared distances | Runways with declared distances |
|---|---|---|---|---|---|---|
| **Anchorage International** | Yes | Yes | No | 0 | No | |
| **Baton Rouge Metropolitan** | Yes | No | Yes | 4 | Yes | 4L-22R, 4R-22L, 13-31 |
| **Boston Logan International** | No | No | Yes | 5 | No | |
| **Denver International** | Yes | Yes | No | 0 | Yes | 8, 34R, 25 |
| **Minneapolis–St. Paul International** | No | Yes | Yes | 8 | Yes | 12L |
| **Nashville International** | Yes | No | Yes | 2 | Yes | 1331 |
| **New York Kennedy International** | Yes | Yes | Yes | 3 | No | |
| **New York La Guardia Airport** | Yes | No | Yes | 2 | No | |
| **Pittsburgh International** | No | Yes | Yes | 1 | Yes | 28R |
| **Roanoke Regional** | Yes | No | Yes | 3 | Yes | 24 |
| **San Diego International** | Yes | No | Yes | 2 | Yes | 9, 27 |
| **Seattle Tacoma International** | No | Yes | No | 0 | Yes | All |
| **Teterboro** | Yes | No | Yes | 2 | No | |
| **Washington National** | Yes | No | Yes | 4 | No | |

*(continued)*

**Table B-1. (Continued).**

| Airport Name | No. EMAS Arrestors | EMAS 1 R/W Designation | EMAS 1 Set Back [ft] | EMAS 1 Length [ft] | EMAS 1 Width [ft] | EMAS 1 Standard 70 knots |
|---|---|---|---|---|---|---|
| **Anchorage International** | 0 | | | | | |
| **Baton Rouge Metropolitan** | 1 | 31 | 75 | 300 | 150 | Yes |
| **Boston Logan International** | 2 | 4L | 5 | 190 | 170 | No |
| **Denver International** | 0 | | | | | |
| **Minneapolis–St. Paul International** | 1 | 12R | 630 | 160 | 216 | Yes |
| **Nashville International** | 0 | | | | | |
| **New York Kennedy International** | 2 | 4R | 35 | 392 | 200 | No |
| **New York La Guardia Airport** | 2 | 22 | 35 | 275 | 170 | No |
| **Pittsburgh International** | 0 | | | | | |
| **Roanoke Regional** | 1 | 33 | 300 | 299 | 169 | Yes |
| **San Diego International** | 1 | 27 | 65 | 315 | 218 | No |
| **Seattle Tacoma International** | 0 | | | | | |
| **Teterboro** | 1 | 24 | 35 | 251 | 170 | No |
| **Washington National** | 0 | | | | | |

*(continued on next page)*

**Table B-1. Selected data from survey of U.S. airport operators.**

| Airport Name | EMAS 2 R/W Designation | EMAS 2 Setback [ft] | EMAS 2 Length [ft] | EMAS 2 Width [ft] | EMAS 2 Standard 70 knots? |
|---|---|---|---|---|---|
| **Anchorage International** | | | | | |
| **Baton Rouge Metropolitan** | | | | | |
| **Boston Logan International** | 15R | 15 | 158 | 170 | No |
| **Denver International** | | | | | |
| **Minneapolis–St. Paul International** | | | | | |
| **Nashville International** | | | | | |
| **New York Kennedy International** | 22L | 35 | 405 | 227 | Yes |
| **New York La Guardia Airport** | 13 | 41 | 327 | 170 | No |
| **Pittsburgh International** | | | | | |
| **Roanoke Regional** | | | | | |
| **San Diego International** | | | | | |
| **Seattle Tacoma International** | | | | | |
| **Teterboro** | | | | | |
| **Washington National** | | | | | |

*(continued)*

## B.2. Other Aviation Organizations

The names of aviation organizations, number of individuals contacted from each, and their survey status are shown in Table B-2. The comments of respondents were discussed in Section 3.8.2.

**Table B-2. Aviation organizations.**

| Organization | No. people contacted | Survey returned |
|---|---|---|
| **A.A.A.E.** | 2 | No |
| **South Central A.A.A.E.** | 1 | No |
| **I.C.A.O.** | 3 | Yes |
| **A.C.I.** | 1 | No |
| **A.L.P.A.** | 2 | No |
| **A.O.P.A.** | 1 | No |
| **Flight Safety Foundation** | 2 | Yes |
| **Flag Air Carriers/Delta** | 1 | No |
| **U.S. Airways** | 3 | No |
| **Southwest Airlines** | 1 | No |
| **United Airlines** | 2 | No |
| **F.A.A./F.S.D.O.** | 3 | No |
| **Aviation consultant** | 1 | Yes |

APPENDIX C

# EMAS Calculations

Appendix C provides the technical details of calculations supporting the EMAS sensitivity analysis discussed in Chapter 5.

## C.1. Data

The data for the EMAS performance calculations were obtained from the manufacturer. Specifically, the manufacturer conducted three simulations of an arrest using in-house software. The three cases were distinguished by the type of aircraft used. The three types of aircraft were a CRJ 200 ER, B737-800, and B747-400. For all cases, the exit speed was 70 knots; the compressive strength of the material was 60 psi; the setback was 35 ft; there was no reverse thrust; and there was a braking friction coefficient of 0.25. Given these initial conditions, the length of the bed was minimized. Plots of aircraft speed with respect to nose-gear travel were provided.

## C.2. Calculations

### C.2.1. Performance of an EMAS

In order to characterize the performance of aircraft within the EMAS bed, for each given design case, a total of 10 to 15 data points were extracted from the manufacturer plots once the aircraft had entered the bed. That is, the initial point in the plots was the point at which the aircraft entered the bed.

These extracted data points were plotted discretely and a polynomial trend line was fitted to the discrete data. The polynomial trend line was then used to generate points of aircraft speed and aircraft travel in the bed for an arbitrary aircraft travel step. Elementary kinematic relations were applied over each travel step to obtain deceleration of the aircraft. The data with a trend line and extracted deceleration profile for the B737-800 are shown in Figure C-1 (a) and (b) respectively.

Deceleration due to braking in the setback area and reverse thrust during the arrest were added to the deceleration due to the EMAS bed. Thus, it was possible to estimate the speed profile for any setback, braking coefficient of friction, and reverse thrust. Reverse thrust in such cases was simply taken as a lumped deceleration value. This value was varied to observe the sensitivity of the response and to determine the criticality of the assumed reverse thrust level. At 70 knots and lower, the reverse thrust contribution is generally minimal. Therefore, in all comparative calculations, the standard assumption of zero reverse thrust was used.

A plot of exit speed with respect to stopping distance was obtained from a plot of the absorbed energy. That is, the force applied to the aircraft by braking, reverse thrust, and EMAS bed engagement was obtained from the resultant deceleration profile of the aircraft and its MTOW. This profile was then numerically integrated to obtain the energy absorbed during the arrest. For every quantity of absorbed energy there was a corresponding stopping distance. The absorbed energy was set equal to the kinetic energy of the aircraft at its exit from the runway, as shown in Equation C-1. In order to extend the domain of exit speed to 80 knots, the steady-state portion of the absorbed energy curve was linearly extended to an absorbed energy corresponding with 80-knot exit speed. The resultant absorbed energy profile for the B737-800 is shown in Figure C-2. Figure C-3 shows stopping distance with respect to exit speed for the three design aircraft.

$$\frac{1}{2}mv^2 = \int_0^L F(x)\,dx \qquad \text{(Equation C-1)}$$

$m$ = mass of aircraft
$v$ = aircraft exit speed
$F(x)$ = instantaneous force applied to the aircraft as function of position
$L$ = distance required to arrest the aircraft

For a given bed width and setback, the cost of an EMAS was calculated as a function of stopping distance, or, put

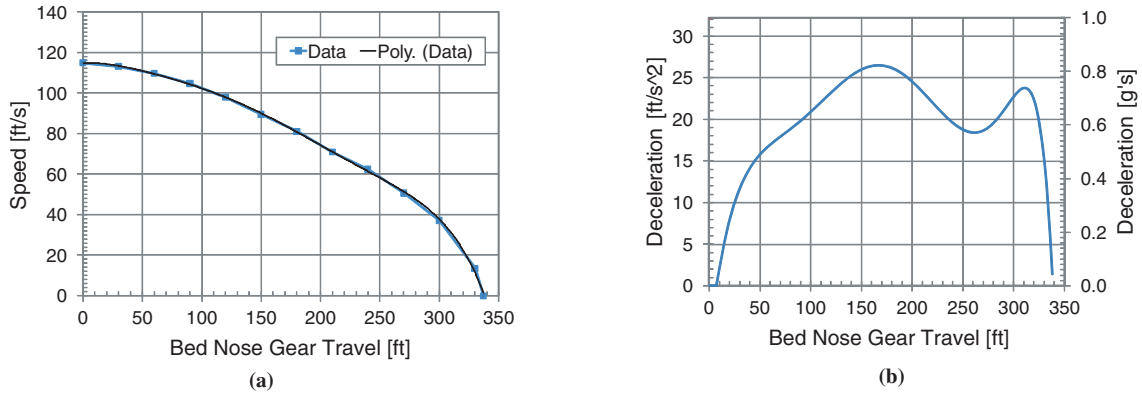


*Figure C-1. (a) Speed and (b) deceleration profile of B737-800 in EMAS bed.*

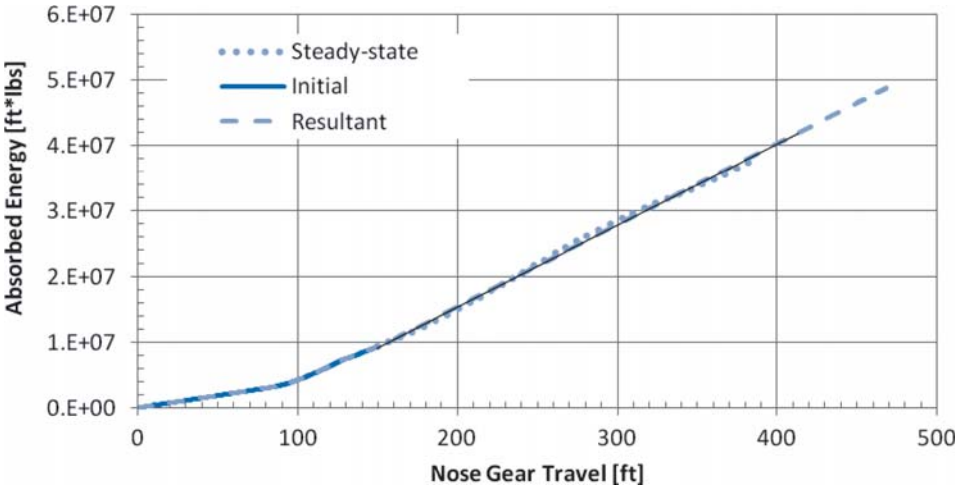


*Figure C-2. Energy vs. exit speed for B737-800.*

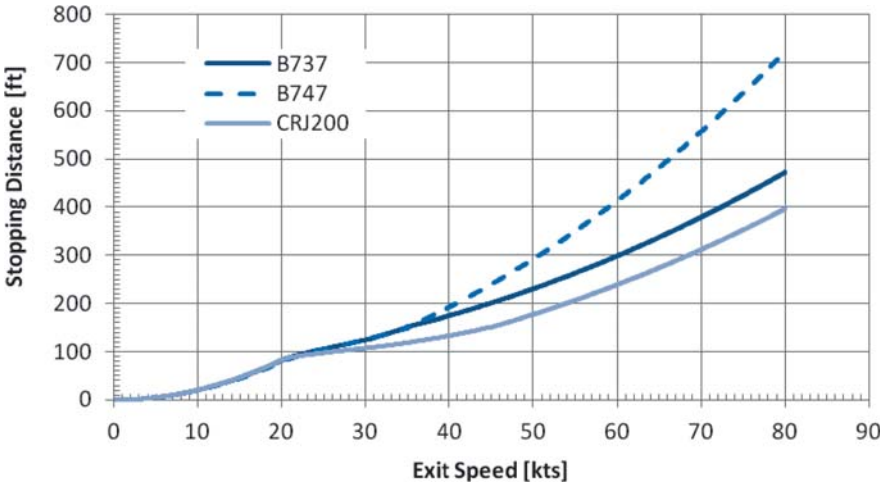


*Figure C-3. Stopping distance vs. exit speed for three aircraft.*

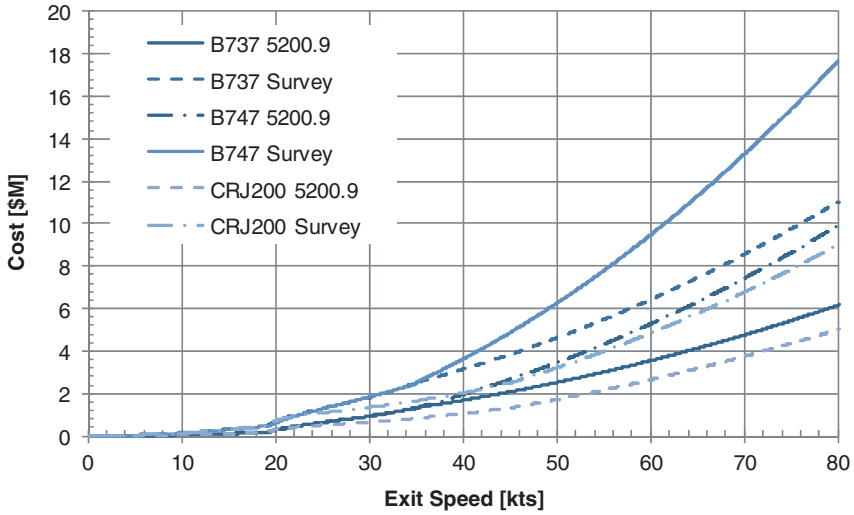


*Figure C-4. Cost vs. exit speed for three aircraft.*

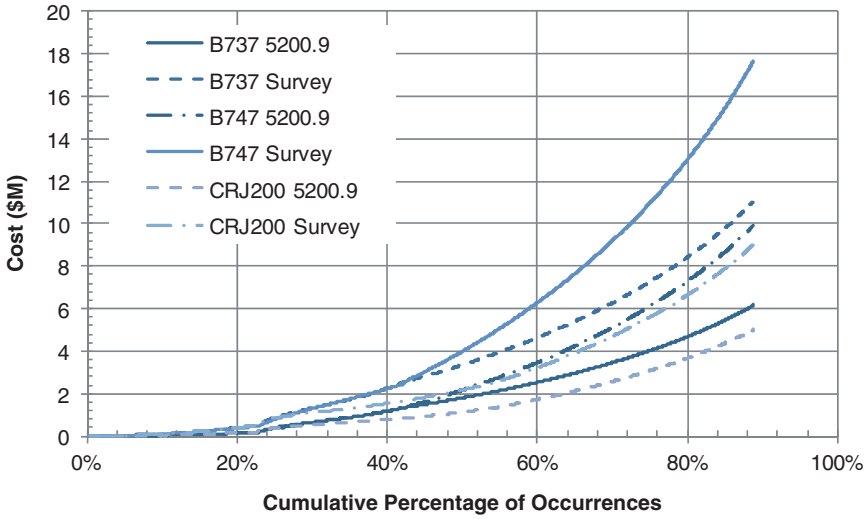


*Figure C-5. Cost vs. reliability for three aircraft using revised overrun probability curve.*

another way, minimum bed length. As discussed in Chapter 5, design cost numbers are reported in FAA Order 5200.9 (*29*) and were obtained as part of the Survey of U.S. Airport Operators (Chapter 3). Furthermore, as was also discussed in Section 4-4, DOT/FAA/CT-93/80 (*5*) and more recent ACRP research (*24*) provided data for relating exit speed to cumulative percentage of overrun occurrences. Therefore, for the three aircraft design cases, it was possible to generate several sets of curves where the paired parameters were either stopping distance, cost, exit speed, and reliability. The resulting curves are shown in Figure C-4 through Figure C-8.

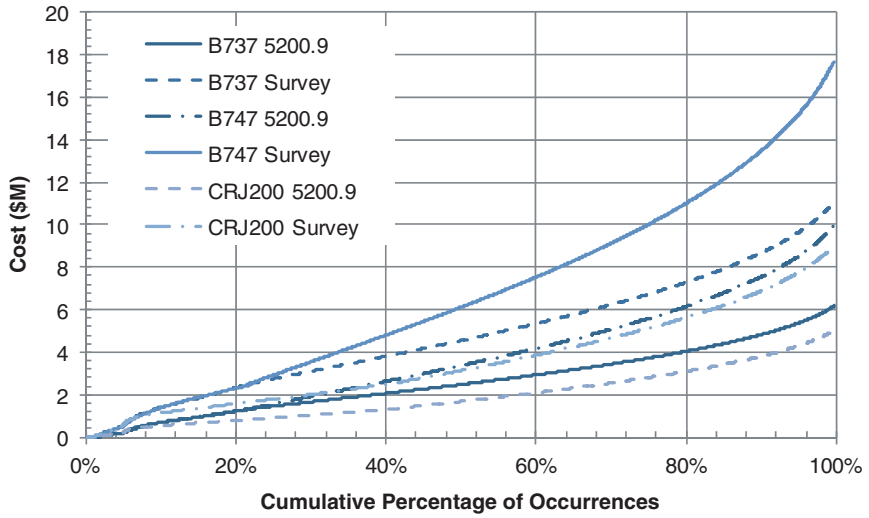


*Figure C-6. Cost vs. reliability for three aircraft using CT-93/80 overrun probability curve.*

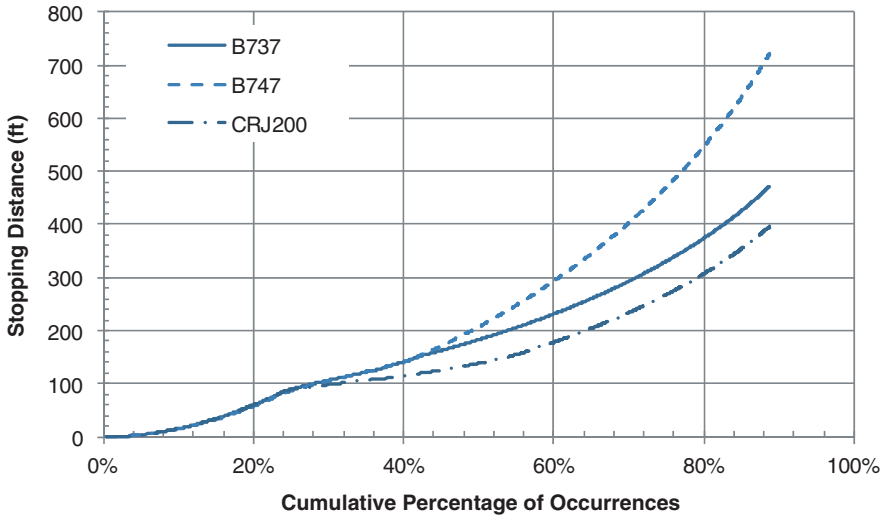


*Figure C-7. Stopping distance vs. reliability for three aircraft using revised overrun probability curve.*

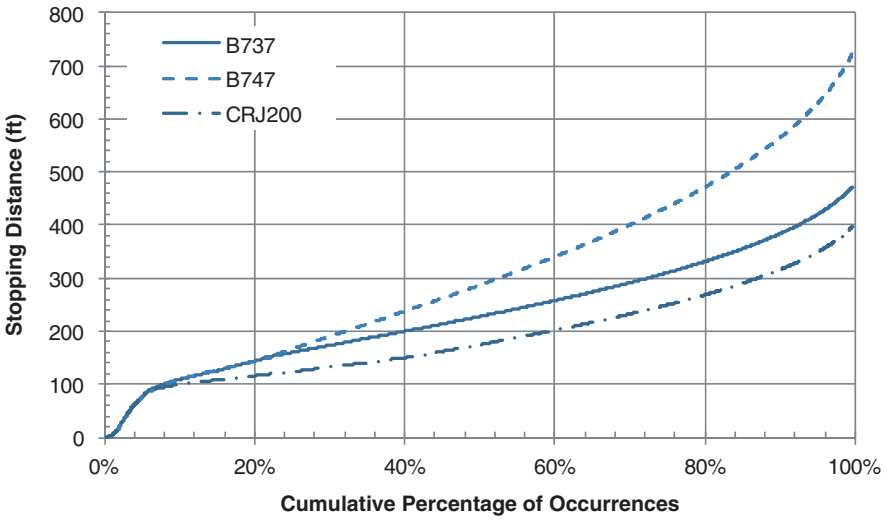


*Figure C-8. Stopping distance vs. reliability for three aircraft using CT-93/80 overrun probability curve.*

APPENDIX D

# Active Arrestor Calculations

This appendix supplies the technical details supporting the assessment of the cable-based arrestor in Section 7.7.

## D.1. Mechanical Parameters

The mechanical input parameters considered in the cable-based arrestor sensitivity analysis and associated output parameters are shown in Table D-1. The geometry parameters—distance between the brake units and slack in the cable—influenced the loading on the main landing gear by changing the angle θ. The limiting lateral and longitudinal loads were determined from FAR part 25 for a Boeing 737-800 (*44*).

## D.2. Dynamics

Figure D-1 shows a cable-based arrest in which the tension in the cable is $T_{c1}$. Figure D-2 is a detail of the main landing gear engaged by the cable with tension $T_{c1}$. The load in the cable between the main gear struts is $T_{c2}$. The lateral load on the landing gear strut is the transverse resultant of $T_{c1}$ and $T_{c2}$, and the transverse resultant depends on the coefficient of friction between the cable and the strut. As the distance from the arresting engines increases, the angle θ decreases. As θ decreases, the projection of $T_{c1}$ on the transverse axis decreases, causing more of the load from $T_{c2}$ to be resisted only by the strut.

## D.3. Calculation Methodology

The cable arresting simulations were performed using Microsoft Excel™, in a time-marching transient calculation.

After an assumed transient, linear increase in the tension of the arresting cable, the tension in the cable was determined by taking the equilibrium of one of the struts (Figure D-2). The longitudinal load on the strut was assumed to be the FAR 25 limiting load. The aircraft was stepped through the arrest length in 0.5-ft increments, and the tension in the cable was determined by equilibrium at each position. The tension in the cable decreased as the aircraft stepped through the arrest length because θ decreased with each arrest length increment. Equilibrium of the entire aircraft provided the deceleration of the aircraft at each step. That deceleration was used to determine the speed at each step. This iterative process was continued until the speed of the aircraft was zero.

This iterative process was performed for numerous cases of the inputs listed in Table D-1. Of particular interest was the effect of the coefficient of friction between the cable and the strut on the lateral load applied to the strut. The lateral load was determined using the equilibrium of the strut and the bearing friction equation.

## D.4. Interface Friction Study

A simulation was developed to determine whether, for a typical arrest case, the lateral load on the landing gear would reach a limiting value. Preliminary simulations showed that if the maximum tension in the cable were kept below a critical value, the lateral load on the landing gear remained below the limiting lateral load, implied by FAR part 25, regardless of the strut-cable coefficient of friction (*44*). This fact is illustrated in Figure D-3. For a braking coefficient of 0.25 and no reverse thrust, simulations were run for a B737-800 in which the strut-cable coefficient of friction was varied and the maximum lateral load on the landing gear was recorded. These maximum lateral loads were normalized by the limiting lateral load. As shown in Figure D-3, the maximum lateral load nearly reached 90% of the limiting lateral load for a strut-cable coefficient of friction of approximately 0.7. Therefore, on the basis of preliminary investigation, if the maximum tension in the cable is limited to the critical value, lateral collapse of the landing gear can be prevented.

## D.5. Load and Deceleration Histories

For a given set of input parameters, the speed and deceleration profiles for the aircraft were determined in the following way. A limiting deceleration of the aircraft was assumed.

**Table D-1. Cable-based arrestor sensitivity analysis parameters.**

| Input Parameters to Vary | Output Parameters from Models |
|---|---|
| Exit speed – arbitrary | Stopping distance |
| Geometry | Max lateral load |
| • Distance between brake units | Max longitudinal load |
| • Slack in cable | |
| Maximum tension in cable | |
| Strut-cable coefficient of friction | |
| Aircraft type – B737-800 | |
| • Limiting lateral load | |
| • Limiting longitudinal load | |
| Aircraft braking condition | |
| • Braking | |
| • Skidding | |
| • Free-rolling | |
| Reverse thrust – arbitrary | |

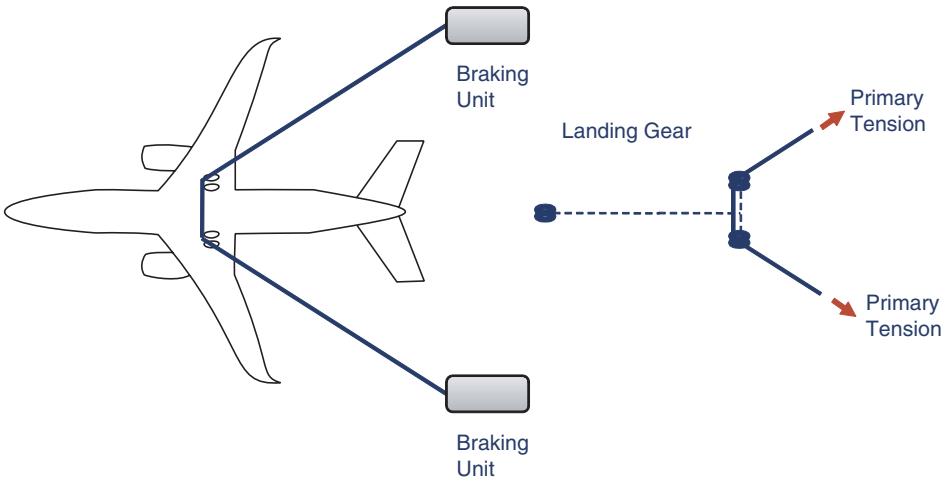


***Figure D-1. Cable-based arrest of aircraft with tension in cable $T_{c1}$.***

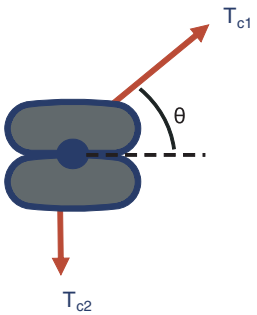


***Figure D-2. Detail of cable and lateral loads on main gear strut.***

Two sources of limiting deceleration were the commonly assumed 1-g deceleration to prevent occupant injury and the limiting longitudinal load on the main gear, caused by both the engaged cable and braking. Preliminary investigation revealed that the limiting longitudinal load controlled. Once a limiting deceleration was inferred, dynamic equilibrium was imposed on the aircraft, and the tension in the cable was determined. A reasonable limit was then imposed on the maximum tension in the cable. Linear interpolation from a tension of zero at the runway exit point to the point of maximum tension was used to generate a resultant tension in the cable. The resultant curve for tension in the cable is shown in Figure D-4 (a). All forces in the plots were normalized by

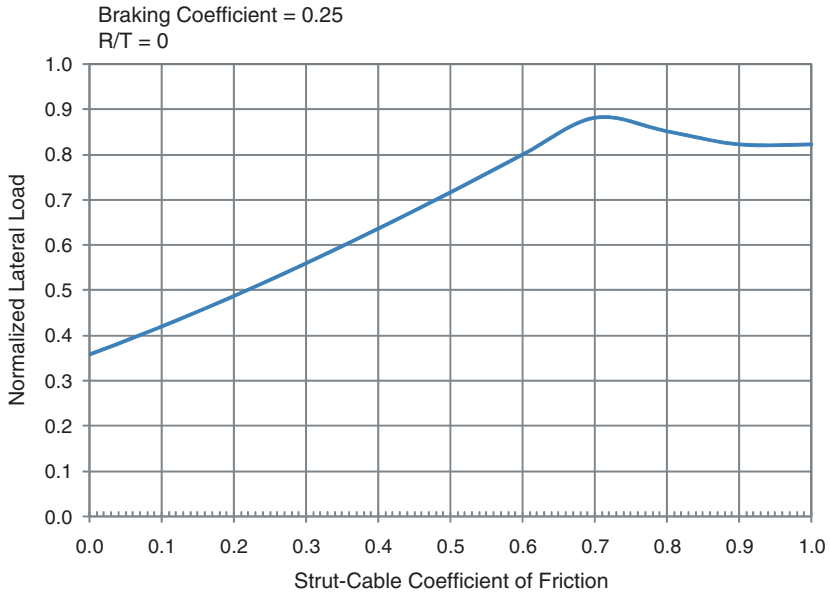


***Figure D-3. Dependence of lateral load on strut-cable coefficient of friction.***

the MTOW of the aircraft. Thus, the primary vertical axis is labeled "Force Ratio."

Figure D-4 (b) shows the normalized forces of $T_{c2}$, the tension in the cable between the main gear landing struts as illustrated in Figure D-2, and the lateral and longitudinal loading on the main gear. $T_{c2}$ was obtained from $T_{c1}$ using the bearing friction equation. The lateral and longitudinal loads were obtained by taking the equilibrium of the strut. The force ratios shown in Figure D-4 (b) were obtained using a strut-cable coefficient of friction of 0.40 to illustrate force ratio trends. Furthermore, the braking coefficient was 0.25 with no reverse thrust.

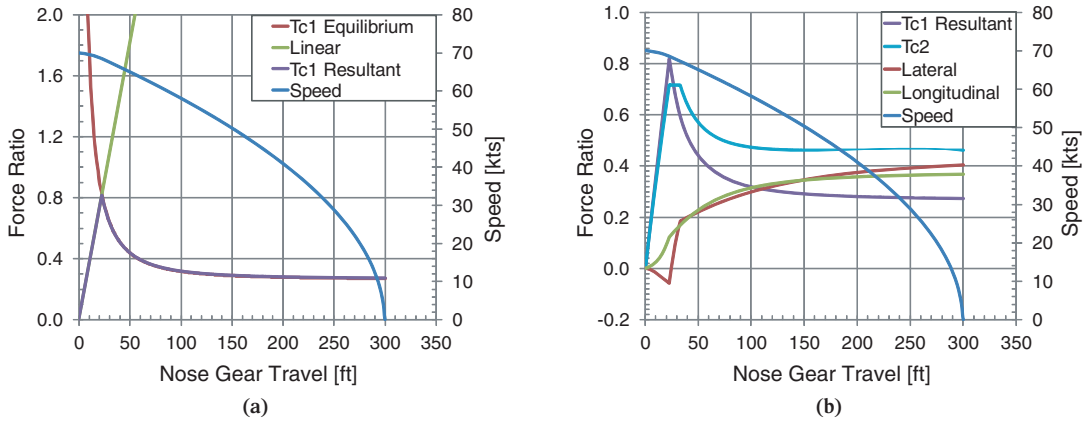


***Figure D-4. (a) Resultant tension $T_{c1}$ in the cable (b) lateral and longitudinal loads.***

APPENDIX E

# Human Injury Study

A previous study (*31*) investigating the effectiveness of arresting systems for civil aircraft suggested a deceleration limit of 1 g for this type of analysis but provided no reference for this design requirement. To establish a design requirement for the airplane with a medical basis, literature from the development of ejection seats, high-g maneuvers, and airplane crash reconstructions were reviewed. From this review, human injuries were related to the deceleration of the fixture volunteers were riding. This appendix is a summary of the literature review. It provides insight into the human tolerance to deceleration for a wide range of durations and suggests deceleration limits for the evaluation of arrestor systems.

## E.1. Range of Human Tolerance to Deceleration

To obtain an evaluation criterion based on human tolerance levels, reports from ejection seat tests, airplane deceleration tests, and aeronautical accident reconstructions were reviewed. The range of decelerations reviewed was from 2 g to 220 g, with durations from 0.002 seconds up to 115 seconds. This encompasses the range of decelerations within which aircraft arrestor systems will most likely stop an airplane. From the literature reviewed, this deceleration range has been broken down, based on the duration of the deceleration pulse, into three broad categories as shown in Table E-1: (1) less than 0.2 seconds, (2) 0.2 to 3 seconds and (3) greater than 3 seconds (*45*). Each category is also graphically represented in Figure E-1 to illustrate the trends in the data. The following sections describe in more detail the types of injuries observed within each category.

### E.1.1. Deceleration Durations Less Than 0.2 Seconds

For decelerations less than 0.2 seconds (200 ms) in duration (Figure E-1 – Region 1) and when the body is sufficiently restrained (i.e., the body does not come in contact with any objects inside the cabin), the risk of injuries has been attributed to the rapid displacement of body fluids. The rate of displacement, and therefore the human tolerance to the deceleration forces, is primarily determined by the rate of application of force acting on the fluids. The rate of application of force is the third derivative of motion, called "Jerk," with the units of g-per-second (g/sec). The literature documents that, in this category, the point of reversible incapacitation is 38 g when the rate of application is 1350 g/sec and increases to 50 g when the rate of application is reduced to 500 g/sec or less (*46*). Reversible incapacitation is defined as momentary lack of awareness of an individual that can limit their ability to extricate themselves from the airplane if necessary. These symptoms can range from disorientation to blackout and last for just a few seconds to several days. The lower bound for these effects begins within the human body at 10 g (*45*).

In addition to the displacement of body fluids, injuries can be also induced by the interaction of the body with the restraining device or the motion of unrestrained body regions such as the head and limbs. These injuries are similar to those observed in automotive crashes. These injuries include bruising (*46, 47*), muscle strains, muscle tears, concussions (mild traumatic brain injuries) (*45*), and fractures when the body impacts the seatbelt with force (*48*) or strikes an object inside the cabin. In an exercise examining the injury threshold for the occurrence of traumatic brain injuries (TBI) based on idealized deceleration curves, the results suggested that injuries to the brain can be induced by deceleration starting at 10 g for impact durations of 0.2 sec. These findings are based on the response of the average male occupant. The response can vary slightly based on the gender and age of the occupant. This difference is illustrated by the upper and lower bounds in addition to age and gender. Simple items such as foam pads on the back of the seat can also significantly change the peak deceleration and the impact duration (*49*); there-

**Table E-1. Summary of the human response to deceleration from the literature reviewed.**

| Decel (g) | Ave Δt (sec) | Reported Injury | Cited |
|---|---|---|---|
| **220** | 0.060 | Lethal in Anesthetized Hogs | (*45*) |
| **125** | 0.060 | Reversible Injury in Anesthetized Hogs | (*45*) |
| **70** | 0.130 | Lung Injury in Chimp Similar to Blast Lung | (*45*) |
| **50** | 0.200 | Reversible Loss of Consciousness (500 g/sec) | (*45*) |
| **45** | 0.050 | Concussion | (*45*) |
| **38** | 0.200 | Reversible Loss of Consciousness (1350 g/sec) | (*45*),(*55*),(*56*) |
| **26** | 0.002 | Back Muscle Soreness | (*47*) |
| **18** | 0.100 | Upper Limit Head and Limb Motion Can be Braked by Musculature | (*57*) |
| **17** | 0.300 | Sudden Pressure to the Epigastrium and Rib Margin | (*55*) |
| **16** | 0.090 | FAA Std for Peak Floor Deceleration | (*52*) |
| **15** | — | Suggested Human Tolerance Limit | (*57*) |
| **14** | >0.200 | Lumbar Fx if Max Torso Flexion is Attained | (*45*) |
| **13** | >0.200 | Abdominal Strain | (*47*) |
| **12** | >0.200 | Where Seat Belt Rides Up | (*46*) |
| **10** | 0.002 | Bruising | (*46*), (*47*) |
| **10** | 0.200 | Hydrostatic Pressure Effects Begin | (*45*),(*56*) |
| **9** | — | FAA Std for Seat Decal Limit | (*52*) |
| **8** | 0.310 | Neck Muscle Soreness | (*46*) |
| **8** | 60.0 | 150% Loss in Respiratory Capacity | (*57*) |
| **6** | 3.0 | Pilot Can Still Maneuver Plane | (*58*) |
| **6** | 60.0 | 15% Loss in Respiratory Capacity | (*57*) |
| **4** | 2.0 | Eye and Sinus Hemorrhages | (*46*) |
| **4** | 80.0 | Dimming of Vision | (*59*) |
| **2** | 115.0 | Flatting of T-Wave (Serious Arrhythmia) | (*59*) |

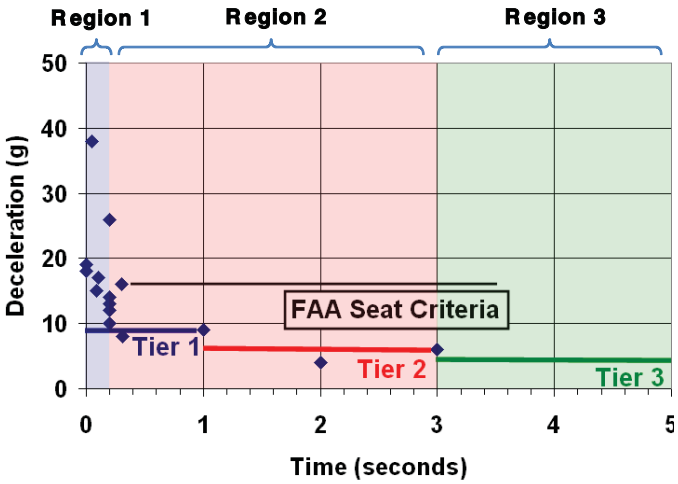


***Figure E-1. Decelerations with documented human response.***

fore, great care should be exercised when using an aircraft deceleration of 10 g as an injury criterion by itself.

In a review of aircraft accidents, Moseley (*50*) observed that although the aircraft's deceleration was within human tolerance limits (<10 g), injuries were still sustained. In the Moseley report, many of the injuries sustained were due to unrestrained body regions striking objects in front of them (*50*). One possible reason for the higher rate of injury, as reported by the Committee for Aeronautics, is that the accelerations measured in the instrumented Anthropomorphic Test Device's (ATD) chest were 1.2 to 1.5 times the peak acceleration measured at the floor (*48*). Therefore, a sled deceleration of 40 g approaches the injury threshold for the chest as specified by the 3 ms clip criterion. The 3 ms clip criterion is an automotive injury criterion that specifies that an acceleration of the chest greater than 60 g can cause serious injuries (*51*).

For emergency crash landings for which the deceleration duration is typically very short, the FAA has set standards for airplane safety. The FAA standard stipulates that the peak floor deceleration of the plane must not exceed 16 g, or have a rate of application (jerk) greater than 178 g/sec (*52*). The structures within the aircraft must be able to withstand the forces generated by this deceleration pulse for at least 3 seconds. From this deceleration pulse, the standard also requires that the peak deceleration experienced by the occupant must not exceed 9 g (*52*).

### E.1.2. Deceleration Durations from 0.2 to 3 Seconds

If the duration of the deceleration pulse is lengthened to between 0.2 and 3 seconds (Figure E-1 – Region 2), a greater transfer of energy to the fluid systems of the body can be expected (*46*). In this range, injuries reported for rapid displacement of body fluids at 10 g now begin at 4 g due to the longer deceleration duration (*45*). In this interval, the heart and circulatory system has time to react, and is working at maximum output to counteract the effects of the deceleration. This increased cardiac output, in some individuals tested, led to an irregular, rapid, and inefficient heartbeat (tachycardia) (*53*). If not corrected, extreme tachycardia cases can be life threatening (*54*). In addition to circulatory problems, the deceleration forces can force fluids to pool in body regions, exceeding the elasticity of tissues and causing blood vessel rupturing (*45*). These injuries can be observed as ruptures of the blood vessels in the eyes and skin. In the evaluation of pilots' responses it was determined that pilots still had the cognitive facilities to control the plane if exposed to accelerations of 6 g for up to 3 seconds. We hypothesize that passengers of an aircraft could extricate themselves from the cabin after a similar experience.

### E.1.3. Deceleration Durations Greater Than 3 Seconds

When the duration of the deceleration exposure is 3 seconds or greater (Figure E-1 – Region 3), the observed injuries are primarily determined by the hypoxic effects (*45*). The hypoxia is caused by a combination of poor blood circulation and poor respiratory output. Since the deceleration occurs over a period of time up to 120 seconds, the onset of symptoms will be more gradual. The initially reported symptom is dimming of vision (*53*), then loss of breath, dizziness and ultimately, for long duration deceleration, loss of consciousness (*55*). The injury threshold for these long duration deceleration pulses is between 2 and 8 g.

## E.2. Injury-Based Criteria for Evaluating Arrestor Systems

To define the human tolerance to deceleration and suggest a human tolerance limit for use in the analysis of existing and future arresting systems, literature was reviewed and an exercise examining the injury threshold for the occurrence of TBI was undertaken. The results of the literature review indicate that a single injury criterion is not applicable for the full range of deceleration durations anticipated in the evaluation of the arresting systems. Therefore, a three-tiered deceleration limit for the evaluation is proposed (Figure E-1). The first is for decelerations with durations under one second, the second for decelerations with durations between one and three seconds, and the third for deceleration durations over three seconds.

For deceleration durations less than 1 second, the data reviewed indicates that 9 g is a reasonable limit. For this tier, the risk of incapacitation or injury due to rapid displacement of body fluids is minimized. In addition to a lower risk of incapacitation, there is a reduced risk of bodily injury. For these short decelerations below 9 g, the airplane cabin will remain intact and is within the design limit for the seat anchors. By remaining within the design limits of the airplane structure, the potential of injury from the body striking objects inside the cabin is reduced. If the head comes into contact with the structures inside the cabin, the potential for injury is estimated to be low.

For the analysis of airplane deceleration between one and three seconds, the peak acceptable deceleration must be reduced to 6 g. By limiting the peak deceleration to 6 g, the literature suggests that the forces placed on the body by the longer deceleration will not affect the passengers' cognitive ability to extricate themselves from the cabin.

When the duration of the deceleration exposure is 3 seconds or greater, it is proposed that the criterion be further reduced to 4 g. The reduction should minimize the occurrence of reported symptoms such as dimming of vision, loss of breath, dizziness, and ultimately, for long duration deceleration, loss of consciousness. All these symptoms could contribute to the passenger's ability to exit the airplane after an incident.

The results of this effort indicate that a tiered approach is required for the analysis of airplane arresting systems. For deceleration durations less than 1 second, the proposed injury threshold is 9 g to reduce the risk of incapacitation or injury due to rapid displacement of body fluids and head impacts to interior structures within the cabin, respectively. For the analysis of airplane deceleration between one and three seconds, the peak acceptable deceleration proposed is 6 g. When the duration of the deceleration exposure is 3 seconds or greater, it is proposed the criterion be further reduced to 4 g. By maintaining the deceleration to these limits, passengers should have the physical and cognitive ability to safely exit the plane.

APPENDIX F

# Tire Models

In order to predict landing gear loads effectively, computer models were required for both the arrestor materials and the tires of the three subject aircraft. This appendix discusses the tire model development, while Chapters 9 through 12 discuss the modeling of the candidate arrestor systems.

## F.1. Subject Tires Modeled

Manufacturer references give the tire sizes, pressures, and load limits for the three aircraft of interest (*60*). Table F-1 lists the main- and nose-gear tires for each aircraft, and Table F-2 provides specifications for the tires. The tire designations give three numbers, referring to the diameter, width, and ply rating, respectively. The leading "H" appearing in some tires indicates a bias-ply tire designed for high deformations.

Goodyear supplied load-deflection curves for the tires listed, which were used for later tire calibration and validation.

## F.2. Tire Modeling Approach

Tire modeling can be a highly detailed process, involving discrete representation of the treads, carcass material, reinforcing fiber layers, the tire–rim interface, inflation pressures, and so on. Modeling these facets is required for accurate prediction of stresses within the tire, oscillatory behavior, tread wear, and so on. However, for arrestor bed modeling, such detail did not necessarily offer added value. A number of these facets would constitute higher order (and lower importance) effects when applied to the simulation of crushable material interactions.

A tire model was needed that could produce a realistic rut through an arrestor bed. A realistic rut would feature the correct penetration depth and cross-sectional shape. Since the energy dissipation is largely based on the crushed volume of material, a rut of the correct dimensions would tend to produce the correct energy dissipation and hence the correct drag load. Under a static vertical load with steady forward motion, this means that the tire would deform and settle to a steady-state depth in the material, producing a rut of the correct depth and width for that loading condition.

For a tire model to create such a rut, it would have to replicate two critical behaviors:

1. Correct deformation shape under loading, and
2. Correct interface loading (ground pressure) against the arrestor material.

After a review of available tire modeling methods and mechanical phenomena, the tire model priorities were set per Table F-3.

### F.2.1. Tire Dimensions

The tire models needed to accurately represent the gross dimensions of the actual aircraft tires. Ensuring such a match was actually more complicated than it appeared. During inflation, the tire model stretched, which altered its original gross dimensions. Therefore, the dimensional criterion applied to the match of the inflated model tire with the inflated actual tire.

### F.2.2. Ground Pressure

The ground pressure that the tire produced strongly depended on its inflation pressure and governed the penetration of the tire into the arrestor material. Provided that the gross dimensions were correct and the load-deflection performance matched, the model would produce a ground pressure that would be sufficiently accurate for the soft-ground interaction.

### F.2.3. Load-Deflection Performance

Goodyear provided load versus deflection curves, both in quasi-static and dynamic loading regimes. The load-deflection performance is analogous to a spring deflection curve. Typical efficiencies for a tire are slightly less than an ideal spring,

**Table F-1. Tires for subject aircraft.**

| Aircraft | Tire | Tire Designation |
|---|---|---|
| **CRJ-200** | Main Tire | H29x9.0-15 |
| | Auxiliary Tire | 18x4.4 |
| **B737-800** | Main Tire | H44.5x16.5-21 |
| | Auxiliary Tire | 27x7.75R15 |
| **B747-400** | Main Tire | H49x19.0-22 |
| | Auxiliary Tire | H49x19.0-22 |

at nominally 45 to 47%, a quasi-linear behavior that applies to the bulk of the loading domain (*14*). This linear behavior ceases during very high "bottoming" loading of the tire, when the deflection is high enough to allow the wheel rim to "bottom out." Bottoming loads are most likely during hard landing impacts, but do not occur in an aircraft in a steady roll with properly inflated tires. As such, replication of the tire performance during bottoming was deemed non-essential to this research. The domain of concern was limited to 80% of bottoming loads for each tire (Figure F-1).

## F.3. Model Construction

### F.3.1. Modeling Methods

Finite element tire models for each aircraft were constructed in LS-DYNA. The tire models were developed using a simple tire carcass with a smeared-property orthotropic material (*61*). The smeared properties represented the combination of all materials in the actual tire: tread, bulk rubber, reinforcement plies, and so on. This approach was attractive due to its simplicity, and it produced correct deformation within the loading range of interest. It was also practical since little detail was known about the inner construction of the actual tires: proprietary manufacturer data would be required to effectively model the various components individually.

The tire model used two-dimensional shell elements for the carcass in order to obtain the best computational efficiency. For a full tire, the carcass contained 4,608 shell elements in 2.5-degree increments; usually a quarter- or half-symmetry version was used, with the element count reduced accordingly (Figure F-2).

A constant pressure was applied to the inner surface of the tire to simulate pneumatic pressure. When loaded vertically, the tire models deflected realistically, forming an increasingly large flat contact area with the ground (Figure F-3).

### F.3.2. Model Calibration

In using a smeared approach, the material properties of the tire carcass required calibration, such that the load-deflection behavior of the model matched that of the actual tire. Using LS-OPT, this calibration was accomplished in a systematic fashion. Two optimization criteria were defined:

1. Match the load-deflection curve for the actual tire as closely as possible, and

**Table F-2. Data for subject aircraft main-gear tires (*60*).**

| Tire Designation | 18x4.4 | 27x7.75R15 | H29x9.0-15 | H44.5x16.5-21 | H49x19-22 | Units |
|---|---|---|---|---|---|---|
| **Rated Speed** | 210 | 225 | 210 | 225 | 235 | *mph* |
| **Rated Load** | 4,350 | 9,650 | 14,500 | 44,700 | 56,600 | *lbf* |
| **Rated Inflation Pressure** | 225 | 200 | 196 | 214 | 205 | *psi* |
| **Maximum Bottoming Load** | 13,000 | 28,950 | 39,200 | 121,000 | 152,800 | *lbf* |

**Table F-3. Aspects of tire dynamics for inclusion and exclusion.**

| Aspects to Replicate | Aspects to Neglect |
|---|---|
| • Tire dimensions | • Internal tire stresses |
| • Ground pressure | • Heat generation |
| • Load versus vertical deflection performance | • Tread features |
| • Correct mode of deformation | • Ground traction and slip |
| • Computational efficiency | • Lateral loading deformations |
| | • High frequency effects, noise, vibration |

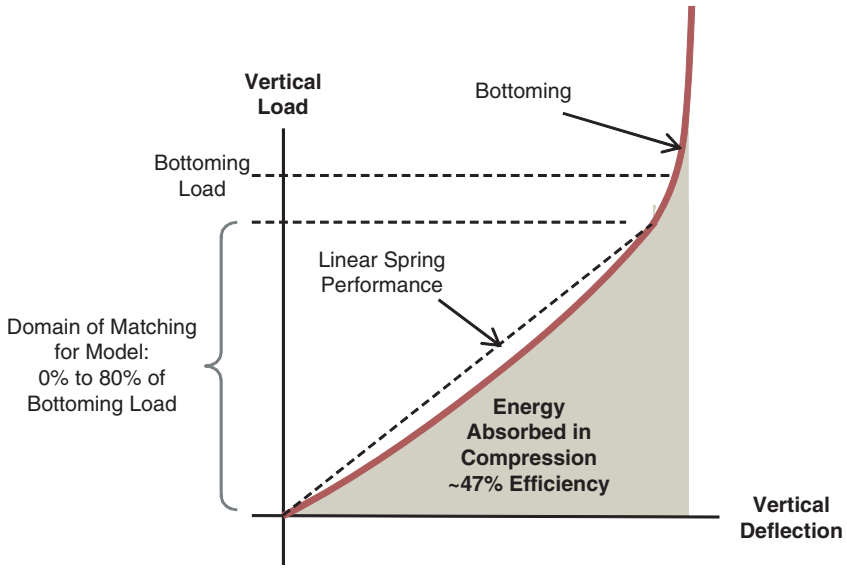


*Figure F-1. Tire load curve and modeling domain of interest.*

2. Match the inflated dimensions for the actual tire as closely as possible.

The load-deflection objective was defined by the mean-squared-error (MSE) between the load curves of the simulated and actual tires. The inflated dimensions were compared by measuring the tire just after the inflation process completed.

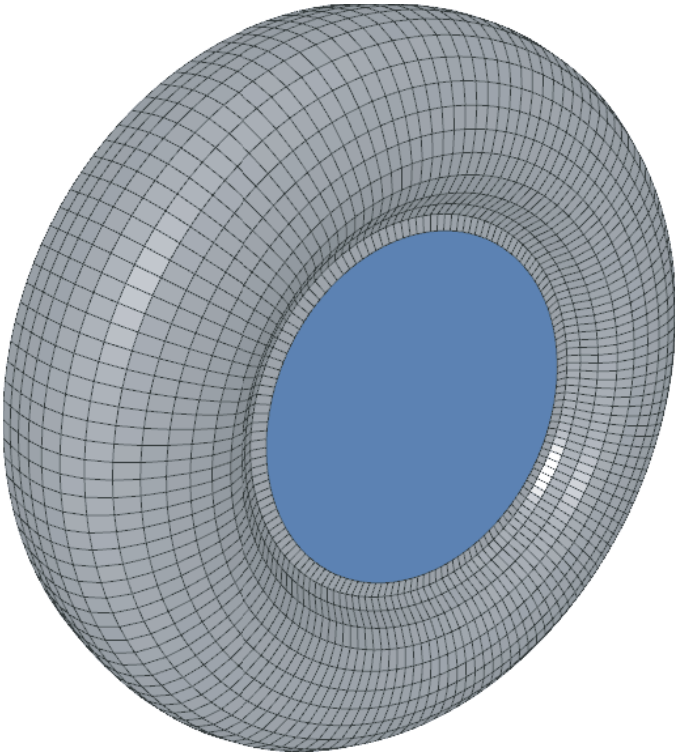

*Figure F-2. 44.5-in. tire model.*

Many simulations were conducted in batches over multiple iterations. Using a sequential response surface methodology (SRSM), the design parameters were gradually narrowed until LS-OPT had determined an optimum set of material properties (*62*). These best-case properties produced the closest overall match between the model and the actual tire performance.

Table F-4 summarizes the tire calibration results. As shown in the lower half of the table, nearly all the criteria were met to within 2% of the objective values. The RMSE values indicate how closely the load-deflection curves match the real tires (Figure F-4). The inflated dimension error represents how closely the final tire diameter matched the actual tire. Practically speaking, these values indicate that the tires have the correct shape and respond with the correct loading as the tire is compressed.

## F.4. Summary of Tire Model Development

The selected tire modeling approach struck a balance between accuracy and efficiency. The orthotropic smeared-property method neglected details required for nuanced tire design models, but it still replicated the overall tire deformation and loading pertinent to arrestor simulation.

When compared with the prior state-of-the-art in arrestor modeling—the radial spring tire model—the FEM approach adopted herein offers an increase in fidelity. This three-dimensional model does not depend on ellipsoid contact surface assumptions and includes lateral tire bulging.

The five tires developed in this task replicate the main- and nose-gear tires of the three subject aircraft. Each mimics the actual tire performance well, typically with less than 2% error for inflated dimensions and load-deflection behavior. The iterative optimization process using LS-OPT made this accurate calibration possible.

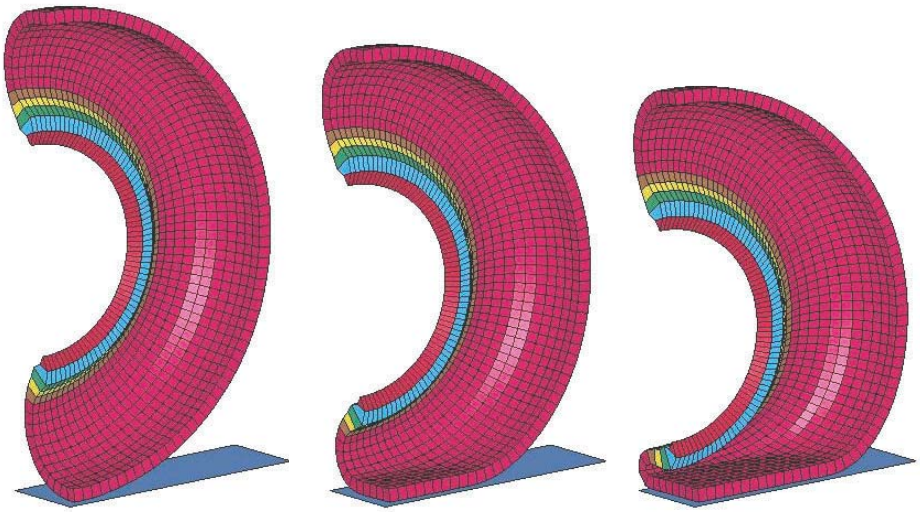

*Figure F-3. Quarter symmetry 44.5-in. tire model undergoing vertical deflection.*

**Table F-4. Summary of tire calibration.**

| | Tire | 18x4.4 | 27x7.75R15 | H29x9-15 | H44.5x16.5-21 | H49x19-22 |
|---|---|---|---|---|---|---|
| **Simulation Parameters** | RSM Type | Quadratic | Quadratic | Quadratic | Linear | Linear |
| | Open Variables | 3 | 3 | 2 | 3 | 3 |
| | Simulations Per Iteration | 16 | 16 | 10 | 7 | 7 |
| | Number of Iterations (Pre Final) | 10 | 20 | 4 | 5 | 7 |
| | Total Simulations | 161 | 321 | 41 | 36 | 50 |
| **Quality of Optimized Design** | RMSE for Load-Deflection Curve Match | 1.6% | 7.4% | 2.0% | 2.0% | 1.7% |
| | Error for Targeted Inflation Dimensions | 2.65% | 1.1% | 2.2% | 1.9% | 0.08% |

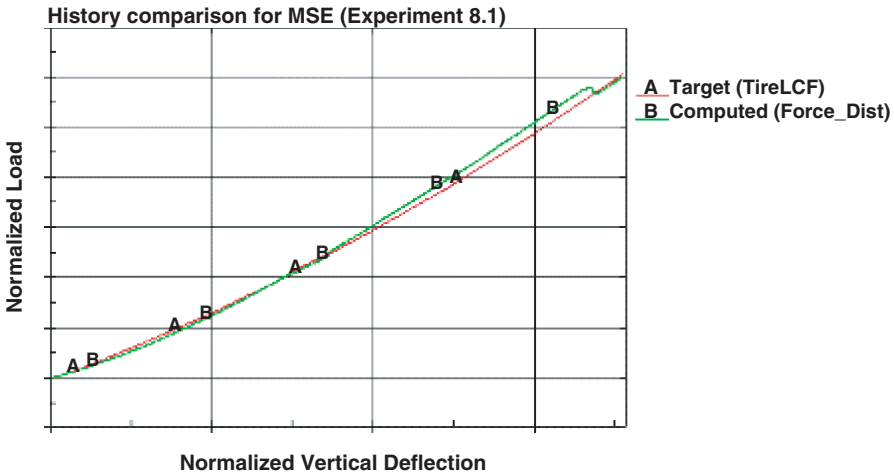


*Figure F-4. Sample load-deflection curve comparison to 80% of bottoming load (units omitted).*

APPENDIX G

# Arrestor Prediction Code

## G.1. APC Overview

The APC was developed to simulate aircraft arrestments for the different arrestor concepts. The APC allows experimentation with different aircraft, arrestor geometries, and material strengths. Built with a generalized framework, essentially any arrestor bed concept could be simulated with the APC.

Figure G-1 shows that the APC has four principal inputs:

1. **Metamodel data,** which defines the aircraft landing gear interaction with the arrestor bed;
2. **Tire load-deflection data,** which defines the landing gear interaction with solid surfaces;
3. **Aircraft library,** which defines the aircraft dimensions, weights, and other properties; and
4. **Arrestor design definitions,** which define the bed dimensions and aircraft conditions for a given scenario.

Using these four inputs, the APC runs a time-marching simulation to predict the dynamic loads on the aircraft, the arresting distance, and so on. A typical APC simulation for an aircraft arrest takes 1.5 to 2 minutes to run. After completion of the simulation, the APC provides graphical plots and tabular data output.

The APC was written in MATLAB, a scientific programming language and coding environment. Overall, the APC has nine modules (m-files) with nominally 1,500 lines of code.

## G.2. FAA ARRESTOR Code

The FAA previously developed the ARRESTOR code, which performed similar predictions as the APC. It featured three aircraft (B707, B727, and B747) and could be used to model different foam arresting bed geometries. Initially, modification of the ARRESTOR code was considered in lieu of developing a new predictive tool. If the evaluation had been restricted to crushable foam materials only, this could have proven advantageous. However, the ARRESTOR code was not inherently capable of simulating the aggregate and aggregate foam systems, which do not behave as an analog to either crushable foams or soils. The APC was, therefore, more generalized than ARRESTOR and could simulate a broader variety of system concepts.

## G.3. Suspension Model

### G.3.1. Concept Description

At the core of APC is an aircraft suspension model that calculates the dynamic loads and motion of an aircraft as it rolls through an arrestor bed. The arrestor bed exerts loads on both the nose and main gear, and the aircraft responds by pitching forward, bouncing, sinking into the bed, and decelerating to an eventual stop. The upper portion of Figure G-2 illustrates the loads on the aircraft during such an event.

The dynamic behavior of the aircraft was represented mathematically using the component model illustrated in the lower portion of Figure G-2. The component model is composed of lumped masses, springs, and damper elements in order to approximate the aircraft fuselage, wings, and landing gear. Although an effective wing mass, spring, and damper were included, this was done as a placeholder provision within the mathematical framework of the model. In practice, the wing motion was neglected by using null values for those parameters.

### G.3.2. Scope of Capabilities

The APC was developed specifically to simulate aircraft arresting scenarios. Consequently, its intended capabilities and limitations were defined *a priori.* General performance objectives for the suspension model include:

- Allowing the modeling of general arrestor beds of various geometries,

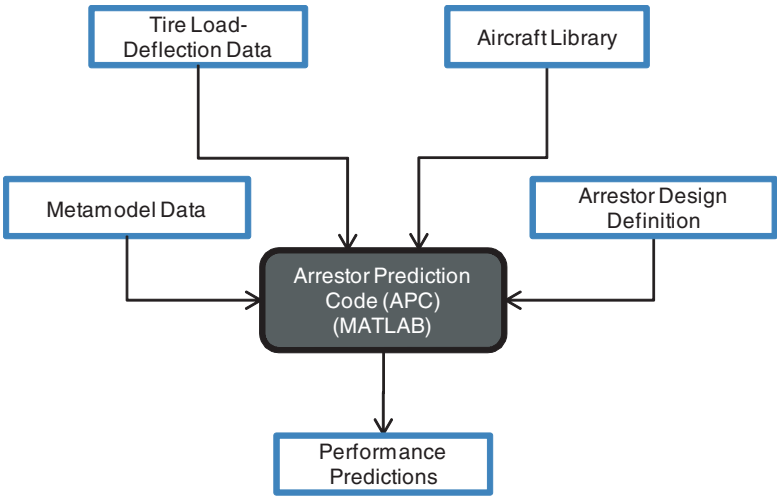


*Figure G-1. Simplified diagram of the APC.*

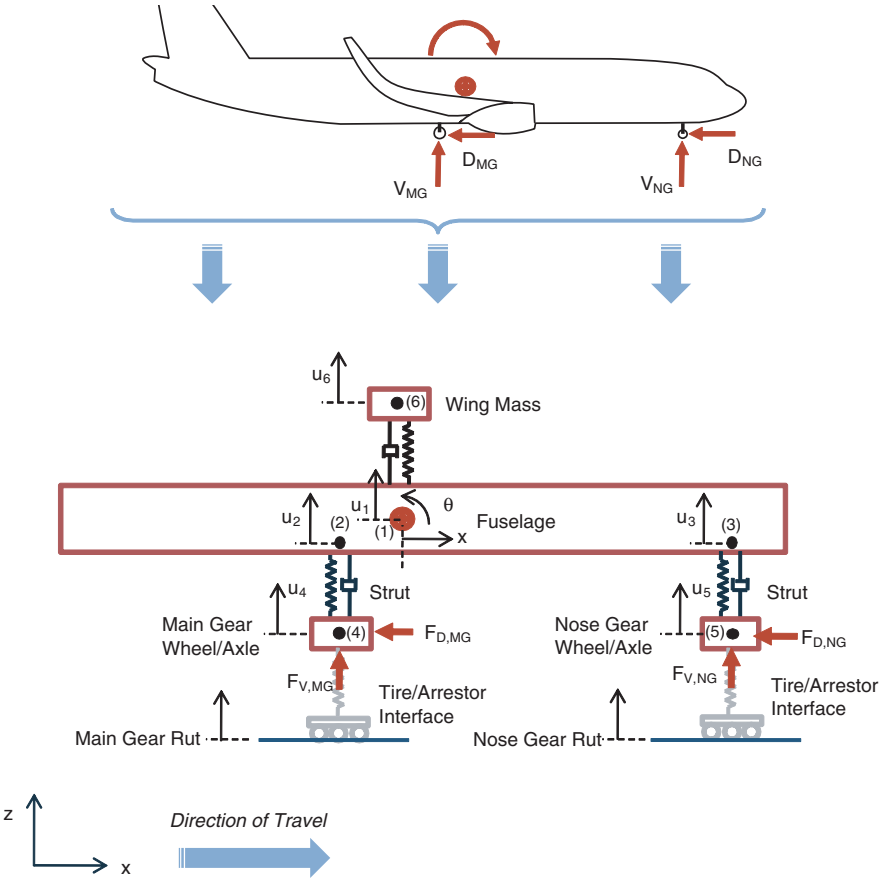


*Figure G-2. Aircraft dynamics transformed into suspension model.*

- Modeling of material response accomplished through metamodels,
- Prediction of gross loading on landing-gear struts for damage estimation,
- Prediction of stopping distance for arrestor concepts,
- Prediction of porpoising effect with transient load spikes,
- Prediction of arrestor efficiency compared with idealized deceleration, and
- Prediction of fleet-wide performance (versatility) of an arrestor.

General limitations for the suspension model include:

- No steerage (yawing) or other lateral motion effects,
- No tire slippage or heat generation effects,
- No lateral load prediction on gear struts, and
- No higher order effects or frequency analysis.

### G.3.3. Simplifying Assumptions

In light of the APC scope of capabilities, the mathematical suspension model involves several simplifying assumptions:

- The fuselage only pitches at relatively small angles, less than +/–10 degrees;
- The motion is two-dimensional with no yawing;
- The airframe remains effectively rigid; and
- The landing-gear struts can be approximated with constant stiffness and damping factors.

These assumptions were appropriate because the simulations assume an aircraft in a ground rolling state. Non-linear strut spring and damping factors were considered, but ultimately were not necessary due to the relatively low loading rates and minimal strut travel.

Given these assumptions, the model has seven degrees of freedom. Since the two rut-depth degrees of freedom are implicitly defined by the metamodel data, only five degrees of freedom are included in the governing equations. This produced a system stiffness matrix that was 10 x 10.

Additionally, linear approximations were made for the angle ($\theta$) and the angular velocity ($\omega$) that were accurate to within less than one percent for the angle range specified.

### G.3.4. User-Defined Problems

The APC permits the user to define arrestor scenarios using many parameters, as summarized in Table G-1.

## G.4. Aircraft Parameter Definition

The aircraft library indicated in Figure G-1 was developed to provide input parameters required by the suspension model for the three test aircraft: the CRJ-200, B737-800, and B747-400. These properties included aircraft weights, landing gear configuration, design strengths of the struts, and overall dimensions. In all, 36 parameters were required to define each plane. These properties were obtained from published manufacturer data, a generalized aircraft model, and the FAR requirements for passenger aircraft.

### G.4.1. Published Manufacturer Data

Published aircraft data generally included information regarding aircraft weight, gross dimensions, landing gear strut configurations, and the types of tires used. This information was acquired through open-source websites and airport guidance documents published by the manufacturers (*42, 60*). Goodyear also provided load curve data for the tires used by the three subject aircraft.

Aircraft manufacturers were approached directly for additional information regarding strut properties and landing gear design strengths. However, these requests were ultimately unfruitful due to the proprietary nature of the specifications.

**Table G-1. User-defined parameters for simulations.**

| Aircraft | Arrestor | Simulation Controls |
|---|---|---|
| • Type<br>• Initial speed<br>• Braking conditions inside and outside of the bed | • Type<br>• Bed length and depth<br>• Depth at which the bed is recessed vertically<br>• Setback distance<br>• Tapering length for bed thickness<br>• Increase or decrease arrestor material strength | • Time step for computations and data output intervals<br>• Plotting and tabular data saving options |

### G.4.2. Generalized Aircraft Model

In the absence of the remaining properties, which were needed to complete the aircraft definitions, alternative means were sought to develop reasonable estimates. Sources found during the literature review provided the means to calculate approximate values.

Chester outlines a modeling approach for a generalized aircraft of arbitrary size, with a focus on landing gear dynamics and overall airframe response (*16*). Based on this method, properties such as strut stiffness, the pitching moment of inertia, and various unspecified dimensions were estimated.

Currey provided excellent guidance with regard to landing gear mechanics (*14*). Non-linear strut compression curves were developed based on oleo-pneumatic strut design principles. Ultimately, however, constant spring stiffnesses were used for simplicity. Statistical information in this reference regarding typical landing gear weights was used to estimate the travelling mass for the wheel assemblies of each strut.

The strut damping coefficients were estimated as a percentage of critical damping, assuming the estimated strut stiffness and a mass equivalent to the vertical static load on the strut. Generally, damping factors less than 1.0 (underdamped) produced oscillatory behavior, noise, and instability. After experimentation, it was determined that a simple factor of 1.0 (critically damped) would suffice for the simulations. Aside from basic system stability, the damping factor was not found to have a substantial effect on the predictions.

### G.4.3. Federal Aviation Regulations

The load limits for the landing gear were among the most critical properties to define for each aircraft. Such values were not available from published data or the aircraft manufacturers. Discussions with the manufacturers and the FAA produced a straightforward alternative: the limit and ultimate landing-gear loads as specified by the FAR were taken as design strengths for the aircraft.

The limit/ultimate loads were calculated for the nose and main gear from multiple criteria in FAR Part 25. Vertical load limits were not of high importance since the rolling arrestments did not substantially affect them. The rearward drag load limits were critical, however, particularly for the nose gear.

For the nose gear, the highest drag loads resulted from Section 25.509, "Towing Loads," conditions 1 and 2. For the main gear, the highest drag loads resulted from Section 25.493, "Braked Roll Conditions." Values for drag-direction limit and ultimate loads based on these two criteria were employed in the APC as performance thresholds.

### G.4.4. Summary of Aircraft Parameters

Based on the preceding discussion, the different aircraft parameters and related data sources can be summarized as in Table G-2.

For inline wheel sets, "shadowed wheels" were those behind the leading wheel. The leading wheel was responsible for producing the drag load when interacting with the arrestor bed, while the shadowed wheels were assumed not to contribute drag load.

## G.5. Arrestor and Tire Interface

### G.5.1. Contrast of APC and ARRESTOR

The APC uses a different premise than ARRESTOR for calculating the landing-gear loads. The ARRESTOR method calculated the loads on the tire based on the geometry of interface and the foam compression strength (radial spring tire assumptions) (*63*). These loads were calculated in real-time, during the course of the simulation. This quasi-analytical method proved sufficient for crushable foam arrestors (cellular cement, polymer foam, etc.). However, the approach is not as well-suited to more chaotic and non-linear arrestor materials (aggregates, foam aggregates, etc.).

The APC method uses high-fidelity numerical models of the tire/arrestor interface to build a large database of loads for a broad range of conditions, which are defined in the metamodels discussed in Table G-4. Because high-fidelity models are used for the load calculations *a priori,* the load predictions have higher accuracy than using a simplified analytical model. Further, there is no inherent limitation on the arrestor beds that can be assessed; a suitable numerical code can be chosen for whatever system is desired (LS-DYNA, EDEM, others). The contrasts of the APC and ARRESTOR methods are summarized in Table G-3.

### G.5.2. Metamodel Interface with Suspension Model

During each simulation, the loads on a tire are determined based on the penetration depth of the tire into the arrestor, the speed of travel, and the arrestor bed depth. Given these conditions, the APC queries the correct metamodel for the vertical and drag loads on the tire. This process is essentially a database lookup except that the database is a multi-dimensional metamodel. When the tire was on a hard surface, rather than in an arrestor bed, tire load-deflection data was used in place of the metamodel data.

Figure G-3 illustrates the transformation of the tire/arrestor interface into a virtual spring/roller assembly in the suspension model (refer to Figure G-2).

**Table G-2. Summary of aircraft parameters.**

| Group | | Parameter | Source |
|---|---|---|---|
| **Overall Aircraft** | Mass | Weight (maximum take-off) | Published data |
| | | Pitching moment of inertia | Generalized model |
| | Dimensions | Wheel base | Published data |
| | | Distances from center of gravity (CG) to nose and main gear | Supplemented using generalized model |
| | | Height to CG | |
| **Main & Nose Gear** | Configuration | Number of struts | Published data |
| | | Wheels per strut | |
| | | Number of shadowed wheels | |
| | Mass | Travelling weight | Generalized model |
| | Strut | Stiffness | Generalized model |
| | | Damping | |
| | Tire | Diameter | Published data |
| | | Static deflection | |
| | | Static load | |
| | | Maximum deflection | |
| | | Maximum load | |
| | Load limits | Drag limit load | FAR Part 25 |
| | | Drag ultimate load | |
| **Wings** | Mass | Weight | Not used |
| | Spring properties | Stiffness | |
| | | Damping | |

**Table G-3. Contrast of ARRESTOR and APC methods for landing-gear load calculations.**

| | ARRESTOR | APC |
|---|---|---|
| **Tire Model** | Radial spring analytical model | Numerical model, dependent on software choice<br>• LS-DYNA: finite element tire model<br>• EDEM: rigid tire form, with deflection adjustment |
| **Arrestor Material Model** | Simplified quasi-analytical crushable foam model | Numerical model using appropriate method<br>• Crushable: LS-DYNA smooth particle hydrodynamics (SPH) formulation<br>• Aggregate: EDEM discrete element (DEM) formulation |
| **Load Calculation Method** | Analytical calculation based on area of tire/arrestor interface | Batch simulations utilizing numerical model<br>• Many simulations to create data set<br>• Metamodel for loading created as a fit to the data set |
| **Timing of Load Calculation** | Real-time, during simulation | A priori, using high-fidelity models to create metamodels.<br>Metamodels referenced in real-time during simulation. |

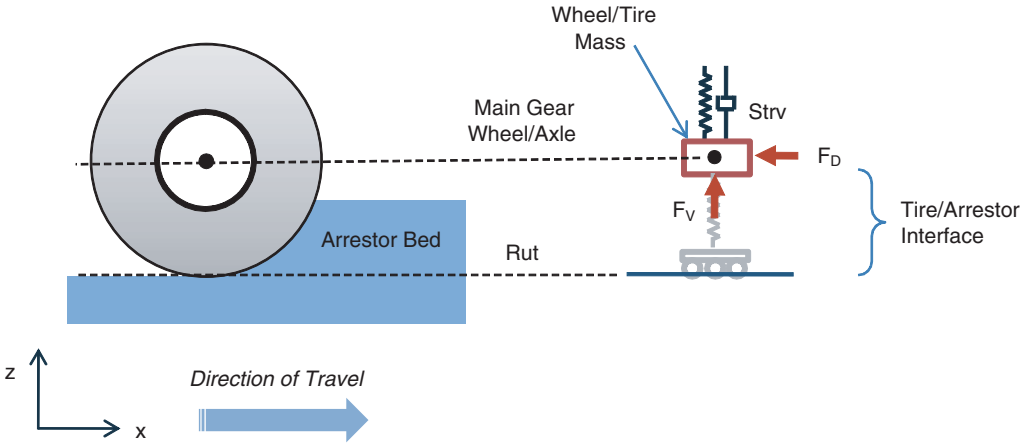


*Figure G-3. Arrestor interface dynamics transformed into suspension model.*

### G.5.3. Metamodel Dimensions

The metamodels generated for each arrestor type had three independent variables: speed, bed depth, and depth of penetration into the bed. For each condition set, two response values were available: the drag and vertical loads (Table G-4). Considered from the standpoint of the suspension model, there were additional parameters that could have been included as additional variables, such as wheel spin, vertical translation velocity, braking torque, and so on. For simplicity, these variables were neglected in the current analysis. Therefore, the current metamodels were four-dimensional, having three independent variables and one response variable each. Ultimately, metamodels could be seven-dimensional if the additional independent variables were included.

The primary limitation of the metamodel data used in these simulations is the lack of vertical speed as an independent variable. Without vertical wheel velocity information, high frequency response predictions, such as small bumps and noise, could be realistically simulated. The overall assumption for the metamodel data was that steady-state loading at various penetration depths was sufficiently accurate for the required predictions. Overall, transient vertical loads were not of significant interest when compared with the overall drag loads. Given the soft nature of the arrestor materials, this assumption was reasonable.

Additional metamodel data could be generated to include vertical speed and could be implemented with little alteration of the software. However, this additional complexity was deemed unnecessary for the current effort.

**Table G-4. Metamodel variables and responses.**

| | Variables | Responses |
|---|---|---|
| **Included in Metamodels** | Forward speed | Vertical load |
| | Bed depth | Drag load |
| | Penetration depth of tire | |
| **Neglected in Metamodels** | Vertical speed | Torque on tire |
| | Spin rate | |
| | Braking torque | |

## G.6. Overall Program Function

The overall process followed by the APC is illustrated by Figure G-4. Starting from the initial conditions specified by the user (upper left), the program calculates a steady-state rolling solution for the aircraft, including initial strut and tire deflections, weight distribution for the aircraft, and so on.

The program then enters the main loop, which computes the time-marching dynamic behavior of the aircraft and arrestor bed. The loop calculates the current load state based on the component locations and velocities. Using the core suspension model stiffness matrix (gray box), the system velocity matrix is determined. Numerical time integration produces new displacements from the velocity matrix. After updating the stiffness matrix constants, the loop begins a new iteration. This process continues until the aircraft comes to rest. At that point, data files and plots are output per user specifications.

## G.7. Conclusions

The APC effectively simulated aircraft arrestments across a wide range of aircraft and for a set of dissimilar arrestor mediums. Because it was not dependent on simplified analytical tire or arrestor material models, it provided a generalized framework suitable for simulating nearly any arrestor design.

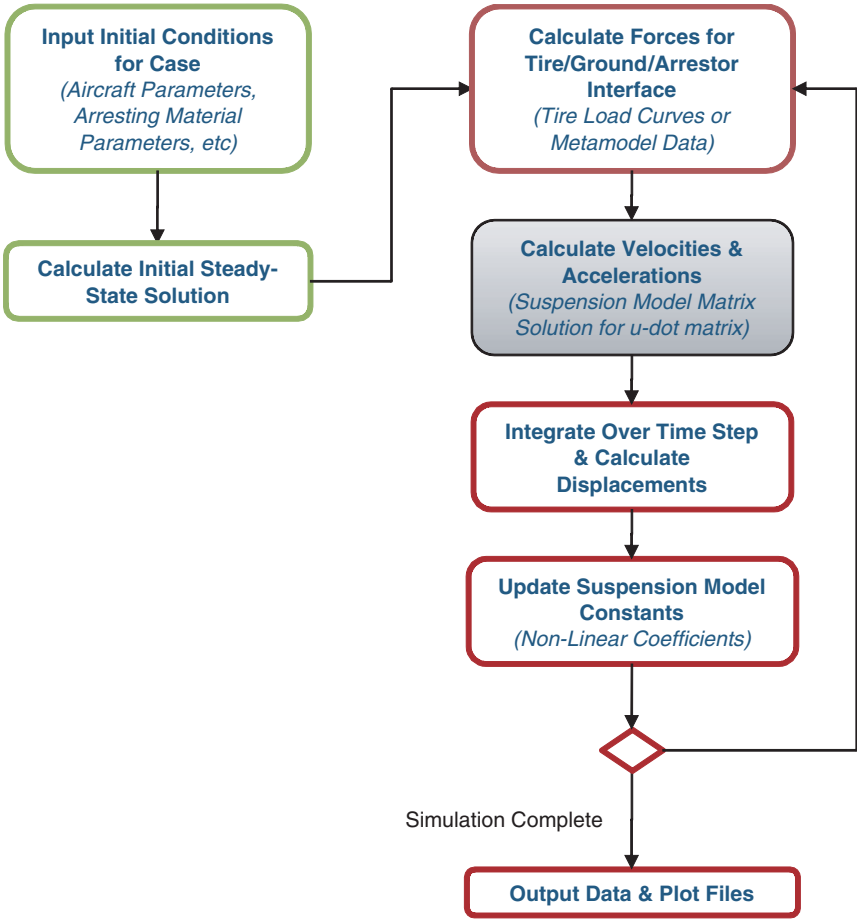


***Figure G-4. Simplified process diagram for the arrestor prediction code.***

# ACRONYMS AND ABBREVIATIONS

| | |
|---|---|
| AASHTO | American Association of State Highway and Transportation Officials |
| AC | Advisory Circular |
| ACRP | Airport Cooperative Research Program |
| APC | Arrestor Prediction Code |
| ARFF | Aircraft Rescue and Fire Fighting index |
| ASTM | American Society for Testing and Materials |
| ATD | Anthropomorphic Test Device |
| CG | Center of Gravity |
| CFR | Code of Federal Regulations |
| CRDA | Cooperative Research and Development Agreement |
| CTEE | Cost to Establish EMAS |
| DOT | Department of Transportation |
| DEM | Discrete Element Modeling (numerical method) |
| EDEM | Discrete Element Modeling Software Available Through DEM Solutions |
| EMAS | Engineered Material Arresting System |
| ERAS | Engineered Root-zone Arresting System |
| ESCO | Engineered Arresting Systems Corporation |
| FAA | Federal Aviation Administration |
| FAR | Federal Aviation Regulations |
| FEM | Finite Element Method (numerical method) |
| JFK | John F. Kennedy International Airport |
| LGA | LaGuardia Airport |
| LS-DYNA | Numerical Modeling Software Available Through LSTC |
| LS-OPT | Optimization Software Available Through LSTC |
| LSTC | Livermore Software Technology Corporation |
| MATLAB | Matrix Laboratory software |
| MG | Main Gear |
| MSP | Minneapolis–St. Paul Airport |
| MTOW | Maximum Takeoff Weight |
| MTW | Maximum Taxi Weight |
| NG | Nose Gear |
| NTSB | National Transportation Safety Board |
| RBF | Radial Basis Function network |
| RMS(E) | Root-Mean-Squared Error |
| RSA | Runway Safety Area |
| RSM | Response Surface Methodology |

| | |
|---|---|
| SPH | Smoothed Particle Hydrodynamics (numerical method) |
| SRSM | Sequential Response Surface Methodology |
| TBI | Traumatic Brain Injury |
| TRB | Transportation Research Board |
| UK | United Kingdom |
| U.S. | United States |

*Abbreviations and acronyms used without definitions in TRB publications:*

| | |
|---|---|
| AAAE | American Association of Airport Executives |
| AASHO | American Association of State Highway Officials |
| AASHTO | American Association of State Highway and Transportation Officials |
| ACI–NA | Airports Council International–North America |
| ACRP | Airport Cooperative Research Program |
| ADA | Americans with Disabilities Act |
| APTA | American Public Transportation Association |
| ASCE | American Society of Civil Engineers |
| ASME | American Society of Mechanical Engineers |
| ASTM | American Society for Testing and Materials |
| ATA | Air Transport Association |
| ATA | American Trucking Associations |
| CTAA | Community Transportation Association of America |
| CTBSSP | Commercial Truck and Bus Safety Synthesis Program |
| DHS | Department of Homeland Security |
| DOE | Department of Energy |
| EPA | Environmental Protection Agency |
| FAA | Federal Aviation Administration |
| FHWA | Federal Highway Administration |
| FMCSA | Federal Motor Carrier Safety Administration |
| FRA | Federal Railroad Administration |
| FTA | Federal Transit Administration |
| IEEE | Institute of Electrical and Electronics Engineers |
| ISTEA | Intermodal Surface Transportation Efficiency Act of 1991 |
| ITE | Institute of Transportation Engineers |
| NASA | National Aeronautics and Space Administration |
| NASAO | National Association of State Aviation Officials |
| NCFRP | National Cooperative Freight Research Program |
| NCHRP | National Cooperative Highway Research Program |
| NHTSA | National Highway Traffic Safety Administration |
| NTSB | National Transportation Safety Board |
| SAE | Society of Automotive Engineers |
| SAFETEA-LU | Safe, Accountable, Flexible, Efficient Transportation Equity Act: A Legacy for Users (2005) |
| TCRP | Transit Cooperative Research Program |
| TEA-21 | Transportation Equity Act for the 21st Century (1998) |
| TRB | Transportation Research Board |
| TSA | Transportation Security Administration |
| U.S.DOT | United States Department of Transportation |